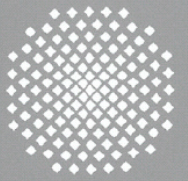
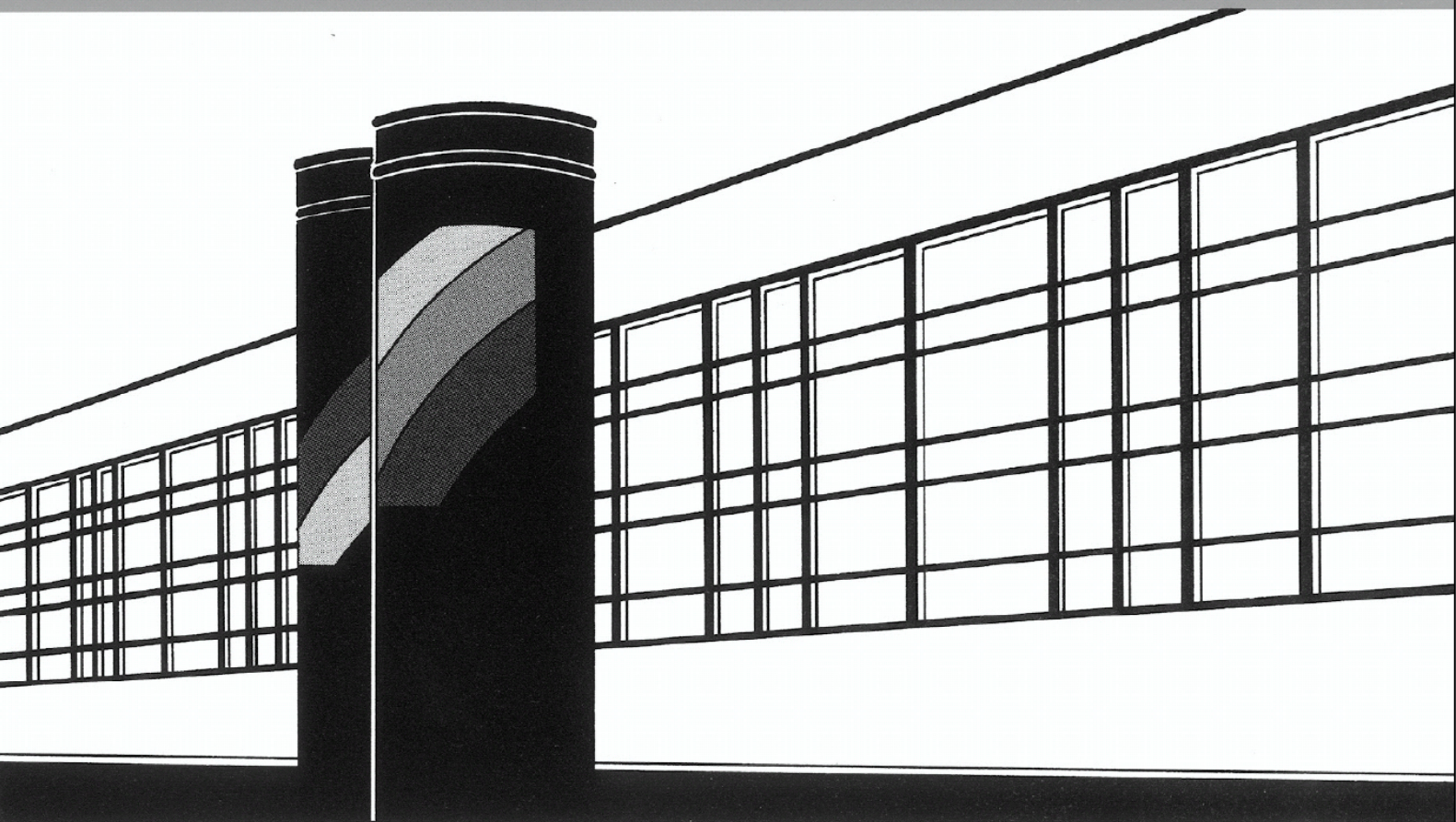


Universität Stuttgart



Institut für Wasser- und Umweltsystemmodellierung

Mitteilungen



Heft 309 Vahid Shoarinezhad

Applying automatic calibration for three-dimensional numerical modeling of hydro-morphological changes in channels and reservoirs

Applying automatic calibration for three-dimensional numerical modeling of hydro-morphological changes in channels and reservoirs

von der Fakultät Bau- und Umweltingenieurwissenschaften
der Universität Stuttgart zur Erlangung der Würde eines
Doktor-Ingenieurs (Dr.-Ing.) genehmigte Abhandlung

vorgelegt von
Vahid Shoarinezhad
aus Täbris, Iran

Hauptberichterin: Prof. Dr.-Ing. Silke Wieprecht
Mitberichter: Prof. Dr.-Ing. Nils Reidar Bøe Olsen
Mitberichter: PD Dr. Stefan Haun

Tag der mündlichen Prüfung: 27. März 2024

Institut für Wasser- und Umweltsystemmodellierung
der Universität Stuttgart
2024

Heft 309 **Applying automatic calibration
for three-dimensional
numerical modeling of hydro-
morphological changes in
channels and reservoirs**

von
Dr.-Ing.
Vahid Shoarinezhad

D93 Applying automatic calibration for three-dimensional numerical modeling of hydro-morphological changes in channels and reservoirs

Bibliografische Information der Deutschen Nationalbibliothek

Die Deutsche Nationalbibliothek verzeichnet diese Publikation in der Deutschen Nationalbibliografie; detaillierte bibliografische Daten sind im Internet über <http://www.d-nb.de> abrufbar

Shoarinezhad, Vahid:

Applying automatic calibration for three-dimensional numerical modeling of hydro-morphological changes in channels and reservoirs, Universität Stuttgart. - Stuttgart: Institut für Wasser- und Umweltsystemmodellierung, 2024

(Mitteilungen Institut für Wasser- und Umweltsystemmodellierung, Universität Stuttgart: H. 309)

Zugl.: Stuttgart, Univ., Diss., 2024

ISBN 978-3-910293-13-7

NE: Institut für Wasser- und Umweltsystemmodellierung <Stuttgart>: Mitteilungen

Gegen Vervielfältigung und Übersetzung bestehen keine Einwände, es wird lediglich um Quellenangabe gebeten.

Herausgegeben 2024 vom Eigenverlag des Instituts für Wasser- und Umweltsystemmodellierung

Druck: P+K Solutions GmbH & Co. KG, Stuttgart

Acknowledgment

I would like to express my sincere appreciation to Prof. Dr.-Ing. Silke Wieprecht, chair of the Department of Hydraulic Engineering and Water Resources Management (LWW) of the Institute for Modelling Hydraulic and Environmental Systems (IWS), University of Stuttgart. Her unwavering support and invaluable guidance have been the cornerstones of my research journey, enabling me to reach this milestone in my academic life. This thesis would not have come to fruition without her steadfast encouragement and kind support. I hold her professionalism, inspiration, and kindness in high regard and aspire to emulate her exemplary conduct in my life.

I would like to extend my deepest gratitude to my co-supervisor, PD Dr. Stefan Haun, head of the IWS Hydraulic Laboratory. His constructive pieces of advice and admirable mentorship have been instrumental in enhancing the quality of this research. He generously allowed me to foster my ideas while consistently offering his friendly guidance and support, enabling me to sharpen my competencies in the expansive domain of hydraulic engineering. Your challenges pushed me to expand my perspective, and the skills that you have imparted to me are genuinely remarkable.

Furthermore, I wish to convey my heartfelt appreciation to my co-supervisor, Prof. Nils Reidar Bøe Olsen, for his invaluable insights and recommendations regarding numerical modeling.

Your support and contributions have been paramount in shaping this thesis and my academic growth. I am genuinely grateful for the privilege of learning from and collaborating with such esteemed supervisors.

Dr.-Ing. Gabriele M. Hartmann, the course director of the International Doctoral Program "Environment Water" (ENWAT), deserves commendation for her support in handling the administrative tasks related to registration, qualifying examination,

and defense preparation. Her commitment and expert guidance have played a pivotal role in guaranteeing a smooth experience throughout the program.

I am truly thankful for my colleagues' fantastic support and camaraderie, whose constant cooperation has made LWW a delightful and friendly workplace. In this regard, I must extend a very special thanks to our exceptional secretary Maria, whose door was always open for assistance and friendly chats.

I would like to acknowledge the Sustainable Water Management Program (NaWaM) from the Federal Ministry of Education and Research (BMBF) for granting me a scholarship administered through the German Academic Exchange Service (DAAD). Their financial support made it possible for me to conduct and bring this research to completion.

My stellar wife, Maryam, and my awesome brother, Farid, you are simply the best! Your constant love and cheering mean everything to me in this world. My marvelous parents, Roghi and Hasan, and in-laws, Aghi and Amir, your boundless love, sacrifices, and prayers during my toughest times have been my guiding light. Thank you for being the fantastic, loving bunch you are from the depths of my heart.

Abstract

Hydraulic and environmental numerical models with ever-increasing levels of complexity have been developed as a result of advancements in computational speed and power. In this context, the number of variables a model incorporates as input parameters reflects its level of complexity and the ability to consider ongoing processes. While increasing the number of parameters allows for a better and more detailed representation of the investigated system in many cases, it comes at the expense of higher processing costs and a more complicated model design. Moreover, many numerical models used to simulate real-world phenomena rely on empirically developed formulae, introducing a high level of uncertainty that must be considered alongside model simplifications when calibrating the model to accurately replicate physical observations.

Currently, there is a significant demand to utilize the analytical and predictive capabilities of numerical models to address existing knowledge gaps in understanding complex hydro-morphodynamic processes, including erosion, transport, and deposition of sediments. The distinct advantage of such models lies in their ability to replicate the intricate interaction between hydrodynamics, sediment dynamics, and morphological changes. This capability not only enhances our ability to anticipate sediment-related issues but also enables us to apply the gained knowledge in forecasting, decision-making, and management under various conditions.

To date, numerous hydro-morphodynamic sediment transport models have been developed for various purposes and resolved through different numerical techniques. Despite ongoing advancements in computational techniques, challenges persist due to the complex nature of sediment dynamics. Addressing these challenges requires the consideration of model- and sediment-specific parameters for calibration. Since these models are highly parameterized, involving multiple unknown or uncertain parameters, their reliability depends significantly on the quality of calibration.

While optimization methods are commonly used for model calibration in various environmental models, e.g., hydrological models, a noticeable gap exists regarding the application of automated inverse techniques for calibrating hydro-morphodynamic numerical models. This research aims to bridge this gap by investigating the application of optimization methods for calibrating various hydro-morphodynamic numerical models and shed light on the benefits of automatic calibration as a cutting-edge alternative to the conventional trial-and-error calibration technique prevalent in this field. While the trial-and-error approach may suffice when dealing with a single parameter subject to calibration, such as the roughness parameter in hydrodynamic models, the presence of multiple uncertain parameters in hydro-morphodynamic models makes manual calibration impractical, time-consuming and subjective due to the countless combinations involved.

This thesis consists of three research articles discussing the applicability and efficiency of automatic calibration in hydro-morphodynamic numerical modeling of channels and reservoirs. Publication I introduces several optimization algorithms for automatic calibration coupled with a 3D numerical model to compute morphological changes in a channel bend. In this study, the efficiency and accuracy of the proposed algorithms for model calibration are compared based on the number of model runs and computed final bed level changes. In Publication II, the most efficient method identified in the previous study is applied to calibrate numerical models of two laboratory-scale reservoirs. Here, the calculation of bed elevation changes is conducted over different periods and compared with measured bed levels. Subsequently, the selected method is applied to a prototype-scale reservoir in Publication III to investigate morphological changes resulting from a flushing event. In each case study, several sensitive parameters are examined for calibration, and new values are proposed for them. Moreover, various statistical metrics are utilized to compare the results from calibrated models with measured data.

The findings of this study emphasize the effectiveness of employing appropriate optimization algorithms for calibrating hydro-morphodynamic models. Optimization algorithms offer significant benefits, including reduced time for calibration, decreased reliance on user intervention, and subjectivity while improving the accuracy of the calibration process and leading to more reliable model outputs.

Kurzfassung

Durch die zunehmende Rechenleistung und Rechengeschwindigkeit wurden immer komplexere Modelle für die Wasser- und Umweltsystemmodellierung entwickelt. In diesem Zusammenhang spiegelt die Anzahl der Variablen, die ein Modell als Eingabeparameter einbezieht, seine Komplexität und die Möglichkeit auftretende Prozesse zu berücksichtigen wider. Eine verbesserte und detaillierte Darstellung des untersuchten Systems ist in vielen Fällen durch eine Erhöhung der Anzahl an Parametern möglich, allerdings auf Kosten höherer Verarbeitungskosten und komplexerer Modellarchitektur. Viele numerische Modelle, die zur Simulation realer Phänomene verwendet werden, basieren auf empirischen Formeln und enthalten daher einen hohen Grad an Unsicherheiten, welche zusammen mit den Modellvereinfachungen berücksichtigt werden müssen, um physikalische Beobachtungen genau zu replizieren.

Um bestehende Wissenslücken in Bezug auf die komplexen hydromorphologischen Prozesse der Erosion, des Transports und der Ablagerung von Sedimenten zu schließen, werden derzeit vermehrt numerische Modelle und deren analytische und prädiktive Fähigkeiten eingesetzt. Der entscheidende Vorteil numerischer Modelle liegt darin die komplexe Wechselwirkung zwischen Hydrodynamik, Sedimentdynamik und morphologischer Veränderungen zu replizieren. Dies verbessert unsere Möglichkeiten, sedimentbedingte Herausforderungen zu antizipieren und die gewonnenen Erkenntnisse in die Vorhersage, Entscheidungsfindung und Bewirtschaftung unter verschiedenen Bedingungen einzubeziehen.

Bis heute wurden eine Vielzahl an Sedimenttransportmodellen für unterschiedliche Zwecke entwickelt und durch verschiedene numerische Ansätze gelöst. Trotz kontinuierlicher Fortschritte in der Rechenleistung bestehen aufgrund der Komplexität der Sedimentdynamik weiterhin Herausforderungen. Die Bewältigung dieser Herausforderungen erfordert die Berücksichtigung modell- und sedimentspezifischer Parameter für die Kalibrierung. Da diese Modelle

hochparametrisiert sind und mehrere unbekannte oder unsichere Parameter enthalten, hängt ihre Zuverlässigkeit stark von der Qualität ihrer Kalibrierung ab.

Obwohl Optimierungsmethoden üblicherweise für die Modellkalibrierung in verschiedenen Modellen, z. B. in der Hydrologie, verwendet werden, besteht eine spürbare Lücke in Bezug auf die Anwendung automatisierter inverser Techniken für die Kalibrierung hydromorphodynamischer Modelle. Diese Forschungsarbeit zielt darauf ab, diese Lücke zu schließen, indem die Anwendung von Optimierungsmethoden zur Kalibrierung verschiedener hydromorphodynamischer numerischer Modelle untersucht wird und Einblicke in die Vorteile der automatischen Modellkalibrierung als moderne Alternative zur typischen Trial-and-Error-Kalibrierungstechnik gegeben werden. Der Trial-and-Error-Ansatz kann durchaus gute Ergebnisse erzielen, wenn es um die Kalibrierung eines einzelnen Parameters geht, wie die Rauheit in hydrodynamischen numerischen Modellen. Bei mehreren unsicheren Parametern, die in hydromorphodynamischen Modellen vorhanden sind, machen jedoch die unzähligen Kombinationen die manuelle Kalibrierung unpraktisch, zeitaufwendig und anfällig für Subjektivität.

Diese Dissertation besteht aus drei Forschungsartikeln, die sich mit der Anwendbarkeit und Effizienz der automatischen Kalibrierung bei der hydromorphodynamischen numerischen Modellierung von Kanälen und Stauseen befassen. Publikation I stellt mehrere Optimierungsalgorithmen für die automatische Kalibrierung vor, die mit einem 3D-numerischen Modell gekoppelt sind, um morphologische Veränderungen in einer Kanalkrümmung zu berechnen. In dieser Studie werden die Effizienz und Genauigkeit der vorgeschlagenen Algorithmen zur Modellkalibrierung anhand der Anzahl der Modellläufe und der berechneten Änderungen der Betthöhe verglichen. In Publikation II wird die effizienteste Methode, die in der vorherigen Studie identifiziert wurde, verwendet, um numerische Modelle von zwei Reservoirs im Labormaßstab zu kalibrieren. Dabei werden die Berechnungen der Betthöhenänderungen über verschiedene Zeiträume durchgeführt und mit den gemessenen Betthöhen verglichen. Anschließend wird die ausgewählte Methode auf ein Reservoir im Prototyp-Maßstab angewendet, um die morphologischen Veränderungen infolge eines Spülungsereignisses zu untersuchen (Publikation III). In jeder Fallstudie werden mehrere sensitive Parameter zur Kalibrierung untersucht, und es werden neue Werte für sie vorgeschlagen. Darüber hinaus werden verschiedene statistische Metriken verwendet, um die Ergebnisse der kalibrierten Modelle mit den gemessenen Daten zu vergleichen.

Die Haupteckennis dieser Studie unterstreicht die Wirksamkeit des Einsatzes geeigneter Optimierungsalgorithmen zur Kalibrierung hydromorphodynamischer Modelle. Optimierungsalgorithmen bieten erhebliche Vorteile, einschließlich reduzierter Zeit für die Kalibrierung, geringerer Abhängigkeit von Benutzerangaben und daraus resultierender Subjektivität, während sie gleichzeitig die Genauigkeit des Kalibrierungsprozesses verbessern und zu zuverlässigeren Modellergebnissen führen.

Contents

1. Introduction.....	1
1.1 Background and motivation.....	3
1.2 Research objectives	6
1.3 Structure of the thesis	6
2. Fluvial sediment transport and reservoir sedimentation	9
2.1 Sediment properties.....	10
2.2 Incipient motion of sediments.....	11
2.3 Modes of sediment transport	12
Bedload transport modeling.....	13
Suspended load transport modeling.....	15
Bed-material load transport modeling.....	16
2.4 Reservoir sedimentation	17
3. Materials and methods	23
3.1 Numerical modeling.....	23
3.2 Model calibration	25
3.3 Case studies	28
180° curved channel.....	28
Lozenge- and hexagon-shaped reservoirs.....	29

Bodendorf reservoir	29
4. Summary of the scientific papers	31
4.1 <i>Publication I</i> : Comparison of local and global optimization methods for calibration of a 3D morphodynamic model of a curved channel	31
4.2 <i>Publication II</i> : Applying optimization methods for automatic calibration of 3D morphodynamic numerical models of shallow reservoirs: comparison between lozenge- and hexagon-shaped reservoirs.....	32
4.3 <i>Publication III</i> : Using automatic model calibration for 3D morphological simulations: a case study of the Bodendorf reservoir flushing.....	34
5. Conclusions and outlook	37
6. References	41
Appendix I Comparison of local and global optimization methods for calibration of a 3D morphodynamic model of a curved channel	65
Appendix II Applying optimization methods for automatic calibration of 3D morphodynamic numerical models of shallow reservoirs: comparison between lozenge- and hexagon-shaped reservoirs	85
Appendix III Using automatic model calibration for 3D morphological simulations: a case study of the Bodendorf reservoir flushing.....	103

List of Figures

Fig. 1.1 Involving factors affecting the reliability of model predictions or "imperfect paths to knowledge" described by Oden et al. [52]	4
Fig. 2.1 Schematic of different modes of sediment transport.....	13
Fig. 2.2 Typical reservoir sedimentation pattern (modified after Julien [239])	18
Fig. 2.3 Classification of strategies for reservoir sedimentation management (modified after Morris [249])	20

List of Tables

Table 5.1 Metadata of Publication I	66
Table 5.2 Metadata of Publication II.....	86
Table 5.3 Metadata of Publication III.....	104

Notations

d	[mm]	diameter of a particle
d_{16}	[mm]	particle diameter representing the 16% cumulative percentile value
d_{50}	[mm]	particle diameter representing the 50% cumulative percentile value
d_{84}	[mm]	particle diameter representing the 84% cumulative percentile value
q_b	[m ² /s]	volumetric bedload transport rate
q_s	[m ² /s]	volumetric suspended load transport rate
Re^*	[-]	dimensionless grain Reynolds number
u_*	[m/s]	shear velocity
w_s	[m/s]	particle fall velocity
κ	[-]	von Kármán constant
τ	[Pa]	bed shear stress
τ_c	[Pa]	critical bed shear stress
τ_{c^*}	[-]	dimensionless critical shear stress
Φ_b	[-]	bedload transport intensity

Abbreviations

BB-BC	Big Bang Big Crunch algorithm
CFD	Computational Fluid Dynamics
CMA-ES	Covariance Matrix Adaptation Evolution Strategy algorithm
ICOLD	International Commission on Large Dams
GML	Gauss-Marquardt-Levenberg algorithm
MPM	Meyer-Peter and Müller bed load equation
PEST	Parameter Estimation tool
PSO	Particle Swarm Optimization algorithm
RANS	Reynolds-averaged Navier-Stokes equations
SCE-UA	Shuffled Complex Evolution algorithm
SIMPLE	Semi-Implicit Method for Pressure-Linked Equations
SSIIM	Sediment Simulation In Intakes with Multiblock option

Chapter 1

Introduction

Since the formation of early civilizations, rivers have served as a central point of human engagement. These natural streams have been perpetually subjected to various alterations and constructions, disturbing their equilibrium conditions and changing their morphological characteristics. To date, humans have been involved in a wide range of activities related directly or indirectly to rivers, including but not limited to water extraction (e.g., for irrigation, drinking water supply, and industrial production), hydroelectricity generation, flood control, navigation, and recreational pursuits. Consequently, rivers confront ongoing anthropogenic impediments or "pressure factors" (e.g., river fragmentation, flow regulation, sediment trapping, water consumption, and infrastructure development in floodplains and riparian areas as defined by Grill et al. [1]), which impair their natural spatiotemporal connectivity and affect the fundamental processes and features of healthy rivers [2–4]. Because of its significant importance, there has been a perpetual interest among geomorphologists, sedimentologists, and hydraulic engineers in investigating complex fluvial processes such as floodplain dynamics, the formation of river channels, and their morphological features [5]. The processes of erosion, transport, and deposition of sediments mainly affect river morphology (shape, size, slope, and bed material composition), as well as hydraulic structures, such as reservoirs, and the surrounding areas. In order to acquire an understanding of the dynamic nature of these systems, it is

necessary to analyze sediment transport mechanisms and address questions and concerns related to erosion and deposition.

The problems associated with sediments are becoming more severe due to hydrological and climate changes (altered precipitation patterns, increased temperatures, and more frequent extreme events). Additionally, persistent human interventions in regulating natural systems, such as constructions, excavations, mining, agricultural activities, deforestation, urbanization, and other land use/cover changes escalate the challenges [6–13]. A number of problems resulting from erosion and sedimentation include changes in channel morphology, damages to infrastructure, navigational issues, exacerbation of the risk of flooding and landslides, and reservoir siltation. Sediments can also contribute to the degradation of water quality (e.g., an increase in pollutants such as nutrients and heavy metals due to contaminated sediment and a decrease in dissolved oxygen levels), loss of soil fertility (reduction of agricultural productivity and food security), habitat destruction (affecting flora and fauna, leading to the loss of biodiversity in aquatic ecosystems), and climate change by affecting soil carbon sequestration [14–26]. Hence, the processes of erosion and sedimentation have significant environmental, economic, and social impacts, which require implementing sustainable management practices and proper sediment control measures to mitigate their impacts [27]. In this regard, there is a remarkable demand to use numerical models' analytical and predictive capabilities for bridging the existing knowledge gaps in understanding the complex processes of erosion, transport, and deposition of sediments. Their unique advantage in replicating the intricate interaction between hydrodynamics, sediment dynamics, and morphological changes improves our ability to anticipate sediment-related issues under various conditions [28,29].

Across various disciplines, from research to engineering applications, numerical models have become indispensable tools to represent physical reality. Nevertheless, the users who rely on information provided by numerical simulations are still concerned about the precision and reliability of the predictions. In this context, it is critically important to adhere to the "good modeling practice" paradigm (i.e., model setup, calibration, validation, application) [30–33]. Thus, evaluating the credibility and trustworthiness of

computer simulations of physical processes remains an issue that needs comprehensive assessment [34,35]. While employing numerical models to investigate sediment transport is viable, without careful model calibration and validation, such modeling may yield findings lacking the accuracy or dependability necessary for valuable design or decision-making purposes.

1.1 Background and motivation

Numerical models are inherently simplified yet practical and versatile representatives of complex systems, providing a better understanding of real-world phenomena [36]. Although simplifications may not lead to severely unrealistic simulation results, a certain level of uncertainty is involved in computational simulations. Therefore, despite its promising potential, numerical modeling presents challenges that originate from the inherent uncertainties resulting from our limited comprehension of natural phenomena, errors associated with the model's structure (i.e., assumptions, simplifications, approximations, initial and boundary conditions), as well as inadequate, imprecise and/or erratic data used for model construction, calibration, and validation [37,38]. The sequence of these uncertainties raises the vital question of "*How should confidence in modeling and simulation be critically assessed?*" [39–41]. More specifically, computational fluid dynamics (CFD) simulations have received increased attention regarding reliability assessment and confidence level enhancement [42,43]. The reliability, accuracy, and authenticity of numerical simulations strongly depend on the quality of [44–51]:

- Mathematical description of the physical process (e.g., boundary conditions, governing equations, empirical formulae)
- Numerical scheme used for discretization of differential equations
- Solution method for the discretized algebraic equations
- Implementation of the numerical solution in a computational code and verification
- Model calibration and validation

As depicted in Fig. 1.1, a physical reality can be encapsulated in a mathematical model (conceptual model), in an abstraction form, that quantitatively represents and describes the knowledge about the system or process of interest. These models are then discretized and treated as computational models [52–54]. Mathematical models typically incorporate input parameters that are imprecise or sometimes even undefinable. This requires the process of model calibration and validation using sufficient information (measured field data, experiments, expert knowledge, and experience) to better reflect the phenomenon for which predictions are targeted. However, uncertainties exist in observational data used for model setup and calibration owing to errors and deficiencies associated with measuring equipment and techniques [55,56]. The uncertainties are even augmented by converting a mathematical model into a computational model through discretization [57–59]. Hence, it is essential to comprehend the ramifications of uncertainties on the model's output [60,61].

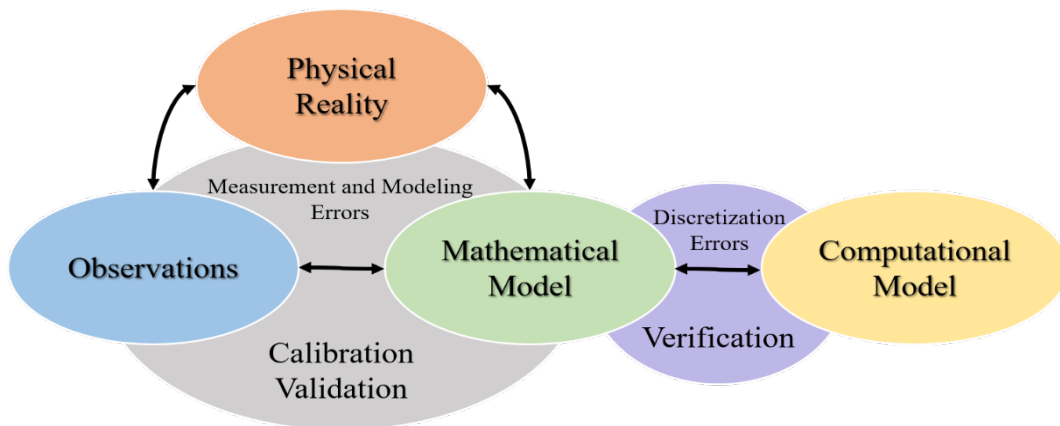


Fig. 1.1 Involving factors affecting the reliability of model predictions or "imperfect paths to knowledge" described by Oden et al. [52]

The models for simulating fluvial hydrodynamics and sediment transport have evolved from simple numerical solvers into advanced hydroinformatic tools over multiple "generations" of numerical modeling in hydraulics, as described by Abbott et al. [62,63]. In light of rapid advancements in computational technology and efficient solvers, hydro-morphodynamic numerical models have emerged as flexible and cost-effective tools to analyze sediment transport mechanisms. Hydro-morphodynamic modeling involves the numerical solution of the governing differential equations (i.e.,

momentum, energy, and continuity) describing the flow field together with simulating sediment transport and morphological evolution within an investigated domain. Because of the multiple processes involved in describing the dynamics of flow-sediment interactions, a substantial quantity of empirical parameters and input data are required [64]. Despite rapid developments in this field and increased knowledge of computational techniques, modelers still face a significant challenge in minimizing inevitable misfits between simulation outcomes and corresponding measured data [65,66]. Since these models are extensively parameterized, they are particularly subject to a significant amount of parametric uncertainty in addition to the aforementioned sources of uncertainty, such as model structure complexity [67–74]. This means that some input parameters required for model setup cannot be quantified at a desired scale or location for a specified period due to challenges associated with continuous in-situ monitoring, while some others cannot be recorded at all owing to physical constraints [75–77]. As a result, the accuracy of hydro-morphodynamic model predictions is constrained by the integrity and spatiotemporal coverage of available data.

Model calibration constitutes the foremost step in accrediting such models as trustworthy tools for predictions and decision-making and addressing the issues encountered by institutions involved in water resource supply and management [78–80]. Calibration is generally applied to authenticate the model's capability to generate results corresponding to the actual data. Entailing the systematic adjustment of model parameters, calibration can be defined as an inverse iterative procedure that aims to mitigate uncertainty through the successive refinement of the model outputs. The ultimate goal is to obtain a rational agreement with a reasonable tolerance between observations and computational outcomes by recurrent comparisons [81–85]. Over the past decades, numerous research works have been conducted on the application of function optimization techniques for model calibration (automatic calibration) as a means to circumvent the laborious, subjective, time- and cost-consuming, and sometimes impractical process of manual calibration in various types of environmental models [86–96]. Automatic model calibration is state-of-the-art in many disciplines, replacing the general trial-and-error calibration procedure, especially when dealing with a high

degree of nonlinearity due to numerous uncertain input parameters and considering the non-uniqueness nature of the solution for the inverse problem. Although applying optimization methods is the conventional approach for model calibration in related fields such as hydrological models [97–99], there is a remarkable research gap regarding the use of automated inverse techniques to calibrate hydro-morphodynamic models [100–105]. This thesis tries to give new insight to the modelers in this field and propagates the application of automatic calibration routine as an essential step in the modeling process.

1.2 Research objectives

This dissertation investigates optimization methods for calibrating various hydro-morphodynamic numerical models and provides insight into the advantages of automatic model calibration as a cutting-edge alternative to the typical trial-and-error calibration technique used in this field. The main research question is: *can the proposed methodology for automatic model calibration be reasonably applied to environmental models with morphological activity?*

In this regard, the following specific objectives were defined:

- Development of 3D hydro-morphodynamic models of a curved channel, two laboratory-scale and one prototype-scale reservoirs.
- Performing parameter identification (sensitivity analysis) and parameter estimation (automatic calibration) using various algorithms.
- Comparison of different optimization methods and finding the most efficient one regarding the computational time and accuracy.

1.3 Structure of the thesis

This doctoral thesis is organized in a cumulative style. In addition to the five chapters, it comprises three methodically developed research papers to assess the performance of automatically calibrated models considering hydro-morphological processes in channels and reservoirs from laboratory to prototype scale.

The first chapter provides an overview of the subject matter, discussing the background and motivation for conducting this research. Chapter 2 presents the fundamentals of sediment transport mechanisms and reservoir sedimentation. Materials and methods used for developing the numerical models and the algorithms for automatic calibration are introduced in Chapter 3. The summaries of the main findings of the published papers, as well as the conclusions and recommendations, are included in Chapters 4 and 5, respectively. Finally, the scientific papers are attached as appendices (Publication I, II, and III).

Chapter 2

Fluvial sediment transport and reservoir sedimentation

Sediment transport mechanisms are among the most intricate and poorly understood natural phenomena. Scholars are still striving to solve ongoing challenges by developing novel approaches and models that provide further insight into the complex fluvial hydrodynamics and sediment transport processes. The formation and arrangement of alluvial channels through the complex interaction between flowing water and sediment materials constitute the core principle of fluvial morphology. Over time, natural streams and rivers undergo continuous adjustments, modifying their characteristics, e.g., slope, shape, and grain distribution. These dynamic processes (degradation and aggradation) involve the scouring of channel beds, transporting sediment particles in suspension or as bedload, and depositing materials depending on the flow velocity to establish a balance between sediment supply and transport capacity [106]. Thus, fluvial systems exhibit a tendency to adapt to disturbances by transitioning toward an equilibrium state through morphodynamic processes.

Sediments are produced in the catchment due to a range of physical and chemical mechanisms known as denudation processes. These mechanisms

lead to the breakdown of rocks into smaller fragments (weathering) in drainage basins. The soil surface undergoes erosion primarily due to the impact of raindrops and surface flow, which may either move in thin layers as sheet erosion or within specific channels as rill and gully erosion. In areas with moderate rainfall, sheet erosion constitutes the primary contributor to the overall sediment load, whereas in arid and semi-arid regions, a substantial portion of the load is supplied by gully and stream-channel erosion [107,108]. Additionally, the downslope movement of loose soil (mass wasting) further contributes to the ongoing process of denudation. Hence, the sediment yield of a catchment depends on extensive interactions among geological and topographical features, soil types, vegetal cover, and climate conditions, which is expedited by human activities.

This chapter aims to briefly overview essential topics related to non-cohesive sediment transport mechanisms, reservoir sedimentation, and hydro-morphodynamic numerical modeling without going into detail or providing extensive empirical/theoretical equations in this field.

2.1 Sediment properties

The sediment transport mechanism is directly related to the size and shape of particles. The size of sediment particles can be categorized into a wide range based on the diameter grade scale, from very fine clay ($0.0005 > d > 0.00024$ mm) to very coarse boulders ($4000 > d > 2000$ mm) [109]. Fluvial sediment typically consists of a heterogeneous combination of varying-sized particles, usually presented as a *particle size distribution curve*. The non-uniformity of a sediment mixture can be described by the *geometric standard deviation of size distribution* and *gradation coefficient* parameters, which are the functions of characteristic particle sizes of the mixture d_{16} , d_{50} , and d_{84} (sizes for which 16, 50, and 84 percent of the sediment sample by weight are finer). The other factors related to sediment particles, as required input parameters for hydro-morphodynamic numerical modeling, are the *angle of repose*, *settling velocity*, and *porosity*.

The angle of repose refers to the slope angle formed by sediment particles that are on the verge of sliding, which typically varies between 30° (sand) and

42° (cobble and boulder) [46,110–112]. The settling velocity is a key variable in sediment transport studies, particularly when suspended load transport predominates. This variable depends on several parameters such as sediment size, shape, submerged specific weight, fluid viscosity, turbulence intensity, and suspended sediment concentration. High sediment concentration in turbid water significantly decreases the settling velocity compared to clear water, referred to as the hindered settling effect. Stokes [113] made the first attempt to formulate settling velocity for spherical particles in laminar clear water. Since then, numerous researchers have proposed a variety of empirical and semi-theoretical relationships for the fall velocity of natural sediment particles with irregular shapes and rough surfaces. A wide range of such formulae can be found in the literature, e.g., [114–121]. *Porosity*, defined as the volume of void per unit total volume of the sediment deposit, can also be approximated according to available empirical formulae [122].

2.2 Incipient motion of sediments

Sediment mobilization occurs when the hydrodynamic forces (drag and lift) exerted on a particle exceed a threshold value to overcome the stabilizing forces (particle submerged weight and friction). Determining this threshold for particle movement is essential in studying sediment transport, the design of stable channels, and managing river and channel systems. Various approaches have been developed to establish criteria for the incipient motion of uniform and non-uniform sediments. These approaches encompass the determination of threshold bed shear stress, critical discharge, critical near-bed or average velocity [123–128], probabilistic concepts [129–134], as well as approaches considering the impact of near-bed turbulence structures on sediment entrainment [135–142]. According to the literature, the most renowned and widely used approach can be traced back to the pioneering work of Shields [143], based on the critical bed shear stress concept for uniform non-cohesive sediment on a horizontal surface [144–147]. Shields developed a diagram grounded in his experimental data, wherein the *dimensionless critical shear stress* (or *Shields parameter*, τ_{c*}) is correlated with the *dimensionless grain Reynolds number* (R_{e*}) that is a function of the shear velocity and grain size. The flow condition associated with the area above the curve in the Shields diagram

indicates sediment mobility for a certain sediment size, whereas the area below the curve denotes no sediment motion. The original Shields diagram, however, has been modified by several researchers to address its practical shortcomings and enhance its predictive applicability across a wider range of flow and sediment conditions [148–157]. As mentioned earlier, the work of Shields and its modified versions specifically apply to uniform sediments on nearly horizontal surfaces. In the case of steep streamwise or lateral gradients, the influence of the downslope gravity component on the incipient motion of sediments should also be considered (see, for example, [158–165]). The initiation of motion in multi-fraction sediment mixtures is governed by a more complex mechanism known as the *hiding-exposure* effect. Regarding non-uniform sediments, coarse particles have a higher likelihood of being exposed to the flow, whereas fine particles are prone to being concealed by coarser material. Therefore, a correction factor should be considered in determining the critical bed shear stress of a given size fraction in accordance with the particle size distribution [166–168].

2.3 Modes of sediment transport

Bedload and suspended load are two primary forms of sediment transport (Fig. 2.1). Bedload transport involves the movement of coarse sediment particles that stay in continuous contact with the bed (*sliding/rolling*) and the particles jumping or bouncing along near-bed trajectories (*saltation*). On the other hand, suspended load transport pertains to the movement of fine particles transported in suspension through the water column. As turbulence intensity significantly decreases, such as when a river flows into a reservoir or lake, most suspended particles eventually settle on the bed according to their settling velocity. The following criteria provide an approximate range based on the ratio of particle fall velocity w_s to shear velocity u_* , to distinguish between different types of sediment transport modes¹ [172]:

¹ Although the threshold condition for sediment suspension is generally defined based on the *Rouse number* ($= w_s/\kappa u_*$, κ is von Kármán constant), the critical values may vary in different literature. For other values, see, for example, Wu [46] and Armanini [169]. Furthermore, the threshold of sediment suspension can also be defined according to the Shields parameter [170] or probabilistic approaches [171].

- Sliding and rolling $6 > w_s/u_* \geq 2$
- Saltation $2 > w_s/u_* \geq 0.6$
- Suspension $0.6 > w_s/u_*$

The proportion of bedload to suspended load may exhibit significant variation from case to case depending on factors such as sediment characteristics and flow conditions. However, bedload generally represents a smaller percentage of the total transported sediment load (about 5 - 25%) compared to the suspended load [172–175]. Additionally, the wash load that occurs near the water surface in the form of semi-permanent suspension involves very fine particles with extremely low settling velocities, which has a practically negligible contribution to the sedimentation process and channel morphology. These particles are transported over long distances through the channel and rarely come in contact with the bed layer, unlike the suspended load that continuously exchanges with the bed. In contrast to the two main modes of sediment transport, the transport rate of wash load is not necessarily dependent on flow characteristics but more on climate conditions and watershed geology (i.e., the presence of fine-grained sediments resulting from chemical weathering or geologic formations) [176–178].

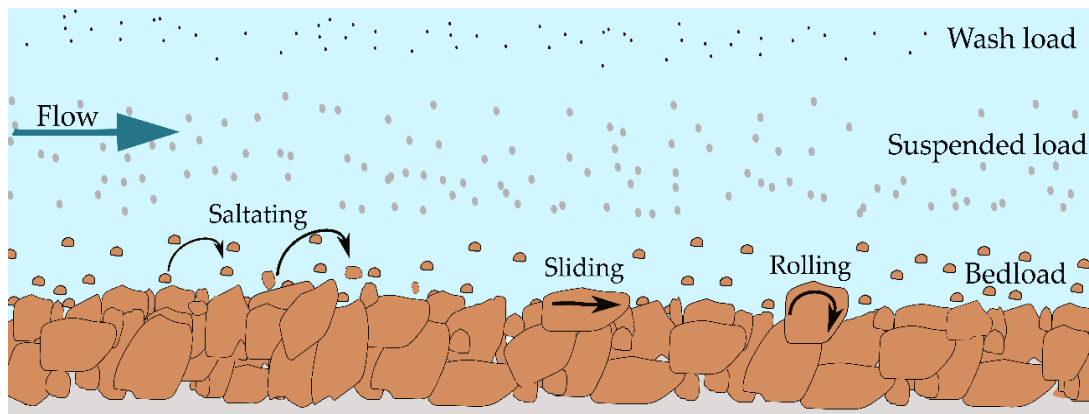


Fig. 2.1 Schematic of different modes of sediment transport

Bedload transport modeling

When the excess bed shear stress ($\tau - \tau_c$) is relatively low, the bedload transport typically proceeds in contact with the bed layer in rolling and sliding manners, where the lift force exerted on particles is equal to or less than the

submerged weight. As the shear stress increases and the lift force exceeds the submerged weight, sediments momentarily lose contact with the riverbed. Then, the streamwise movement of sediment particles occurs in a rapid and successive jumping or bouncing form mainly governed by the hydrodynamic lift and drag forces, as well as the bed roughness and the impact force after hitting the bed. Consequently, most of the momentum of these saltating particles is transferred to the bed as horizontal impulses, which may induce the initiation of motion of surface sediments, commonly referred to as *surface creep*. The bedload transport rate q_b can be expressed as the solid volume of transported particles per unit time and width. It can also be expressed in a dimensionless form known as bedload transport intensity Φ_b . Over the past century, researchers have developed numerous formulae to estimate the bedload transport rate based on various approaches, from empirical to more complex theoretical ones [179–182]. Commonly employed approaches include:

- **Excess bed shear stress concept** considers the difference between the bed shear stress acting on particles and the threshold shear stress for initiation of motion; e.g., formulae of Meyer-Peter and Müller [183], Fernandez Luque and van Beek [184], Paintal [185], Parker [186], and Cheng [187].
- **Energy balance concept** considers the amount of energy available in flow to transport sediments, which is typically defined as the stream power (per unit bed area, expressed as the product of average velocity and bed shear stress) or unit stream power (energy expenditure per unit weight of water, defined as the product of average velocity and bed slope) [188,189]; e.g., formulae of Bagnold [190–194] and Yang [195].
- **Probabilistic concept** based on the idea that the entrainment of individual sediment particles is stochastic, considering the randomness of particle geometry and the fluctuating nature of the turbulent flow field, which exerts a complex set of forces on sediments. The exchange of particles between the bed surface and bed layer and their movement are analyzed in terms of the probability that the applied forces on a grain surpass the resisting forces at a specific time and location; e.g., formulae of Einstein (empirical [196] and semi-theoretical [197]), Wang et al. [198], and Engelund and Fredsøe [199].

It should be noted that most of the bedload transport equations are only applicable for nearly horizontal flows or mild slopes. However, the downslope gravitational component should also be considered for steep slopes. The formulae for bedload transport over steep gradients can be found in Smart [200], Graf and Suszka [201], Suszka [202], Tsujimoto [203], Rickenmann [204], and Damgaard et al. [205], among others. Furthermore, the fractional transport rate of bedload, which is typical in natural streams with non-uniform sediment mixtures, has been investigated by some researchers following the pioneering work of Einstein [197], e.g., formulae of Parker et al. [167], Misri et al. [206], Samaga et al. [207], Bridge and Bennett [208], Hsu and Holly [209], Patel and Ranga Raju [210], and Wu et al. [168].

Suspended load transport modeling

With a further rise in excess bed shear stress, turbulence formation in the vicinity of the bed and its fluctuations cause finer particles to be lifted upwards from the bed and carried in suspension over a relatively long period [211]. Bagnold [190] described sediment suspension as the process where the submerged weight of particles is balanced by the upward diffusion of turbulent eddies.

According to Einstein [197], the suspended load transport rate q_s , expressed in volume per unit time and width, can be determined by integrating the product of flow velocity and local sediment concentration over the flow depth based on the advection–diffusion concept of sediment concentration. Other formulae to estimate q_s based on the diffusion approach can be found in the works of Lane and Kaliske [212], Guo and Wood [213], Bijker [214], and van Rijn [215].

The concentration gradient follows an exponential pattern, with the highest concentration (*reference concentration*) near the bed (*reference level*), which decreases with an increase in flow elevation. The vertical distribution of suspended sediment concentration can be approximated according to Rouse's equation [216] as well as similar distribution functions [215,217–221], considering the equilibrium sediment suspension by balancing entrainment flux due to upward turbulent diffusion and depositional flux (volumetric

settling rate per unit area) due to gravity. The reference level on top of the bed layer (boundary for supplying sediment to the suspended load) and the concentration at this level are essential parameters in quantifying the suspended load transport rate. Numerous researchers have proposed different criteria to determine the reference level, which can be proportional to the flow depth [222,223], particle size [197,199,224], bed roughness, or bedform height [214,215,225]. Accordingly, they have developed formulae for calculating the concentration at this level. However, the direct measurement of near-bed suspended load concentration is practically not feasible to verify the reliability of these formulae. Instead, it has to be extrapolated based on measurements taken in the upper flow layers using the vertical concentration distribution functions.

In addition to the mentioned diffusion concept for estimating the suspended load transport rate, there are also formulae based on the energy concept or stream power, e.g., Bagnold [191] and Wu et al. [168].

Bed-material load transport modeling

Bed-material load (sometimes called total load by neglecting the wash load) is the sum of the transported bedload and suspended load per unit time and width. Therefore, the bed-material load transport rate can be calculated indirectly by defining and summing the transport rate of bedload and suspended load, e.g., formulae of Einstein [197], Chang et al. [226], Bagnold [191], van Rijn [151,215], and Wu et al. [168]. The other method is the direct estimation of bed-material load without breaking it down into two separate components. For example, Laursen [227] established a formula considering size fractions in calculating the total concentration of bed-material load. Engelund and Hansen [228] used the stream power concept and the similarity principle to develop their total load transport equation. Ackers and White [229] used the stream power approach and introduced a mobility factor based on dimensional analysis in their formula. Yang [230,231] related the total load transport rate to the unit stream power. Karim [232] introduced a formula for non-uniform sediment mixtures, including particle hiding and exposure for fractional transport rate of bed-material load. Yang and Lim [233] and Yang

[234] developed an equation for the total load transport rate, including the wash load.

Selecting an appropriate sediment transport formula for a particular case may be challenging due to the extensive number of available equations, each with its certain range of applicability. These formulae have been developed based on different approaches and under specific conditions, such as sediment size, shape, sorting, flow conditions, and bed slope. Therefore, the optimal choice depends on a thorough understanding of the unique attributes of a specific case, including the sediment characteristics and hydraulic conditions.

2.4 Reservoir sedimentation

Reservoirs, as anthropogenic elements of river systems disturbing the watercourse continuity, are built for diverse purposes (e.g., water supply, hydropower production, and flood control). Reservoirs are susceptible to the progressive process of sedimentation owing to relatively low flow velocities, limited turbulence intensity, and restricted transport capacity of the sediment-laden water. Reservoir sedimentation is influenced by factors such as reservoir characteristics (size, slope, geometry), reservoir operation, watershed characteristics and its hydrological features, river regime and sediment inflow rate. The majority of bedload sediment and heavier particles of suspended load contribute to the formation of delta deposits at the head of the reservoir and cause an increase in the backwater profile in the upstream channel, whereas fine particles are carried into the reservoir, resulting in depositions over the whole reservoir. Fine sediment usually reaches the dam structure, also by density currents or stratified flows (Fig. 2.2). The accumulation of sediment leads to a reduction in reservoir storage capacity over time and is a significant threat to the long-term viability and functionality of reservoirs. Sedimentation not only limits the reservoir's useful lifespan but also alters the sediment balance in the riverine environment, introduces safety concerns, restricts the benefits provided by dams, and negatively impacts the up- and downstream river regions [235].

The effects resulting from reservoir sedimentation can be classified according to their location as [236–238]:

- Upstream region: delta formation and backwater effect, streambed aggradation, higher flood levels, impaired navigational clearance, affecting upstream water intakes, elevated groundwater levels, waterlogging riparian agricultural soil, and soil salinization
- Reservoir area: storage loss (e.g., affecting hydropower generation, water supply, flood control benefits, recreational and commercial navigation), and operational problems (e.g., clogging of intake structures and abrasion of hydromechanical equipment)
- Downstream part: channel incision below the dam, bed-material coarsening and bed armoring, destabilization of streambanks and accelerated bank erosion, lowering of groundwater levels, limited nutrient delivery to downstream ecosystems, and accelerated coastal erosion

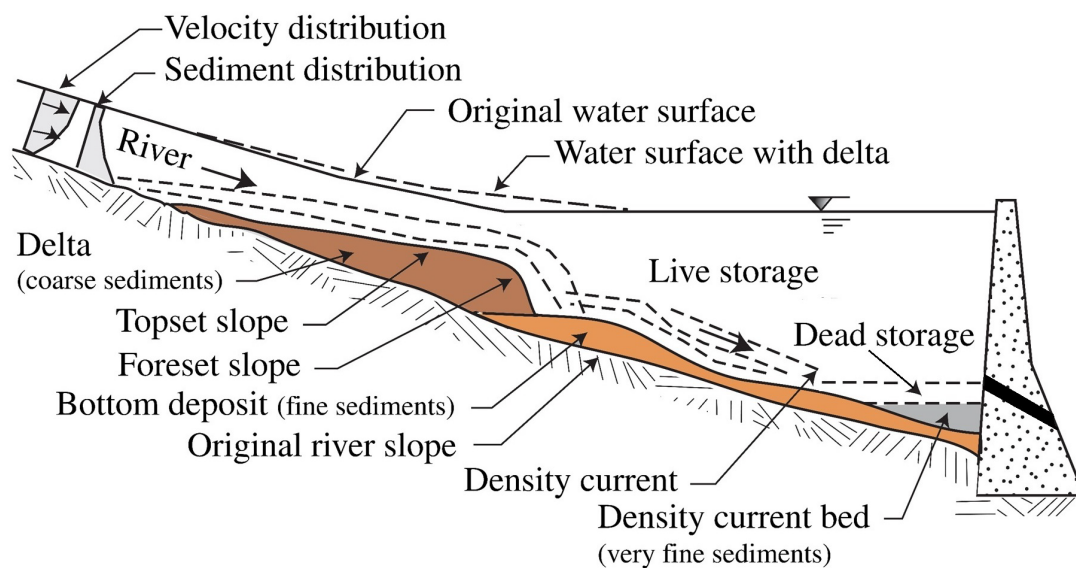


Fig. 2.2 Typical reservoir sedimentation pattern (modified after Julien [239])

According to the International Commission on Large Dams (ICOLD), as of 2020, there are currently around 58,700 registered large dams worldwide with a cumulative storage volume of 7,000–8,300 km³. With a growing population resulting in increased demands for water storage, food, and renewable energy, the necessity for new dams and storage reservoirs is continuously rising

[240,241]. As a result of this ongoing development, ecological and environmental consequences, such as increasing river fragmentation due to dam construction and further reservoir sedimentation, are anticipated. Although sedimentation rates are highly site-specific and are not uniform worldwide, since the 1987 World Bank report [242], it has been consistently highlighted in the literature that reservoir sedimentation reduces global storage capacity by 0.5–1 % per year [243–245]. According to Annandale [246] and Schleiss et al. [247], the annual average global loss of storage capacity due to sedimentation exceeds the capacity growth achieved through the construction of new reservoirs, which indicates that reservoirs are generally not sustainable. Therefore, urgent mitigation measures are necessary to ensure the reliable and efficient management of existing reservoirs in order to extend their useful lifespan.

Sediment management strategies aim to achieve equilibrium in the watershed-river–reservoir-dam system by manipulating its components to preserve storage capacity while minimizing socioeconomic and environmental costs. These strategies can be categorized into the following groups (Fig. 2.3) [235,244,248,249]:

- Measures to decrease the proportion of sediment yield that flows into reservoirs
- Measures to minimize the entry and deposition of sediment inside reservoirs
- Measures to recover the storage volume by sediment removal techniques
- Adaptive strategies to mitigate sedimentation impacts without adjusting the sediment balance

Significant long-term reduction in sediment yield can result from soil conservation measures (nonstructural measures), generally by promoting vegetative cover. However, the downstream reaction to land-use changes upstream may undergo a time lag of several decades. Structures for erosion control, such as check dams, contribute significantly by stabilizing eroding channels, but their storage capacity is typically limited compared to the sediment yield, and they require ongoing maintenance [249]. According to

Wang and Kondolf [250], in regions with high sediment yield, sustainable strategies for managing reservoir sedimentation should prioritize the passing of sediment downstream rather than trapping it upstream. It is due to the expenses associated with construction and maintaining upstream structures, along with their restricted sediment trapping capacity.

Routing strategies aim to minimize deposition by passing the sediment-laden flow around (off-stream reservoir or bypass tunnel/channel) or through the reservoir. An off-stream reservoir can be constructed outside the main channel (e.g., across a tributary) to divert the clear water into storage (by pumping or gravity) through an intake, while sediment-laden flow bypasses the reservoir. Furthermore, the muddy water can be diverted by a tunnel/channel around the instream reservoir to a location below the dam [237,251,252]. Sediment can pass through the reservoir by releasing turbidity currents or sluicing (lowering the water level during a flood event, allowing the flow to pass the reservoir at the same rate it enters).

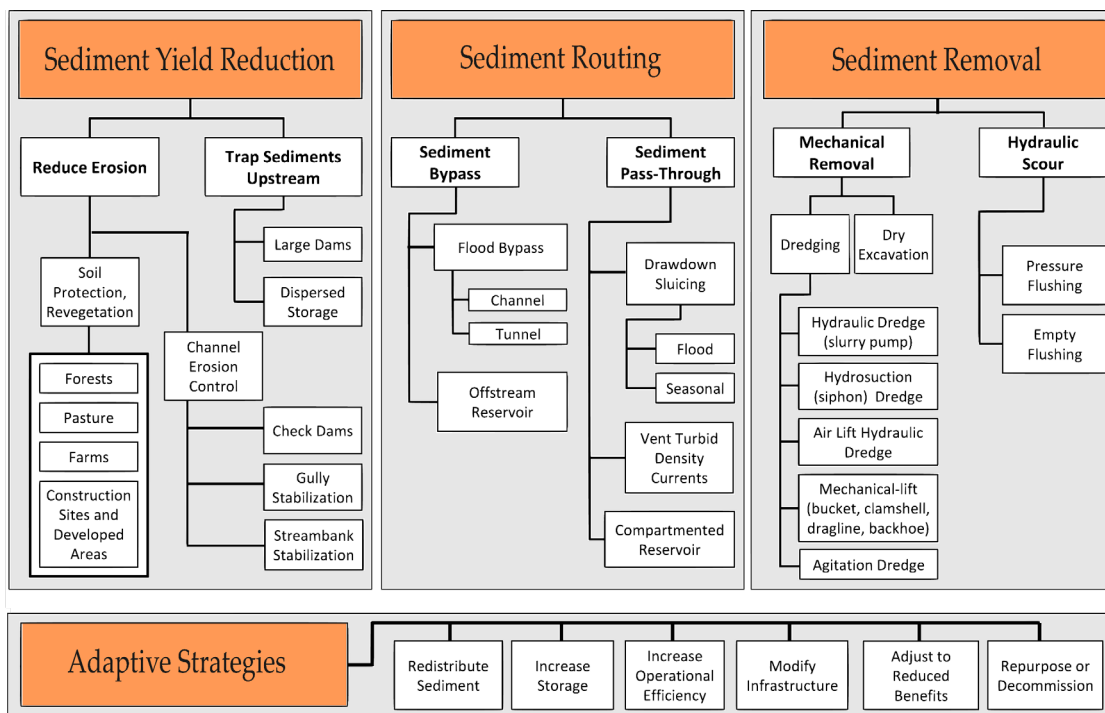


Fig. 2.3 Classification of strategies for reservoir sedimentation management (modified after Morris [249])

Among the sediment removal techniques (e.g., using hydraulic forces or mechanical equipment), reservoir flushing is a commonly used method to counteract sediment accumulation by eroding a portion of the deposited materials. This technique has been regarded as one of the most efficient methods for reservoir desiltation [235,253]. Increased velocities and flow-induced shear forces acting on deposits lead to the mobilization and transport of sediment, along with scouring of a flushing channel typically following the river thalweg when the water level is sufficiently lowered to reach the free-flow conditions (full drawdown or empty flushing). Moreover, pressure flushing (partial drawdown), which is not as efficient as empty flushing, occurs when low-level outlets are opened to discharge sediment while the water level is high. Subsequently, a scour cone forms in front of the outlets, and sediment removal is confined to the region immediately upstream of the outlets. The effectiveness of flushing is dependent upon several factors, such as reservoir geometry, flow discharge, sediment characteristics, and outlet size, among others. The large quantity of particles being flushed and the high suspended sediment concentration in the outflow may negatively impact the overall health of the downstream environment. Therefore, it is essential to evaluate the compatibility of sediment flushing activities with the conservation of the downstream ecosystem, considering the socioeconomic impacts [254–258], which requires careful monitoring.

To conclude, the management strategies applicable to each reservoir may differ based on several factors, such as hydrological and environmental considerations, technical requirements, as well as financial aspects and legal conditions. Certain strategies can be implemented simultaneously, while others can be applied in a sequential manner. An optimal method often involves an integration of proactive and adaptive strategies for long-term sustainable use [249]. For a detailed and comprehensive overview of different management strategies applied to reservoirs worldwide, see [235,237,244,253,259–263].

Chapter 3

Materials and methods

In this thesis, three case studies are examined. A fully three-dimensional CFD code is employed for calculating hydraulics and morphological changes. The models are automatically calibrated using various optimization algorithms. This chapter offers a concise overview of the methodology used, while detailed information for the three case studies is available in Appendices I, II, and III.

3.1 Numerical modeling

Computational hydro-morphodynamic models can be classified based on different aspects, e.g., dimensionality (section-averaged 1D, depth- or width-averaged 2D, and 3D), flow state (steady, quasi-steady, and unsteady), discretization methods for governing equations (e.g., finite volume, finite difference, and finite element methods), as well as sediment related aspects (equilibrium or non-equilibrium transport state, uniform or non-uniform size fraction, and sediment transport modes). The selection of a model depends upon the nature and complexity of the problem, the model's ability to accurately simulate the problem, the availability of data for model calibration and verification, as well as the overall time and budget assigned for the simulation [28,46]. The flow dynamics in natural streams exhibit three-

dimensional characteristics, particularly in areas such as meander bends or local expansions. Three-dimensional hydro-morphodynamic models typically employ the Reynolds-averaged form of the Navier–Stokes equations (momentum conservation) and the continuity equation (mass conservation) of fluid along with the sediment continuity equation, incorporating equations of varying complexity to address turbulence closure [264–267] as well as required equations to calculate free-flow surface, suspended load transport, bedload transport, and bed evolution. A comprehensive overview of related governing equations, turbulence models, and numerical solutions can be found in textbooks on fluid dynamics [46,268–275].

The numerical model SSIIM (Sediment Simulation In Intakes with Multiblock option) [276] is used for modeling hydraulics and morphological changes in all three case studies in this thesis. SSIIM is a freely available CFD code that has been successfully employed in numerous studies focused on hydraulics and sediment transport [277–292]. SSIIM solves the Reynolds-averaged Navier–Stokes (RANS) equations with the continuity equation on a three-dimensional unstructured and non-orthogonal adaptive grid. The adaptive grid refinement is based on the implemented wetting/drying algorithm, which relies on the alterations in the free water surface and bed levels. This algorithm computes the number of cells generated in the vertical direction after each time step based on the water depth. Consequently, the computational domain undergoes spatiotemporal changes and can be adapted for the subsequent time step. For spatial discretization, SSIIM uses the finite volume method, and an implicit scheme is employed for temporal discretization, allowing the use of larger time steps. Concerning the RANS equations, the convective term can be modeled using different schemes (e.g., power-law or second-order upwind scheme). The pressure term is addressed through the semi-implicit method for pressure-linked equations (SIMPLE). The Reynolds stress term is computed using Boussinesq approximation with the concept of eddy viscosity, and it involves the application of different turbulence models (e.g., standard or RNG $k-\epsilon$) for turbulence closure. The free water surface can be calculated based on several methods (e.g., computed pressure field or diffusive wave equations) [293]. Regarding the up- and downstream boundary conditions, SSIIM uses the Dirichlet boundary

condition and Neumann type zero gradient boundary condition for all variables, respectively. The movement of suspended sediment is modeled by solving the transient convection-diffusion equation using an equilibrium near-bed sediment concentration. Several bedload transport formulae (e.g., van Rijn or Meyer-Peter and Müllers) have also been implemented in SSIIM. The critical shear stress can be calculated according to the Shields curve, and the shear stress for the bed and side boundaries is computed according to the wall law.

3.2 Model calibration

Calibration is a multi-step, inverse problem aimed at reducing uncertainty by updating the parameter values of a model and comparing computational and measured data to achieve improved agreement within a reasonable tolerance. In this context, the model output deviates minimally from the actual data as specified in performance criteria. Since hydro-morphodynamic models involve a multitude of imprecise or unknown input parameters, in-depth calibration and validation are imperative for the reliable use of such models in making accurate predictions about hydraulics, sediment transport, and morphological processes, ensuring the model's trustworthiness. However, model calibration is a challenging task. According to Wang and Wu [294], calibrated values may sometimes fall outside the reasonable range (even to an order of magnitude), but they still yield satisfactory results when compared with the measured data. This happens because the model user employs a limited number of calibrated parameters to account for all simplifications of the model. Moreover, it can be argued that if a model is calibrated based on a specific aspect (e.g., morphological change), there is no guarantee that other simulated parameters (e.g., flow velocities and sediment transport rate) agree with their corresponding measurements [295]. Thus, calibrated models still encompass a potential degree of uncertainty and have shortcomings arising from model errors (approximations, simplifications, and assumptions) and data errors (the absence of error-free observations with sufficient spatial and temporal resolutions for calibration), thereby contributing to discrepancies [296]. Hence, despite the validity of calibrated parameters for a specific site during the time period when the data was collected, it cannot be assured that the calibrated values will remain valid for other periods at the same site or at

a different location (spatiotemporal dependency) [32]. The calibration process, which can be done in a manual trial-and-error or automatic manner, comprises two major stages [297,298]:

1. Parameter specification: where sensitive parameters, whose variations significantly influence the model's output, are identified. The proper selection of parameters through sensitivity analysis is of utmost importance since the adjustment of irrelevant or non-sensitive parameters may result in extra dimensionality and computing burden.

2. Parameter estimation: where optimal or quasi-optimal values for the specified parameters are determined in order to achieve the best alignment between the model's predictions and observed or measured data.

Hydro-morphodynamic model calibration is typically carried out through trial-and-error procedures, which, aside from being inefficient and intricate (highly time-consuming), is subjective and depends on the experience of modelers [299]. These challenges emphasize the necessity to automate the calibration procedure using optimization techniques. In the process of automatic calibration, parameters are adjusted automatically following a specified optimization algorithm and sequential assessments of goodness-of-fit (objective function) until reaching the termination criterion, enabling the explicit statement of confidence in model simulations [300]. Automatic calibration of hydro-morphodynamic numerical models is still in its initial stage compared to other fields, such as hydrologic models, which demand further investigations [301,302].

The model-independent nonlinear Parameter ESTimation and predictive analysis tool (PEST) [303], using the gradient-based Gauss–Marquardt–Levenberg (GML) local optimization algorithm, is employed for the calibration of the numerical models in all three case studies in this thesis. PEST iteratively alters uncertain parameters within a predetermined range to minimize the difference between calculated and measured values based on the residual sum of squares as the objective function. Employing the GML algorithm, which combines the gradient descent method and Gauss–Newton algorithm, PEST runs the model and linearizes the relationship between model outcomes and

input parameters through Taylor's expansion of the actual parameter set. The number of model runs in a single PEST iteration is equal to the number of calibration parameters. In each iteration, a Jacobian matrix, which consists of the partial derivatives of the model outputs, is calculated. This is then utilized to derive an upgrade vector for modifying the parameters in the subsequent iteration. This process continues until either the minimum of the objective function is reached or termination requirements are fulfilled.

Since there is a possibility for local optimization algorithms to be trapped in local minima points on the objective function surface, a series of global optimization algorithms are also employed to validate the results obtained by PEST, as follows:

- **Shuffled Complex Evolution (SCE-UA)** uses a combination of competitive evolution, local direct search of the downhill simplex approach, controlled random search, and complex shuffling. The optimization begins by picking a population of points dispersed randomly over the parameter space, which are then grouped into several complexes. Each complex evolves independently to search the domain in diverse directions, employing the downhill simplex algorithm. The population is rearranged at regular intervals, and candidate solutions are transferred to new groups to exchange information gathered from prior complexes throughout their evolution phase. The process of evolution and shuffling is iteratively performed until the convergence condition is met [304].
- **Covariance Matrix Adaptation Evolution Strategy (CMA-ES)** is a stochastic algorithm designed for the real-parameter optimization of nonlinear and nonconvex functions. It employs evolution strategies' general operators, including recombination, mutation, and selection. Every iteration begins by sampling a population of candidate solutions from a multivariate normal search distribution. Subsequently, solutions are assessed based on their performance metrics, and the parameters of the multivariate normal distribution are adjusted to direct the search towards the region with lower objective function values. The series of iterations persists until a termination condition is satisfied [305].

- **Particle Swarm Optimization (POS)** is a metaheuristic global optimization approach. This method involves initializing the search space by distributing particles, which serve as possible solutions, to create a swarm. Particles consist of position and velocity vectors, moving in random directions while maintaining records of the best positions they have individually discovered and the overall best position achieved by the entire swarm. The fitness of particles is evaluated based on an objective function. In each generation, the velocity vector is adjusted according to the previous best position of each particle and the best position of the entire swarm. Subsequently, the new position is calculated concerning the updated velocity [306].
- **Big Bang Big Crunch (BB–BC)** is inspired by a theory for the universe's evolution. The Big Bang phase involves the uniform generation of the initial population by dispersing random candidate solutions across the entire search space. Following this, the fitness value for each candidate solution is computed (representing the "mass" of each particle). In the subsequent Big Crunch phase, the randomly distributed population shrinks to a single point, referred to as the "center of mass". In the subsequent Big Bang, new individuals are primarily generated around the previously calculated center of mass following a normal distribution. The standard deviation of the normal distribution decreases as the optimization progresses. This phase is succeeded by a contraction based on calculating the new center of mass [307].

3.3 Case studies

180° curved channel

- Geometry: U-shaped channel with 1 m width and 4 m central radius including up- and downstream reaches of 11.5 m length attached to the bend, having a slope of 2 ‰
- Flow condition: unsteady flow with a base flow rate of 0.02 m³/s and a depth of 0.054 m, using a triangular-shaped hydrograph

- Sediment characteristics: 0.2 m of nonuniform sand on the bed with a median diameter of 1 mm, a geometric standard deviation of 2.5, and a density of 2,650 kg/m³, modeled by 8 size fractions
- Sediment transport formulae: Engelund-Hansen, van Rijn, and Wu
- Optimization algorithms: GML, SCE-UA, CMA-ES, PSO
- Calibration parameters: roughness height, active layer thickness, and volume fraction of compacted sediments in bed
- Data for calibration: measured bed elevations of 54 points along different longitudinal and cross-sections

Lozenge- and hexagon-shaped reservoirs

- Geometry: two shallow reservoirs having lozenge and hexagon shapes with maximum inner dimensions of 4.0 m in width and 6.0 m in length, having a flat bed
- Flow condition: constant flow discharge of 0.007 m³/s with a water depth of 0.2 m
- Sediment characteristics: suspended sediment inflow containing nonuniform walnut shells with a median diameter of 0.05 mm, a geometric standard deviation of 2.4, and a density of 1,500 kg/m³, modeled by 7 size fractions
- Sediment transport formula: van Rijn
- Optimization algorithms: GML, BB-BC
- Calibration parameters: roughness height and active layer thickness
- Data for calibration: measured bed elevations of 8,600 and 16,500 points along different longitudinal and cross-sections for the lozenge- and hexagon-shaped reservoirs, respectively

Bodendorf reservoir

- Geometry: 2.5 km long reservoir with an average width of 40 m (between 35 m and 120 m), an average slope of 3.8 ‰ (between 0.5 ‰ and 7 ‰), and a designed storage capacity of 900,000 m³
- Flow condition: 31 hours of drawdown flushing with a maximum discharge of 134 m³/s under free flow conditions

- Sediment characteristics: size range between 1 mm and 80 mm with different proportion distribution along the reservoir having a density of $2,550 \text{ kg/cm}^3$, modeled by 9 size fractions
- Sediment transport formulae: Meyer-Peter and Müller, van Rijn, and Wu
- Optimization algorithms: GML
- Calibration parameters: four empirical parameters in van Rijn's bedload transport formula, coefficient of Meyer-Peter and Müller's sediment transport formula, hiding-exposure correction factor, roughness height, active layer thickness, and volume fraction of compacted sediments in bed
- Data for calibration: measured bed elevations of 1,300 points in 10 cross-sections along the reservoir

Chapter 4

Summary of the scientific papers

This chapter briefly summarizes the scientific publications presented in Appendices I, II, and III. Each summary outlines the main findings of the respective study. Further details regarding the results for calibrated values and the statistical performance of the models can be found in the corresponding articles.

4.1 *Publication I: Comparison of local and global optimization methods for calibration of a 3D morphodynamic model of a curved channel*

The measured data obtained from a well-documented laboratory experiment conducted on a U-shaped channel is utilized to set up and calibrate the numerical model. This case study has been typically employed as a benchmark for hydro-morphodynamic numerical studies. In this paper, a local (GML) and three global optimization algorithms (SCE-UA, CMA-ES, and PSO) are coupled with the numerical model SSIIM for automatic calibration. The objective of this study is to investigate the applicability and efficiency of automatic calibration by comparing different algorithms in terms of model runs and the accuracy of their output.

Additionally, the most appropriate algorithm is used to calibrate further models using different discharge rates.

The automatic calibration in this study focuses on three input parameters: roughness height, active layer thickness, and sediment volume relative to water at the bed. All methods contribute to streamlining the calibration process by reducing the need for user intervention. Comparing the outcomes of the GML algorithm of the PEST software with the three global optimization algorithms reveals a notable concurrence in the calibrated parameter values. This highlights the capability of PEST to calibrate the model on a global scale (without being trapped in local minimum points) while using a local optimization technique. Furthermore, in terms of convergence speed, the GML algorithm stands out as considerably more efficient than the other methods, requiring fewer model runs, which offers a significant benefit in the calibration of hydro-morphodynamic models with long simulation times. Therefore, PEST is further used to calibrate a total of nine models using three distinct discharge rates and sediment transport formulae of van Rijn, Wu, and Engelund-Hansen. Models calibrated using Wu's formula demonstrate superior predictive capability in capturing the general characteristics of bed deformations, including regions of deposition, erosion, and their magnitudes. The van Rijn formula also yields reasonably acceptable results. However, models employing the Engelund-Hansen formula exhibit the highest disagreement with the observations.

The main scientific contribution of this paper lies in developing an efficient methodology for the automatic calibration of hydro-morphodynamic models.

4.2 *Publication II: Applying optimization methods for automatic calibration of 3D morphodynamic numerical models of shallow reservoirs: comparison between lozenge- and hexagon-shaped reservoirs*

This paper examines the performance of the 3D numerical model SSIIM in conjunction with the automatic calibration tool PEST to assess the morphological changes in two symmetric laboratory-scale shallow reservoirs with hexagonal and

lozenge geometries. Numerical modeling of symmetric expansions presents complex challenges, where the entering jet can randomly follow one side of the expanded area. This complexity introduces the possibility of multiple solutions for the Navier–Stokes equations. Moreover, the presence of secondary currents in recirculation zones and 3D stretching vortices necessitates using 3D models.

In this study, to validate PEST's ability to identify the global optimum point across the search space and avoid local minima, the models are also calibrated using the global optimization algorithm BB–BC. Following a sensitivity analysis, two parameters, roughness and active layer thickness, are chosen for calibration. Obtaining nearly identical calibrated parameter values from PEST and BB-BC confirms PEST's ability to identify the global minimum point. This shows the repeatability and robustness of the auto-calibration procedure using the GML algorithm of PEST to calibrate the models globally. Moreover, the number of model runs required for calibration in PEST is about an order of magnitude fewer than BB–BC, which reveals the efficiency of PEST and its potential for calibrating hydro-morphodynamic models. Regarding the hexagonal reservoir, characterized by a stable straight flow structure, sediment particles tend to settle primarily along the central longitudinal section. Nevertheless, the unstable fluctuating flow pattern within the lozenge-shaped reservoir results in sediment distribution along the sides of the reservoir. Comparisons between the calculated bed levels and the measured topography of the physical models at various time steps indicate that the calibrated numerical models can reasonably replicate similar patterns, considering the key features of both reservoirs, including the flow field, jet direction, recirculation zones, and bed level changes.

According to the literature, the hydro-morphodynamic numerical studies of symmetric expansions are typically limited to rectangular reservoirs with a 90° expansion angle. The primary scientific contribution of this paper involves the numerical modeling and calibration of lower expansion angles to investigate their effect on the flow field development and sedimentation patterns.

4.3 *Publication III*: Using automatic model calibration for 3D morphological simulations: a case study of the Bodendorf reservoir flushing

In this paper, the insights gained from automatic calibration using PEST software in the former two case studies are applied to calibrate a numerical model simulating a reservoir flushing event in a prototype scale. Due to the relatively longer simulation time compared to the previous two cases, global optimization algorithms are omitted from this investigation.

After conducting a sensitivity analysis, nine parameters are chosen for calibration (four empirical parameters in van Rijn's bedload transport formula, coefficient of Meyer-Peter and Müller's sediment transport formula, hiding-exposure correction factor, roughness, active layer thickness, and volume fraction of sediments in bed). The calibration process involves utilizing bed elevation data collected at ten cross-sections, comprising around 1,300 points along the reservoir. The formulae of Meyer-Peter and Müller (MPM), van Rijn, and Wu are used in simulations. During the optimization process, modifications are made to van Rijn and MPM formulae by adjusting their empirical parameters. Additionally, the parameter related to the hiding-exposure behavior of non-uniform sediments, as proposed by Wu, is altered. The findings of model calibration indicate that calibrated values are highly dependent on the initial model components, and an optimized parameter set may not be the best set if the model configuration changes. Therefore, employing optimized values resulting from calibrating a hydro-morphodynamic model and applying them to the same model with a different sediment transport formula, a practice often observed in manual calibration, may not always yield the optimal outcome. The models utilizing the van Rijn and Wu formulae demonstrate better performance compared to the model calculated using the MPM formula, as evidenced by lower error amounts and higher correlations. Both models using the formulae of van Rijn and Wu demonstrate similar performance levels, with no clear statistical evidence of one performing better. This is further supported by the Brier skill score, where both van Rijn and Wu models achieve nearly identical scores, indicating their "good" performance. In contrast, the model simulated by the MPM formula is

classified as having a "reasonable/fair" performance based on the evaluation criteria of the Brier skill score.

The simulation of hydro-morphodynamic models in a prototype scale is inherently time-consuming. Their calibration is further complicated and demands considerable time investment. Consequently, the limited studies on the automatic calibration of such models have focused on using representative metamodels (surrogate models) for calibration. The contribution of this paper lies in demonstrating the efficient automatic calibration of an actual 3D hydro-morphodynamic model for simulating a reservoir flushing event in a prototype scale.

Chapter 5

Conclusions and outlook

Hydro-morphodynamic numerical models incorporate numerous imprecise or unknown input parameters, leading to substantial uncertainty in their outputs. Hence, it is imperative to calibrate these models using available measured data and assess their uncertainty before applying them for forecasting, decision-making, and management purposes. Most studies on numerical modeling of fluvial sediment transport, reservoir sedimentation, and reservoir flushing have traditionally focused on individual parameters during calibration, employing manual trial-and-error and one-at-a-time approaches based on the user's understanding of the model structure and environmental system properties. This means each sensitive parameter is calibrated independently while holding others constant. However, it is often the case that the overall optimal fit does not arise from the individual calibration of each parameter, which means there could be significant conflicts between evaluated parameters, and manual calibration may not capture these trade-offs. Hence, when dealing with several uncertain parameters, many potential combinations make manual calibration more complex, time-consuming, and costly. Moreover, due to the subjective nature of manual model calibration, there is no assurance that the optimal parameter

combination can be attained. Therefore, applying optimization techniques to the model fitting procedure offers a more objective and convenient alternative. In order to assess the performance, efficiency, and reliability of optimization techniques, three case studies are modeled and automatically calibrated against measured data in this thesis. In the first and second case studies, the performance of a gradient-based local optimization method (GML algorithm of PEST software) is compared with several global optimization techniques. Since the calibrated values obtained from all methods are identical in each case, it can be concluded that the GML algorithm is able to calibrate the models globally without getting stuck in the local minimum points of the objective function surface. In terms of efficiency, the GML algorithm requires significantly fewer model runs than other algorithms, making it superior without sacrificing reliability. The overall conclusion of this study emphasizes the efficacy of employing appropriate optimization algorithms for calibrating hydro-morphodynamic models, a practice not commonly adopted by researchers in this domain. Such techniques can substantially reduce calibration time, minimize user intervention and subjectivity, enable uncertainty quantification, and concurrently enhance the precision of the calibration process.

Nevertheless, it is essential to note that since GML is a gradient-based algorithm, it starts the optimization procedure from a single point on the objective function surface towards the nearest optimum point, and hence, there is a possibility of missing the global optimum. Therefore, to confirm the ability of the GML algorithm to find the global optimum point across the search space and avoid local minima, it is beneficial to reassess the calibration either by using different initial values within the parameter space or by employing global optimization algorithms. However, this reassessment may only be reasonable for computationally inexpensive models. Regarding large-scale models with extended simulation times, such as long-term reservoir sedimentation modeling, an alternative approach could involve surrogate modeling (metamodels). This method facilitates the utilization of global optimization algorithms or Bayesian calibration. Nonetheless, metamodels serve as approximations of full-complexity numerical models and can only be

utilized to expedite the calibration procedure if a sufficient number of model runs (training iterations) are conducted to construct the metamodel.

Moreover, enhancing the validity and reliability of automatic calibration of hydro-morphodynamic models could involve employing multi-objective optimization approaches. These methods consider additional aspects of the model (e.g., using velocities in addition to the bed levels for calibration), moving beyond a single value for uncertain parameters. Instead, they identify a set of equally optimal and non-dominated solutions.

References

1. Grill, G.; Lehner, B.; Thieme, M.; Geenen, B.; Tickner, D.; Antonelli, F.; Babu, S.; Borrelli, P.; Cheng, L.; Crochetiere, H.; et al. Mapping the world's free-flowing rivers. *Nature* **2019**, *569*, 215–221, doi:10.1038/s41586-019-1111-9.
2. Nilsson, C.; Berggren, K. Alterations of Riparian Ecosystems Caused by River Regulation: Dam operations have caused global-scale ecological changes in riparian ecosystems. How to protect river environments and human needs of rivers remains one of the most important questions of our time. *BioScience* **2000**, *50*, 783–792, doi:10.1641/0006-3568(2000)050[0783:AORECB]2.0.CO;2.
3. Syvitski, J.P.M.; Kettner, A.J.; Overeem, I.; Hutton, E.W.H.; Hannon, M.T.; Brakenridge, G.R.; Day, J.; Vörösmarty, C.; Saito, Y.; Giosan, L.; et al. Sinking deltas due to human activities. *Nature Geoscience* **2009**, *2*, 681–686, doi:10.1038/ngeo629.
4. Vörösmarty, C.J.; McIntyre, P.B.; Gessner, M.O.; Dudgeon, D.; Prusevich, A.; Green, P.; Glidden, S.; Bunn, S.E.; Sullivan, C.A.; Liermann, C.R.; et al. Global threats to human water security and river biodiversity. *Nature* **2010**, *467*, 555–561, doi:10.1038/nature09440.
5. Garde, R.J. *River Morphology*; New Age International Ltd: New Delhi, 2006; ISBN 978-81-224-1864-4.
6. Brown, L.R. The global loss of topsoil. *Journal of Soil and Water Conservation* **1984**, *39*, 162–165.
7. Beusen, A.H.W.; Dekkers, A.L.M.; Bouwman, A.F.; Ludwig, W.; Harrison, J. Estimation of global river transport of sediments and associated particulate C, N, and P. *Global Biogeochemical Cycles* **2005**, *19*, doi:10.1029/2005GB002453.
8. Thorslund, J.; Jarsjö, J.; Chalov, S.R.; Belozerova, E.V. Gold mining impact on riverine heavy metal transport in a sparsely monitored region: the upper Lake Baikal Basin case. *Journal of Environmental Monitoring* **2012**, *14*, 2780–2792, doi:10.1039/C2EM30643C.
9. Chalov, S.; Jarsjö, J.; Kasimov, N.S.; Romanchenko, A.O.; Pietroń, J.; Thorslund, J.; Promakhova, E.V. Spatio-temporal variation of sediment transport in the Selenga River Basin, Mongolia and Russia. *Environmental Earth Sciences* **2015**, *73*, 663–680, doi:10.1007/s12665-014-3106-z.
10. Panagos, P.; Borrelli, P.; Meusburger, K.; Yu, B.; Klik, A.; Jae Lim, K.; Yang, J.E.; Ni, J.; Miao, C.; Chattopadhyay, N.; et al. Global rainfall erosivity assessment based on high-temporal resolution rainfall records. *Scientific Reports* **2017**, *7*, 4175, doi:10.1038/s41598-017-04282-8.

11. Murphy, J.C. Changing suspended sediment in United States rivers and streams: linking sediment trends to changes in land use/cover, hydrology and climate. *Hydrology and Earth System Sciences* **2020**, *24*, 991–1010, doi:10.5194/hess-24-991-2020.
12. Best, J. Anthropogenic stresses on the world's big rivers. *Nature Geoscience* **2019**, *12*, 7–21, doi:10.1038/s41561-018-0262-x.
13. Fagundes, H.O.; Fan, F.M.; Paiva, R.C.D.; Siqueira, V.A.; Buarque, D.C.; Kornowski, L.W.; Laipelt, L.; Collischonn, W. Sediment Flows in South America Supported by Daily Hydrologic-Hydrodynamic Modeling. *Water Resources Research* **2021**, *57*, doi:10.1029/2020WR027884.
14. Martin, J.M.; Meybeck, M. Elemental mass-balance of material carried by major world rivers. *Marine Chemistry* **1979**, *7*, 173–206, doi:10.1016/0304-4203(79)90039-2.
15. Vitousek, P.M.; Mooney, H.A.; Lubchenco, J.; Melillo, J.M. Human Domination of Earth's Ecosystems. *Science* **1997**, *277*, 494–499, doi:10.1126/science.277.5325.494.
16. Lal, R. Soil erosion and the global carbon budget. *Environment International* **2003**, *29*, 437–450, doi:10.1016/S0160-4120(02)00192-7.
17. Walling, D.E.; Fang, D. Recent trends in the suspended sediment loads of the world's rivers. *Global and Planetary Change* **2003**, *39*, 111–126, doi:10.1016/S0921-8181(03)00020-1.
18. Stone, P.; Shanahan, J. *Sediment matters A practical guide to sediment and its impacts in UK rivers*; Environment Agency, Bristol, 2011.
19. Mouri, G.; Golosov, V.; Chalov, S.; Takizawa, S.; Oguma, K.; Yoshimura, K.; Shiiba, M.; Hori, T.; Oki, T. Assessment of potential suspended sediment yield in Japan in the 21st century with reference to the general circulation model climate change scenarios. *Global and Planetary Change* **2013**, *102*, 1–9, doi:10.1016/j.gloplacha.2013.01.002.
20. Galy, V.; Peucker-Ehrenbrink, B.; Eglinton, T. Global carbon export from the terrestrial biosphere controlled by erosion. *Nature* **2015**, *521*, 204–207, doi:10.1038/nature14400.
21. Tan, Z.; Leung, L.R.; Li, H.; Tesfa, T.; Vanmaercke, M.; Poesen, J.; Zhang, X.; Lu, H.; Hartmann, J. A Global Data Analysis for Representing Sediment and Particulate Organic Carbon Yield in Earth System Models. *Water Resources Research* **2017**, *53*, 10674–10700, doi:10.1002/2017WR020806.
22. Hajigholizadeh, M.; Melesse, A.M.; Fuentes, H.R. Erosion and Sediment Transport Modelling in Shallow Waters: A Review on Approaches, Models and Applications. *International Journal of Environmental Research and Public Health* **2018**, *15*, 518, doi:10.3390/ijerph15030518.
23. Hauer, C.; Leitner, P.; Unfer, G.; Pulg, U.; Habersack, H.; Graf, W. The Role of Sediment and Sediment Dynamics in the Aquatic Environment. In *Riverine Ecosystem Management: Science for Governing Towards a Sustainable Future*; Schmutz,

-
- S., Sendzimir, J., Eds.; Aquatic Ecology Series; Springer International Publishing: Cham, 2018; pp. 151–169 ISBN 978-3-319-73250-3.
24. Sartori, M.; Philippidis, G.; Ferrari, E.; Borrelli, P.; Lugato, E.; Montanarella, L.; Panagos, P. A linkage between the biophysical and the economic: Assessing the global market impacts of soil erosion. *Land Use Policy* **2019**, *86*, 299–312, doi:10.1016/j.landusepol.2019.05.014.
25. Andualem, T.G.; Hewa, G.A.; Myers, B.R.; Peters, S.; Boland, J. Erosion and Sediment Transport Modeling: A Systematic Review. *Land* **2023**, *12*, 1396, doi:10.3390/land12071396.
26. Debie, E.; Awoke, Z. Assessment of the effects of land use/cover changes on soil loss and sediment export in the Tul Watershed, Northwest Ethiopia using the RUSLE and InVEST models. *International Journal of River Basin Management* **2023**, 1–16, doi:10.1080/15715124.2023.2187399.
27. Apitz, S.E. Conceptualizing the role of sediment in sustaining ecosystem services: Sediment-ecosystem regional assessment (SEcoRA). *Science of The Total Environment* **2012**, *415*, 9–30, doi:10.1016/j.scitotenv.2011.05.060.
28. Papanicolaou, A.N.; Elhakeem, M.; Krallis, G.; Prakash, S.; Edinger, J. Sediment Transport Modeling Review—Current and Future Developments. *Journal of Hydraulic Engineering* **2008**, *134*, 1–14, doi:10.1061/(ASCE)0733-9429(2008)134:1(1).
29. James, S.C.; Jones, C.A.; Grace, M.D.; Roberts, J.D. Advances in sediment transport modelling. *Journal of Hydraulic Research* **2010**, *48*, 754–763, doi:10.1080/00221686.2010.515653.
30. Scholten, H.; van Waveren, R.H.; Groot, S.; van Geer, F.C.; Wösten, J.H.M.; Koezee, R.D.; Noort, J.J. Good modelling practice in water management. In Proceedings of the 4th International Conference on Hydroinformatics; Cedar Rapids, IA, USA, 2000.
31. Cunge, J.A. Of data and models. *Journal of Hydroinformatics* **2003**, *5*, 75–98, doi:10.2166/hydro.2003.0007.
32. Refsgaard, J.C.; Henriksen, H.J. Modelling guidelines—terminology and guiding principles. *Advances in Water Resources* **2004**, *27*, 71–82, doi:10.1016/j.advwatres.2003.08.006.
33. Vidal, J.-P.; Moisan, S.; Faure, J.-B.; Dartus, D. Towards a reasoned 1D river model calibration. *Journal of Hydroinformatics* **2005**, *7*, 91–104, doi:10.2166/hydro.2005.0009.
34. Thomann, R.V. The Future “Golden Age” of Predictive Models for Surface Water Quality and Ecosystem Management. *Journal of Environmental Engineering* **1998**, *124*, 94–103, doi:10.1061/(ASCE)0733-9372(1998)124:2(94).
35. Riedmaier, S.; Danquah, B.; Schick, B.; Diermeyer, F. Unified Framework and Survey for Model Verification, Validation and Uncertainty Quantification. *Archives of Computational Methods in Engineering* **2021**, *28*, 2655–2688, doi:10.1007/s11831-020-09473-7.

36. Silberstein, R.P. Hydrological models are so good, do we still need data? *Environmental Modelling & Software* **2006**, *21*, 1340–1352, doi:10.1016/j.envsoft.2005.04.019.
37. Trucano, T.G.; Swiler, L.P.; Igusa, T.; Oberkampf, W.L.; Pilch, M. Calibration, validation, and sensitivity analysis: What's what. *Reliability Engineering & System Safety* **2006**, *91*, 1331–1357, doi:10.1016/j.ress.2005.11.031.
38. Ruark, M.D.; Niemann, J.D.; Greimann, B.P.; Arabi, M. Method for Assessing Impacts of Parameter Uncertainty in Sediment Transport Modeling Applications. *Journal of Hydraulic Engineering* **2011**, *137*, 623–636, doi:10.1061/(ASCE)HY.1943-7900.0000343.
39. Oberkampf, W.L.; Trucano, T.G.; Hirsch, C. Verification, validation, and predictive capability in computational engineering and physics. *Applied Mechanics Reviews* **2004**, *57*, 345–384, doi:10.1115/1.1767847.
40. Babuska, I.; Oden, J.T. Verification and validation in computational engineering and science: basic concepts. *Computer Methods in Applied Mechanics and Engineering* **2004**, *193*, 4057–4066, doi:10.1016/j.cma.2004.03.002.
41. Rebba, R.; Mahadevan, S.; Huang, S. Validation and error estimation of computational models. *Reliability Engineering & System Safety* **2006**, *91*, 1390–1397, doi:10.1016/j.ress.2005.11.035.
42. Mehta, U.B. Some Aspects of Uncertainty in Computational Fluid Dynamics Results. *Journal of Fluids Engineering* **1991**, *113*, 538–543, doi:10.1115/1.2926512.
43. Oberkampf, W.L.; Blottner, F.G. Issues in Computational Fluid Dynamics Code Verification and Validation. *AIAA Journal* **1998**, *36*, 687–695, doi:10.2514/2.456.
44. Hornung, U. Mathematical aspects of inverse problems, model calibration, and parameter identification. *Science of The Total Environment* **1996**, *183*, 17–23, doi:10.1016/0048-9697(95)04970-3.
45. Pace, D.K. Modeling and Simulation Verification and Validation Challenges. *Johns Hopkins APL Technical Digest (Applied Physics Laboratory)* **2004**, *25*, 163–172.
46. Wu, W. *Computational River Dynamics*; Taylor & Francis Group, London, 2007.
47. Babuška, I.; Nobile, F.; Tempone, R. Reliability of computational science. *Numerical Methods for Partial Differential Equations* **2007**, *23*, 753–784, doi:10.1002/num.20263.
48. Oberkampf, W.L.; Trucano, T.G. Verification and validation benchmarks. *Nuclear Engineering and Design* **2008**, *238*, 716–743, doi:10.1016/j.nucengdes.2007.02.032.
49. Oberkampf, W.L.; Roy, C.J. *Verification and Validation in Scientific Computing*; Cambridge University Press, 2010; ISBN 978-1-139-49176-1.
50. Roy, C.J.; Oberkampf, W.L. A comprehensive framework for verification, validation, and uncertainty quantification in scientific computing. *Computer*

-
- Methods in Applied Mechanics and Engineering* **2011**, *200*, 2131–2144, doi:10.1016/j.cma.2011.03.016.
51. Sankararaman, S.; Mahadevan, S. Integration of model verification, validation, and calibration for uncertainty quantification in engineering systems. *Reliability Engineering & System Safety* **2015**, *138*, 194–209, doi:10.1016/j.res.2015.01.023.
52. Oden, J.; Moser, R.; Ghattas, O. Computer Predictions with Quantified Uncertainty, Part I. *SIAM News* **2010**, *43*, 1–3.
53. Sargent, R.G. Verification and validation of simulation models. *Journal of Simulation* **2013**, *7*, 12–24, doi:10.1057/jos.2012.20.
54. Geffray, C.; Gerschenfeld, A.; Kudinov, P.; Mickus, I.; Jeltsov, M.; Kööp, K.; Grishchenko, D.; Pointer, D. Verification and Validation and Uncertainty Quantification. In *Thermal Hydraulics Aspects of Liquid Metal Cooled Nuclear Reactors*; Roelofs, F., Ed.; Woodhead Publishing: Cambridge, UK, 2019; pp. 383–405.
55. McIntyre, N.; Wheeler, H.; Lees, M. Estimation and propagation of parametric uncertainty in environmental models. *Journal of Hydroinformatics* **2002**, *4*, 177–198, doi:10.2166/hydro.2002.0018.
56. Uniyal, B.; Jha, M.K.; Verma, A.K. Parameter identification and uncertainty analysis for simulating streamflow in a river basin of Eastern India. *Hydrological Processes* **2015**, *29*, 3744–3766, doi:10.1002/hyp.10446.
57. Radwan, M.; Willems, P.; Berlamont, J. Sensitivity and uncertainty analysis for river quality modelling. *Journal of Hydroinformatics* **2004**, *6*, 83–99, doi:10.2166/hydro.2004.0008.
58. Pathak, C.S.; Teegavarapu, R.S.V.; Olson, C.; Singh, A.; Lal, A.M.W.; Polatel, C.; Zahraiefard, V.; Senarath, S.U.S. Uncertainty Analyses in Hydrologic/Hydraulic Modeling: Challenges and Proposed Resolutions. *Journal of Hydrologic Engineering* **2015**, *20*, doi:10.1061/(ASCE)HE.1943-5584.0001231.
59. Oden, J.T.; Babuška, I.; Faghihi, D. Predictive Computational Science: Computer Predictions in the Presence of Uncertainty. In *Encyclopedia of Computational Mechanics Second Edition*; John Wiley & Sons, Ltd, 2017; pp. 1–26 ISBN 978-1-119-17681-7.
60. Refsgaard, J.C.; van der Sluijs, J.P.; Brown, J.; van der Keur, P. A framework for dealing with uncertainty due to model structure error. *Advances in Water Resources* **2006**, *29*, 1586–1597, doi:10.1016/j.advwatres.2005.11.013.
61. Mullins, J.; Mahadevan, S. Bayesian Uncertainty Integration for Model Calibration, Validation, and Prediction. *Journal of Verification, Validation and Uncertainty Quantification* **2016**, *1*, doi:10.1115/1.4032371.
62. Abbott, M.B.; Havn, K.; Lindberg, S. The fourth generation of numerical modelling in hydraulics. *Journal of Hydraulic Research* **1991**, *29*, 581–600, doi:10.1080/00221689109498978.

63. Abbott, M.B.; Babovic, V.M.; Cunge, J.A. Towards the hydraulics of the hydroinformatics era. *Journal of Hydraulic Research* **2001**, *39*, 339–349, doi:10.1080/00221680109499839.
64. Sabatine, S.M.; Niemann, J.D.; Greimann, B.P. Evaluation of Parameter and Model Uncertainty in Simple Applications of a 1D Sediment Transport Model. *Journal of Hydraulic Engineering* **2015**, *141*, doi:10.1061/(ASCE)HY.1943-7900.0000992.
65. Vidal, J.-P.; Moisan, S.; Faure, J.-B.; Dartus, D. River model calibration, from guidelines to operational support tools. *Environmental Modelling & Software* **2007**, *22*, 1628–1640, doi:10.1016/j.envsoft.2006.12.003.
66. Acuña, G.J.; Ávila, H.; Canales, F.A. River Model Calibration Based on Design of Experiments Theory. A Case Study: Meta River, Colombia. *Water* **2019**, *11*, 1382, doi:10.3390/w11071382.
67. Kennedy, M.C.; O'Hagan, A. Bayesian calibration of computer models. *Journal of the Royal Statistical Society Series B: Statistical Methodology* **2001**, *63*, 425–464, doi:10.1111/1467-9868.00294.
68. Snowling, S.D.; Kramer, J.R. Evaluating modelling uncertainty for model selection. *Ecological Modelling* **2001**, *138*, 17–30, doi:10.1016/S0304-3800(00)00390-2.
69. Murray, A.B. Reducing model complexity for explanation and prediction. *Geomorphology* **2007**, *90*, 178–191, doi:10.1016/j.geomorph.2006.10.020.
70. Jin, X.; Xu, C.-Y.; Zhang, Q.; Singh, V.P. Parameter and modeling uncertainty simulated by GLUE and a formal Bayesian method for a conceptual hydrological model. *Journal of Hydrology* **2010**, *383*, 147–155, doi:10.1016/j.jhydrol.2009.12.028.
71. Villaret, C.; Hervouet, J.-M.; Kopmann, R.; Merkel, U.; Davies, A.G. Morphodynamic modeling using the Telemac finite-element system. *Computers & Geosciences* **2013**, *53*, 105–113, doi:10.1016/j.cageo.2011.10.004.
72. Xue, C.; Chen, B.; Wu, H. Parameter Uncertainty Analysis of Surface Flow and Sediment Yield in the Huolin Basin, China. *Journal of Hydrologic Engineering* **2014**, *19*, 1224–1236, doi:10.1061/(ASCE)HE.1943-5584.0000909.
73. Li, Y.; Tang, C.; Zhu, J.; Pan, B.; Anim, D.O.; Ji, Y.; Yu, Z.; Acharya, K. Parametric uncertainty and sensitivity analysis of hydrodynamic processes for a large shallow freshwater lake. *Hydrological Sciences Journal* **2015**, *60*, 1078–1095, doi:10.1080/02626667.2014.948444.
74. Wu, D.; Lu, Z.; Wang, Y.; Cheng, L. Model validation and calibration based on component functions of model output. *Reliability Engineering & System Safety* **2015**, *140*, 59–70, doi:10.1016/j.ress.2015.03.024.
75. Vrugt, J.A.; Ter Braak, C.J.F.; Clark, M.P.; Hyman, J.M.; Robinson, B.A. Treatment of input uncertainty in hydrologic modeling: Doing hydrology backward with Markov chain Monte Carlo simulation. *Water Resources Research* **2008**, *44*, doi:10.1029/2007WR006720.

-
76. Her, Y.; Chaubey, I. Impact of the numbers of observations and calibration parameters on equifinality, model performance, and output and parameter uncertainty. *Hydrological Processes* **2015**, *29*, 4220–4237, doi:10.1002/hyp.10487.
77. Reisenbüchler, M.; Bui, M.D.; Skublics, D.; Rutschmann, P. Enhancement of a numerical model system for reliably predicting morphological development in the Saalach River. *International Journal of River Basin Management* **2020**, *18*, 335–347, doi:10.1080/15715124.2019.1628034.
78. Johnson, P.A. Uncertainty of Hydraulic Parameters. *Journal of Hydraulic Engineering* **1996**, *122*, 112–114, doi:10.1061/(ASCE)0733-9429(1996)122:2(112).
79. Beckers, F.; Noack, M.; Wieprecht, S. Uncertainty analysis of a 2D sediment transport model: an example of the Lower River Salzach. *Journal of Soils and Sediments* **2018**, *18*, 3133–3144, doi:10.1007/s11368-017-1816-z.
80. Cheng, Y.; Li, Y.; Wang, Y.; Tang, C.; Shi, Y.; Sarpong, L.; Li, R.; Acharya, K.; Li, J. Uncertainty and sensitivity analysis of spatial distributed roughness to a hydrodynamic water quality model: a case study on Lake Taihu, China. *Environmental Science and Pollution Research* **2022**, *29*, 13688–13699, doi:10.1007/s11356-021-16623-2.
81. Oreskes, N.; Shrader-Frechette, K.; Belitz, K. Verification, Validation, and Confirmation of Numerical Models in the Earth Sciences. *Science* **1994**, *263*, 641–646, doi:10.1126/science.263.5147.641.
82. Kleijnen, J.P.C. Verification and validation of simulation models. *European Journal of Operational Research* **1995**, *82*, 145–162, doi:10.1016/0377-2217(94)00016-6.
83. Oberkampf, W.L.; Trucano, T.G. Verification and validation in computational fluid dynamics. *Progress in Aerospace Sciences* **2002**, *38*, 209–272, doi: 10.1016/S0376-0421(02)00005-2.
84. Chau, K.W. Selection and calibration of numerical modeling in flow and water quality. *Environmental Modeling & Assessment* **2005**, *9*, 169–178, doi:10.1007/s10666-005-3797-3.
85. Moore, C.; Doherty, J. Role of the calibration process in reducing model predictive error. *Water Resources Research* **2005**, *41*, doi:10.1029/2004WR003501.
86. Gupta, V.K.; Sorooshian, S. The Automatic Calibration of Conceptual Catchment Models Using Derivative-Based Optimization Algorithms. *Water Resources Research* **1985**, *21*, 473–485, doi:10.1029/WR021i004p00473.
87. Beven, K.; Binley, A. The future of distributed models: Model calibration and uncertainty prediction. *Hydrological Processes* **1992**, *6*, 279–298, doi:10.1002/hyp.3360060305.
88. Yapo, P.O.; Gupta, H.V.; Sorooshian, S. Multi-objective global optimization for hydrologic models. *Journal of Hydrology* **1998**, *204*, 83–97, doi:10.1016/S0022-1694(97)00107-8.

89. Gupta, H.V.; Sorooshian, S.; Yapo, P.O. Toward improved calibration of hydrologic models: Multiple and noncommensurable measures of information. *Water Resources Research* **1998**, *34*, 751–763, doi:10.1029/97WR03495.
90. Gupta, H.V.; Sorooshian, S.; Yapo, P.O. Status of Automatic Calibration for Hydrologic Models: Comparison with Multilevel Expert Calibration. *Journal of Hydrologic Engineering* **1999**, *4*, 135–143, doi:10.1061/(ASCE)1084-0699(1999)4:2(135).
91. Boyle, D.P.; Gupta, H.V.; Sorooshian, S. Toward improved calibration of hydrologic models: Combining the strengths of manual and automatic methods. *Water Resources Research* **2000**, *36*, 3663–3674, doi:10.1029/2000WR900207.
92. Madsen, H. Parameter estimation in distributed hydrological catchment modelling using automatic calibration with multiple objectives. *Advances in Water Resources* **2003**, *26*, 205–216, doi:10.1016/S0309-1708(02)00092-1.
93. Calvello, M.; Finno, R.J. Selecting parameters to optimize in model calibration by inverse analysis. *Computers and Geotechnics* **2004**, *31*, 410–424, doi:10.1016/j.compgeo.2004.03.004.
94. Kim, S.M.; Benham, B.L.; Brannan, K.M.; Zeckoski, R.W.; Doherty, J. Comparison of hydrologic calibration of HSPF using automatic and manual methods. *Water Resources Research* **2007**, *43*, doi:10.1029/2006WR004883.
95. Gamerith, V.; Gruber, G.; Muschalla, D. Single- and Multievent Optimization in Combined Sewer Flow and Water Quality Model Calibration. *Journal of Environmental Engineering* **2011**, *137*, 551–558, doi:10.1061/(ASCE)EE.1943-7870.0000356.
96. Chlumsky, R.; Mai, J.; Craig, J.R.; Tolson, B.A. Simultaneous Calibration of Hydrologic Model Structure and Parameters Using a Blended Model. *Water Resources Research* **2021**, *57*, doi:10.1029/2020WR029229.
97. Abbaspour, K.C.; Johnson, C.A.; van Genuchten, M.Th. Estimating Uncertain Flow and Transport Parameters Using a Sequential Uncertainty Fitting Procedure. *Vadose Zone Journal* **2004**, *3*, 1340–1352, doi:10.2136/vzj2004.1340.
98. Tolson, B.A.; Shoemaker, C.A. Dynamically dimensioned search algorithm for computationally efficient watershed model calibration. *Water Resources Research* **2007**, *43*, doi:10.1029/2005WR004723.
99. Moradkhani, H.; Sorooshian, S. General Review of Rainfall-Runoff Modeling: Model Calibration, Data Assimilation, and Uncertainty Analysis. In *Hydrological Modelling and the Water Cycle*; Sorooshian, S., Hsu, K.-L., Coppola, E., Tomassetti, B., Verdecchia, M., Visconti, G., Eds.; Springer: Berlin/Heidelberg, Germany, 2008; Vol. 63, pp. 1–24 ISBN 978-3-540-77842-4.
100. Wasantha Lal, A.M. Calibration of Riverbed Roughness. *Journal of Hydraulic Engineering* **1995**, *121*, 664–671, doi:10.1061/(ASCE)0733-9429(1995)121:9(664).

-
101. Khatibi, R.H.; Williams, J.J.R.; Wormleaton, P.R. Identification Problem of Open-Channel Friction Parameters. *Journal of Hydraulic Engineering* **1997**, *123*, 1078–1088, doi:10.1061/(ASCE)0733-9429(1997)123:12(1078).
 102. Dung, N.V.; Merz, B.; Bárdossy, A.; Thang, T.D.; Apel, H. Multi-objective automatic calibration of hydrodynamic models utilizing inundation maps and gauge data. *Hydrology and Earth System Sciences* **2011**, *15*, 1339–1354, doi:10.5194/hess-15-1339-2011.
 103. Jahandideh-Tehrani, M.; Helfer, F.; Zhang, H.; Jenkins, G.; Yu, Y. Hydrodynamic modelling of a flood-prone tidal river using the 1D model MIKE HYDRO River: calibration and sensitivity analysis. *Environmental Monitoring and Assessment* **2020**, *192*, doi:10.1007/s10661-019-8049-0.
 104. Ranji, Z.; Soltanpour, M. Optimization of Bottom Friction Coefficient Using Inverse Modeling in the Persian Gulf. *Ocean Science Journal* **2021**, *56*, 331–343, doi:10.1007/s12601-021-00040-0.
 105. Clare, M.C.A.; Kramer, S.C.; Cotter, C.J.; Piggott, M.D. Calibration, inversion and sensitivity analysis for hydro-morphodynamic models through the application of adjoint methods. *Computers & Geosciences* **2022**, *163*, 105104, doi:10.1016/j.cageo.2022.105104.
 106. Noack, M. Modeling Approach for Interstitial Sediment Dynamics and Reproduction of Gravel-Spawning Fish. PhD Thesis, Universität Stuttgart, Institut für Wasser-und Umweltsystemmodellierung: Stuttgart, Germany, 2012.
 107. Charlton, R. *Fundamentals of Fluvial Geomorphology*; Routledge, Abingdon, 2007; ISBN 978-1-134-31349-5.
 108. Huggett, R.; Shuttleworth, E. *Fundamentals of Geomorphology*; 5th ed.; Routledge: London, 2022; ISBN 978-1-00-325115-6.
 109. Vanoni, V.A. *Sedimentation Engineering*, Manuals & Reports on Engineering Practice, 54, ASCE: New York, NY, USA, 1975.
 110. Li, Z.; Komar, P.D. Laboratory measurements of pivoting angles for applications to selective entrainment of gravel in a current. *Sedimentology* **1986**, *33*, 413–423, doi:10.1111/j.1365-3091.1986.tb00545.x.
 111. Simons, D.B.; Şentürk, F. *Sediment Transport Technology: Water and Sediment Dynamics*; Water Resources Publication: Colorado, USA, 1992; ISBN 978-0-918334-66-4.
 112. Julien, P.Y. *River Mechanics*; 2nd ed.; Cambridge University Press: UK, 2018; ISBN 978-1-107-46277-9.
 113. Stokes, G.G. On the Effect of the Internal Friction of Fluids on the Motion of Pendulums. *Transactions of the Cambridge Philosophical Society* **1851**, *9*, 8.
 114. Hallermeier, R.J. Terminal settling velocity of commonly occurring sand grains. *Sedimentology* **1981**, *28*, 859–865, doi:10.1111/j.1365-3091.1981.tb01948.x.

115. Dietrich, W.E. Settling velocity of natural particles. *Water Resources Research* **1982**, *18*, 1615–1626, doi:10.1029/WR018i006p01615.
116. Cheng, N.-S. Simplified Settling Velocity Formula for Sediment Particle. *Journal of Hydraulic Engineering* **1997**, *123*, 149–152, doi:10.1061/(ASCE)0733-9429(1997)123:2(149).
117. Ahrens, J.P. A Fall-Velocity Equation. *Journal of Waterway, Port, Coastal, and Ocean Engineering* **2000**, *126*, 99–102, doi:10.1061/(ASCE)0733-950X(2000)126:2(99).
118. Jiménez, J.A.; Madsen, O.S. A Simple Formula to Estimate Settling Velocity of Natural Sediments. *Journal of Waterway, Port, Coastal, and Ocean Engineering* **2003**, *129*, 70–78, doi:10.1061/(ASCE)0733-950X(2003)129:2(70).
119. Ferguson, R.I.; Church, M. A Simple Universal Equation for Grain Settling Velocity. *Journal of Sedimentary Research* **2004**, *74*, 933–937, doi:10.1306/051204740933.
120. She, K.; Trim, L.; Pope, D. Fall velocities of natural sediment particles: a simple mathematical presentation of the fall velocity law. *Journal of Hydraulic Research* **2005**, *43*, 189–195, doi:10.1080/00221686.2005.9641235.
121. Camenen, B. Simple and General Formula for the Settling Velocity of Particles. *Journal of Hydraulic Engineering* **2007**, *133*, 229–233, doi:10.1061/(ASCE)0733-9429(2007)133:2(229).
122. Wu, W.; Wang, S.S.Y. Formulas for Sediment Porosity and Settling Velocity. *Journal of Hydraulic Engineering* **2006**, *132*, 858–862, doi:10.1061/(ASCE)0733-9429(2006)132:8(858).
123. Hjulström, F. Studies of the morphological activity of rivers as illustrated by the River Fyris. PhD Thesis, Uppsala University: Uppsala, Sweden, 1935.
124. Neill, C.R. Mean-Velocity Criterion for Scour of Coarse Uniform Bed-Material. In Proceedings of the 12th Congress of the International Association of Hydraulics Research; Fort Collins, Colorado, 1967; Vol. 3, pp. 46–54.
125. Garde, R.J. Initiation of Motion on a Hydrodynamically Rough Surface, Critical Water Velocity Approach. *Journal of Irrigation Power* **1970**, *27*, 271–282.
126. Yang, C.T. Incipient Motion and Sediment Transport. *Journal of the Hydraulics Division* **1973**, *99*, 1679–1704, doi:10.1061/JYCEAJ.0003766.
127. Prakash, H. Velocity Approach for Incipient Motion. *ISH Journal of Hydraulic Engineering* **2010**, *16*, 47–58, doi:10.1080/09715010.2010.10515001.
128. Simões, F.J.M. Shear velocity criterion for incipient motion of sediment. *Water Science and Engineering* **2014**, *7*, 183–193, doi:10.3882/j.issn.1674-2370.2014.02.006.
129. Gessler, J. Self-Stabilizing Tendencies of Alluvial Channels. *Journal of the Waterways, Harbors and Coastal Engineering Division* **1970**, *96*, 235–249, doi:10.1061/AWHCAR.0000016.
130. Grass, A. Initial Instability of Fine Bed Sand. *Journal of Hydraulic Division* **1970**, *96*, <https://doi.org/10.1061/JYCEAJ.000236>.

-
131. He, M.; Han, Q. Stochastic Model of Incipient Sediment Motion. *Journal of the Hydraulics Division* **1982**, *108*, 211–224, doi:10.1061/JYCEAJ.0005816.
132. Dancey, C.L.; Diplas, P.; Papanicolaou, A.; Bala, M. Probability of Individual Grain Movement and Threshold Condition. *Journal of Hydraulic Engineering* **2002**, *128*, 1069–1075, doi:10.1061/(ASCE)0733-9429(2002)128:12(1069).
133. Papanicolaou, A.N.; Diplas, P.; Evaggelopoulos, N.; Fotopoulos, S. Stochastic Incipient Motion Criterion for Spheres under Various Bed Packing Conditions. *Journal of Hydraulic Engineering* **2002**, *128*, 369–380, doi:10.1061/(ASCE)0733-9429(2002)128:4(369).
134. Wu, F.-C.; Chou, Y.-J. Rolling and Lifting Probabilities for Sediment Entrainment. *Journal of Hydraulic Engineering* **2003**, *129*, 110–119, doi:10.1061/(ASCE)0733-9429(2003)129:2(110).
135. Sutherland, A.J. Proposed mechanism for sediment entrainment by turbulent flows. *Journal of Geophysical Research (1896-1977)* **1967**, *72*, 6183–6194, doi:10.1029/JZ072i024p06183.
136. Nelson, J.M.; Shreve, R.L.; McLean, S.R.; Drake, T.G. Role of Near-Bed Turbulence Structure in Bed Load Transport and Bed Form Mechanics. *Water Resources Research* **1995**, *31*, 2071–2086, doi:10.1029/95WR00976.
137. Cao, Z. Turbulent Bursting-Based Sediment Entrainment Function. *Journal of Hydraulic Engineering* **1997**, *123*, 233–236, doi:10.1061/(ASCE)0733-9429(1997)123:3(233).
138. Sechet, P.; Le Guennec, B. Bursting phenomenon and incipient motion of solid particles in bed-load transport. *Journal of Hydraulic Research* **1999**, *37*, 683–696, doi:10.1080/00221689909498523.
139. Zanke, U.C.E. On the influence of turbulence on the initiation of sediment motion. *International Journal of Sediment Research* **2003**, *18*, 17–31.
140. Dey, S.; Sarkar, S.; Solari, L. Near-Bed Turbulence Characteristics at the Entrainment Threshold of Sediment Beds. *Journal of Hydraulic Engineering* **2011**, *137*, 945–958, doi:10.1061/(ASCE)HY.1943-7900.0000396.
141. Ali, S.Z.; Dey, S. Origin of the scaling laws of sediment transport. *Proceedings of the Royal Society A: Mathematical, Physical and Engineering Sciences* **2017**, *473*, 20160785, doi:10.1098/rspa.2016.0785.
142. Li, S.; Katul, G. Cospectral budget model describes incipient sediment motion in turbulent flows. *Physical Review Fluids* **2019**, *4*, 093801, doi:10.1103/PhysRevFluids.4.093801.
143. Shields, A. *Anwendung Der Ähnlichkeitsmechanik Und Der Turbulenzforschung Auf Die Geschiebebewegung (Application of the Similarity in Mechanics and Turbulence Research on the Mobility of Bed Load)*; Preußische Versuchsanstalt für Wasserbau und Schiffbau: Berlin, Germany, 1936; Vol. 26.

144. Dey, S.; Papanicolaou, A. Sediment threshold under stream flow: A state-of-the-art review. *KSCE Journal of Civil Engineering* **2008**, *12*, 45–60, doi:10.1007/s12205-008-8045-3.
145. Church, M.; Ferguson, R.I. Morphodynamics: Rivers beyond steady state. *Water Resources Research* **2015**, *51*, 1883–1897, doi:10.1002/2014WR016862.
146. Shahmohammadi, R.; Afzalimehr, H.; Sui, J. Assessment of Critical Shear Stress and Threshold Velocity in Shallow Flow with Sand Particles. *Water* **2021**, *13*, 994, doi:10.3390/w13070994.
147. Hadian, S.; Afzalimehr, H.; Sui, J. Incipient Motion of Bed Material in a Channel with Varying Width and Vegetated Channel Walls. *Water* **2023**, *15*, 3691, doi:10.3390/w15203691.
148. Miller, M.C.; McCave, I.N.; Komar, P.D. Threshold of sediment motion under unidirectional currents. *Sedimentology* **1977**, *24*, 507–527, doi:10.1111/j.1365-3091.1977.tb00136.x.
149. Mantz, P.A. Incipient Transport of Fine Grains and Flakes by Fluids — Extended Shields Diagram. *Journal of the Hydraulics Division* **1977**, *103*, 601–615, doi:10.1061/JYCEAJ.0004766.
150. Yalin, M.S.; Karahan, E. Inception of Sediment Transport. *Journal of the Hydraulics Division* **1979**, *105*, 1433–1443, doi:10.1061/JYCEAJ.0005306.
151. van Rijn, L.C. Sediment Transport, Part I: Bed Load Transport. *Journal of Hydraulic Engineering* **1984**, *110*, 1431–1456, doi:10.1061/(ASCE)0733-9429(1984)110:10(1431).
152. Buffington, J.M.; Montgomery, D.R. A systematic analysis of eight decades of incipient motion studies, with special reference to gravel-bedded rivers. *Water Resources Research* **1997**, *33*, 1993–2029, doi:10.1029/96WR03190.
153. Soulsby, R.L.; Whitehouse, R.J. Threshold of Sediment Motion in Coastal Environments. In *Pacific Coasts and Ports '97: Proceedings of the 13th Australasian Coastal and Ocean Engineering Conference and the 6th Australasian Port and Harbour Conference*; Centre for Advanced Engineering, University of Canterbury: Christchurch, New Zealand, 1997; Vol. 1, pp. 149–154.
154. Buffington, J.M. The Legend of A. F. Shields. *Journal of Hydraulic Engineering* **1999**, *125*, 376–387, doi:10.1061/(ASCE)0733-9429(1999)125:4(376).
155. Wu, W.; Wang, S.S.Y. Movable Bed Roughness in Alluvial Rivers. *Journal of Hydraulic Engineering* **1999**, *125*, 1309–1312, doi:10.1061/(ASCE)0733-9429(1999)125:12(1309).
156. Paphitis, D. Sediment movement under unidirectional flows: an assessment of empirical threshold curves. *Coastal Engineering* **2001**, *43*, 227–245, doi:10.1016/S0378-3839(01)00015-1.

-
157. Cao, Z.; Pender, G.; Meng, J. Explicit Formulation of the Shields Diagram for Incipient Motion of Sediment. *Journal of Hydraulic Engineering* **2006**, *132*, 1097–1099, doi:10.1061/(ASCE)0733-9429(2006)132:10(1097).
158. Ikeda, S. Incipient Motion of Sand Particles on Side Slopes. *Journal of the Hydraulics Division* **1982**, *108*, 95–114, doi:10.1061/JYCEAJ.0005812.
159. Whitehouse, R.J.S.; Hardisty, J. Experimental assessment of two theories for the effect of bedslope on the threshold of bedload transport. *Marine Geology* **1988**, *79*, 135–139, doi:10.1016/0025-3227(88)90162-4.
160. Chiew, Y.-M.; Parker, G. Incipient sediment motion on non-horizontal slopes. *Journal of Hydraulic Research* **1994**, *32*, 649–660, doi:10.1080/00221689409498706.
161. Iversen, J.D.; Rasmussen, K.R. The effect of surface slope on saltation threshold. *Sedimentology* **1994**, *41*, 721–728, doi:10.1111/j.1365-3091.1994.tb01419.x.
162. Dey, S.; Debnath, K. Influence of Streamwise Bed Slope on Sediment Threshold under Stream Flow. *Journal of Irrigation and Drainage Engineering* **2000**, *126*, 255–263, doi:10.1061/(ASCE)0733-9437(2000)126:4(255).
163. Seminara, G.; Solari, L.; Parker, G. Bed load at low Shields stress on arbitrarily sloping beds: Failure of the Bagnold hypothesis. *Water Resources Research* **2002**, *38*, 31-1-31–16, doi:10.1029/2001WR000681.
164. Dey, S. Critical bed shear for initial movement of sediments on a combined lateral and longitudinal slope. *Hydrology Research* **2004**, *35*, 153–164, doi:10.2166/nh.2004.0011.
165. Chen, X.; Ma, J.; Dey, S. Sediment Transport on Arbitrary Slopes: Simplified Model. *Journal of Hydraulic Engineering* **2010**, *136*, 311–317, doi:10.1061/(ASCE)HY.1943-7900.0000175.
166. Egiazaroff, I.V. Calculation of Nonuniform Sediment Concentrations. *Journal of the Hydraulics Division* **1965**, *91*, 225–247, doi:10.1061/JYCEAJ.0001277.
167. Parker, G.; Klingeman, P.C.; McLean, D.G. Bedload and Size Distribution in Paved Gravel-Bed Streams. *Journal of the Hydraulics Division* **1982**, *108*, 544–571, doi:10.1061/JYCEAJ.0005854.
168. Wu, W.; Wang, S.S.Y.; Jia, Y. Nonuniform sediment transport in alluvial rivers. *Journal of Hydraulic Research* **2000**, *38*, 427–434, doi:10.1080/00221680009498296.
169. Armanini, A. *Principles of River Hydraulics*; Springer International Publishing: Cham, 2018; ISBN 978-3-319-68099-6.
170. Celik, I.; Rodi, W. Suspended Sediment-Transport Capacity for Open Channel Flow. *Journal of Hydraulic Engineering* **1991**, *117*, 191–204, doi:10.1061/(ASCE)0733-9429(1991)117:2(191).
171. Cheng, N.-S.; Chiew, Y.-M. Analysis of Initiation of Sediment Suspension from Bed Load. *Journal of Hydraulic Engineering* **1999**, *125*, 855–861, doi:10.1061/(ASCE)0733-9429(1999)125:8(855).

172. Dey, S. *Fluvial Hydrodynamics: Hydrodynamic and Sediment Transport Phenomena*; GeoPlanet: Earth and Planetary Sciences; Springer-Verlag: Berlin/Heidelberg, 2014; ISBN 978-3-642-19061-2.
173. Church, M. Bed Material Transport and the Morphology of Alluvial Rivers. *Annual Review of Earth and Planetary Sciences* **2006**, *34*, 325–354, doi:10.1146/annurev.earth.33.092203.122721.
174. Cantalice, J.R.B.; da Silva Souza, W.L.; Agra Bezerra Silva, Y.J.; Guerra, S.M.S.; Araújo, A.M.; Monteiro Cavalcante, D.; Cordeiro Atanzio Cruz Silva, C.M. Bedload and Suspended Sediment of a Watershed Impacted by Dams. In *Effects of Sediment Transport on Hydraulic Structures*; Vlassios Hrissanthou, Ed.; IntechOpen: Rijeka, 2015.
175. Yang, C.-Y.; Julien, P.Y. The ratio of measured to total sediment discharge. *International Journal of Sediment Research* **2019**, *34*, 262–269, doi:10.1016/j.ijsrc.2018.11.005.
176. Komar, P.D. Modes of sediment transport in channelized water flows with ramifications to the erosion of the Martian outflow channels. *Icarus* **1980**, *42*, 317–329, doi:10.1016/0019-1035(80)90097-4.
177. Woo, H.S.; Julien, P.Y.; Richardson, E.V. Washload and Fine Sediment Load. *Journal of Hydraulic Engineering* **1986**, *112*, 541–545, doi:10.1061/(ASCE)0733-9429(1986)112:6(541).
178. Khullar, N.K.; Kothiyari, U.C.; Ranga Raju, K.G. Suspended Wash Load Transport of Nonuniform Sediments. *Journal of Hydraulic Engineering* **2010**, *136*, 534–543, doi:10.1061/(ASCE)HY.1943-7900.0000223.
179. Gomez, B.; Church, M. An assessment of bed load sediment transport formulae for gravel bed rivers. *Water Resources Research* **1989**, *25*, 1161–1186, doi:10.1029/WR025i006p01161.
180. Gomez, B. Bedload Transport. *Earth-Science Reviews* **1991**, *31*, 89–132, doi:10.1016/0012-8252(91)90017-A.
181. Ancey, C. Bedload transport: a walk between randomness and determinism. Part 1. The state of the art. *Journal of Hydraulic Research* **2020**, *58*, 1–17, doi:10.1080/00221686.2019.1702594.
182. Ancey, C. Bedload transport: a walk between randomness and determinism. Part 2. Challenges and prospects. *Journal of Hydraulic Research* **2020**, *58*, 18–33, doi:10.1080/00221686.2019.1702595.
183. Meyer-Peter, E.; Müller, R. Formulas for Bed-Load Transport. In *Proceeding of 2nd IAHR Congress*, Stockholm, 1948.
184. Fernandez Luque, R.; Van Beek, R. Erosion And Transport Of Bed-Load Sediment. *Journal of Hydraulic Research* **1976**, *14*, 127–144, doi:10.1080/00221687609499677.

-
185. Paintal, A.S. Concept Of Critical Shear Stress In Loose Boundary Open Channels. *Journal of Hydraulic Research* **1971**, 9, 91–113, doi:10.1080/00221687109500339.
 186. Parker, G. Hydraulic Geometry of Active Gravel Rivers. *Journal of the Hydraulics Division* **1979**, 105, 1185–1201, doi:10.1061/JYCEAJ.0005275.
 187. Cheng, N.-S. Exponential Formula for Bedload Transport. *Journal of Hydraulic Engineering* **2002**, 128, 942–946, doi:10.1061/(ASCE)0733-9429(2002)128:10(942).
 188. Ferguson, R.I. Estimating critical stream power for bedload transport calculations in gravel-bed rivers. *Geomorphology* **2005**, 70, 33–41, doi:10.1016/j.geomorph.2005.03.009.
 189. Gomez, B.; Soar, P.J. Bedload transport and the stream power approach. *Proceedings of the Royal Society A: Mathematical, Physical and Engineering Sciences* **2023**, 479, 20220783, doi:10.1098/rspa.2022.0783.
 190. Bagnold, R.A. The flow of cohesionless grains in fluids. *Philosophical Transactions of the Royal Society of London. Series A, Mathematical and Physical Sciences* **1956**, 249, 235–297, doi:10.1098/rsta.1956.0020.
 191. Bagnold, R.A. *An Approach to the Sediment Transport Problem from General Physics*; U.S. Geological Survey: Washington D.C., USA, 1966.
 192. Bagnold, R.A. The nature of saltation and of 'bed-load' transport in water. *Proceedings of the Royal Society of London. A. Mathematical and Physical Sciences* **1973**, 332, 473–504, doi:10.1098/rspa.1973.0038.
 193. Bagnold, R.A. Bed load transport by natural rivers. *Water Resources Research* **1977**, 13, 303–312, doi:10.1029/WR013i002p00303.
 194. Bagnold, R.A. An Empirical Correlation of Bedload Transport Rates in Flumes and Natural Rivers. *Proceedings of the Royal Society of London. A. Mathematical and Physical Sciences* **1980**, 372, 453–473, doi:10.1098/rspa.1980.0122.
 195. Yang, C.T. Unit Stream Power Equation for Gravel. *Journal of Hydraulic Engineering* **1984**, 110, 1783–1797, doi:10.1061/(ASCE)0733-9429(1984)110:12(1783).
 196. Einstein, H.A. Formulas for the Transportation of Bed Load. *Transactions of the American Society of Civil Engineers* **1942**, 107, 561–577, doi:10.1061/TACEAT.0005468.
 197. Einstein, H.A. *The Bed-Load Function for Sediment Transportation in Open Channel Flows*. Technical Bulletin No. 1026; United States Department of Agriculture, Soil Conservation Service, Washington D.C., USA, 1950;
 198. Wang, X.; Zheng, J.; Li, D.; Qu, Z. Modification of the Einstein Bed-Load Formula. *Journal of Hydraulic Engineering* **2008**, 134, 1363–1369, doi:10.1061/(ASCE)0733-9429(2008)134:9(1363).
 199. Engelund, F.; Fredsøe, J. A Sediment Transport Model for Straight Alluvial Channels. *Hydrology Research* **1976**, 7, 293–306, doi:10.2166/nh.1976.0019.
 200. Smart, G.M. Sediment Transport Formula for Steep Channels. *Journal of Hydraulic Engineering* **1984**, 110, 267–276, doi:10.1061/(ASCE)0733-9429(1984)110:3(267).

201. Graf, W.H.; Suszka, L. Sediment Transport in Steep Channels. *Journal of Hydrosience and Hydraulic Engineering* **1987**, *5*, 11–26.
202. Suszka, L. Modification of transport rate formula for steep channels. In *Fluvial Hydraulics of Mountain Regions*; Armanini, A., Di Silvio, G., Eds.; Springer: Berlin, Heidelberg, 1991; pp. 59–70.
203. Tsujimoto, T. Bed-Load Transport in Steep Channels. In *Fluvial Hydraulics of Mountain Regions*; Armanini, A., Di Silvio, G., Eds.; Springer: Berlin, Heidelberg, 1991; pp. 89–102.
204. Rickenmann, D. Hyperconcentrated Flow and Sediment Transport at Steep Slopes. *Journal of Hydraulic Engineering* **1991**, *117*, 1419–1439, doi:10.1061/(ASCE)0733-9429(1991)117:11(1419).
205. Damgaard, J.S.; Whitehouse, R.J.S.; Soulsby, R.L. Bed-Load Sediment Transport on Steep Longitudinal Slopes. *Journal of Hydraulic Engineering* **1997**, *123*, 1130–1138, doi:10.1061/(ASCE)0733-9429(1997)123:12(1130).
206. Misri, R.L.; Garde, R.J.; Ranga Raju, K.G. Bed Load Transport of Coarse Nonuniform Sediment. *Journal of Hydraulic Engineering* **1984**, *110*, 312–328, doi:10.1061/(ASCE)0733-9429(1984)110:3(312).
207. Samaga, B.R.; Raju, K.G.R.; Garde, R.J. Bed Load Transport of Sediment Mixtures. *Journal of Hydraulic Engineering* **1986**, *112*, 1003–1017, doi:10.1061/(ASCE)0733-9429(1986)112:11(1003).
208. Bridge, J.S.; Bennett, S.J. A model for the entrainment and transport of sediment grains of mixed sizes, shapes, and densities. *Water Resources Research* **1992**, *28*, 337–363, doi:10.1029/91WR02570.
209. Hsu, S.M.; Holly, F.M. Conceptual Bed-Load Transport Model and Verification for Sediment Mixtures. *Journal of Hydraulic Engineering* **1992**, *118*, 1135–1152, doi:10.1061/(ASCE)0733-9429(1992)118:8(1135).
210. Patel, P.L.; Ranga Raju, K.G. Fractionwise calculation of bed load transport. *Journal of Hydraulic Research* **1996**, *34*, 363–379, doi:10.1080/00221689609498485.
211. Dey, S.; Ali, S.Z.; Padhi, E. Terminal fall velocity: the legacy of Stokes from the perspective of fluvial hydraulics. *Proceedings of the Royal Society A: Mathematical, Physical and Engineering Sciences* **2019**, *475*, 20190277, doi:10.1098/rspa.2019.0277.
212. Lane, E.W.; Kalinske, A.A. Engineering calculations of suspended sediment. *Transactions American Geophysical Union* **1941**, *22*, 603–607, doi:10.1029/TR022i003p00603.
213. Guo, J.; Wood, W.L. Fine Suspended Sediment Transport Rates. *Journal of Hydraulic Engineering* **1995**, *121*, 919–922, doi:10.1061/(ASCE)0733-9429(1995)121:12(919).
214. Bijker, E.W. Longshore Transport Computations. *Journal of the Waterways, Harbors and Coastal Engineering Division* **1971**, *97*, 687–701, doi:10.1061/AWHCAR.0000122.

-
215. van Rijn, L.C. Sediment Transport, Part II: Suspended Load Transport. *Journal of Hydraulic Engineering* **1984**, *110*, 1613–1641, doi:10.1061/(ASCE)0733-9429(1984)110:11(1613).
216. Rouse, H. Modern Conceptions of the Mechanics of Fluid Turbulence. *Transactions of the American Society of Civil Engineers* **1937**, *102*, 463–505, doi:10.1061/taceat.0004872.
217. Hunt, J.N. The turbulent transport of suspended sediment in open channels. *Proceedings of the Royal Society of London. Series A. Mathematical and Physical Sciences* **1954**, *224*, 322–335, doi:10.1098/rspa.1954.0161.
218. Zagustin, K. Sediment Distribution In Turbulent Flow. *Journal of Hydraulic Research* **1968**, *6*, 163–172, doi:10.1080/00221686809500227.
219. McTigue, D.F. Mixture Theory for Suspended Sediment Transport. *Journal of the Hydraulics Division* **1981**, *107*, 659–673, doi:10.1061/JYCEAJ.0005678.
220. Ni, J.R.; Qian Wang, G. Vertical Sediment Distribution. *Journal of Hydraulic Engineering* **1991**, *117*, 1184–1194, doi:10.1061/(ASCE)0733-9429(1991)117:9(1184).
221. Umeyaina, M. Vertical Distribution of Suspended Sediment in Uniform Open-Channel Flow. *Journal of Hydraulic Engineering* **1992**, *118*, 936–941, doi:10.1061/(ASCE)0733-9429(1992)118:6(936).
222. Itakura, T.; Kishi, T. Open Channel Flow with Suspended Sediments. *Journal of the Hydraulics Division* **1980**, *106*, 1325–1343, doi:10.1061/JYCEAJ.0005483.
223. Garcia, M.; Parker, G. Entrainment of Bed Sediment into Suspension. *Journal of Hydraulic Engineering* **1991**, *117*, 414–435, doi:10.1061/(ASCE)0733-9429(1991)117:4(414).
224. Zyserman, J.A.; Fredsøe, J. Data Analysis of Bed Concentration of Suspended Sediment. *Journal of Hydraulic Engineering* **1994**, *120*, 1021–1042, doi:10.1061/(ASCE)0733-9429(1994)120:9(1021).
225. Smith, J.D.; McLean, S.R. Spatially averaged flow over a wavy surface. *Journal of Geophysical Research* **1977**, *82*, 1735–1746, doi:10.1029/JC082i012p01735.
226. Chang, F.M.; Simons, D.B.; Richardson, E.V. Total bed-material discharge in alluvial channels; In Proceedings of 12th Congress IAHR, Fort Collins, Colorado, 1967, 132–140.
227. Laursen, E.M. The Total Sediment Load of Streams. *Journal of the Hydraulics Division* **1958**, *84*, 1–36, doi:10.1061/JYCEAJ.0000158.
228. Engelund, F.; Hansen, E. *A Monograph on Sediment Transport in Alluvial Streams*; Teknisk Vorlag: Copenhagen, Denmark, 1967.
229. Ackers, P.; White, W.R. Sediment Transport: New Approach and Analysis. *Journal of the Hydraulics Division* **1973**, *99*, 2041–2060, doi:10.1061/JYCEAJ.0003791.
230. Yang, C.T. Unit Stream Power and Sediment Transport. *Journal of the Hydraulics Division* **1972**, *98*, 1805–1826, doi:10.1061/JYCEAJ.0003439.

231. Yang, C.T. Unit stream power equations for total load. *Journal of Hydrology* **1979**, *40*, 123–138, doi:10.1016/0022-1694(79)90092-1.
232. Karim, F. Bed Material Discharge Prediction for Nonuniform Bed Sediments. *Journal of Hydraulic Engineering* **1998**, *124*, 597–604, doi:10.1061/(ASCE)0733-9429(1998)124:6(597).
233. Yang, S.-Q.; Lim, S.-Y. Total Load Transport Formula for Flow in Alluvial Channels. *Journal of Hydraulic Engineering* **2003**, *129*, 68–72, doi:10.1061/(ASCE)0733-9429(2003)129:1(68).
234. Yang, S.-Q. Prediction of total bed material discharge. *Journal of Hydraulic Research* **2005**, *43*, 12–22, doi:10.1080/00221680509500107.
235. Morris, G.L.; Fan, J. *Reservoir Sedimentation Handbook: Design and Management of Dams, Reservoirs, and Watersheds for Sustainable Use*; McGraw Hill Professional: New York, NY, USA, 1998; ISBN 978-0-07-043302-1.
236. García, M.H. *Sedimentation Engineering: Processes, Measurements, Modeling, and Practice*; Environmental and Water Resources Institute (EWRI), ASCE Manuals and Reports on Engineering Practice, American Society of Civil Engineers: Reston, VA, USA, 2008; ISBN 978-0-7844-0814-8.
237. Annandale, G.W.; Morris, G.L.; Karki, P. *Extending the Life of Reservoirs: Sustainable Sediment Management for Dams and Run-of-River Hydropower*; The World Bank: Washington, D.C., USA, 2016; ISBN 978-1-4648-0838-8.
238. ICOLD *Sedimentation and Sustainable Use of Reservoirs and River Systems*; Sedimentation Committee 2009; Draft ICOLD Bulletin; ICOLD: Paris, France, 2009.
239. Julien, P.Y. *Erosion and Sedimentation*; 2nd ed.; Cambridge University Press: Cambridge, 2010; ISBN 978-0-521-83038-6.
240. Mulligan, M.; van Soesbergen, A.; Sáenz, L. GOODD, a global dataset of more than 38,000 georeferenced dams. *Scientific Data* **2020**, *7*, 31, doi:10.1038/s41597-020-0362-5.
241. Hariri-Ardebili, M.A.; Salazar, F.; Pourkamali-Anaraki, F.; Mazzà, G.; Mata, J. Soft Computing and Machine Learning in Dam Engineering. *Water* **2023**, *15*, 917, doi:10.3390/w15050917.
242. Mahmood, K. Reservoir Sedimentation-Impact, Extent and Mitigation. Technical paper No. WTP 71, International Bank for Reconstruction and Development, Washington, DC, USA, 1987.
243. Yoon, Y.N. The state and the perspective of the direct sediment removal methods from reservoirs. *International Journal of Sediment Research* **1992**, *7*, 99–115.
244. White, R. *Evacuation of Sediments from Reservoirs*; Thomas Telford Publishing: London, UK, 2001; ISBN 978-0-7277-2953-8.

-
245. Basson, G.R. Management of Siltation in Existing and New Reservoirs. In Proceedings of the 23rd Congress of the Int. Commission on Large Dams CIGB-ICOLD; 2009; Vol. 2.
246. Annandale, G.W. Reservoir Sedimentation. In *Encyclopedia of Hydrological Sciences*; John Wiley & Sons, Ltd, 2006; ISBN 978-0-470-84894-4.
247. Schleiss, A.J.; Franca, M.J.; Juez, C.; De Cesare, G. Reservoir Sedimentation. *Journal of Hydraulic Research* **2016**, *54*, 595–614, doi:10.1080/00221686.2016.1225320.
248. Kondolf, G.M.; Gao, Y.; Annandale, G.W.; Morris, G.L.; Jiang, E.; Zhang, J.; Cao, Y.; Carling, P.; Fu, K.; Guo, Q.; et al. Sustainable sediment management in reservoirs and regulated rivers: Experiences from five continents. *Earth's Future* **2014**, *2*, 256–280, doi:10.1002/2013EF000184.
249. Morris, G.L. Classification of Management Alternatives to Combat Reservoir Sedimentation. *Water* **2020**, *12*, 861, doi:10.3390/w12030861.
250. Wang, H.-W.; Kondolf, G.M. Upstream Sediment-Control Dams: Five Decades of Experience in the Rapidly Eroding Dahan River Basin, Taiwan. *JAWRA Journal of the American Water Resources Association* **2014**, *50*, 735–747, doi:10.1111/jawr.12141.
251. Boes, R.M.; Auel, C.; Hagmann, M.; Albayrak, I. Sediment bypass tunnels to mitigate reservoir sedimentation and restore sediment continuity. In *Reservoir Sedimentation*; Schleiss, A.J., de Cesare, G., Franca, M.J., Pfister, M., Eds.; CRC Press: Boca Raton, FL, USA, 2014; pp. 221–228 ISBN 978-0-429-22680-9.
252. Auel, C. Sediment Bypassing – A Sustainable and Eco-Friendly Strategy Against Reservoir Sedimentation. In Proceedings of the 26th ICOLD Congress, Vienna, Austria. Intl. Commission on Large Dams: Paris, France, 2018.
253. Batuca, D.G.; Jordaan Jr, J.M. *Silting and Desilting of Reservoirs*; Taylor and Francis, London, 2000.
254. Crosa, G.; Castelli, E.; Gentili, G.; Espa, P. Effects of suspended sediments from reservoir flushing on fish and macroinvertebrates in an alpine stream. *Aquatic Sciences* **2010**, *72*, 85–95, doi:10.1007/s00027-009-0117-z.
255. Espa, P.; Castelli, E.; Crosa, G.; Gentili, G. Environmental Effects of Storage Preservation Practices: Controlled Flushing of Fine Sediment from a Small Hydropower Reservoir. *Environmental Management* **2013**, *52*, 261–276, doi:10.1007/s00267-013-0090-0.
256. Espa, P.; Brignoli, M.L.; Crosa, G.; Gentili, G.; Quadroni, S. Controlled sediment flushing at the Cancano Reservoir (Italian Alps): Management of the operation and downstream environmental impact. *Journal of Environmental Management* **2016**, *182*, 1–12, doi:10.1016/j.jenvman.2016.07.021.
257. Moridi, A.; Yazdi, J. Sediment Flushing of Reservoirs under Environmental Considerations. *Water Resources Management* **2017**, *31*, 1899–1914, doi:10.1007/s11269-017-1620-y.

258. Antoine, G.; Camenen, B.; Jodeau, M.; Némery, J.; Esteves, M. Downstream erosion and deposition dynamics of fine suspended sediments due to dam flushing. *Journal of Hydrology* **2020**, *585*, 124763, doi:10.1016/j.jhydrol.2020.124763.
259. Atkinson, E. *The Feasibility of Flushing Sediment from Reservoirs*; HR Wallingford Report OD 137 to British Overseas Development Admin: London, UK, 1996; p. 99.
260. Bhattacharyya, K.; Singh, V.P. *Reservoir Sedimentation: Assessment and Environmental Controls*; CRC Press: Boca Raton, FL, USA, 2019; ISBN 978-1-351-02750-2.
261. Tigrek, S.; Aras, T. *Reservoir Sediment Management*; CRC Press: London, 2012; ISBN 978-0-429-08695-3.
262. Hauer, C.; Wagner, B.; Aigner, J.; Holzapfel, P.; Flödl, P.; Liedermann, M.; Tritthart, M.; Sindelar, C.; Pulg, U.; Klösch, M.; et al. State of the art, shortcomings and future challenges for a sustainable sediment management in hydropower: A review. *Renewable and Sustainable Energy Reviews* **2018**, *98*, 40–55, doi:10.1016/j.rser.2018.08.031.
263. Haun, S. Advanced Methods for a Sustainable Sediment Management of Reservoirs. Habilitation thesis, Universität Stuttgart, Institut für Wasser-und Umweltsystemmodellierung: Stuttgart, Germany, 2022.
264. Launder, B.E.; Spalding, D.B. *Lectures in Mathematical Models of Turbulence*; Academic Press: London, 1972.
265. Rodi, W. *Turbulence Models and Their Application in Hydraulics: A State of the Art Review*, IAHR Monograph; 3rd ed.; A.A. Balkema, Rotterdam, Netherlands, 1993; ISBN 978-0-203-73489-6.
266. Wilcox, D.C. *Turbulence Modeling for CFD*; 3rd ed.; DCW Industries: La Canada, CA, 2006; ISBN 978-1-928729-08-2.
267. Rodi, W. Turbulence Modeling and Simulation in Hydraulics: A Historical Review. *Journal of Hydraulic Engineering* **2017**, *143*, 03117001, doi:10.1061/(ASCE)HY.1943-7900.0001288.
268. Bates, P.D., Lane, S.N., Ferguson, R.I. *Computational Fluid Dynamics: Applications in Environmental Hydraulics*; John Wiley & Sons, Ltd.: Chichester, UK, 2005.
269. Versteeg, H.K.; Malalasekera, W. *An Introduction to Computational Fluid Dynamics: The Finite Volume Method*; 2nd ed.; Pearson Education Ltd: Harlow, UK, 2007; ISBN 978-0-13-127498-3.
270. Tanguy, J.-M. *Environmental Hydraulics: Numerical Methods*; 1st ed.; Wiley-ISTE: London, 2010; Vol. 3; ISBN 978-1-84821-155-1.
271. Andersson, B.; Andersson, R.; Håkansson, L.; Mortensen, M.; Sudiyo, R.; Wachem, B. van *Computational Fluid Dynamics for Engineers*; Cambridge University Press: Cambridge, 2011; ISBN 978-1-139-50556-7.

-
272. Moukalled, F.; Mangani, L.; Darwish, M. *The Finite Volume Method in Computational Fluid Dynamics: An Advanced Introduction with OpenFOAM and Matlab*; 1st ed.; Springer Publishing Company, Incorporated, 2015; ISBN 978-3-319-16873-9.
273. Kondolf, G.M., Piégay, H. *Tools in Fluvial Geomorphology*; 2nd ed.; John Wiley & Sons, Ltd, Chichester, UK, 2016.
274. Schlichting, H.; Gersten, K. *Boundary-Layer Theory*; 9th ed.; Springer: Berlin, 2017; ISBN 978-3-662-52917-1.
275. Ferziger, J.H.; Perić, M.; Street, R.L. *Computational Methods for Fluid Dynamics*; 4th ed.; Springer International Publishing: Cham, Switzerland, 2020; ISBN 978-3-319-99691-2.
276. Olsen, N.R.B. *A Three Dimensional Numerical Model for Simulation of Sediment Movement in Water Intakes with Multiblock Option*; Department of Hydraulic and Environmental Engineering, The Norwegian University of Science and Technology: Trondheim, Norway, 2014.
277. Haun, S.; Olsen, N.R.B.; Feurich, R. Numerical Modeling of Flow Over Trapezoidal Broad-Crested Weir. *Engineering Applications of Computational Fluid Mechanics* **2011**, *5*, 397–405, doi:10.1080/19942060.2011.11015381.
278. Haun, S.; Olsen, N.R.B. Three-dimensional numerical modelling of the flushing process of the Kali Gandaki hydropower reservoir. *Lakes & Reservoirs: Science, Policy and Management for Sustainable Use* **2012**, *17*, 25–33, doi:10.1111/j.1440-1770.2012.00491.x.
279. Haun, S.; Olsen, N.R.B. Three-dimensional numerical modelling of reservoir flushing in a prototype scale. *International Journal of River Basin Management* **2012**, *10*, 341–349, doi:10.1080/15715124.2012.736388.
280. Haun, S.; Kjærås, H.; Løvfall, S.; Olsen, N.R.B. Three-dimensional measurements and numerical modelling of suspended sediments in a hydropower reservoir. *Journal of Hydrology* **2013**, *479*, 180–188, doi:10.1016/j.jhydrol.2012.11.060.
281. Esmaili, T.; Sumi, T.; Kantoush, S.A.; Kubota, Y.; Haun, S.; Rütther, N. Three-Dimensional Numerical Study of Free-Flow Sediment Flushing to Increase the Flushing Efficiency: A Case-Study Reservoir in Japan. *Water* **2017**, *9*, 900, doi:10.3390/w9110900.
282. Esmaili, T.; Sumi, T.; Kantoush, S.A.; Kubota, Y.; Haun, S.; Rütther, N. Numerical Study of Discharge Adjustment Effects on Reservoir Morphodynamics and Flushing Efficiency: An Outlook for the Unazuki Reservoir, Japan. *Water* **2021**, *13*, 1624, doi:10.3390/w13121624.
283. Olsen, N.R.B.; Hillebrand, G. Long-time 3D CFD modeling of sedimentation with dredging in a hydropower reservoir. *Journal of Soils and Sediments* **2018**, *18*, 3031–3040, doi:10.1007/s11368-018-1989-0.
284. Olsen, N.R.B. 3D numerical modelling of braided channel formation. *Geomorphology* **2021**, *375*, 107528, doi:10.1016/j.geomorph.2020.107528.

285. Hillebrand, G.; Klassen, I.; Olsen, N.R.B. 3D CFD modelling of velocities and sediment transport in the Iffezheim hydropower reservoir. *Hydrology Research* **2017**, *48*, 147–159, doi:10.2166/nh.2016.197.
286. Fischer-Antze, T.; Rütger, N.; Olsen, N.R.B.; Gutknecht, D. Three-dimensional (3D) modeling of non-uniform sediment transport in a channel bend with unsteady flow. *Journal of Hydraulic Research* **2009**, *47*, 670–675, doi:10.3826/jhr.2009.3252.
287. Baranya, S.; Olsen, N.R.B.; Józsa, J. Flow Analysis of a River Confluence with Field Measurements and Rans Model with Nested Grid Approach. *River Research and Applications* **2015**, *31*, 28–41, doi:10.1002/rra.2718.
288. Radan, P.; Vaghefi, M. Flow and scour pattern around submerged and non-submerged T-shaped spur dikes in a 90° bend using the SSIIM model. *International Journal of River Basin Management* **2016**, *14*, 219–232, doi:10.1080/15715124.2016.1159570.
289. Almeland, S.K.; Olsen, N.R.B.; Bråveit, K.; Aryal, P.R. Multiple solutions of the Navier-Stokes equations computing water flow in sand traps. *Engineering Applications of Computational Fluid Mechanics* **2019**, *13*, 199–219, doi:10.1080/19942060.2019.1566094.
290. Isaac, N.; Eldho, T.I. Experimental and numerical simulations of the hydraulic flushing of reservoir sedimentation for planning and design of a hydropower project. *Lakes & Reservoirs: Science, Policy and Management for Sustainable Use* **2019**, *24*, 259–274, doi:10.1111/lre.12278.
291. Oveici, E.; Tayari, O.; Jalalkamali, N. Flow Field in a Sloped Channel with Damaged and Undamaged Piers: Numerical and Experimental Studies. *KSCE Journal of Civil Engineering* **2021**, *25*, 4240–4251, doi:10.1007/s12205-021-1511-x.
292. Zhang, Q.; Hillebrand, G.; Hoffmann, T.; Hinkelmann, R. Assessing long-term evolution of the fine sediment budget in the Iffezheim reservoir: temporal upscaling of numerical simulations. *International Journal of River Basin Management* **2022**, *20*, 475–486, doi:10.1080/15715124.2021.1885419.
293. Olsen, N.R.B. Four free surface algorithms for the 3D Navier–Stokes equations. *Journal of Hydroinformatics* **2015**, *17*, 845–856, doi:10.2166/hydro.2015.012.
294. Wang, S.S.Y.; Wu, W. River Sedimentation and Morphology Modeling—The State of the Art and Future Development. In Proceedings of the 9th International Symposium on River Sedimentation; Yichang, China, 2004; pp. 71–94.
295. Wang, S.S.Y.; Wu, W. Computational Simulation of River Sedimentation and Morphology: A Review of the State of the Art. *International Journal of Sediment Research* **2005**, *20*, 7–29.
296. Muleta, M.K.; Nicklow, J.W. Sensitivity and uncertainty analysis coupled with automatic calibration for a distributed watershed model. *Journal of Hydrology* **2005**, *306*, 127–145, doi:10.1016/j.jhydrol.2004.09.005.

-
297. Chang, C.; Yang, J.; Tung, Y. Sensitivity and uncertainty analysis of a sediment transport model: a global approach. *Stochastic Hydrology and Hydraulics* **1993**, *7*, 299–314, doi:10.1007/BF01581617.
298. Gou, J.; Miao, C.; Duan, Q.; Tang, Q.; Di, Z.; Liao, W.; Wu, J.; Zhou, R. Sensitivity Analysis-Based Automatic Parameter Calibration of the VIC Model for Streamflow Simulations Over China. *Water Resources Research* **2020**, *56*, doi:10.1029/2019WR025968.
299. Shoarinezhad, V.; Wieprecht, S.; Haun, S. Automatic Calibration of a 3D Morphodynamic Numerical Model for Simulating Bed Changes in a 180° Channel Bend. In *Recent Trends in Environmental Hydraulics, GeoPlanet: Earth and Planetary Sciences*; Kalinowska, M.B., Mrokowska, M.M., Rowiński, P.M., Eds.; Springer International Publishing: Cham, 2020; pp. 253–262.
300. Shoarinezhad, V.; Wieprecht, S.; Haun, S. Comparison of Local and Global Optimization Methods for Calibration of a 3D Morphodynamic Model of a Curved Channel. *Water* **2020**, *12*, 1333, doi:10.3390/w12051333.
301. Shoarinezhad, V.; Wieprecht, S.; Kantoush, S.A.; Haun, S. Applying optimization methods for automatic calibration of 3D morphodynamic numerical models of shallow reservoirs: comparison between lozenge- and hexagon-shaped reservoirs. *Journal of Hydroinformatics* **2023**, *25*, 85–100, doi:10.2166/hydro.2022.094.
302. Shoarinezhad, V.; Olsen, N.R.B.; Wieprecht, S.; Haun, S. Using automatic model calibration for 3D morphological simulations: a case study of the Bodendorf reservoir flushing. *Environmental Fluid Mechanics* **2024**, doi:10.1007/s10652-023-09961-x.
303. Doherty, J. *PEST Model-Independent Parameter Estimation User Manual Part I, 6th ed.*; Watermark Numerical Computing: Brisbane, Australia, 2016.
304. Duan, Q.Y.; Gupta, V.K.; Sorooshian, S. Shuffled complex evolution approach for effective and efficient global minimization. *Journal of Optimization Theory and Applications* **1993**, *76*, 501–521, doi:10.1007/BF00939380.
305. Hansen, N. The CMA evolution strategy: A tutorial. *arXiv* **2016**, arXiv:1604.00772.
306. Kennedy, J.; Eberhart, R. Particle swarm optimization. In Proceedings of the ICNN'95—International Conference on Neural Networks; IEEE: Perth, WA, Australia, 1995; Vol. 4, pp. 1942–1948.
307. Erol, O.K.; Eksin, I. A new optimization method: Big Bang–Big Crunch. *Advances in Engineering Software* **2006**, *37*, 106–111, doi:10.1016/j.advengsoft.2005.04.005.

Appendix I

Comparison of local and global optimization methods for calibration of a 3D morphodynamic model of a curved channel

Table 5.1. Metadata of Publication I

Title	Comparison of local and global optimization methods for calibration of a 3D morphodynamic model of a curved channel
Authors	Vahid Shoarinezhad, Silke Wieprecht, Stefan Haun
Journal	Water
Submitted	03 April 2020
Accepted	04 May 2020
Published	08 May 2020
DOI	https://doi.org/10.3390/w12051333

Article

Comparison of Local and Global Optimization Methods for Calibration of a 3D Morphodynamic Model of a Curved Channel

Vahid Shoarinezhad * , Silke Wieprecht  and Stefan Haun 

Institute for Modelling Hydraulic and Environmental Systems, University of Stuttgart, Pfaffenwaldring 61, 70569 Stuttgart, Germany; silke.wieprecht@iws.uni-stuttgart.de (S.W.); stefan.haun@iws.uni-stuttgart.de (S.H.)

* Correspondence: vahid.shoarinezhad@iws.uni-stuttgart.de

Received: 3 April 2020; Accepted: 4 May 2020; Published: 8 May 2020



Abstract: In curved channels, the flow characteristics, sediment transport mechanisms, and bed evolution are more complex than in straight channels, owing to the interaction between the centrifugal force and the pressure gradient, which results in the formation of secondary currents. Therefore, using an appropriate numerical model that considers this fully three-dimensional effect, and subsequently, the model calibration are substantial tasks for achieving reliable simulation results. The calibration of numerical models as a subjective approach can become challenging and highly time-consuming, especially for inexperienced modelers, due to dealing with a large number of input parameters with respect to hydraulics and sediment transport. Using optimization methods can notably facilitate and expedite the calibration procedure by reducing the user intervention, which results in a more objective selection of parameters. This study focuses on the application of four different optimization algorithms for calibration of a 3D morphodynamic numerical model of a curved channel. The performance of a local gradient-based method is compared with three global optimization algorithms in terms of accuracy and computational time (model runs). The outputs of the optimization methods demonstrate similar sets of calibrated parameters and almost the same degree of accuracy according to the achieved minimum of the objective function. Accordingly, the most efficient method concerning the number of model runs (i.e., local optimization method) is selected for further investigation by setting up additional numerical models using different sediment transport formulae and various discharge rates. The comparisons of bed topography changes in several longitudinal and cross-sections between the measured data and the results of the calibrated numerical models are presented. The outcomes show an acceptable degree of accuracy for the automatically calibrated models.

Keywords: 3D hydro-morphodynamic model; automatic calibration; optimization algorithms; curved channel; SSIIM; PEST

1. Introduction

Numerical models have become useful behavioral representatives of complex environmental systems. In water-related domains, the growth of knowledge about the underlying processes and recent developments regarding numerical solvers and computational techniques have increased the performance and speed of simulations. However, a significant challenge remains for modelers to minimize the misfit between simulation outputs and corresponding physical observations, which is necessary to obtain a reliable predictive model [1,2]. Hydro-morphodynamic models are characterized by a large number of input parameters dealing with a considerable amount of uncertainty. This uncertainty arises from the sophisticated behavior of environmental fluid systems, the simplified structure of models, implemented empirical equations, unknown boundary conditions,

and imprecise input data. Some of the physical input parameters, which are subject to calibration, can only be quantified at specific locations over a limited period, and for some it is not physically feasible to measure them.

Modeling practice can be defined as a four-step task, involving model setup, calibration, validation, and application [3]. Consequently, the model accuracy depends not only on the model structure and the quality of input data but also on the model calibration and validation. Calibration of numerical models is the foremost step for quantifying and accrediting computational simulations, involving two major stages: parameter specification (i.e., selection of sensitive parameters that are subject to adjustment) and parameter estimation (i.e., determination of optimal or quasi-optimal values of specified parameters). Calibration is an inverse, multistep problem, with the aim of uncertainty diminution by updating the model through subsequent comparisons between observations and computational results, in order to achieve a good agreement with a reasonable tolerance [4]. In other words, calibration is the process of model adaption by adjusting independent variables to gain accordance between computed and measured distributions of dependent variables, so that the model output deviates marginally from the real data specified in the performance criteria [5,6]. Nevertheless, even calibrated models potentially involve a certain amount of uncertainty and seldom address the underlying deficiencies because of both model errors (modeling assumptions, simplifications, and approximations) and data errors (the lack of error-free measurements) [7,8]. Hence, a calibrated model needs to be validated before applying it to practical problems to ensure reliable predictions [9–11]. On the other hand, according to Refsgaard and Henriksen [12], a validated model operates in a precise manner with regards to site-specific applications and predefined accuracy criteria, and thus the validity of a model is always limited in terms of time, space, boundary conditions, and the type of application.

Model calibration can be accomplished manually, automatically, or by using a multistep method combining the two approaches [13–15]. The most widely used trial-and-error method is not only highly dependent on users' knowledge of the model structure and their level of expertise, but also on their understanding of the environmental system characteristics and the properties of measured data [16]. The trial-and-error method follows the simple approach of manual adjustment of uncertain or unknown parameters and the comparison of predictions with measured values, involving human judgment to attain the best fit for model parameters [17]. As the model structure becomes complicated, the manual calibration procedure becomes laborious, time- and cost-consuming, and for models with a large number of uncertain or unknown variables (e.g., morphological models), sometimes impractical. The demanding practice related to the manual method has been persuading modelers to improve the complex inverse calibration technique based on optimization algorithms (e.g., deterministic, metaheuristic, stochastic, or uncertainty-based). This can be done by coupling the model with an optimization engine, with the aim of speeding up the calibration process and establishing an objective scheme to address the "user-subjectivity" issue [18–20]. As an example of the user influence on model calibration results, Botterweg [21] compared the outcomes of a hydrological model that was calibrated independently by two users with an identical set of measured data and reported how different sets of calibrated parameter values could yield reasonable results.

Principally, automated calibration consists of three elements: an objective function to assess the differences between model outputs and observations, an optimization algorithm for sequential adjustment of preselected model parameters with regard to the reduction of the objective function's value, and a convergence criterion [22–24]. Optimization algorithms can be categorized into two classes: global methods based on sampling the proposed values of parameters over the entire space, and local methods based on point estimation by finding the optimum point where no further progress can be achieved in the adjacent space of the parameter. Regarding the local methods, which are computationally efficient and need far fewer model runs, the initial values should be chosen carefully, as model calibration proceeds from this point towards the gradient descent of the objective function. If nonlinearity affects the model, there is no assurance that the inverse problem is unimodal, which means local methods can be simply trapped in local minima points instead

of finding the global minimum. Therefore, since the calibration process is strongly dependent on the initial starting point, it is required that the user continuously assesses results, adjusts starting values, and restarts the model [25–27]. “Equifinality”, as described by Beven [28,29], should also be considered regarding the automated calibration, which may propose the same model prediction by using different parameter sets (also see Straten and Keesman [30] for the term “equally possible” parameter sets). In other words, uncertainty-based calibration methods such as Generalized Likelihood Uncertainty Estimation (GLUE) [31–33] or the Metropolis–Hastings algorithm of Markov Chain Monte Carlo (MCMC) method [34], which sample different parameter combinations to produce a calibrated probability distribution, detect several feasible parameter sets, unlike the other methods, which focus on pinpointing a single optimal solution [35].

The performance of autocalibration techniques has been extensively studied for environmental models in the fields of hydrology and groundwater over several decades. However, in the field of fluvial hydraulics, there are relatively few studies available in the literature regarding the application of automated inverse methods for calibrating hydro-morphodynamic models [36–42]. In the present study, a 3D hydro-morphodynamic model of a 180° curved channel is developed according to a physical model and calibrated against the measured bed elevations of 54 points along different longitudinal and cross-sections. The model calibration is carried out with a local optimization method (Gauss–Marquardt–Levenberg method), using the Parameter ESTimation (PEST) package [43] and three population-based global optimization algorithms: Particle Swarm Optimization (PSO) [44], Shuffled Complex Evolution (SCE-UA) [45], and Covariance Matrix Adaptation Evolution Strategy (CMA-ES) [46]. The used methodology is further explained in Section 2. This work aims to evaluate the efficiency of the automatic calibration procedure based on the local optimization method as compared to the global methods, with the main objective of predicting a single set of optimal parameter values for the model, which is presented in Section 3.1. Further, in order to test the performance of the most efficient method, different experimental runs with various discharge rates are used to set up and calibrate additional models, presented in Section 3.2. Finally, the results are summarized and conclusions are presented in Section 4.

2. Methodology

2.1. Experimental Data

Yen and Lee [47] conducted a series of experiments to investigate the bed topography evolution and transverse sediment sorting in a 180° curved channel under unsteady flow conditions. The rectangular U-shaped channel measured 1 m in width and had a 4 m central radius. Two straight up- and downstream reaches measuring 11.5 m in length were attached to the bend to ensure uniform and fully turbulent flow. A 20 cm flat layer of nonuniform sand with a median diameter of $d_{50} = 1$ mm and a geometric standard deviation of $\sigma_g = 2.5$ was placed on the bed, having a final slope of 2‰. Further details regarding the sediment characteristics can be seen in Table 1, which also includes the fall velocity of particles calculated according to the empirical equation of Ferguson and Church [48], by assuming $\rho_s = 2650$ kg/m³ as the density of sediments. The base flow rate for all experiments was set to $Q_0 = 0.02$ m³/s, according to the incipient motion of sediment particles, with a flow depth of $h_0 = 5.44$ cm. During the experiments, the discharge was linearly increased up to a maximum value and then progressively lowered to the base flow discharge (triangular-shaped hydrograph). In total, five different experiments were conducted with different durations and peak discharge values.

Table 1. Sediment characteristics of the experiments that were applied in the numerical model.

	Sediment Size Classes							
	0.25	0.42	0.84	1.19	2.00	3.36	4.76	8.52
Size (mm)	0.25	0.42	0.84	1.19	2.00	3.36	4.76	8.52
Proportion (%)	6.55	10.56	25.36	15.06	20.11	13.02	4.88	4.46
Cumulative proportion (%)	6.55	17.11	42.47	57.53	77.64	90.66	95.54	100
Fall velocity (m/s)	0.03	0.06	0.11	0.14	0.20	0.26	0.32	0.43

2.2. Numerical Model

Due to the three-dimensional nature of the flow field in bends caused by the interaction of centrifugal force and the lateral pressure gradient, which results in a helical flow structure, the use of a 3D numerical model is imperative. In the present study, the fully three-dimensional numerical model SSIIM 2 (Sediment Simulation In Intakes with Multiblock option) [49] is employed to simulate hydraulics and morphological bed changes. This Computational Fluid Dynamics (CFD) code has been successfully used to model several cases with different scales in the fields of hydraulic and sedimentation engineering by many researchers [50–61]. The numerical model SSIIM 2 solves the Reynolds-averaged Navier–Stokes (RANS) equations together with the continuity equation (Equations (1) and (2)) on an adaptive three-dimensional non-orthogonal and unstructured grid, by using a finite volume approach for the spatial discretization and an implicit scheme for the temporal discretization to compute the water motion for turbulent flow.

$$\frac{\partial U_i}{\partial t} + U_j \frac{\partial U_i}{\partial x_j} = \frac{1}{\rho} \frac{\partial}{\partial x_j} (-P\delta_{ij} - \rho \overline{u_i u_j}) \quad (1)$$

$$\frac{\partial U_i}{\partial x_i} = 0 \quad i = 1, 2, 3 \quad (2)$$

where U is the averaged velocity over the time t ; x is the space direction; ρ is the water density; P is the dynamic pressure; δ_{ij} is the Kronecker delta, which can be either 1 if $i = j$ or 0 if $i \neq j$ [62]; and $-\rho \overline{u_i u_j}$ is the turbulent Reynolds stress term. Regarding the RANS equations, the convective term is modeled by using the second-order upwind (SOU) scheme [49]. The semi-implicit method for pressure-linked equations (SIMPLE) is used to evaluate the pressure term [63] by computing pressure-correction from the water continuity defect in a cell. The Reynolds stress term is computed by the concept of eddy viscosity with the standard k – ϵ turbulence model [64], using the Boussinesq approximation. The free water surface is calculated according to the computed pressure gradient using the Bernoulli equation [65]. A Dirichlet boundary condition is applied for the inflow and a zero gradient boundary condition is defined for variables at the outflow boundary. Wall laws for rough boundaries are used for the bed and the side walls [66].

The grid size is chosen according to a similar study by Fischer-Antze et al. [67], containing $254 \times 20 \times 5$ cells in streamwise, lateral, and vertical directions, respectively. The number of cells in the adaptive grid is adjusted during the computations according to the implemented wetting–drying algorithm [68]. Three different bedload transport formulae by Engelund-Hansen [69], van Rijn [70], and Wu [71] are used for the sediment transport computation. Using Wu’s correction factor, the hiding and exposure effect of nonuniform sediments is applied for the formulae by Engelund-Hansen and van Rijn, which by default do not consider the interaction between different size fractions in calculating the fractional transport rate of nonuniform sediments (i.e., they take the transport of each size individually into account).

2.3. Calibration Procedure

2.3.1. Local Optimization Method

The model-independent Parameter ESTimation tool (PEST) has been successfully used for calibration, sensitivity, and uncertainty analysis of environmental models in the fields of hydrology [72], groundwater [73], ecology and water quality [74–76], and flood modeling [77], providing promising results. PEST uses the gradient-based Gauss–Marquardt–Levenberg (GML) [78,79] algorithm for

nonlinear parameter estimation through iterative progress refinement and by employing the weighted sum of the squared residuals as the objective function (Equation (3)).

$$SSR = \sum_{i=1}^n w_i r_i^2 \quad (3)$$

where r is the residual, defined as the difference between model-generated bed levels and corresponding measured topographic elevation; and w is the weighting factor, which is considered to be 1 for all observations in this study.

The GML algorithm combines the gradient descent method (when the function is far from the minimum) with the Gauss–Newton algorithm (when the function is around the minimum), resulting in a fast and efficient convergence to the minimum of the objective function. PEST invokes the model by using the initial parameter values prespecified by the user. Through Taylor’s expansion of the actual parameter set, PEST linearizes the relationship between input parameters and model outputs. At the first iteration, according to the number of adjustable parameters, PEST runs the model several times and fills the Jacobian matrix containing the partial derivatives of each model output (i.e., filling the Jacobian matrix requires as many runs as the number of adjustable parameters). Subsequently, the upgrade vector is calculated (Equation (4)) with the aim of defining a damping factor, and parameters are changed within the user-defined bounds. This procedure is repeated for each iteration by using the updated values from the previous one until the minimum of the objective function is found.

$$u = (J^T Q J + \lambda I)^{-1} J^T Q r \quad (4)$$

where J is the ($n \times m$) Jacobian matrix, which has n columns according to the number of adjustable parameters and m rows following the number of model outputs; the superscript T stands for the transpose operator; Q is an ($m \times m$) diagonal weight matrix; λ is a damping parameter (i.e., Marquardt lambda), which is adjusted during each iteration; I is an ($n \times n$) identity matrix; and r is the vector of residuals for the current parameter set.

A reliable estimation of calibrated parameters in PEST highly depends on the predefined starting values. The reason is that in the case of getting trapped in a local minimum point on the objective function surface, the GML algorithm may not be able to leave this region. Therefore, in this study, the model calibration is done with four different initial parameter values for PEST to ensure its stability in finding the global minimum.

2.3.2. Global Optimization Methods

- The Shuffled Complex Evolution-University of Arizona (SCE-UA)

The SCE-UA method was initially developed for calibration of conceptual rainfall-runoff models [45], which uses a global optimization algorithm. The algorithm is based on the competitive evolution [80], the local direct search of downhill simplex method [81], a controlled random search [82], and the concept of complex shuffling. The optimization starts by sampling a population of randomly distributed points over the feasible parameter space and partitioning the points into several groups (complexes). Each complex contains $2n + 1$ points (n is the number of parameters to be optimized) and evolves independently to explore the domain in different directions, using the downhill simplex algorithm. Periodically, the population is shuffled and candidate solutions are reassigned to new complexes to share the information obtained from previous complexes during their evolution phase. The evolution and shuffling are progressively repeated until the convergence criterion is reached (i.e., the entire population moves gradually to converge towards the global minimum point). For more details about the algorithm see [83,84].

- Covariance Matrix Adaptation Evolution Strategy (CMA-ES)

CMA-ES is a derivative-free stochastic method for real-parameter optimization of nonlinear and nonconvex functions, using the general operators of evolution strategies, i.e., recombination, mutation, and selection. Each iteration (generation) is initiated by sampling a new population of individuals or candidate solutions from a multivariate normal search distribution. This is followed by the evaluation of individuals according to their performance measures and by updating the parameters of the multivariate normal distribution to guide the search towards the area with lower objective function values. The sequence of iterations is continued until a user-defined termination criterion is met. CMA-ES adapts the covariance matrix representing the pairwise dependencies between the variables in the distribution. The algorithm follows two principles for the parameter adaptation: (a) the maximum likelihood principle for updating the mean of the normal distribution in a way that the likelihood of previously successful candidate solutions is maximized; (b) using two evolution paths, one for the covariance matrix adaptation and the other one for adjusting the mutation strength (or the step size, which is defined as the standard deviation of the normal distribution). For a detailed description of the algorithm see [85].

- Particle Swarm Optimization (PSO)

The PSO algorithm, inspired by the social behavior of swarming animals (e.g., bird flocks or fish schools), is a metaheuristic stochastic global optimization approach. In this method, the search space is initialized with randomly positioned particles as potential solutions forming a swarm. Particles are composed of two vectors (position and velocity vectors) and move in random directions, keeping track of the best position (solution) found by themselves (having intelligence) and the one achieved by the whole swarm (with social interaction). The fitness of particles is measured by an objective function. In each generation, the velocity vector (reflecting the travel direction of particles across the search trajectory) is updated according to the previous best position of each particle (personal best or cognitive component) and that of the entire swarm population (global best or social component). Finally, the new position is computed with regard to the updated velocity. The process is iterated until a termination condition is satisfied [44,86].

2.3.3. Investigated Parameters

Among several uncertain input parameters in SSIIM 2 numerical model, the three most sensitive parameters are selected for calibration through a manual sensitivity analysis as follows:

1. *Roughness height at the bed (k_s):* For fixed beds, this parameter is typically assumed to be proportional to the representative grain size d_n (the diameter where $n\%$ of sediment grains are finer) (i.e., Nikoradse's equivalent grain roughness). For movable beds, however, the roughness caused by bedforms has to be added to the grain roughness, which may increase it with a higher factor than the grain roughness itself. A collection of different equations regarding the roughness height can be found in the literature (e.g., [87]). In this study, despite the dynamic nature of the roughness coefficient due to the formation of bedforms, the roughness height is considered to be uniform along the whole domain, because of the focus on the automatic calibration procedure. The range of this parameter is selected to be between d_{50} and $10d_{90}$.
2. *Active layer thickness (ALT):* This parameter is described as a function of the representative grain diameter and the bedform height as a dynamic value that depends on the sediment properties and the flow conditions. ALT determines the maximum depth of erosion during one time-step in the numerical model. For this study, a constant value of ALT is also chosen, with a range between d_{50} and $5d_{max}$ [88,89].
3. *The volume fraction of compacted sediments (VFS):* This parameter describes the proportion of deposited sediments in the bed compared to the water content, which depends on the bulk density as a function of grain size distribution and packing of sediment depositions. This parameter's range is adjusted between 40% and 60% in the calibration process.

2.4. Work Structure

Among the five experiments conducted by Yen and Lee [47], three different discharge rates—Run#1 (the highest discharge), Run#3 (the middle discharge), and Run#5 (the lowest discharge)—are used in this study for model calibration in order to cover different discharge characteristics. First, Run#5 is selected to test all of the optimization algorithms. Afterwards, the most efficient method is also applied for Run#1 and Run#3 to test the performance of the selected method. It should be mentioned that Run#1 and Run#3 show the formation of bedforms at the outer bend in the experimental setup. However, the employed numerical model in this study cannot precisely simulate the bedforms. Table 2 presents the features of the three applied hydrographs.

Table 2. Characteristics of the three hydrographs used in this study.

Run#	Peak Flow Discharge (m ³ /s)	Peak Flow Depth (cm)	Duration (min)
1	0.0750	12.9	180
3	0.0613	11.3	240
5	0.0436	9.10	420

3. Results and Discussion

3.1. Testing the Performance of Different Optimization Methods

In order to evaluate the performance of the four selected calibration methods, in the first step, the numerical model of Run#5 is calibrated as a test case, using Wu's bedload transport formula, which considers the fractional transport of nonuniform sediments. The initial values of the investigated parameters are defined for all methods to be: $k_s = d_{90}$, $ALT = d_{max}$, and $VFS = 50\%$. However, for ensuring the survival of the gradient-based method by using PEST from being trapped in a local minimum point, three additional starting values are also proposed as:

- PEST#2 ($k_s = d_{90}$, $ALT = 2d_{max}$, and $VFS = 55\%$)
- PEST#3 ($k_s = 2d_{90}$, $ALT = 4d_{max}$, and $VFS = 45\%$)
- PEST#4 ($k_s = 5d_{90}$, $ALT = 2d_{max}$, and $VFS = 50\%$)

Table 3 summarizes the values for the calibrated parameters obtained from the four PEST runs (four different starting conditions) and those obtained by the three global optimization methods. In addition, the minimum of the achieved objective function (sum of the squared residuals, *SSR*) and the number of models runs are presented in the table.

Table 3. Calibration results for the numerical model Run#5 by local and global optimization methods, using Wu's sediment transport formula.

Calibration Results	Calibration Method						
	PEST#1	PEST#2	PEST#3	PEST#4	SCE-UA	CMA-ES	PSO
k_s (cm)	0.904	0.894	0.899	0.903	0.898	0.892	0.904
ALT (cm)	1.639	1.644	1.629	1.638	1.635	1.631	1.647
VFS (%)	48.1	47.9	48.4	48	48.1	48.1	47.9
Minimum of <i>SSR</i> (cm)	0.28249	0.28251	0.28240	0.28249	0.28247	0.28247	0.28241
Number of model runs	26	30	28	27	176	440	448

Note: k_s , roughness height at the bed; ALT , active layer thickness; VFS , the volume fraction of compacted sediments; *SSR*, sum of the squared residuals.

According to the results presented in Table 3, PEST returns very similar outputs by using different initial values. This reveals that the software explored the whole parameter space and did not stick to a local minimum point. By comparing the results of PEST with the three global optimization

algorithms, a good agreement can be found between them regarding the calibrated parameter values, which proves the ability of PEST to calibrate the model globally by applying a local optimization algorithm. Nevertheless, by taking the number of model runs into account, considerably fewer runs are used by PEST, representing an advantage for the calibration of morphological models, for which long simulation time occurs.

3.2. Application of the Selected Calibration Method for Additional Numerical Setups

Based on its efficient performance in model calibration, PEST is selected to calibrate additional numerical models (i.e., Run#1, Run#3, and Run#5, with the sediment transport formulae of Wu, van Rijn, and Engelund-Hansen; nine model calibrations in total). From Table 4, which presents the calibration results for nine models, it can be seen that the active layer thickness (*ALT*), as well as the roughness height (k_s), gain higher values with increase of the flow discharge. It can be argued that the formation and evolution of bedforms along the channel bottom account for this effect.

Table 4. Calibrated values of the three selected parameters for nine simulations.

Calibration Parameters	Sediment Transport Formula								
	Wu			Van Rijn			Engelund-Hansen		
	Run#1	Run#3	Run#5	Run#1	Run#3	Run#5	Run#1	Run#3	Run#5
k_s (cm)	1.52	1.34	0.90	0.63	0.61	0.37	0.48	0.31	0.25
<i>ALT</i> (cm)	2.04	1.85	1.64	2.20	1.94	1.24	1.31	1.12	0.74
<i>VFS</i> (%)	49	51	48	60	60	60	52	51	53

The volume fraction of sediments (*VFS*) compared to the water volume is quite constant for the simulations using the formulae of Wu and Engelund-Hansen (around 50%). However, a value of 60% is found by employing the sediment transport formula of van Rijn, which corresponds to the upper predefined boundary for the search algorithm, indicating that the best solution for the optimization problem may lie outside the physically realistic bounds. As already mentioned, the selection of threshold values, between which the optimization algorithm adjusts parameters, should be taken according to a reasonable range for each parameter.

Figures 1–3 show longitudinal sections of the initial and final bed levels after Run#1 (the highest discharge), Run#3 (the mid discharge), and Run#5 (the lowest discharge), respectively. The results are presented along the sections: (a) 10 cm from the inner convex bank, (b) the central line, and (c) 10 cm from the outer concave bank.

In Run#1, according to the measurements, the maximum deposition occurs near the inner wall at the 75° cross-section, which is well predicted in terms of position and magnitude by the numerical model using the formula of Wu. The model using Engelund-Hansen's formula also predicts the location of this point at the same cross-section (75°), with just a minor discrepancy. Nevertheless, the model of van Rijn shows higher bed levels compared to the measurements. In this case, the position of the point bar is at the central cross-section (90°), having a slightly higher magnitude (Figure 1a). Along the central longitudinal-section (Figure 1b), the predicted patterns of bed elevations by all of the numerical models have a similar trend compared to the measurements, with a modest overestimation of the deposition for the last 40° range of the bend (140°–180°). Near the outer bend, the maximum scour depth in the experiment can be seen at the 165° cross-section, whereas the numerical models give this point at the 180° cross-section. In the second half of the bend (90°–180°), measurements show larger fluctuations caused by the development of bedforms compared to the smoother patterns obtained from the simulations (Figure 1c).

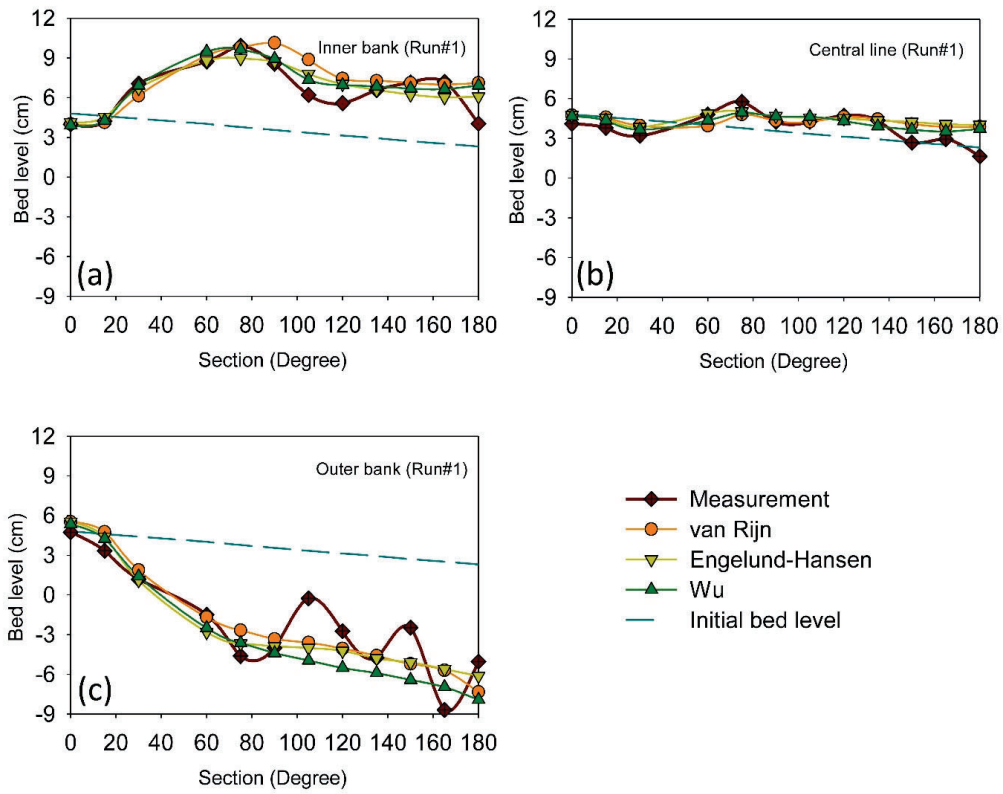


Figure 1. Initial and final bed levels of Run#1 along three longitudinal sections, (a) 10 cm from the inner bank, (b) the central line, and (c) 10 cm from the outer bank.

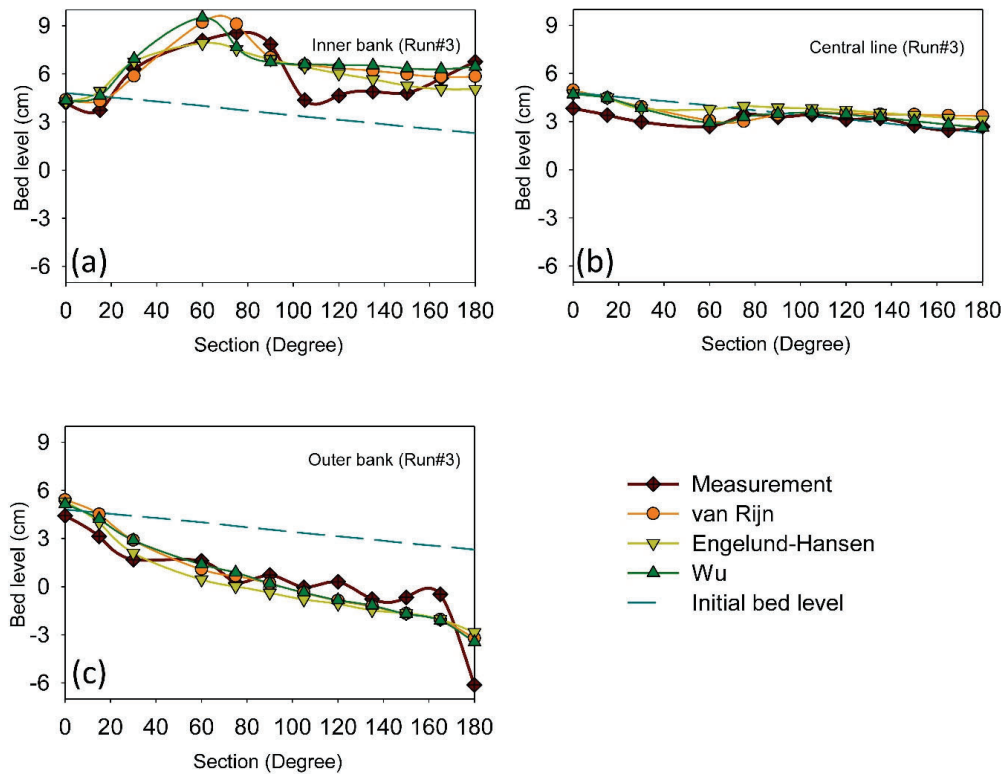


Figure 2. Initial and final bed levels of Run#3 along three longitudinal sections, (a) 10 cm from the inner bank, (b) the central line, and (c) 10 cm from the outer bank.

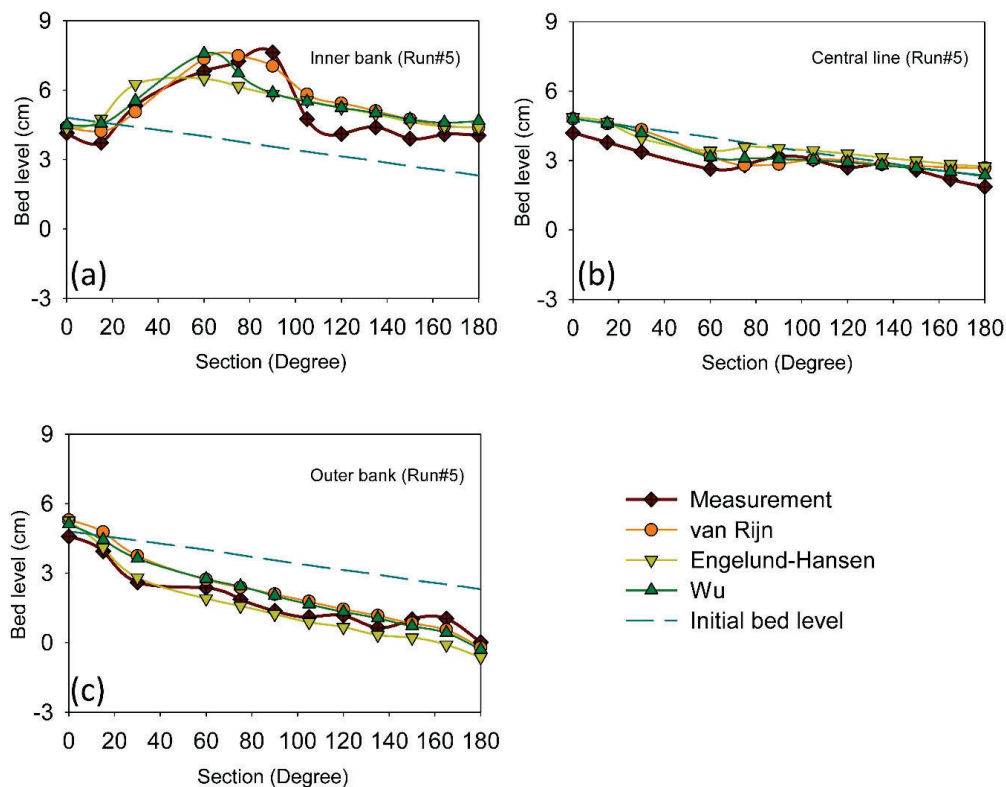


Figure 3. Initial and final bed levels of Run#5 along three longitudinal sections, (a) 10 cm from the inner bank, (b) the central line, and (c) 10 cm from the outer bank.

Regarding Run#3, near the inner bank, the maximum calculated deposition point is slightly shifted to the upstream compared to the experiment. The location of this point is at around 60° – 70° according to the numerical models, although measurements show it at about 75° (Figure 2a). Additionally, in the range of 90° – 160° , higher bed levels can be seen in the numerical models compared to the experiment. Along the central line (Figure 2b), numerical models marginally underpredict the erosion part up to the 60° cross-section. However, the overall patterns of the bed levels are similar to the experiment. Although having almost identical patterns near the outer bend (Figure 2c), a contrast can be found in the range of the last 30° of the bend between the simulations and measurements, especially the underestimation of the maximum erosion depth at the 180° cross-section.

In Run#5, similar to Run#3, the position of the maximum bed level near the inner wall (Figure 3a) is shifted further to the upstream in the numerical models. Here, the results of the model using Engelund-Hansen’s formula diverge largely from the measured data. Although showing some degree of underprediction regarding the erosion part up to the 60° cross-section, the simulated bed levels along the central line and near the concave bank are in good agreement with the experimental data (Figure 3b,c).

In Figure 4a–f, the cross-sectional bed profiles for all three runs are plotted at the locations of the maximum deposition height (Run#1: 75° ; Run#3: 75° ; Run#5: 90°) and the maximum scour depth (Run#1: 165° ; Run#3: 180° ; Run#5: 180°), according to the experiments. It can be seen that the results of the numerical models are in good agreement with the experimental data regarding the pattern and magnitude of the bed levels. However, the models using the formula of Engelund-Hansen are not successful in accurately predicting the steepness of the scour flank and its depth in the downstream part while increasing the discharge rate (compare Figure 4b,d,f).

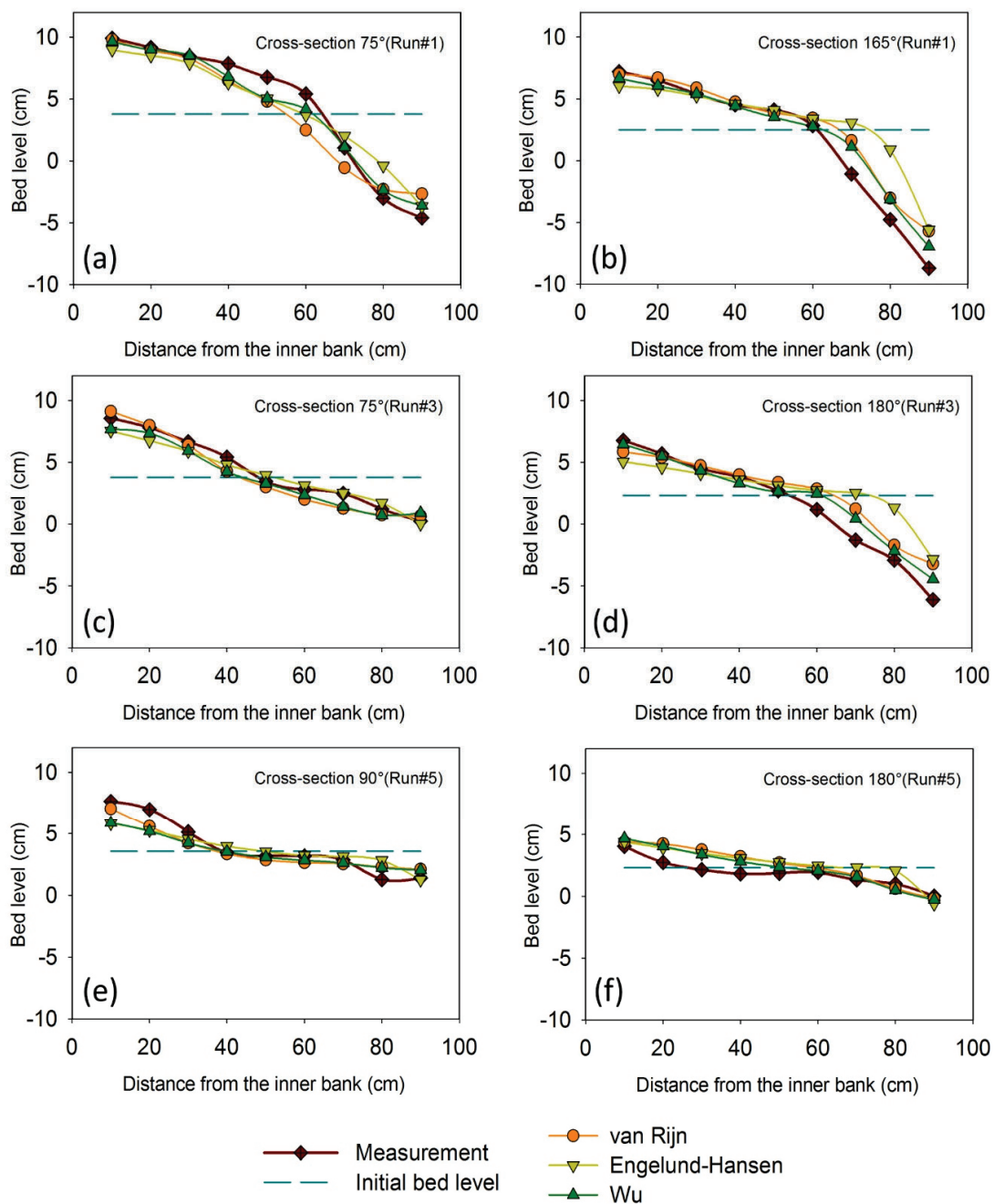


Figure 4. Cross-sectional bed levels for all runs in the maximum deposition (a,c,e) and erosion (b,d,f) sections according to the experiments.

According to Table 5, which presents the overall performance of the models based on the coefficient of determination (R^2) and the root mean squared error ($RMSE$) statistics, all three calibrated models using Wu’s formula have the best agreement with the observations, with R^2 values ranging between 0.89 and 0.95 and $RMSE$ values ranging between 0.67 cm and 1.49 cm. The simulation results with van Rijn’s formula show similar statistical performance as those obtained with Wu’s formula. Nevertheless, the results for the models using Engelund-Hansen’s formula have the lowest correlation and the highest error compared to the measured data.

Table 5. Goodness of fit for the calibrated models with different sediment transport formulae.

Goodness of Fit	Sediment Transport Formula								
	Wu			Van Rijn			Engelund-Hansen		
	Run#1	Run#3	Run#5	Run#1	Run#3	Run#5	Run#1	Run#3	Run#5
R^2 (-)	0.90	0.89	0.95	0.90	0.89	0.94	0.88	0.83	0.90
RMSE (cm)	1.49	1.04	0.67	1.57	1.08	0.69	1.63	1.33	0.81

Note: R^2 , the coefficient of determination; RMSE, the root mean squared error.

In Figure 5, the bed level changes normalized by the base water depth ($\Delta Z/h_0$, where $h_0 = 5.44$ cm) are presented for all runs using Wu’s formula (right side), and are compared with the experimental data (left side).

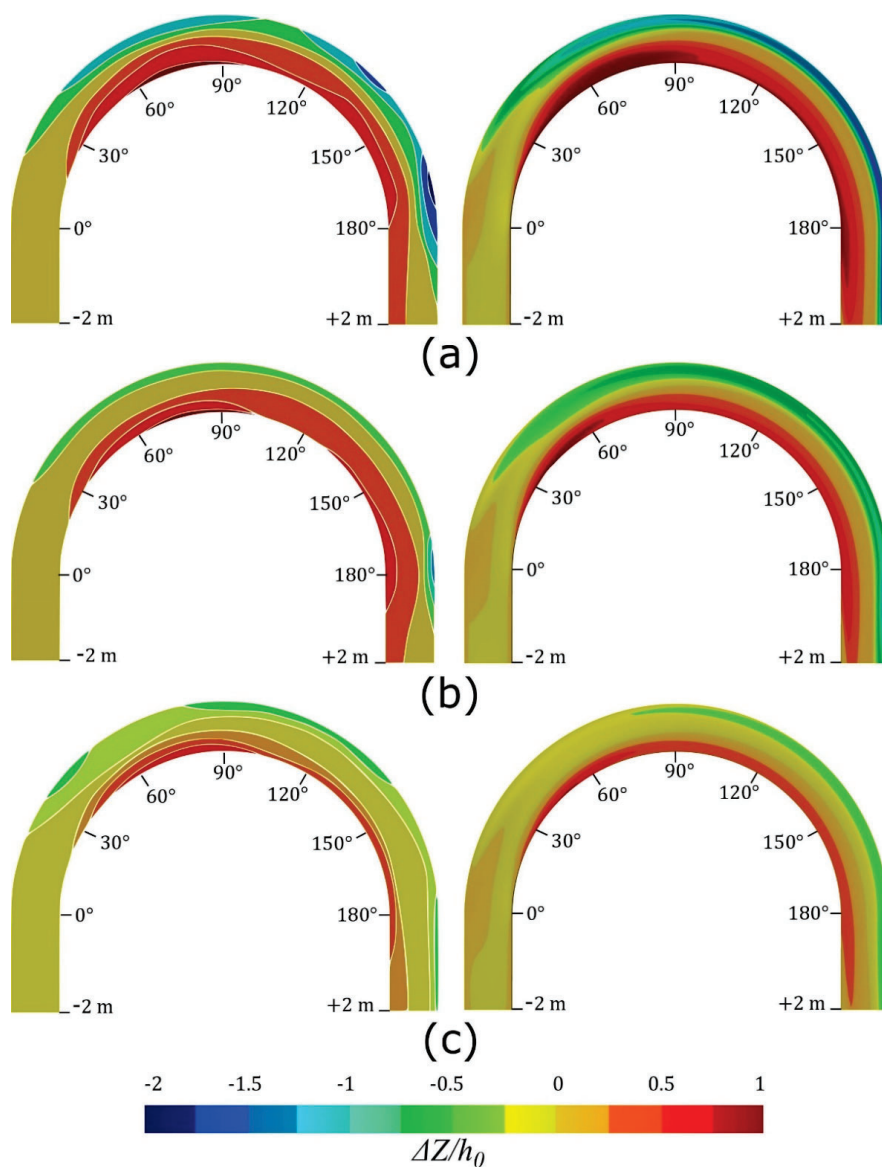


Figure 5. Plan view of the normalized bed deformations for (a) Run#1, (b) Run#3, and (c) Run#5, comparing the simulations (right) to the measurements (left).

4. Summary and Conclusions

In the present study, four different optimization methods (GML, SCE-UA, CMA-ES, and PSO) are employed for automatic calibration of a 3D morphodynamic numerical model of a 180° bend. Three input parameters, namely roughness height, active layer thickness, and the sediment volume compared to water at the bed, are selected for calibration, using their initial values and a reasonable range based on the literature. The results of the model calibration using all optimization methods (a local method and three global methods) show very similar calibrated values. All of the methods facilitate the calibration process by reducing the user intervention. However, considering the convergence speed, using the GML algorithm of PEST software is considerably more efficient compared to the other methods, as it needs far fewer model runs. Accordingly, PEST is selected for further investigation (In total, nine models are calibrated by using three different discharge rates and the sediment transport formulae of van Rijn, Wu, and Engelund-Hansen). Nonetheless, as PEST uses a gradient-based algorithm, it potentially involves a high risk of being trapped in a local minimum point over the search space rather than finding the global minimum. Therefore, the initial parameter values should be taken with care. It is also worthwhile reassessing the calibration procedure with different starting values to ensure that PEST finds the global minimum of the objective function. Moreover, characters and discontinuous values, which are defined in models (such as the selection of the sediment transport formula), cannot be processed by PEST and have to be adjusted manually.

The final bed levels predicted by the calibrated numerical models are compared with the measurements at various longitudinal and cross-sections. The overall capabilities of the numerical models are evaluated using the coefficient of determination and the root mean squared error statistics. It is concluded that the calibrated models using Wu's formula can predict the general characteristics of bed deformations (regions of deposition, erosion, and their magnitudes) better than the other two formulae by having the highest correlation and the lowest error between simulations and experimental data. The formula of van Rijn also gives reasonably acceptable results. However, the models which use the formula of Engelund-Hansen have the highest disagreement with the observations. It can also be mentioned that the bedforms, developed at the outer bend by increasing the discharge rate, cannot be accurately simulated by the numerical model. This effect is independent of the selection of the sediment transport formula and the calibration routine.

Author Contributions: Conceptualization, V.S., S.W., and S.H.; methodology, V.S. and S.H.; software, V.S.; validation, V.S., S.W., and S.H.; formal analysis, V.S. and S.H.; investigation, V.S., S.W., and S.H.; resources, V.S. and S.H.; data curation, V.S. and S.H.; writing—original draft preparation, V.S.; writing—review and editing, V.S., S.W., and S.H.; visualization, V.S.; supervision, S.W.; project administration, S.H. All authors have read and agreed to the published version of the manuscript.

Funding: This research received no external funding.

Acknowledgments: The first author received a Ph.D. scholarship from the German Federal Ministry of Education and Research (BMBF) through the German Academic Exchange Service (DAAD scholarship program NaWaM).

Conflicts of Interest: The authors declare no conflict of interest.

References

1. McIntyre, N.; Wheater, H.; Lees, M. Estimation and propagation of parametric uncertainty in environmental models. *J. Hydroinf.* **2002**, *4*, 177–198. [[CrossRef](#)]
2. Thomann, R.V. The future “golden age” of predictive models for surface water quality and ecosystem management. *J. Environ. Eng.* **1998**, *124*, 94–103. [[CrossRef](#)]
3. Cunge, J.A. Of data and models. *J. Hydroinf.* **2003**, *5*, 75–98. [[CrossRef](#)]
4. Oberkampf, W.L.; Trucano, T.G.; Hirsch, C. Verification, validation, and predictive capability in computational engineering and physics. *Appl. Mech. Rev.* **2004**, *57*, 345–384. [[CrossRef](#)]
5. Kleijnen, J.P.C. Verification and validation of simulation models. *Eur. J. Oper. Res.* **1995**, *82*, 145–162. [[CrossRef](#)]

6. Oreskes, N.; Shrader-Frechette, K.; Belitz, K. Verification, validation, and confirmation of numerical models in the earth sciences. *Science* **1994**, *263*, 641–646. [[CrossRef](#)]
7. Bahremand, A.; De Smedt, F. Distributed hydrological modeling and sensitivity analysis in Torysa Watershed, Slovakia. *Water Resour. Manag.* **2008**, *22*, 393–408. [[CrossRef](#)]
8. Muleta, M.K.; Nicklow, J.W. Sensitivity and uncertainty analysis coupled with automatic calibration for a distributed watershed model. *J. Hydrol.* **2005**, *306*, 127–145. [[CrossRef](#)]
9. Sargent, R.G. Verification and validation of simulation models. *J. Simul.* **2013**, *7*, 12–24. [[CrossRef](#)]
10. Oberkampf, W.L.; Trucano, T.G. Verification and validation benchmarks. *Nucl. Eng. Des.* **2008**, *238*, 716–743. [[CrossRef](#)]
11. Rebba, R.; Mahadevan, S.; Huang, S. Validation and error estimation of computational models. *Reliab. Eng. Syst. Saf.* **2006**, *91*, 1390–1397. [[CrossRef](#)]
12. Refsgaard, J.C.; Henriksen, H.J. Modelling guidelines—Terminology and guiding principles. *Adv. Water Resour.* **2004**, *27*, 71–82. [[CrossRef](#)]
13. Acuña, G.J.; Ávila, H.; Canales, F.A. River model calibration based on design of experiments theory. A case study: Meta River, Colombia. *Water* **2019**, *11*, 1382.
14. Troy, T.J.; Wood, E.F.; Sheffield, J. An efficient calibration method for continental-scale land surface modeling: Efficient calibration for large-scale land surface modeling. *Water Resour. Res.* **2008**. [[CrossRef](#)]
15. Hogue, T.S.; Sorooshian, S.; Gupta, H.; Holz, A.; Braatz, D. A multistep automatic calibration scheme for river forecasting models. *J. Hydrometeorol.* **2000**, *1*, 524–542. [[CrossRef](#)]
16. Madsen, H. Automatic calibration of a conceptual rainfall–runoff model using multiple objectives. *J. Hydrol.* **2000**, *235*, 276–288. [[CrossRef](#)]
17. Moradkhani, H.; Sorooshian, S. General review of rainfall–runoff modeling: Model calibration, data assimilation, and uncertainty analysis. In *Hydrological Modelling and the Water Cycle*; Sorooshian, S., Hsu, K.-L., Coppola, E., Tomassetti, B., Verdecchia, M., Visconti, G., Eds.; Springer: Berlin/Heidelberg, Germany, 2008; Volume 63, pp. 1–24.
18. Madsen, H.; Wilson, G.; Ammentorp, H.C. Comparison of different automated strategies for calibration of rainfall–runoff models. *J. Hydrol.* **2002**, *261*, 48–59. [[CrossRef](#)]
19. Boyle, D.P.; Gupta, H.V.; Sorooshian, S. Toward improved calibration of hydrologic models: Combining the strengths of manual and automatic methods. *Water Resour. Res.* **2000**, *36*, 3663–3674. [[CrossRef](#)]
20. Gupta, H.V.; Sorooshian, S.; Yapo, P.O. Status of automatic calibration for hydrologic models: Comparison with multilevel expert calibration. *J. Hydrol. Eng.* **1999**, *4*, 135–143. [[CrossRef](#)]
21. Botterweg, P. The user’s influence on model calibration results: An example of the model SOIL, independently calibrated by two users. *Ecol. Model.* **1995**, *81*, 71–81. [[CrossRef](#)]
22. Vidal, J.-P.; Moisan, S.; Faure, J.-B.; Dartus, D. River model calibration, from guidelines to operational support tools. *Environ. Model. Softw.* **2007**, *22*, 1628–1640. [[CrossRef](#)]
23. Vidal, J.-P.; Moisan, S.; Faure, J.-B.; Dartus, D. Towards a reasoned 1D river model calibration. *J. Hydroinf.* **2005**, *7*, 91–104. [[CrossRef](#)]
24. Madsen, H. Parameter estimation in distributed hydrological catchment modelling using automatic calibration with multiple objectives. *Adv. Water Resour.* **2003**, *26*, 205–216. [[CrossRef](#)]
25. Mugunthan, P.; Shoemaker, C.A.; Regis, R.G. Comparison of function approximation, heuristic, and derivative-based methods for automatic calibration of computationally expensive groundwater bioremediation models. *Water Resour. Res.* **2005**. [[CrossRef](#)]
26. Abbaspour, K.C.; Schulin, R.; van Genuchten, M.T. Estimating unsaturated soil hydraulic parameters using ant colony optimization. *Adv. Water Resour.* **2001**, *24*, 827–841. [[CrossRef](#)]
27. Finley, J.R.; Pintér, J.D.; Satish, M.G. Automatic model calibration applying global optimization techniques. *Environ. Model. Assess.* **1998**, *3*, 117–126. [[CrossRef](#)]
28. Beven, K. A manifesto for the equifinality thesis. *J. Hydrol.* **2006**, *320*, 18–36. [[CrossRef](#)]
29. Beven, K. Prophecy, reality and uncertainty in distributed hydrological modelling. *Adv. Water Resour.* **1993**, *16*, 41–51. [[CrossRef](#)]
30. Straten, G.T.V.; Keesman, K.J. Uncertainty propagation and speculation in projective forecasts of environmental change: A lake-eutrophication example. *J. Forecast.* **1991**, *10*, 163–190. [[CrossRef](#)]
31. Beven, K.; Binley, A. GLUE: 20 years on. *Hydrol. Process.* **2014**, *28*, 5897–5918. [[CrossRef](#)]

32. Beven, K.; Freer, J. Equifinality, data assimilation, and uncertainty estimation in mechanistic modelling of complex environmental systems using the GLUE methodology. *J. Hydrol.* **2001**. [[CrossRef](#)]
33. Beven, K.; Binley, A. The future of distributed models: Model calibration and uncertainty prediction. *Hydrol. Process.* **1992**, *6*, 279–298. [[CrossRef](#)]
34. Bates, B.C.; Campbell, E.P. A markov Chain Monte Carlo scheme for parameter estimation and inference in conceptual rainfall-runoff modeling. *Water Resour. Res.* **2001**, *37*, 937–947. [[CrossRef](#)]
35. Razavi, S.; Tolson, B.A.; Matott, L.S.; Thomson, N.R.; MacLean, A.; Seglenieks, F.R. Reducing the computational cost of automatic calibration through model preemption: Model preemption approach in automatic calibration. *Water Resour. Res.* **2010**. [[CrossRef](#)]
36. Meert, P.; Pereira, F.; Willems, P. Surrogate modeling-based calibration of hydrodynamic river model parameters. *J. Hydro. Environ. Res.* **2018**, *19*, 56–67. [[CrossRef](#)]
37. Deslauriers, S.; Mahdi, T.-F. Flood modelling improvement using automatic calibration of two dimensional river software SRH-2D. *Nat. Hazards* **2018**, *91*, 697–715. [[CrossRef](#)]
38. Evangelista, S.; Giovinco, G.; Kocaman, S. A multi-parameter calibration method for the numerical simulation of morphodynamic problems. *J. Hydrol. Hydromech.* **2017**, *65*, 175–182. [[CrossRef](#)]
39. Lavoie, B.; Mahdi, T.-F. Comparison of two-dimensional flood propagation models: SRH-2D and Hydro_AS-2D. *Nat. Hazards* **2017**, *86*, 1207–1222. [[CrossRef](#)]
40. McKibbin, J.; Mahdi, T.-F. Automatic calibration tool for river models based on the MHYSER software. *Nat. Hazards* **2010**, *54*, 879–899. [[CrossRef](#)]
41. Fabio, P.; Aronica, G.T.; Apel, H. Towards automatic calibration of 2-D flood propagation models. *Hydrol. Earth Syst. Sci.* **2010**, *14*, 911–924. [[CrossRef](#)]
42. Wasantha Lal, A.M. Calibration of riverbed roughness. *J. Hydraul. Eng.* **1995**, *121*, 664–671. [[CrossRef](#)]
43. Doherty, J. *PEST Model-Independent Parameter Estimation User Manual Part I*, 6th ed.; Watermark Numerical Computing: Brisbane, Australia, 2016.
44. Kennedy, J.; Eberhart, R. Particle swarm optimization. In Proceedings of the ICNN'95—International Conference on Neural Networks, Perth, WA, Australia, 27 November–1 December 1995; Volume 4, pp. 1942–1948.
45. Duan, Q.; Sorooshian, S.; Gupta, V. Effective and efficient global optimization for conceptual rainfall-runoff models. *Water Resour. Res.* **1992**, *28*, 1015–1031. [[CrossRef](#)]
46. Hansen, N.; Ostermeier, A. Adapting arbitrary normal mutation distributions in evolution strategies: The covariance matrix adaptation. In Proceedings of the IEEE International Conference on Evolutionary Computation, Nagoya, Japan, 20–22 May 1996.
47. Yen, C.; Lee, K.T. Bed topography and sediment sorting in channel bend with unsteady flow. *J. Hydraul. Eng.* **1995**, *121*, 591–599. [[CrossRef](#)]
48. Ferguson, R.I.; Church, M. A Simple universal equation for grain settling velocity. *J. Sediment. Res.* **2004**, *74*, 933–937. [[CrossRef](#)]
49. Olsen, N.R.B. *A Three Dimensional Numerical Model for Simulation of Sediment Movement in Water Intakes with Multiblock Option*; Department of Hydraulic and Environmental Engineering, The Norwegian University of Science and Technology: Trondheim, Norway, 2014.
50. Saam, L.; Mouris, K.; Wieprecht, S.; Haun, S. Three-dimensional numerical modelling of reservoir flushing to obtain long-term sediment equilibrium. In Proceedings of the 38th IAHR World Congress, Panama City, Panama, 1–6 September 2019.
51. Mouris, K.; Beckers, F.; Haun, S. Three-dimensional numerical modeling of hydraulics and morphodynamics of the Schwarzenbach reservoir. *E3s Web Conf.* **2018**, *40*, 03005. [[CrossRef](#)]
52. Esmaeili, T.; Sumi, T.; Kantoush, S.; Kubota, Y.; Haun, S.; Rütther, N. Three-dimensional numerical study of free-flow sediment flushing to increase the flushing efficiency: A case-study reservoir in Japan. *Water* **2017**, *9*, 900. [[CrossRef](#)]
53. Harb, G.; Haun, S.; Schneider, J.; Olsen, N.R.B. Numerical analysis of synthetic granulate deposition in a physical model study. *Int. J. Sediment Res.* **2014**, *29*, 110–117. [[CrossRef](#)]
54. Haun, S.; Kjærås, H.; Løvfall, S.; Olsen, N.R.B. Three-dimensional measurements and numerical modelling of suspended sediments in a hydropower reservoir. *J. Hydrol.* **2013**, *479*, 180–188. [[CrossRef](#)]
55. Haun, S.; Olsen, N.R.B. Three-dimensional numerical modelling of the flushing process of the Kali Gandaki hydropower reservoir. *Lakes Reserv. Sci. Policy Manag. Sustain. Use* **2012**, *17*, 25–33. [[CrossRef](#)]

56. Haun, S.; Olsen, N.R.B.; Feurich, R. Numerical modeling of flow over trapezoidal broad-crested weir. *Eng. Appl. Comput. Fluid Mech.* **2011**, *5*, 397–405. [[CrossRef](#)]
57. Wilson, C.A.M.E.; Yagci, O.; Rauch, H.-P.; Olsen, N.R.B. 3D numerical modelling of a willow vegetated river/floodplain system. *J. Hydrol.* **2006**, *327*, 13–21. [[CrossRef](#)]
58. Rütther, N.; Olsen, N.R. Three-dimensional modeling of sediment transport in a narrow 90° channel bend. *J. Hydraul. Eng.* **2005**, *131*, 917–920. [[CrossRef](#)]
59. Olsen, N.R.B. Three-dimensional CFD modeling of self-forming meandering channel. *J. Hydraul. Eng.* **2003**, *129*, 366–372. [[CrossRef](#)]
60. Booker, D.J. Hydraulic modelling of fish habitat in urban rivers during high flows. *Hydrol. Process.* **2003**, *17*, 577–599. [[CrossRef](#)]
61. Wilson, C.A.M.E.; Boxall, J.B.; Guymmer, I.; Olsen, N.R.B. Validation of a three-dimensional numerical code in the simulation of pseudo-natural meandering flows. *J. Hydraul. Eng.* **2003**, *129*, 758–768. [[CrossRef](#)]
62. Versteeg, H.K.; Malalasekera, W. *An Introduction to Computational Fluid Dynamics: The Finite Volume Method*, 2nd ed.; Pearson Education Ltd.: Harlow, UK, 2007.
63. Patankar, S.V. *Numerical Heat Transfer and Fluid Flow*; McGraw-Hill: New York, NY, USA, 1980.
64. Rodi, W. *Turbulence Models and Their Application in Hydraulics*, 1st ed.; Routledge: Rotterdam, The Netherlands, 1993.
65. Olsen, N.R.B.; Haun, S. Free surface algorithms for 3D numerical modelling of reservoir flushing. In Proceedings of the River flow 2010, Federal Waterways Engineering and Research Institute (BAW), Braunschweig, Germany, 8–10 September 2010; Volume 2010, pp. 1105–1110.
66. Schlichting, H. *Boundary Layer Theory*; McGraw-Hill: New York, NY, USA, 1979.
67. Fischer-Antze, T.; Rütther, N.; Olsen, N.R.B.; Gutknecht, D. Three-dimensional (3D) modeling of non-uniform sediment transport in a channel bend with unsteady flow. *J. Hydraul. Res.* **2009**, *47*, 670–675. [[CrossRef](#)]
68. Haun, S.; Olsen, N.R.B. Three-dimensional numerical modelling of reservoir flushing in a prototype scale. *Int. J. River Basin Manag.* **2012**, *10*, 341–349. [[CrossRef](#)]
69. Engelund, F.; Hansen, E. *A Monograph on Sediment Transport in Alluvial Streams*; Teknisk Forlag: Copenhagen, Denmark, 1967.
70. Van Rijn, L.C. Sediment transport, part I: Bed load transport. *J. Hydraul. Eng.* **1984**, *110*, 1431–1456. [[CrossRef](#)]
71. Wu, W.; Wang, S.S.Y.; Jia, Y. Nonuniform sediment transport in alluvial rivers. *J. Hydraul. Res.* **2000**, *38*, 427–434. [[CrossRef](#)]
72. Soltani, M.; Laux, P.; Mauder, M.; Kunstmann, H. Inverse distributed modelling of streamflow and turbulent fluxes: A sensitivity and uncertainty analysis coupled with automatic optimization. *J. Hydrol.* **2019**, *571*, 856–872. [[CrossRef](#)]
73. Usman, M.; Reimann, T.; Liedl, R.; Abbas, A.; Conrad, C.; Saleem, S. Inverse parametrization of a regional groundwater flow model with the aid of modelling and GIS: Test and application of different approaches. *ISPRS Int. J. Geo. Inf.* **2018**, *7*, 22. [[CrossRef](#)]
74. Nécipalová, M.; Anex, R.P.; Fienen, M.N.; Del Grosso, S.J.; Castellano, M.J.; Sawyer, J.E.; Iqbal, J.; Pantoja, J.L.; Barker, D.W. Understanding the DayCent model: Calibration, sensitivity, and identifiability through inverse modeling. *Environ. Model. Softw.* **2015**, *66*, 110–130. [[CrossRef](#)]
75. Rode, M.; Suhr, U.; Wriedt, G. Multi-objective calibration of a river water quality model—Information content of calibration data. *Ecol. Model.* **2007**, *204*, 129–142. [[CrossRef](#)]
76. Baginska, B.; Milne-Home, W.; Cornish, P.S. Modelling nutrient transport in Currency Creek, NSW with AnnAGNPS and PEST. *Environ. Model. Softw.* **2003**, *18*, 801–808. [[CrossRef](#)]
77. Liu, C.; Batelaan, O.; Smedt, F.D.; Poórová, J.; Velcická, L. Automated calibration applied to a GIS-based flood simulation model using PEST. In *Floods, from Defence to Management*; van Alphen, J., van Beek, E., Taal, M., Eds.; Taylor-Francis Group: London, UK, 2005; pp. 317–326.
78. Marquardt, D.W. An algorithm for least-squares estimation of nonlinear parameters. *J. Soc. Ind. Appl. Math.* **1963**, *11*, 431–441. [[CrossRef](#)]
79. Levenberg, K. A method for the solution of certain nonlinear problems in least squares. *Q. Appl. Math.* **1944**, *2*, 164–168. [[CrossRef](#)]
80. Holland, J.H. *Adaptation in Natural and Artificial Systems: An Introductory Analysis with Applications to Biology, Control and Artificial Intelligence*; MIT Press: Cambridge, MA, USA, 1992.
81. Nelder, J.A.; Mead, R. A simplex method for function minimization. *Comput. J.* **1965**, *7*, 308–313. [[CrossRef](#)]

82. Price, W.L. Global optimization algorithms for a CAD workstation. *J. Optim. Theory Appl.* **1987**, *55*, 133–146. [[CrossRef](#)]
83. Duan, Q.; Sorooshian, S.; Gupta, V.K. Optimal use of the SCE-UA global optimization method for calibrating watershed models. *J. Hydrol.* **1994**, *158*, 265–284. [[CrossRef](#)]
84. Duan, Q.Y.; Gupta, V.K.; Sorooshian, S. Shuffled complex evolution approach for effective and efficient global minimization. *J. Optim. Theory Appl.* **1993**, *76*, 501–521. [[CrossRef](#)]
85. Hansen, N. The CMA evolution strategy: A tutorial. *arXiv* **2016**, arXiv:1604.00772.
86. Shi, Y.; Eberhart, R.C. Parameter selection in particle swarm optimization. In *Evolutionary Programming VII*; Porto, V.W., Saravanan, N., Waagen, D., Eiben, A.E., Eds.; Springer: Berlin/Heidelberg, Germany, 1998; pp. 591–600.
87. García, M.H. *Sedimentation Engineering: Processes, Measurements, Modeling, and Practice*; Environmental and Water Resources Institute (EWRI), ASCE Manuals and Reports on Engineering Practice, American Society of Civil Engineers: Reston, VA, USA, 2008.
88. Hunziker, R.P. *Fraktionsweiser Geschiebetransport*. Ph.D. Thesis, ETH, Zurich, Switzerland, 1995.
89. Malcherek, A. *Sedimenttransport und Morphodynamik*; Scriptum Institut für Wasserwesen, Bundeswehr University Munich: Munich, Germany, 2007.



© 2020 by the authors. Licensee MDPI, Basel, Switzerland. This article is an open access article distributed under the terms and conditions of the Creative Commons Attribution (CC BY) license (<http://creativecommons.org/licenses/by/4.0/>).

Appendix II

Applying optimization methods for automatic calibration of 3D morphodynamic numerical models of shallow reservoirs: comparison between lozenge- and hexagon- shaped reservoirs

Table 5.2. Metadata of Publication II

Title	Applying optimization methods for automatic calibration of 3D morphodynamic numerical models of shallow reservoirs: comparison between lozenge- and hexagon-shaped reservoirs
Authors	Vahid Shoarinezhad, Silke Wieprecht, Sameh Ahmed Kantoush, Stefan Haun
Journal	Journal of Hydroinformatics
Submitted	28 June 2022
Accepted	02 November 2022
Published	15 November 2022
DOI	https://doi.org/10.2166/hydro.2022.094

Applying optimization methods for automatic calibration of 3D morphodynamic numerical models of shallow reservoirs: comparison between lozenge- and hexagon-shaped reservoirs

Vahid Shoarinezhad ^{a,*}, Silke Wieprecht ^a, Sameh Ahmed Kantoush ^b and Stefan Haun ^a

^a Institute for Modeling Hydraulic and Environmental Systems (IWS), University of Stuttgart, Stuttgart 70569, Germany

^b Disaster Prevention Research Institute (DPRI), Kyoto University, Uji, Kyoto 611-0011, Japan

*Corresponding author. E-mail: vahid.shoarinezhad@iws.uni-stuttgart.de

 VS, 0000-0002-0647-7032; SW, 0000-0001-6776-2446; SAK, 0000-0003-0919-5097; SH, 0000-0002-8202-4633

ABSTRACT

Understanding the complexity of the siltation process and sediment resuspension in shallow reservoirs is vital for maintaining the reservoir functionality and implementing sustainable sediment management strategies. The geometry of reservoirs plays an indispensable role in the appearance of various flow structures inside the basin and, consequently, the pattern of the morphological evolution. In this study, a three-dimensional numerical model, coupled with optimization algorithms, is used to investigate the morphological bed changes in two symmetric shallow reservoirs having hexagon and lozenge shapes. This work aims to evaluate the applicability, efficiency, and accuracy of the automatic calibration routine, which can be a suitable replacement for the time-consuming and subjective method of manual model calibration. In this regard, two sensitive parameters (i.e., roughness height and sediment active layer thickness) are assessed. The goodness-of-fit between the calculated bed levels and the measured topography from physical models are presented by different statistical metrics. From the results, it can be concluded that the automatically calibrated models are in reasonable agreement with the observations. Employing a suitable optimization algorithm, which finds the best possible combination of investigated parameters, can considerably reduce the model calibration time and user intervention.

Key words: 3D hydro-morphodynamic models, automatic model calibration, parameter estimation, reservoir sedimentation, shallow reservoirs

HIGHLIGHTS

- The flow structure and sedimentation pattern in symmetric expansions are numerically studied.
- Local (GML) and a global (BB-BC) optimization algorithms are used to calibrate the numerical models of two symmetric shallow reservoirs.
- GML outperforms BB-BC considering the convergence speed (efficiency) without trapping in local minima by having the same predicted parameter values (robustness).

1. INTRODUCTION

As general multi-purpose hydraulic structures, shallow reservoirs are used in different fields, serving as sediment and pollutant trapping tanks, retention ponds, water storage basins, and also for aquafarming (Dewals *et al.* 2020). Depending on several factors, such as geometrical aspects (i.e., expansion ratio: reservoir width/inlet width; and aspect ratio: reservoir length/reservoir width), hydraulic and boundary conditions, and sediment properties, the velocity field inside a reservoir emerges with various configurations, influencing the sedimentation along the basin. In turn, deposited sediments can further modify the flow pattern (Kantoush 2008; Dufresne *et al.* 2012). The flow behavior in shallow reservoirs, such that the horizontal dimensions are considerably larger than the water depth, can be considered a condition in which the flow passes through a narrow inlet channel into a sudden or moderate expanded basin. Thus, the flow field involves an entering jet associated with large-scale 2D horizontal coherent turbulent structures and recirculation zones, controlling the mass and momentum exchange. In addition, the flow field in symmetric expansions is specified by symmetry-breaking bifurcation

under certain conditions. The importance of this behavior in engineering applications has been a subject of interest among many researchers in the field of fluid dynamics (Fani *et al.* 2012).

A comprehensive experimental study of laminar flow through a planar symmetric sudden expansion dates back to Durst *et al.* (1974), who found that the Reynolds number (Re) strictly governs the flow structure. They defined a critical Re value, beyond which the flow tends to become asymmetric. Cherdron *et al.* (1978) performed a similar study and confirmed that the reason for asymmetric flow formation lies in disturbances generated at the edge of the expansion, which amplify in the shear layers. Sobey & Drazin (1986) investigated the instabilities and bifurcation of flow in slight expansions by asymptotic analysis, numerical methods, and laboratory experiments. Shapira *et al.* (1990) carried out a linear stability analysis of symmetric flow considering different angles at the expansion section. A numerical and experimental investigation of the flow field in a symmetric expansion, indicating a symmetry-breaking (pitchfork) bifurcation point, was published by Fearn *et al.* (1990). They introduced a slight asymmetry in the inlet channel in their numerical model to reproduce the imperfections, which are inevitable in physical models. This small perturbation was also considered by Hawa & Rusak (2000). The effect of different expansion ratios on the occurrence of non-symmetrical flow regimes in symmetric sudden expansions was studied by Drikakis (1997). Many other researchers investigated the discussed phenomenon (i.e., the transition of the symmetric flow into the asymmetric state) in sudden expansions (e.g., Mizushima *et al.* 1996; Sarma *et al.* 2000; Quaini *et al.* 2016). The main focus of these studies is on determining a threshold for the critical Reynolds number as the bifurcation initiating factor and the effect of geometrical aspects on the flow structure.

In contrast to extensive investigations of laminar flow behavior downstream of sudden expansions, relatively limited studies exist about turbulent flow configurations (Escudier *et al.* 2002). As one of the earliest studies, Abbott & Kline (1962) experimentally investigated the turbulent flow through a symmetric plane sudden expansion. They noticed two same-length recirculation zones with a predominant central plane jet after the expansion. However, when the expansion ratio was increased, the asymmetric pattern was observed with two disproportionate recirculation regions by the deflection of the main jet toward one of the walls. They claimed that the reattachment length highly depends on the expansion ratio and is not sensitive to the Reynolds number value (turbulence intensity). Similar results were obtained by Mehta (1981), arguing the insensitivity of the asymmetric pattern for a range of high Reynolds numbers. Among other related studies on turbulent flow through symmetric expansions, the laboratory experiments of Casarsa & Giannattasio (2008) and the numerical simulations by De Zilwa *et al.* (2000) are worth mentioning. Most of these studies report the formation of the asymmetric flow pattern as a function of the expansion ratio.

Narrowing down the discussed phenomenon to shallow reservoirs, Kantoush (2008) and Kantoush *et al.* (2008a, 2008b) performed a comprehensive series of systematic investigations of the flow field with suspended sediments inside different geometries with suddenly expanded regions experimentally and numerically. They studied the effect of reservoir geometry alteration on the flow field, the silting process pattern, and the reservoir trap efficiency. The primary conclusion of these works is that an asymmetric flow pattern appears in symmetric geometries under certain conditions, affecting the process of suspended sediment transport and adjusting the spatial distribution of sediment deposits. Furthermore, the accumulation of deposited sediments due to the additional sediment supply can, in turn, alter the flow pattern. Regarding the related experimental studies in this field, Dufresne *et al.* (2010) classified flow patterns in shallow rectangular reservoirs into four stable categories. They found a symmetric flow pattern containing a straight jet from the inlet to the outlet with two equal-size recirculation zones at the sides for short-length reservoirs (called S_0 type) and three asymmetric patterns with one, two, or three reattachment points (A_1 , A_2 , and A_3) with unequal recirculation regions, depending on the length of the basin, for long-length reservoirs. In reservoirs with intermediate length, an unstable flow field was also identified (S_0/A_1), in which the flow randomly oscillates between the symmetric (S_0) and asymmetric (A_1) patterns. They investigated the effects of dimensionless length and flow depth, lateral expansion ratio, and the Froude number on the median reattachment lengths and defined a shape factor to predict the flow behavior based on the geometric aspects. Similar experimental results to those of Kantoush (2008) were obtained by Camnasio *et al.* (2011), who categorized the flow field inside shallow rectangular reservoirs into a channel-like (CH-L) type for reservoirs with very short width, two symmetric (S_0 and S_1), and two asymmetric (A_1 and A_2) stable types, based on the reservoir expansion and aspect ratios.

Regarding the numerical assessment of the flow behavior in rectangular shallow basins, 2D models using the shallow water equations were employed by Dewals *et al.* (2008) and Dufresne *et al.* (2011). On the other hand, the use of 3D numerical models, employing the Reynolds-averaged Navier–Stokes equations, can be found in Esmaeili *et al.* (2016) and Lakzian *et al.* (2020). Numerical models of symmetric expanding channels are complicated cases where the entering jet can randomly

follow one side of the reservoir. It means that for such cases, multiple solutions for the Navier–Stokes equations can exist, where the presence of an obstacle (deposited sediments), the grid resolution, discretization schemes, and the turbulence model may cause the convergence of the equations with a different flow direction. Hence, in contrast to the extensively studied rectangular geometries, we investigated the performance of a fully 3D numerical model (SSIIM) coupled with an automatic calibration tool (PEST) to evaluate the morphological bed changes in two shallow reservoirs having hexagon and lozenge shapes. The reservoirs are selected based on available high-resolution measurements for calibration and to test the automatic model calibration for cases with complicated flow behavior. Since PEST uses a gradient-based local optimization algorithm, to confirm its ability in finding the global optimum point over the search space and avoid the local minima, the models are also calibrated by a global optimization algorithm.

Due to the fact that hydro-morphodynamic models involve a series of physically unmeasurable parameters, their accuracy and reliability highly depend on the calibration process, which means the adjustment of uncertain input parameters to minimize the misfit between simulation results and corresponding physical measurements. Generally, the calibration of such models has been manually carried out through trial-and-error parameter adjustments based on the user's understanding of the model structure and features of the environmental system until a satisfactory agreement between simulated and measured values can be achieved. By having multiple parameters for manual calibration, the typical way is to consider each parameter separately for tuning by keeping the others constant. The procedure can then be repeated for the rest of the parameters one at a time. However, in reality, the combination of the best values of every single parameter may not result in the overall best fit. Thus, having a complicated model with several uncertain input parameters, the manual calibration method becomes cost- and time-consuming, involving a high degree of subjectivity. Nevertheless, employing optimization algorithms is an ingenious approach to the model fitting process. The application of automatic model calibration in different fields of environmental studies, such as hydrologic or groundwater models, has gained popularity over the last four decades; however, there is a considerable gap in applying automatic calibration in hydro-morphodynamic studies. This work aims to evaluate the efficiency and accuracy of automatic model calibration based on mathematical optimization, which can be an innovative practice to overcome the time-consuming and subjective nature of manual model calibration.

2. MATERIALS AND METHODS

2.1. Experimental data

The experimental data obtained by Kantoush (2008) are used to set up the numerical models and calibrate them against measured bed levels. As an outline of the experimental work, a reference rectangular shallow reservoir with 4.0 m of width, 6.0 m of length, and 0.3 m of depth was constructed at the Laboratory of Hydraulic Constructions (LCH) of the Swiss Federal Institute of Technology (EPFL). There were up- and downstream rectangular channels centrally connected to the reservoir with 0.25 m of width and 1.0 m of length. The walls were made of movable PVC plates, which could be adjusted to create different geometrical shapes. The water-sediment mixture was supplied from a mixing tank into the basin by gravity. The thickness of deposited sediments was measured by a mini echo sounder. Fine ground non-uniform walnut shells were used as sediment particles with a median diameter of $d_{50} = 50 \mu\text{m}$, a geometric standard deviation of particle size gradation of $\sigma_g = \sqrt{d_{84}/d_{16}} = 2.4$, a density of $\rho_s = 1.5 \text{ g/cm}^3$, and an average entrance concentration of $C = 3.0 \text{ g/l}$. Further details regarding the sediment characteristics can be found in Table 1. The discharge rate was constant during different experiments with a value of $Q = 7 \text{ l/s}$ and a corresponding water depth of $h = 0.2 \text{ m}$, which was adjusted by a flap gate at the outlet.

Table 1 | Sediment characteristics used for numerical modeling

	Sediment size classes						
Size (mm)	0.025	0.03	0.05	0.06	0.09	0.125	0.28
Proportion (%)	20	10	20	10	20	10	10
Cumulative proportion (%)	20	30	50	60	80	90	100
Fall velocity (mm/s)	0.2	0.25	0.7	1	2	4.2	20

Among the several investigated reservoir shapes in the laboratory, we used two configurations, lozenge and hexagon (Figure 1), for numerical modeling. The sediment feeding was done in four steps with different periods (3×1.5 hrs + 1×3 hrs for the lozenge-shaped reservoir, and 3×1.5 hrs + 1×4.5 hrs for the hexagonal reservoir). Furthermore, for both cases, the Froude number was small (0.1), and the Reynolds number was high enough (28,000) at the inlet to ensure subcritical, fully developed turbulent flow conditions.

2.2. Numerical modeling

Kantoush (2008) indicated three-dimensional flow characteristics in shallow reservoirs (i.e., the presence of secondary currents and 3D stretching vortices). As long as the effect of secondary currents, generated by the streamline curvature in recirculation zones, could be excluded (such as studying the flow field without considering sediments), using 2D numerical models is reasonable. However, such models cannot directly simulate the 3D effect of secondary currents and their contribution to sedimentation. Although such flows are weaker compared to the primary flow, their role becomes significant in morphological studies with suspended sediment transport and the presence of bedforms. Accordingly, 3D numerical models can provide a more precise assessment of morphological processes in shallow reservoirs (Esmaceli *et al.* 2017). In this work, the fully three-dimensional numerical model SSIIM 2 (Sediment Simulation In Intakes with Multiblock option) (Olsen 2014) is used for hydro-morphodynamic simulations, which has been proven to yield reliable results in the field of reservoir sedimentation/flushing studies (Haun & Olsen 2012; Hillebrand *et al.* 2017; Mohammad *et al.* 2020). This software solves the Reynolds-averaged Navier–Stokes (RANS) equations together with the continuity equation (Equations (1) and (2)). SSIIM 2 generates an adaptive, unstructured, three-dimensional, non-orthogonal grid. The adaptive grid refinement in SSIIM 2 is based on the calculated free water surface and bed level changes resulting from the implemented wetting/drying algorithm. This algorithm calculates the number of cells that can be generated in the vertical direction after each time step as the function of the water depth so that the computational domain changes spatiotemporally and can be adjusted for the next time step. The finite-volume approach is used as the spatial discretization scheme, while an implicit scheme is employed for the

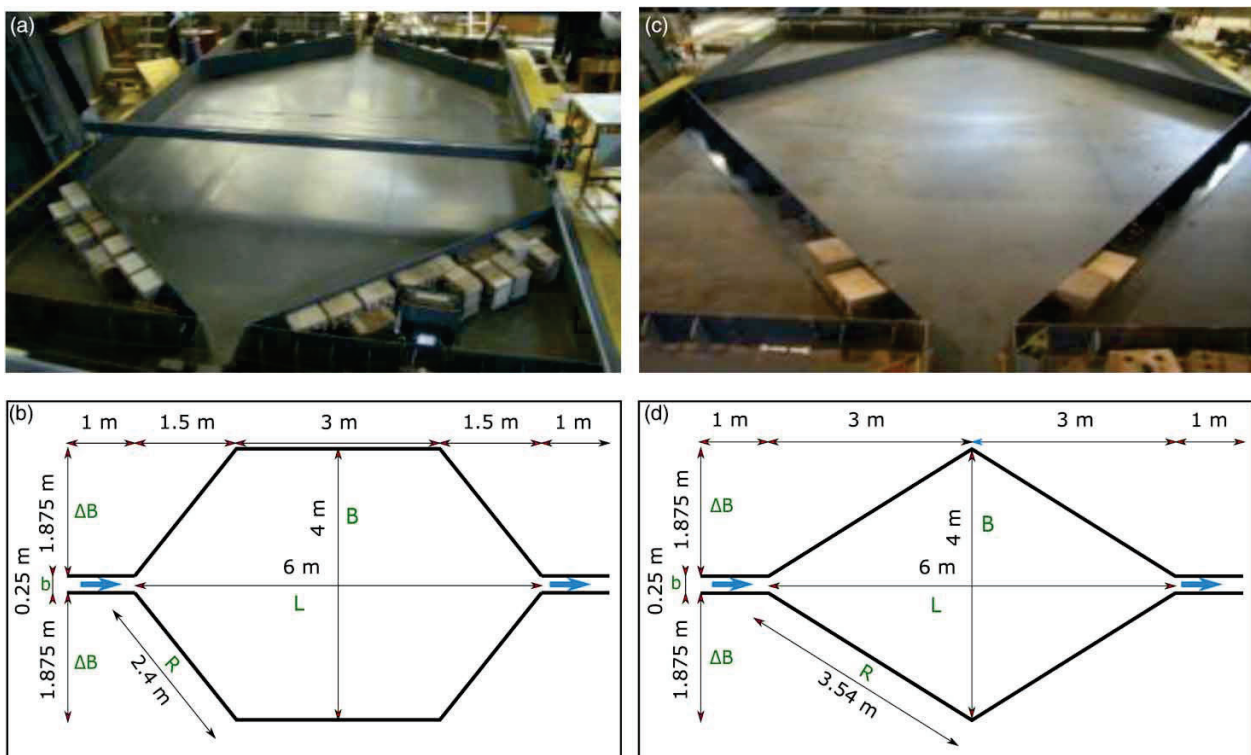


Figure 1 | Photos of the physical models and their sketched plan views for (a and b) hexagonal and (c and d) lozenge-shaped reservoirs.

temporal discretization.

$$\frac{\partial U_i}{\partial t} + U_j \frac{\partial U_i}{\partial x_j} = \frac{1}{\rho} \frac{\partial}{\partial x_j} (-P \delta_{ij} - \rho \overline{u_i u_j}) \quad (1)$$

$$\frac{\partial U_i}{\partial x_i} = 0 \quad i = 1, 2, 3 \quad (2)$$

where U represents the averaged velocity over the time t , x is the space coordinate, ρ is the water density, P is the dynamic pressure, δ_{ij} denotes the Kronecker delta (equal to 1 if $i = j$, or 0 if $i \neq j$), and $-\rho \overline{u_i u_j}$ indicates the turbulent Reynolds stress term. This term is calculated according to Boussinesq's approximation with the concept of eddy viscosity and by applying the standard k - ε model for turbulence closure (Equations (3) and (4)).

$$-\overline{u_i u_j} = \nu_T \left(\frac{\partial U_i}{\partial x_j} + \frac{\partial U_j}{\partial x_i} \right) - \frac{2}{3} k \delta_{ij} \quad (3)$$

$$\nu_T = \frac{c_\mu k^2}{\varepsilon} \quad (4)$$

Turbulent eddy-viscosity ν_T can be determined by turbulent kinetic energy k , turbulent dissipation ε , and a dimensionless constant c_μ equal to 0.09. Regarding the other terms of the RANS equations, the pressure term is handled by the semi-implicit method for pressure-linked equations, and the convective term is modeled by the second-order upwind scheme. The free water surface is calculated based on the computed pressure gradient by using the Bernoulli equation. The flow discharge, turbulence parameters, and inflow sediment concentration are prescribed at the inlet as a Dirichlet boundary condition. At the outlet, the Neumann type zero gradient boundary condition is used for all variables. Wall laws for rough boundaries introduced by Schlichting (1979) are used in the simulations (Equation (5)).

$$\frac{U}{u^*} = \frac{1}{\kappa} \ln \left(\frac{30\Delta}{k_s} \right) \quad (5)$$

where U is the flow velocity, u^* is the shear velocity, κ is the von Kármán constant equal to 0.41, Δ is the distance between the wall and the center of the closest cell, and k_s is the equivalent sediment roughness height.

Concerning the grid resolution, both models (lozenge and hexagon) are composed of $120 \times 80 \times 5$ cells in the streamwise, lateral, and vertical directions, respectively. The suspended sediment transport computation is carried out by solving the advection-diffusion equation (Equation (6)), considering van Rijn's (1984a) formula for the equilibrium near-bed concentration as a boundary condition (Equation (7)).

$$\frac{\partial c_i}{\partial t} + U_j \frac{\partial c_i}{\partial x_j} + w_i \frac{\partial c_i}{\partial z} = \frac{\partial}{\partial x_j} \left(\Gamma_T \frac{\partial c_i}{\partial x_j} \right) \quad (6)$$

where c_i is the sediment concentration of size i , w is the sediment fall velocity, and $\Gamma_T = \nu_T / S_c$ is the turbulent diffusion coefficient, where S_c is the Schmidt number. The value for the Schmidt number is taken to be equal to unity by assuming no deviation between the eddy viscosity and the turbulent diffusivity.

Suspended sediment transport calculation requires the specification of the near-bed sediment concentration, considering a reference level above the bed, where sediment resuspension occurs (reference concentration). The empirical formula of van Rijn is used to calculate the equilibrium suspended sediment concentration in the cells close to the bed as the bottom boundary condition for solving the advection-diffusion equation. The near-bed volumetric sediment concentration for the i th

fraction ($c_{b,i}$) is calculated as follows:

$$c_{b,i} = 0.015 \frac{d_i}{a} \frac{\left(\frac{\tau - \tau_{c,i}}{\tau_{c,i}}\right)^{1.5}}{\left(d_i \left(\frac{(\rho_s - \rho_w)g}{\rho_w \nu^2}\right)^{\frac{1}{3}}\right)^{0.5}} \quad (7)$$

where d_i is the diameter of the i th fraction, a represents the roughness height as the reference level, τ is the bed shear stress, $\tau_{c,i}$ is the critical shear stress for the movement of the i th fraction according to the Shields curve, ρ_s and ρ_w are the density of sediment and water, respectively, g is the gravity acceleration, and ν represents the kinematic viscosity. The sediment resuspension from the bed can be calculated by converting the sediment concentration into the entrainment rate.

The bedload transport is also calculated by the empirical formula of van Rijn (1984b) (Equation (8)), which represents the transport rate of the i th fraction per unit width.

$$q_{b,i} = 0.053 d_i^{1.5} \left(\frac{\rho_s - \rho_w}{\rho_w} g\right)^{0.5} \frac{\left(\frac{\tau - \tau_{c,i}}{\tau_{c,i}}\right)^{2.1}}{d_i^{0.5} \left(\frac{(\rho_s - \rho_w)g}{\rho_w \nu^2}\right)^{0.1}} \quad (8)$$

The sediment continuity equation (Exner equation) is used to calculate the bed elevation changes with respect to the continuity defect in cells close to the bed. The difference between the sediment inflow and outflow in a cell is multiplied by the time step and divided by the horizontal plane area of the cell. The bed is then raised or lowered after each time step, and the grid is regenerated.

Regarding the velocity distribution at the inlet, a minor linear perturbation is introduced to the velocity profile, described by Dewals *et al.* (2008), to provide an initiating factor and a condition for the genesis of the asymmetric flow in symmetric numerical models. This small perturbation can be considered as an initial boundary condition that is unavoidable in experimental set-ups, and can be further damped and become a straight jet regarding the reservoirs with stable-symmetric flow structure. In other words, a perfect symmetric numerical model needs a symmetry-breaking condition to reproduce an asymmetric flow field.

2.3. Model calibration

Model calibration is regarded as the initial stage of appraising the performance of a computational model that represents the complex behavior of a real-world system. This inverse process depends on how sensible the uncertain affecting parameters are adjusted according to the misfit minimization between calculated and corresponding measured values. The traditional manual trial-and-error method of model calibration has nowadays been overshadowed by the concept of mathematical optimization, which paves the way for automatic model calibration owing to its interesting features such as objective-based judgment of goodness-of-fit rather than relying on the user subjectivity and being less time-consuming (Evangelista *et al.* 2017). The principal elements of an automatic calibration routine are: an objective function to evaluate the model performance, an optimization algorithm to explore the parameter space by repetitive adjustment of the uncertain parameters, and a termination criterion to stop the search when the convergence of the objective function or the maximum allowable number of iterations is satisfied (Vidal *et al.* 2007).

In this study, the model-independent nonlinear Parameter ESTimation and predictive analysis package PEST (Doherty 2016), which employs the gradient-based Gauss–Marquardt–Levenberg (GML) local optimization algorithm, is used to calibrate the numerical models. This tool has demonstrated promising results for sensitivity analysis and automatic calibration of numerical models in different environmental studies (Shoarinezhad *et al.* 2020a, 2020b). Further, a global optimization algorithm, Big Bang Big Crunch (BB–BC) (Erol & Eksin 2006), is applied to validate PEST performance in finding the global optimum over the search space.

The numerical models are calibrated in accordance with the measured bed levels in different longitudinal and cross-sections, taking 8,600 and 16,500 points into account for the lozenge- and hexagon-shaped reservoirs, respectively. The

residual sum of squares between measured and calculated bed levels, $RSS = \sum_{i=1}^n (\text{measurement} - \text{prediction})^2$, is used as the optimization objective function for the automatic calibration of the models. The measured points were located in every 10 cm of cross-sections (61 cross-sections) with a lateral distance of about 1 cm from each other. Among the four phases of sediment feeding in the experiments, the measured bed levels from the first 1.5 hrs (considered a warm-up period) are used as the initial bed levels to simulate the following three phases. This is performed to provide an initial condition for the roughness calibration considering the surface friction development from the hydraulically smooth bed surface.

2.3.1. Gauss–Marquardt–Levenberg algorithm of PEST

PEST iteratively adjusts the uncertain parameters within a pre-defined space with the aid of the GML search algorithm until reaching the minimum deviation between the measured and calculated values according to the residual sum of squares as the objective function. Using the GML algorithm, as a combination of the gradient descent method and Gauss–Newton algorithm, PEST runs the model and linearizes the relationship between input parameters and model outputs by Taylor's expansion of the actual parameter set. The number of adjustable parameters, subject to calibration, determines the number of model runs in a single PEST iteration. During each iteration, a Jacobian matrix of partial derivatives of model outputs is generated, followed by an upgrade vector (Equation (9)) to alter the parameters for the next iteration up to reaching either the minimum of the objective function or termination criteria.

$$u = (J^T Q J + \lambda I)^{-1} J^T Q r \quad (9)$$

where u is the parameter upgrade vector, J^T represents the transpose of the Jacobian matrix J , Q is the diagonal weight matrix, λ is the Marquardt lambda acting as a damping factor, I is an identity matrix, and r is the vector of residuals.

2.3.2. Big Bang Big Crunch algorithm

BB–BC is a metaheuristic optimization algorithm inspired by a theory for the evolution of the universe. The initial population is uniformly generated by spreading random candidate solutions over the entire search space in the Big Bang phase. The main concept of this phase is based on the energy dissipation in nature which creates chaos and randomness in the population. Then, the fitness value for each candidate solution is calculated (i.e., the 'mass' of each particle). During the Big Crunch phase, the randomly distributed population shrinks to a single point \bar{x}^c , which is called the 'center of mass', and calculated according to Equation (10).

$$\bar{x}^c = \frac{\sum_{i=1}^N \frac{1}{f^i} \bar{x}^i}{\sum_{i=1}^N \frac{1}{f^i}} \quad (10)$$

Here, \bar{x}^i is the position vector of the i th candidate in an n -dimensional search space, N is the population size, and f^i denotes the fitness value of the i th candidate. In the next Big Bang, new individuals are mainly generated around the former-calculated center of mass according to a normal distribution, where the standard deviation of the normal distribution decreases as the optimization proceeds. This step is followed by a contraction according to the recalculation of the new center of mass. In order to ensure the global convergence of the method, the algorithm always generates a number of new solutions far from the center of mass with a diminishing probability as iterations go forward. Eventually, with regard to a defined termination criterion, this successive two-phase scheme (explosion-contraction) converges to the optimum point (Kaveh & Bakhshpoori 2019).

2.3.3. Parameters selection

A series of sensitivity analyses are performed to find out the significance of uncertain input parameters (e.g., roughness coefficient, the porosity of compacted bed sediments, the coefficient for the bedform smoothing algorithm, the thickness of the upper active sediment layer, and the angle of repose for sediments) on the system behavior as the initial stage prior to the model calibration. SENSAN, a model-independent local SENSitivity ANalyzer as one of the PEST utilities, is used for the sensitivity analysis. SENSAN conducts several runs according to the pre-defined sets of parameter values and records

the model output sensitivities to parameter changes. Among the assessed parameters, the two most sensitive ones are selected for auto-calibration as follows:

- Nikuradse equivalent roughness height (k_s), which is generally considered to be proportionately related to the representative grain size, such that $k_s = \alpha_s d_n$. There are several values for α_s and various sediment sizes as the representative grain size d_n in the literature (e.g., see Dey (2014)). Here, the range of this parameter is set to be $d_{50} \leq k_s \leq 10d_{90}$.
- Active layer thickness (ALT), as the superficial exchange layer depth, engaged in the entrainment and deposition of sediment particles. The sorting mechanism occurs in the active layer, where the sediment continuity equation is computed separately for each size fraction inside a cell during each time step. Depending on the transport regime, ALT scales with the representative grain size of the sediment mixture or is defined as a fraction of bedforms height. The range for this parameter is selected to be $d_{50} \leq ALT \leq 5d_{max}$ (Malcherek 2007).

Since the GML algorithm is a gradient-based approach, it might likely find the local optimum point on the objective function surface rather than the desired global one. Therefore, it is worthwhile to reassess the calibration procedure by using different random initial values within the parameter space in the case of using local optimization algorithms. Here, two different pre-defined starting values are considered for the investigated parameters:

- GML#1: $k_{s1} = d_{90} = 0.013$ cm $ALT_1 = d_{max} = 0.028$ cm
- GML#2: $k_{s2} = 3d_{90} = 0.039$ cm $ALT_2 = 3d_{max} = 0.084$ cm

3. RESULTS AND DISCUSSION

The geometry of a reservoir plays a vital role in the flow field development and, consequently, the sedimentation pattern. Regarding this fact, different relations in the literature can be found, the so-called shape factors, which correlate geometrical aspects with the appearance of various flow field categories (e.g., Kantoush (2008); Dufresne *et al.* (2011)). Above a critical value for the shape factor, the symmetric flow inside a symmetric reservoir evolves toward the asymmetric pattern due to the Coanda effect, where the flow deviates to one side of the reservoir according to a tiny imperfection in the physical symmetric configuration.

Figure 2 shows the calculated final surface velocity magnitude for hexagonal (a, b, c) and lozenge-shaped (d, e, f) reservoirs in different periods (i.e., phases 1, 2, and 3, up to bottom). Concerning the hexagonal configuration, the main jet enters the reservoir and keeps its straight path up to the outlet with recirculation zones on both sides. It is evident that the deposited sediments during different periods do not affect the stability of the velocity field and do not interrupt the flow symmetry (Figure 2(a)–2(c)). Nevertheless, there is a significant deviation in the flow trajectory in the lozenge-shaped reservoir, where the entering jet reattaches to one side, resulting in a single large recirculation zone. Here, the flow field is much more complex, and the unstable nature of the flow gives rise to a shift in the velocity field from one side to the opposite side of the reservoir due to the accumulated sediments. Although there is a gradual shift of the flow pattern from clockwise in phase 1 to counterclockwise in phase 2, the velocity field keeps its counterclockwise route during phase 3 (Figure 2(d)–2(f)).

Figure 3 depicts the middle cross-sectional profile ($x = 3$ m) of (a) hexagonal and (b) lozenge-shaped reservoirs at the end of the final phase. The color contour maps show the calculated streamwise velocity (U_x), where the vectors are the resultant of the lateral (U_y) and vertical (U_z) velocity components.

The auto-calibration process is based on the pairwise comparison of the calculated and measured bed levels. Table 2 shows the calibration results for both reservoirs using GML (with two different starting values for the selected parameters) and BB–BC (with randomly sampled initial values) algorithms. It can be seen that the calibrated values for the investigated parameters ($k_{s \text{ calibrated}}$ and $ALT_{\text{calibrated}}$) are very similar for GML#1 and GML#2 regarding both reservoirs, indicating the repeatability and robustness of the auto-calibration procedure based on the GML algorithm. Moreover, these values are almost the same as the results of the BB–BC algorithm. It means the gradient-based GML algorithm is not affected by local minima, and PEST can reliably calibrate the numerical models in a global manner. Furthermore, among innumerable parameter combinations, PEST calibrates the models with 30–40 runs depending on the starting values, which shows the method's efficiency compared to the BB–BC algorithm.

Considering $d_{90} = 0.013$ cm as the representative grain size, the calibrated values can be rewritten as: $ks \approx 1.64d_{90}$ and $ALT \approx 2.4d_{90}$ for the lozenge-shaped reservoir; and $ks \approx 1.84d_{90}$ and $ALT \approx 2.94d_{90}$ regarding the hexagonal reservoir.

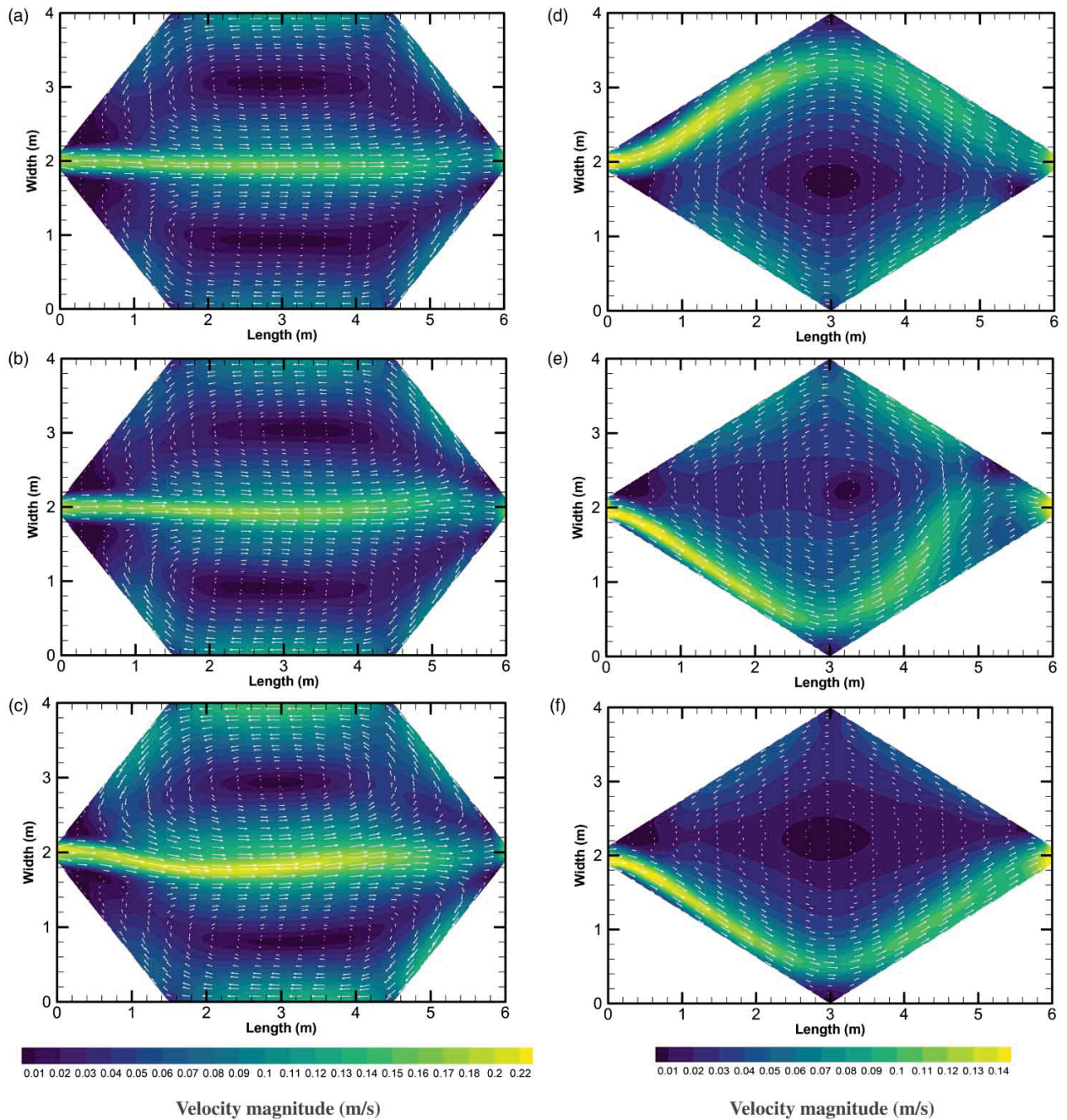


Figure 2 | Contour maps of calculated velocity fields for the two reservoirs in different periods: 1.5 hrs of (a and d) phase 1 and (b and e) phase 2 for both reservoirs; (c) 4.5 hrs and (f) 3 hrs of phase 3 for the hexagonal and lozenge-shaped reservoirs, respectively.

Figures 4 and 5 illustrate plan views of the measured and simulated bed topography at the end of each period (i.e., phases 1, 2, and 3, up to bottom) for hexagonal and lozenge-shaped reservoirs, respectively. In the hexagonal reservoir (Figure 4), the flow field has a stable behavior during different periods with a continuous straight jet. Hence, the main part of sediment particles is settled along this mid-longitudinal section. In addition to the main central flow, two large recirculation zones are in charge of the lateral depositions. In phase 1 (Figure 4(a) and 4(d)), the magnitude of these lateral eddies in the experimental set-up and the numerical model are almost identical. However, in phase 2 (Figure 4(b) and 4(e)), there is a stronger vortex at

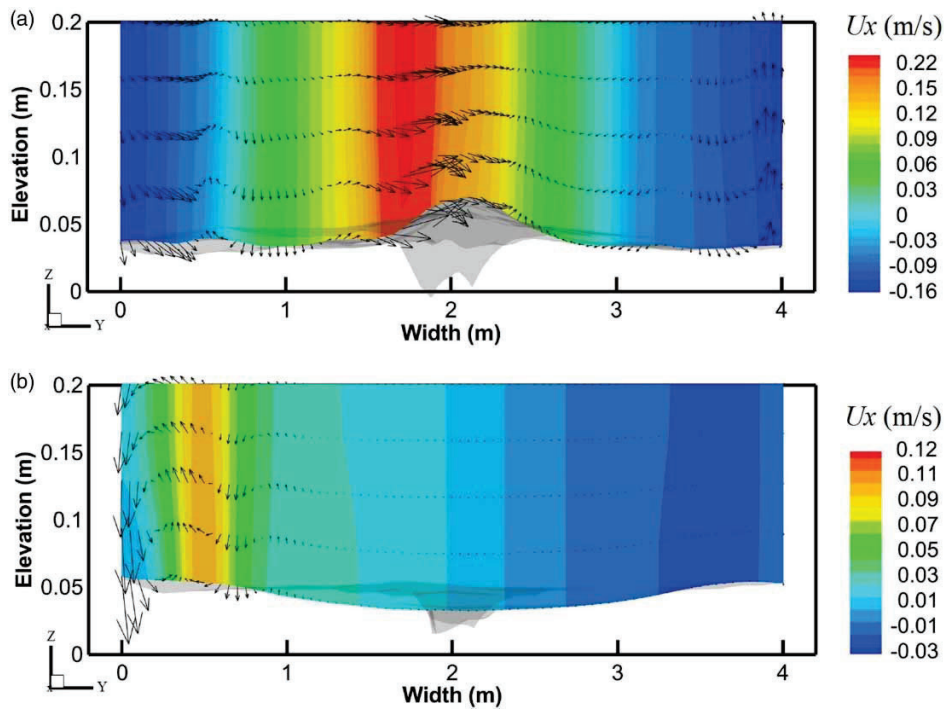


Figure 3 | Central cross-sectional view of the final velocity field for (a) hexagonal and (b) lozenge-shaped reservoirs.

Table 2 | Initial values of the investigated parameters and calibration results (final calibrated values and the number of model runs)

Reservoir shape	Algorithm	Initial values		Calibration results		
		k_s initial	ALT initial	k_s calibrated	ALT calibrated	Model runs
Lozenge	GML#1	0.013	0.028	0.0212	0.0308	32
	GML#2	0.039	0.084	0.0214	0.0311	38
	BB-BC	Randomly sampled		0.0212	0.0309	471
Hexagon	GML#1	0.013	0.028	0.0238	0.0382	31
	GML#2	0.039	0.084	0.0235	0.0377	35
	BB-BC	Randomly sampled		0.0237	0.0380	438

Note: k_s , roughness height at the bed; ALT, active layer thickness. Units are in centimeters.

the right side of the flow direction in the laboratory model. Here, more sediments are transported and settled at the right side of the reservoir in the experimental set-up compared to the uniform pattern of the numerical model. According to the final bed levels for the hexagonal reservoir (Figure 4(c) and 4(f)), a scour hole occurs in the immediate upstream of the experiment, which could not be simulated in the numerical model. The overall patterns of final bed levels are similar, with the maximum deposition along the first half of the central-longitudinal section.

Despite the stable, straight, and symmetric nature of the flow in the hexagonal reservoir, which results in a central-longitudinal pattern of sediment depositions, the flow structure in the lozenge-shaped reservoir is unstable and fluctuating with main sediment deposits at the sides of the reservoir (Figure 5). During the first phase, the flow direction is clockwise, and sediments are mostly settled at the left part, resulting in an asymmetric bed topography (Figure 5(a) and 5(d)). The shift in the flow path during the second phase, due to the deposited sediments that can modify the unstable and sensitive flow structure in the lozenge-shaped reservoir, changes the bed topography to a semi-symmetric pattern (Figure 5(b) and 5(e)). Here, the numerical model underestimates the bed levels at the second half of the right side of the reservoir. Considering the final bed levels, sediments are almost symmetrically deposited along the left and right parts of the basin in the experiment, whereas the

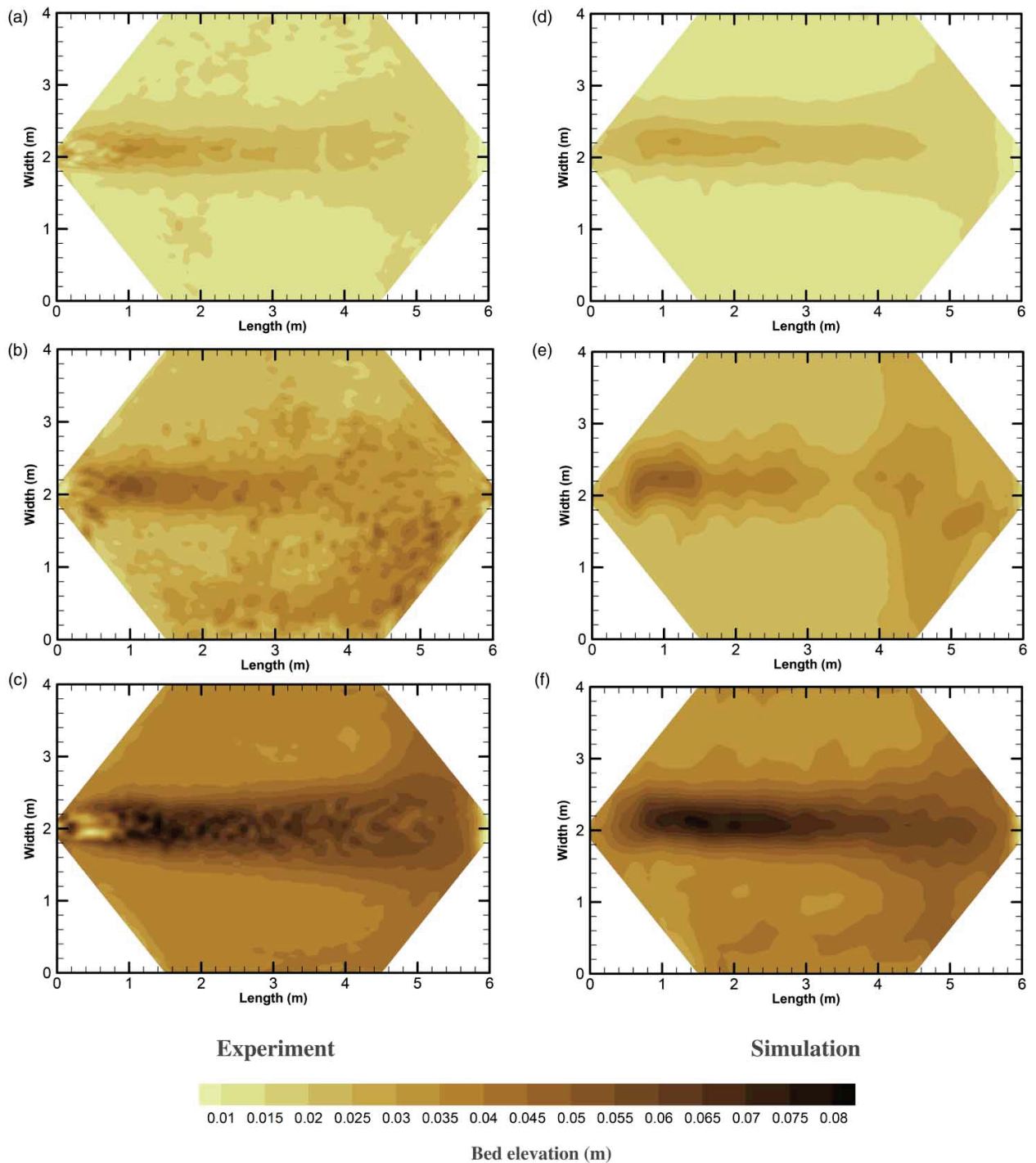


Figure 4 | Comparison of bed level changes in the experiment (left) with the simulation results (right) in (a and d) phase 1, (b and e) phase 2, and (c and f) phase 3 for the hexagonal reservoir.

maximum deposition is along the first half of the right side in the numerical model (Figure 5(c) and 5(f)). Furthermore, in all phases, an erosion area can be seen just in front of the inlet in the experiment, which is deeper and larger in size compared to the results of the numerical model.

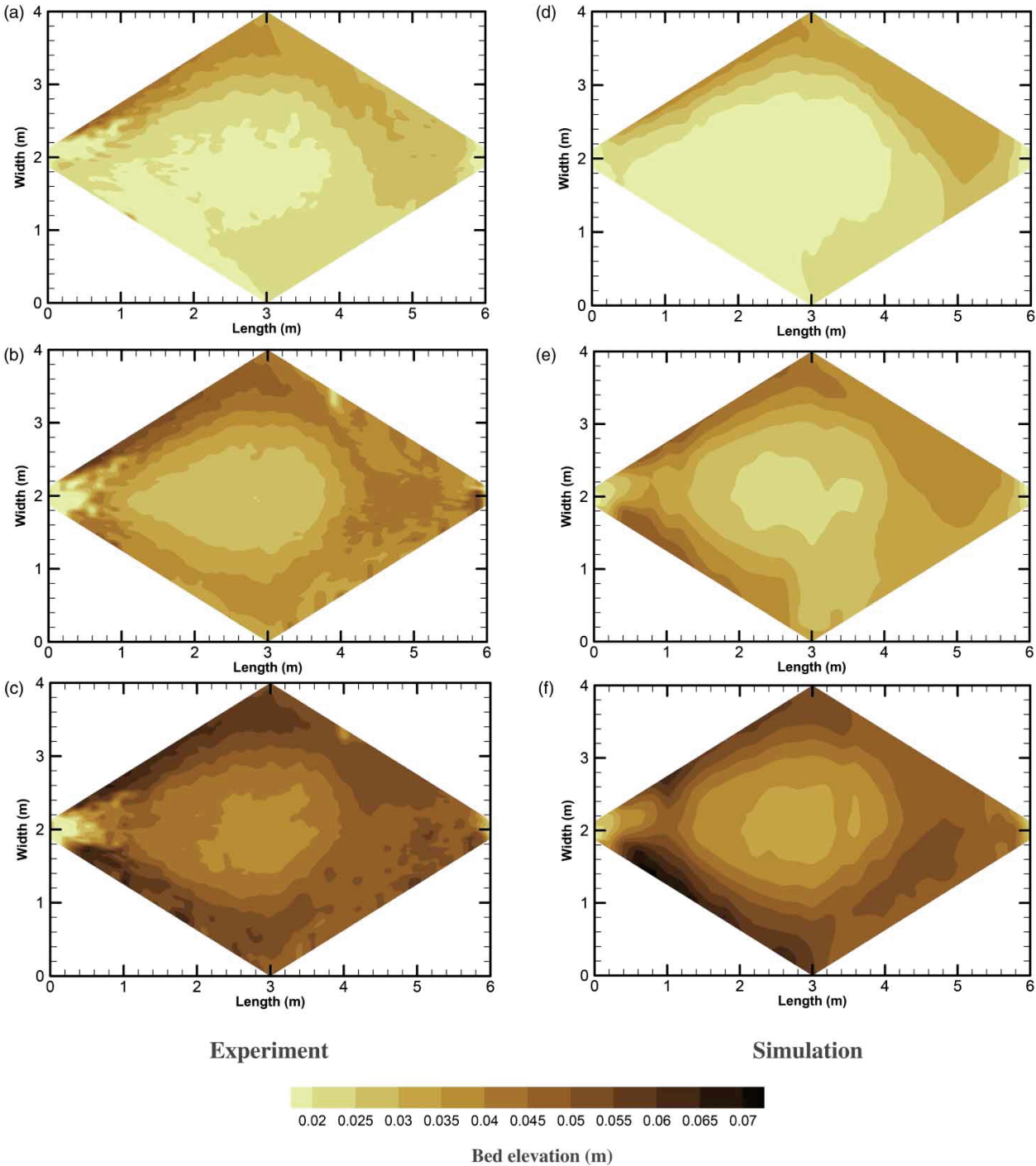


Figure 5 | Comparison of bed level changes in the experiment (left) with the simulation results (right) in (a and d) phase 1, (b and e) phase 2, and (c and f) phase 3 for the lozenge-shaped reservoir.

In order to quantitatively evaluate the overall performance of the automatically calibrated numerical models, various statistical metrics are used to compare the final measured and calculated bed levels, as shown in Table 3. The results of uncalibrated models using the initial parameter values of GML#1 are also presented to see the deviation between the results of the calibrated models and our initial guess. Mean Bias Error (MBE) is applied as a bias indicator, describing the degree of

Table 3 | Statistical performance of the automatic model calibration

Reservoir shape		Goodness-of-fit				
		MBE (cm)	RMSE (cm)	MAE (cm)	R (-)	KG (-)
Lozenge	Calibrated	-0.024	0.054	0.044	0.80	0.77
	Initial guess	-0.061	0.288	0.212	0.56	0.52
Hexagon	Calibrated	-0.013	0.055	0.039	0.86	0.85
	Initial guess	-0.039	0.252	0.208	0.70	0.68

Note: MBE, Mean Bias Error; RMSE, Root Mean Squared Error; MAE, Mean Absolute Error; R, Pearson correlation coefficient; KG, Kling-Gupta efficiency.

underprediction (negative values) or overprediction (positive values) of the model. Root Mean Squared Error (RMSE) and Mean Absolute Error (MAE) both reflect the average magnitude of the error. While MAE indicates a linear behavior of individual errors, RMSE gives more importance to big errors by giving higher weights to them. Pearson correlation coefficient (R) shows the linear correlation between estimated and measured bed levels. As a multi-component goodness-of-fit, Kling-Gupta efficiency (KG) is used, which combines Pearson correlation coefficient, bias, and variability within a single objective function.

According to the negative values of MBE, the numerical models underestimate the final bed levels in both cases. Although having a similar calibrated RMSE, the lower MAE value for the hexagonal model represents its more precise calibration (the best value is 0). This can further be confirmed by higher values of correlation and Kling-Gupta efficiency metrics for the hexagonal model (the best value is 1). Nevertheless, the statistical performance of the calibrated lozenge-shaped model also agrees reasonably with the measured data.

4. SUMMARY AND CONCLUSIONS

In this study, we applied an automatic calibration tool (PEST), which uses the gradient-based Gauss–Marquardt–Levenberg optimization algorithm, to calibrate the 3D morphodynamic numerical models of two reservoirs (hexagonal and lozenge-shaped configurations) against the experimental data. The two most affecting input parameters (roughness height and active layer thickness) in the numerical models are selected for calibration through a sensitivity analysis. In order to verify the ability of the gradient-based optimization algorithm to find the global optimum values of the parameters over the search space rather than sticking to a local optimum point (evaluating the robustness and convergence of the algorithm), in addition to using the global optimization algorithm Big Bang Big Crunch, we tested the gradient-based method with two different pre-defined initial values with a reasonable range based on the literature. Achieving an almost identical set of calibrated values confirmed the accuracy and reliability of the optimization procedure. The parameters are calibrated with 30–40 model runs by PEST, which shows its efficiency and superiority over the trial-and-error manual calibration, suggesting its potential use for hydro-morphodynamic models calibration.

So far, most related research works have been on rectangular reservoirs with a 90° expansion angle. In this work, the effect of lower expansion angles on the flow field development and the sedimentation pattern is assessed numerically. Keeping the maximum inner dimensions constant, the lower expansion angle gives a higher chance of asymmetric flow appearance. Regarding the hexagonal reservoir, which has a stable flow structure, the main part of sediment particles is settled along the mid-longitudinal section. However, the unstable flow pattern inside the lozenge-shaped reservoir causes sediments to be distributed at the sides of the basin. The calculated bed levels are compared with the measured topography of the physical models in different time steps. Considering the primary features and specifications of both reservoirs regarding the flow field, jet direction, recirculation zones, and bed topography in the experimental work, the calibrated numerical models can reasonably reproduce similar patterns. The achieved results regarding the flow fields and erosion/deposition patterns are used as a criterion to judge the ability of the Gauss–Marquardt–Levenberg search algorithm to calibrate the numerical models (optimization performance). A difference between the bed levels in the physical set-up and simulation results is related to the scour hole in front of the inlet, likely due to boundary effects, which cannot be predicted by the numerical model.

The quality and performance of the calibrated numerical models are also investigated by different statistical metrics, comparing the predicted and measured bed levels. The mean bias error shows an underestimation of bed levels in both reservoirs. Nevertheless, according to the low values of the root mean squared error and the mean absolute error; and high values of the

correlation coefficient and Kling-Gupta efficiency, the overall performance of the automatic calibration procedure is reasonable.

The manual trial-and-error model calibration approach with just one parameter subject to alteration may be reasonable and sufficient in most cases. However, if there are several uncertain parameters, their innumerable combinations cause the manual calibration method to become much more complex, time- and cost-consuming, and impractical. What is more, since the issue of subjectivity is involved in manual model calibration, there is no guarantee that the best possible combination of parameters can be achieved. The overall outcome of this study is that using suitable optimization algorithms for hydro-morphodynamic models calibration, which is not a common practice among researchers in this field, can considerably reduce the calibration time and user intervention/subjectivity and concurrently increase the precision of the process.

ACKNOWLEDGEMENTS

The first author received a Ph.D. scholarship from the German Federal Ministry of Education and Research (BMBF) through the Sustainable Water Management-NaWaM program of the German Academic Exchange Service (DAAD). The last author is indebted to the Baden-Württemberg Stiftung for the financial support from the Elite program for Postdocs. The authors also acknowledge Prof. Nils Reidar Bøe Olsen, the developer of SSIIM software, for his valuable suggestion regarding numerical modeling.

DATA AVAILABILITY STATEMENT

All relevant data are included in the paper or its Supplementary Information.

CONFLICT OF INTEREST

The authors declare there is no conflict.

REFERENCES

- Abbott, D. E. & Kline, S. J. 1962 Experimental investigation of subsonic turbulent flow over single and double backward facing steps. *Journal of Basic Engineering* **84**, 317–325. <https://doi.org/10.1115/1.3657313>.
- Camnasio, E., Orsi, E. & Schleiss, A. J. 2011 Experimental study of velocity fields in rectangular shallow reservoirs. *Journal of Hydraulic Research* **49**, 352–358. <https://doi.org/10.1080/00221686.2011.574387>.
- Casarsa, L. & Giannattasio, P. 2008 Three-dimensional features of the turbulent flow through a planar sudden expansion. *Physics of Fluids* **20**, 015103. <https://doi.org/10.1063/1.2832780>.
- Cherdron, W., Durst, F. & Whitelaw, J. H. 1978 Asymmetric flows and instabilities in symmetric ducts with sudden expansions. *Journal of Fluid Mechanics* **84**, 13. <https://doi.org/10.1017/S0022112078000026>.
- Dewals, B. J., Kantoush, S. A., Erpicum, S., Piroton, M. & Schleiss, A. J. 2008 Experimental and numerical analysis of flow instabilities in rectangular shallow basins. *Environmental Fluid Mechanics* **8**, 31–54. <https://doi.org/10.1007/s10652-008-9053-z>.
- Dewals, B., Archambeau, P., Bruwier, M., Erpicum, S., Piroton, M., Adam, T., Delhez, E. & Deleersnijder, E. 2020 Age of water particles as a diagnosis of steady-state flows in shallow rectangular reservoirs. *Water* **12**, 2819. <https://doi.org/10.3390/w12102819>.
- Dey, S. 2014 *Fluvial Hydrodynamics: Hydrodynamic and Sediment Transport Phenomena*. Springer, Berlin, Heidelberg. <https://doi.org/10.1007/978-3-642-19062-9>.
- De Zilwa, S. R. N., Khezzar, L. & Whitelaw, J. H. 2000 Flows through plane sudden-expansions. *International Journal for Numerical Methods in Fluids* **32**, 313–329. [https://doi.org/10.1002/\(SICI\)1097-0363\(20000215\)32:3<313::AID-FLD940>3.0.CO;2-B](https://doi.org/10.1002/(SICI)1097-0363(20000215)32:3<313::AID-FLD940>3.0.CO;2-B).
- Doherty, J. 2016 *PEST Model-Independent Parameter Estimation User Manual Part I, 6th ed.* Watermark Numerical Computing, Brisbane, Australia.
- Drikakis, D. 1997 Bifurcation phenomena in incompressible sudden expansion flows. *Physics of Fluids* **9**, 76–87. <https://doi.org/10.1063/1.869174>.
- Dufresne, M., Dewals, B. J., Erpicum, S., Archambeau, P. & Piroton, M. 2010 Classification of flow patterns in rectangular shallow reservoirs. *Journal of Hydraulic Research* **48**, 197–204. <https://doi.org/10.1080/00221681003704236>.
- Dufresne, M., Dewals, B. J., Erpicum, S., Archambeau, P. & Piroton, M. 2011 Numerical investigation of flow patterns in rectangular shallow reservoirs. *Engineering Applications of Computational Fluid Mechanics* **5**, 247–258. <https://doi.org/10.1080/19942060.2011.11015368>.
- Dufresne, M., Dewals, B., Erpicum, S., Archambeau, P. & Piroton, M. 2012 Flow patterns and sediment deposition in rectangular shallow reservoirs. *Water and Environment Journal* **26**, 504–510. <https://doi.org/10.1111/j.1747-6593.2012.00310.x>.
- Durst, F., Melling, A. & Whitelaw, J. H. 1974 Low reynolds number flow over a plane symmetric sudden expansion. *Journal of Fluid Mechanics* **64**, 111–128. <https://doi.org/10.1017/S0022112074002035>.

- Erol, O. K. & Eksin, I. 2006 A new optimization method: Big Bang–Big Crunch. *Advances in Engineering Software* **37**, 106–111. <https://doi.org/10.1016/j.advengsoft.2005.04.005>.
- Escudier, M. P., Oliveira, P. J. & Poole, R. J. 2002 Turbulent flow through a plane sudden expansion of modest aspect ratio. *Physics of Fluids* **14**, 3641–3654. <https://doi.org/10.1063/1.1504711>.
- Esmaeili, T., Sumi, T., Kantoush, S. A., Haun, S. & Rütther, N. 2016 Three-dimensional numerical modelling of flow field in shallow reservoirs. *Proceedings of the Institution of Civil Engineers-Water Management* **169**, 229–244. <https://doi.org/10.1680/wama.15.00011>.
- Esmaeili, T., Sumi, T., Kantoush, S., Kubota, Y., Haun, S. & Rütther, N. 2017 Three-dimensional numerical study of free-flow sediment flushing to increase the flushing efficiency: a case-study reservoir in Japan. *Water* **9**, 900. <https://doi.org/10.3390/w9110900>.
- Evangelista, S., Giovinco, G. & Kocaman, S. 2017 A multi-parameter calibration method for the numerical simulation of morphodynamic problems. *Journal of Hydrology and Hydromechanics* **65**, 175–182. <https://doi.org/10.1515/johh-2017-0014>.
- Fani, A., Camarri, S. & Salvetti, M. V. 2012 Stability analysis and control of the flow in a symmetric channel with a sudden expansion. *Physics of Fluids* **24**. <https://doi.org/10.1063/1.4745190>.
- Fearn, R. M., Mullin, T. & Cliffe, K. A. 1990 Nonlinear flow phenomena in a symmetric sudden expansion. *Journal of Fluid Mechanics* **211**, 595–608. <https://doi.org/10.1017/S0022112090001707>.
- Haun, S. & Olsen, N. R. B. 2012 Three-dimensional numerical modelling of reservoir flushing in a prototype scale. *International Journal of River Basin Management* **10**, 341–349. <https://doi.org/10.1080/15715124.2012.736388>.
- Hawa, T. & Rusak, Z. 2000 Viscous flow in a slightly asymmetric channel with a sudden expansion. *Physics of Fluids* **12**, 2257–2267. <https://doi.org/10.1063/1.1287610>.
- Hillebrand, G., Klassen, I. & Olsen, N. R. B. 2017 3D CFD modelling of velocities and sediment transport in the Iffezheim hydropower reservoir. *Hydrology Research* **48**, 147–159. <https://doi.org/10.2166/nh.2016.197>.
- Kantoush, S. A. 2008 *Experimental Study on the Influence of the Geometry of Shallow Reservoirs on Flow Patterns and Sedimentation by Suspended Sediments*. PhD Thesis, École Polytechnique Fédérale de Lausanne (EPFL), Lausanne, Switzerland.
- Kantoush, S. A., Bollaert, E. & Schleiss, A. J. 2008a Experimental and numerical modelling of sedimentation in a rectangular shallow basin. *International Journal of Sediment Research* **23**, 212–232. [https://doi.org/10.1016/S1001-6279\(08\)60020-7](https://doi.org/10.1016/S1001-6279(08)60020-7).
- Kantoush, S. A., De Cesare, G., Boillat, J. L. & Schleiss, A. J. 2008b Flow field investigation in a rectangular shallow reservoir using UVP, LSPIV and numerical modelling. *Flow Measurement and Instrumentation* **19**, 139–144. <https://doi.org/10.1016/j.flowmeasinst.2007.09.005>.
- Kaveh, A. & Bakhshpoori, T. 2019 Big Bang-Big Crunch Algorithm. In: *Metaheuristics: Outlines, MATLAB Codes and Examples*. Springer International Publishing, Cham, pp. 31–40. https://doi.org/10.1007/978-3-030-04067-3_4.
- Lakzian, E., Saghi, H. & Kooshki, O. 2020 Numerical simulation of sediment deposition and trapping efficiency estimation in settling basins, considering secondary flows. *International Journal of Sediment Research* **35**, 347–354. <https://doi.org/10.1016/j.ijsrc.2020.02.001>.
- Malcherek, A. 2007 *Sedimenttransport und Morphodynamik*. Scriptum Institut für Wasserwesen, Bundeswehr University Munich, Munich, Germany.
- Mehta, P. R. 1981 Separated flow through large sudden expansions. *Journal of the Hydraulics Division* **107**, 451–460. <https://doi.org/10.1061/JYCEAJ.0005648>.
- Mizushima, J., Okamoto, H. & Yamaguchi, H. 1996 Stability of flow in a channel with a suddenly expanded part. *Physics of Fluids* **8**, 2933–2942. <https://doi.org/10.1063/1.869072>.
- Mohammad, M. E., Al-Ansari, N., Knutsson, S. & Laue, J. 2020 A computational fluid dynamics simulation model of sediment deposition in a storage reservoir subject to water withdrawal. *Water* **12**, 959. <https://doi.org/10.3390/w12040959>.
- Olsen, N. R. B. 2014 *A Three Dimensional Numerical Model for Simulation of Sediment Movement in Water Intakes with Multiblock Option*. Department of Hydraulic and Environmental Engineering, The Norwegian University of Science and Technology, Trondheim, Norway.
- Quaini, A., Glowinski, R. & Čanić, S. 2016 Symmetry breaking and preliminary results about a Hopf bifurcation for incompressible viscous flow in an expansion channel. *International Journal of Computational Fluid Dynamics* **30**, 7–19. <https://doi.org/10.1080/10618562.2016.1144877>.
- Sarma, A. S. R., Sundararajan, T. & Ramjee, V. 2000 Numerical simulation of confined laminar jet flows. *International Journal for Numerical Methods in Fluids* **33**, 609–626. [https://doi.org/10.1002/1097-0363\(20000715\)33:5 < 609::AID-FLD745 > 3.0.CO;2-%23](https://doi.org/10.1002/1097-0363(20000715)33:5 < 609::AID-FLD745 > 3.0.CO;2-%23).
- Schlichting, H. 1979 *Boundary Layer Theory*. McGraw-Hill, New York, USA.
- Shapira, M., Degani, D. & Weihs, D. 1990 Stability and existence of multiple solutions for viscous flow in suddenly enlarged channels. *Computers & Fluids* **18**, 239–258. [https://doi.org/10.1016/0045-7930\(90\)90009-M](https://doi.org/10.1016/0045-7930(90)90009-M).
- Shoarinezhad, V., Wieprecht, S., Haun, S., 2020a Automatic calibration of a 3D morphodynamic numerical model for simulating bed changes in a 180° channel bend. In: *Recent Trends in Environmental Hydraulics, GeoPlanet: Earth and Planetary Sciences* (Kalinowska, M. B., Mrokowska, M. M. & Rowiński, P. M., eds). Springer International Publishing, Cham, pp. 253–262. https://doi.org/10.1007/978-3-030-37105-0_22.
- Shoarinezhad, V., Wieprecht, S. & Haun, S. 2020b Comparison of local and global optimization methods for calibration of a 3D morphodynamic model of a curved channel. *Water* **12**, 1333. <https://doi.org/10.3390/w12051333>.
- Sobey, I. J. & Drazin, P. G. 1986 Bifurcations of two-dimensional channel flows. *Journal of Fluid Mechanics* **171**, 263–287. <https://doi.org/10.1017/S0022112086001441>.

- van Rijn, L. C. 1984a Sediment transport, part II: suspended load transport. *Journal of Hydraulic Engineering* **110**, 1613–1641. [https://doi.org/10.1061/\(ASCE\)0733-9429\(1984\)110:11\(1613\)](https://doi.org/10.1061/(ASCE)0733-9429(1984)110:11(1613)).
- van Rijn, L. C. 1984b Sediment transport, part I: bed load transport. *Journal of Hydraulic Engineering* **110**, 1431–1456. [https://doi.org/10.1061/\(ASCE\)0733-9429\(1984\)110:10\(1431\)](https://doi.org/10.1061/(ASCE)0733-9429(1984)110:10(1431)).
- Vidal, J.-P., Moisan, S., Faure, J.-B. & Dartus, D. 2007 River model calibration, from guidelines to operational support tools. *Environmental Modelling & Software* **22**, 1628–1640. <https://doi.org/10.1016/j.envsoft.2006.12.003>.

First received 28 June 2022; accepted in revised form 2 November 2022. Available online 15 November 2022

Appendix III

Using automatic model calibration for 3D morphological simulations: a case study of the Bodendorf reservoir flushing

Table 5.3. Metadata of Publication III

Title	Using automatic model calibration for 3D morphological simulations: a case study of the Bodendorf reservoir flushing
Authors	Vahid Shoarinezhad, Nils Reidar Bøe Olsen, Silke Wieprecht, Stefan Haun
Journal	Environmental Fluid Mechanics
Submitted	06 September 2023
Accepted	29 November 2023
Published	22 February 2024
DOI	https://doi.org/10.1007/s10652-023-09961-x



Using automatic model calibration for 3D morphological simulations: a case study of the Bodendorf reservoir flushing

Vahid Shoarinezhad¹ · Nils Reidar Bøe Olsen² · Silke Wieprecht¹ · Stefan Haun¹

Received: 6 September 2023 / Accepted: 29 November 2023
© The Author(s) 2024

Abstract

Reservoir sedimentation poses a significant challenge to water resource management. Improving the lifespan and productivity of reservoirs requires appropriate sediment management strategies, among which flushing operations have become more prevalent in practice. Numerical modeling offers a cost-effective approach to assessing the performance of different flushing operations. However, calibrating highly parametrized morphological models remains a complex task due to inherent uncertainties associated with sediment transport processes and model parameters. Traditional calibration methods require laborious manual adjustments and expert knowledge, hindering calibration accuracy and efficiency and becoming impractical when dealing with several uncertain parameters. A solution is to use optimization techniques that enable an objective evaluation of the model behavior by expediting the calibration procedure and reducing the issue of subjectivity. In this paper, we investigate bed level changes as a result of a flushing event in the Bodendorf reservoir in Austria by using a three-dimensional numerical model coupled with an optimization algorithm for automatic calibration. Three different sediment transport formulae (Meyer-Peter and Müller, van Rijn, and Wu) are employed and modified during the calibration, along with the roughness parameter, active layer thickness, volume fraction of sediments in bed, and the hiding-exposure parameter. The simulated bed levels compared to the measurements are assessed by several statistical metrics in different cross-sections. According to the goodness-of-fit indicators, the models using the formulae of van Rijn and Wu outperform the model calculated by the Meyer-Peter and Müller formula regarding bed patterns and the volume of flushed sediments.

Keywords 3D hydro-morphodynamic modeling · Automatic model calibration · Parameter estimation · Reservoir flushing · SSIIM · PEST

1 Introduction

While erosion and sedimentation are natural processes, the rate of these mechanisms may be dramatically accelerated through urbanization and human activities that destabilize soils and alter stream dynamics. As anthropogenic components of river systems, reservoirs are

Extended author information available on the last page of the article

constructed to retain water for various purposes such as irrigation, hydroelectric power generation, drinking water supply, and flood control. Reservoirs are inevitably prone to sedimentation due to regulated flow conditions (relatively low flow velocity and turbulence) and a limited sediment transport capacity. The progressive process of sedimentation occurs at varied rates, depending on a variety of factors, such as hydrological features of the catchment and river basin characteristics [1]. Thus, reservoir sedimentation is a major issue in areas with substantial sediment yield [2]. Sediment accumulation in reservoirs decreases the storage capacity over time, which, in fact, cuts down their useful lifespan, poses safety issues, and limits the advantages provided by dams and reservoirs [3].

The mean annual loss of global storage owing to sedimentation surpasses the growth in capacity by constructing new reservoirs [4, 5]. Following the 1987 World Bank report, it has been frequently stated in the literature that sediment deposition in reservoirs reduces the global storage capacity by 0.5–1% annually [6, 7]. Consequently, to ensure the long-term viability and sustainability of reservoirs, it is of critical importance to implement appropriate management strategies that include measures to minimize the catchment sediment yield and its inflow to reservoirs, as well as adopting sediment removal techniques [8, 9].

Reservoir flushing has been recognized as one of the most cost-effective desiltation methods [10]. By sufficiently lowering the reservoir water level (drawdown flushing), higher flow velocities and flow-induced shear forces imposed on deposits cause the mobilization and transport of particles. The excessive volume of flushed-out particles and high suspended sediment concentration may impair the integrity of the downstream ecosystem, including negative morphological effects, such as river bed clogging. Hence, assessing the compatibility of sediment flushing activities with the preservation of the downstream environment is indispensable. The flushing efficiency is determined by various factors, including sediment characteristics, the discharge and water levels within the reservoir, the reservoir geometry as well as the size and location of outlets, among others. Although there are different indicators in the literature to evaluate the effectiveness of flushing events, such as the sediment balance ratio or the long-term capacity ratio, there is no unified approach and criterion based on which to quantify flushing effectiveness [11].

Numerical models that replicate hydro-morphodynamic processes are beneficial tools for predicting the consequences of flushing operations. The application of numerical simulations to study sediment dynamics and flushing events is well documented in the literature. Depending on the available computational power, features of the study region, and the appropriate level of numerical simplification, researchers have employed a variety of modeling techniques to simulate reservoir flushing events, i.e., 1D [12, 13], 2D [14, 15], 3D [16, 17], and mesh-free Lagrangian models [18]. However, unless a reservoir is characterized as straight and narrow, the three-dimensional behavior of the flow, such as secondary currents in bends, needs to be considered. Although numerical models are promising tools for simulating reservoir flushing, there is a considerable challenge posed by uncertainties arising from the imperfect structure of the model reflecting the nature (i.e., model approximations and simplifications), initial assumptions and boundary conditions, equations derived from limited experimental/field studies, as well as imprecise, sparse and erratic data and measurements for model calibration/validation [19]. Hydro-morphodynamic numerical models are characterized by a large number of input parameters, some of which are physically impractical to be measured, while others can only be quantified at certain places over a limited period. Hence, within the calibration process, uncertain input variables that significantly impact model accuracy and predictive dependability are adapted in a way that simulated values correspond to their measured pairs with a reasonable tolerance.

Most of the related studies on numerical modeling of reservoir flushing have investigated individual parameters in the case of model calibration by manual trial-and-error and one-at-a-time (OAT) approach based on the user's comprehension of the model structure and properties of the environmental system. In other words, the general approach among the researchers in this field for model calibration is to examine each sensitive parameter independently while keeping the others constant. In practice, however, the overall optimum fit may not emerge from the combination of the best values of each component individually. It means there may be a significant conflict between the evaluated parameters, where by using manual OAT calibration, their trade-offs cannot be quantified. As a result, when handling a complex model with many unknown input parameters, the manual calibration approach becomes demanding and time-consuming, involving a high degree of subjectivity. Thus, using optimization methods to accomplish the model fitting procedure is a cutting-edge alternative. Although automatic model calibration has been widely used in various fields of environmental research over the last few decades, such as groundwater or hydrological models, its application to hydro-morphodynamic models is relatively new and limited, indicating a considerable research gap. Related studies in this field mainly focused on using stochastic metaheuristic optimization algorithms [20] as well as Bayesian calibration techniques [21]. Such methods incorporate randomness or probabilistic elements in their core operations to explore the solution space. Nevertheless, the calibration time associated with these methods is significantly high due to the numerous model runs for sampling the entire search space. An approach to overcome this challenge is to use a representative metamodel (surrogate model), which replaces the numerical model and replicates its output trends [22]. However, it should be noted that metamodels are just an approximation of the full-complexity numerical models and may only be employed for accelerating the calibration procedure if sufficient model runs (training iterations) are performed to construct the metamodel. The other alternative for automatic calibration is to use deterministic gradient-based optimization algorithms, which interact directly with the numerical model and require much fewer model runs compared to the sampling-based approaches.

In this study, the flushing operation of the Bodendorf reservoir in Austria is simulated with a fully 3D numerical model. The model is coupled with a gradient-based optimization algorithm and automatically calibrated against the measured flushed bed levels of 10 cross-sections along the reservoir. This work aims to assess the applicability and efficiency of automatic model calibration for reservoir flushing events.

2 Materials and methods

2.1 Study area

The Bodendorf run-of-the-river power plant, with an installed capacity of 7.5 MW and an annual production of about 33 GWh, was constructed between 1979 and 1982 on the River Mur in the federal state of Styria in Austria (47° 06' 27" N, 14° 03' 54" E) (Fig. 1). The reservoir is about 2.5 km long, has an average width of 40 m (between 35 and 120 m), an average slope of 3.8 ‰ (between 0.5 and 7 ‰), and a designed storage capacity of 900,000 m³. The weir system, used for drawdown flushing, consists of two radial gates with an attached top flap. The width and height of each gate are 12 m and 8.5 m, respectively. The average annual amount of siltation is estimated to be approximately 35,000 m³ [23].

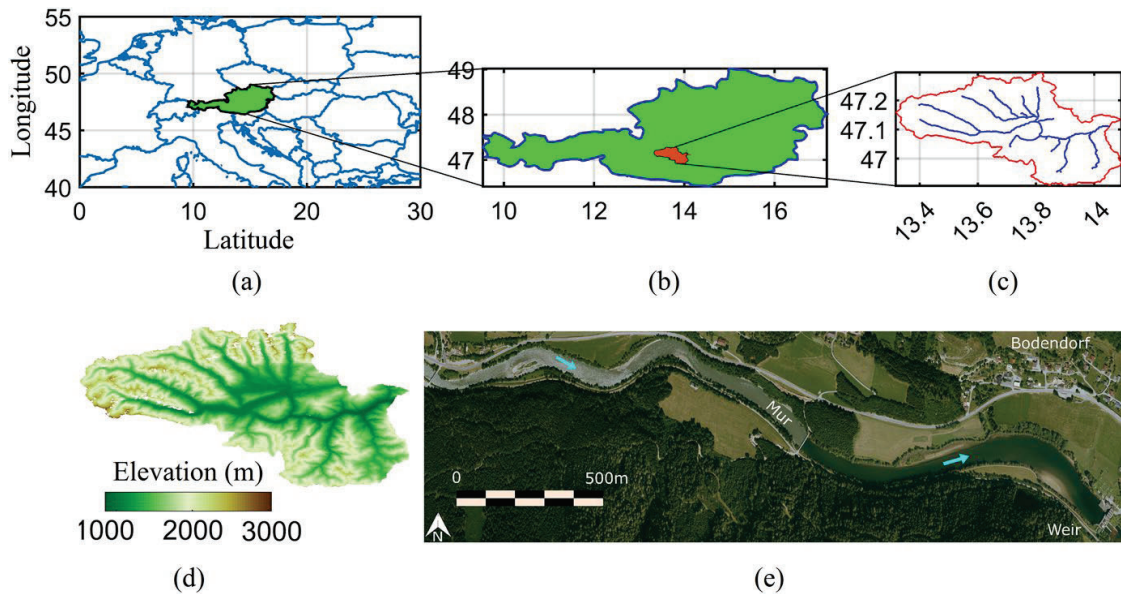


Fig. 1 **a** and **b** Austria (green) and the catchment area (red) that covers parts of the federal states Styria and Salzburg, **c** and **d** the river network and elevation map of the catchment, and **e** aerial photo of the Bodendorf reservoir

Since the first flushing operation in 1996, the reservoir has been subject to regular flushings. To develop sustainable reservoir management strategies for alpine reservoirs, comprehensive monitoring of the Bodendorf reservoir flushing was performed in 2004 within the framework of the EU Interreg IIIB project ALPRESERV, also considering ecological impacts on the downstream river section [24]. The duration of the 2004 flushing was 31 h, where the discharge reached a maximum of $134 \text{ m}^3/\text{s}$ under free flow conditions.

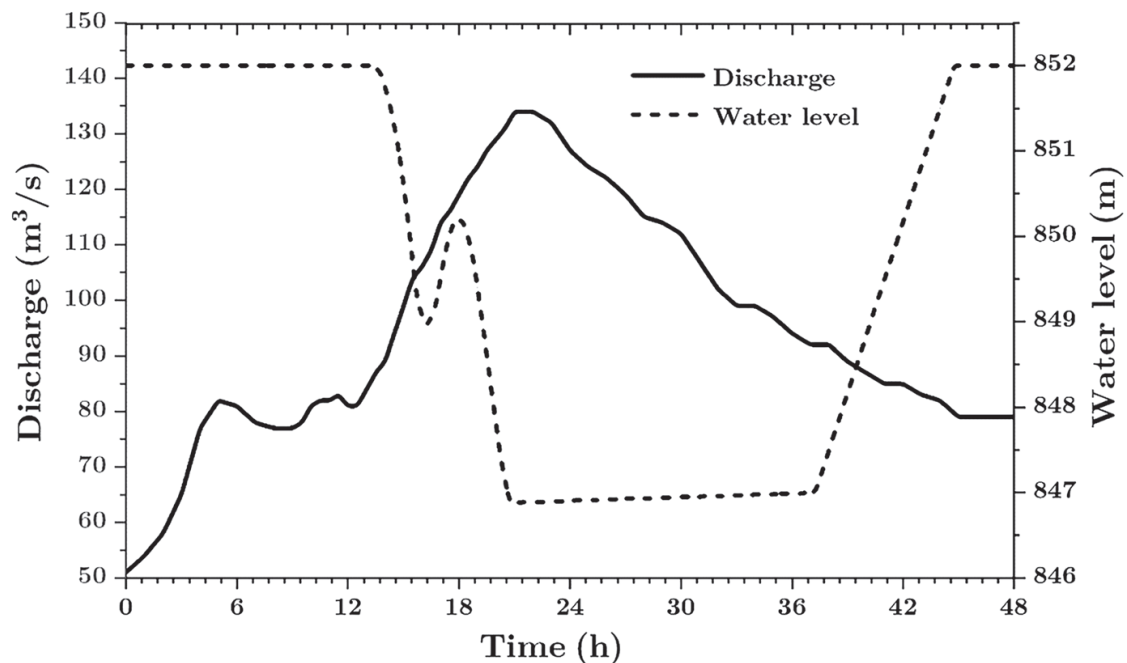


Fig. 2 The inflow discharge rate and the water level at the weir during the Bodendorf reservoir flushing in 2004

Figure 2 depicts the flushing hydrograph together with the corresponding water level at the weir, which is used as the boundary condition for simulations.

According to echo sounder measurements, the flushed-out volume was about 47,300 m³ [23]. The data obtained from bathymetry surveys conducted before and after the flushing are used to set up the numerical model and for automatic calibration.

2.2 Numerical modeling

The flow during reservoir flushing typically has three-dimensional behavior, including the effect of secondary currents in curved parts and in reaches where bedforms develop. This results in complex water–sediment interactions. The fully three-dimensional numerical model SSIIM (Sediment Simulation In Intakes with Multiblock option) is used in this study to calculate the hydraulics and morphological bed changes. SSIIM solves the Reynolds-averaged Navier–Stokes (RANS) equations (Eq. 1) along with the continuity equation (Eq. 2) on an unstructured and non-orthogonal adaptive grid [25]. The model has been successfully used in prototype-scale reservoir flushing studies and has yielded promising outcomes [26–29]. SSIIM employs a finite-volume approach for spatial discretization. An implicit time discretization scheme enables the use of large time steps in the model, which, together with the presence of the adaptive grid, reduces the computational time.

$$\frac{\partial U_i}{\partial t} + U_j \frac{\partial U_i}{\partial x_j} = \frac{1}{\rho} \frac{\partial}{\partial x_j} (-P\delta_{ij} - \rho \overline{u_i u_j}) \quad (1)$$

$$\frac{\partial U_i}{\partial x_i} = 0 \quad i = 1, 2, 3 \quad (2)$$

U is the time-averaged velocity, x represents the geometrical dimension, ρ is the fluid density, P denotes the dynamic pressure, δ_{ij} represents the Kronecker delta ($\delta_{ij} = 1$ if $i = j$, otherwise $\delta_{ij} = 0$), and $-\rho \overline{u_i u_j}$ (Eq. 3) is the turbulent Reynolds stress term [30], which is modeled by the k – ε turbulence closure scheme [31] to estimate the turbulent eddy viscosity ν_T :

$$-\overline{u_i u_j} = \nu_T \left(\frac{\partial U_i}{\partial x_j} + \frac{\partial U_j}{\partial x_i} \right) - \frac{2}{3} k \delta_{ij} \quad (3)$$

The pressure term is computed by the semi-implicit method for pressure-linked equations (SIMPLE) based on the water continuity defect in a cell [32]. The convective term in Eq. 1 is calculated by the power law scheme. The Rhie and Chow [33] momentum interpolation for non-staggered grids is used to estimate the cell-surface flux from the cell-center calculated velocity [34]. The free water surface is modeled by an implicit method based on the diffusive wave equation [35].

A Dirichlet boundary condition is specified for the variables at the upstream boundary, and the Neumann-type zero gradient boundary condition is applied to all variables at the downstream boundary. It means that the derivative (gradient) of variables normal to the boundary is set to zero and their value at the downstream boundary is defined to be equal to the calculated value in the closest cell to the boundary. The logarithmic wall function for rough boundaries (Eq. 4) is defined for the cells close to the bed [36].

$$u = \frac{u^*}{\kappa} \ln \left(\frac{30y}{k_s} \right) \quad (4)$$

where u and u^* are the flow and shear velocities, respectively, κ is the von Kármán constant ($=0.41$), y is the distance from the center of the border cell to the wall, and k_s is the roughness height.

The adaptive grid covers the area between the head of the reservoir and the weir structure; hence, the modeling domain ends at the upstream side of the dam. The grid consists of 20×390 horizontal cells in lateral and streamwise directions, respectively, and a maximum number of 10 vertical cells at the deepest part of the reservoir. The vertical profile refinement is a function of the free water surface and bed elevation changes that arise from the applied wetting/drying algorithm. The algorithm determines the number of cells formed vertically based on the calculated water depth after each time step, allowing the computational domain to vary spatiotemporally and be modified for the following time step. Figure 3 illustrates the computational grid used in this study.

Suspended sediment movement is modeled by solving the transient convection–diffusion equation (Eq. 5) together with the near-bed sediment concentration. The sediment resuspension from the bed is calculated by converting the concentration into the entrainment rate.

$$\frac{\partial c_i}{\partial t} + U_j \frac{\partial c_i}{\partial x_j} + \omega_i \frac{\partial c_i}{\partial z} = \frac{\partial}{\partial x_j} \left(\Gamma_T \frac{\partial c_i}{\partial x_j} \right) + F_{e,i} \quad (5)$$

where c_i is the concentration of the i th size class, ω_i denotes the particle settling velocity, $F_{e,i}$ is the sediment pick-up rate from erosion of i th particle from the bed, and $\Gamma_T = \nu_T / S_c$ is the turbulent diffusion coefficient. By assuming the Schmidt number (S_c) to be equal to 1, the turbulent diffusion is set equal to the eddy viscosity (ν_T). Then $\Gamma_T = \nu_T = c_\mu k^2 / \varepsilon$, where c_μ is a constant equal to 0.09, k is the turbulent kinetic energy, and ε denotes the energy dissipation. To estimate the near-bed equilibrium suspended sediment concentration, the empirical formula of van Rijn [37] is used as the boundary condition (Eq. 6).

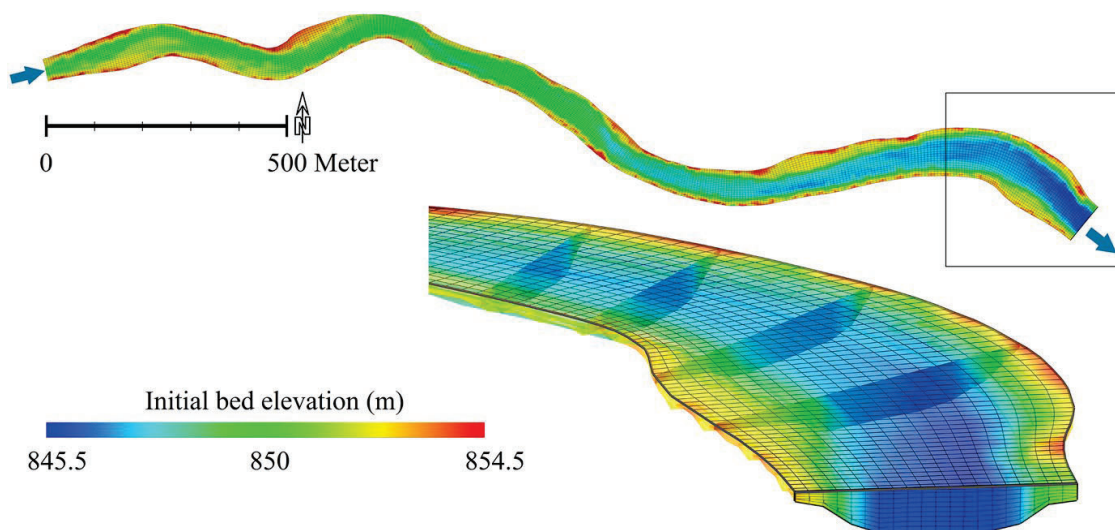


Fig. 3 **a** the computational domain of the Bodendorf reservoir and **b** a detailed view of the section upstream of the weir

$$c_{b,i} = 0.015 \frac{d_i}{a} \frac{\left(\frac{\tau - \tau_{c,i}}{\tau_{c,i}}\right)^{1.5}}{\left(d_i \left(\frac{(\rho_s - \rho_w)g}{\rho_w \nu^2}\right)^{\frac{1}{3}}\right)^{0.3}} \tag{6}$$

where $c_{b,i}$ is the volumetric near-bed concentration (reference concentration) of the i th fraction, d_i is the particle diameter, a denotes the near-bed reference level equal to the roughness height, τ is the bed shear stress, $\tau_{c,i}$ represents the critical bed shear stress for initiation of motion of the i th sediment fraction, obtained from the Shields diagram, ρ_s and ρ_w are sediment and water densities, respectively, g is the acceleration of gravity, and ν is the kinematic viscosity.

The bedload transport is then estimated by the empirical formulae of van Rijn [38]. Alternative sediment transport formulas tested in the current study are given by Wu [39], and Meyer-Peter and Müller [40]. The sediment transport formula gives the transport capacity that can be transformed to an equilibrium sediment concentration in a bed cell (c_e). The erosive ($F_{e,i}$) and deposition ($F_{d,i}$) sediment flux for size i is given in Eqs. 7 and 8, respectively.

$$F_{e,i} = c_{e,i} \omega_i \tag{7}$$

$$F_{d,i} = c_i \omega_i \tag{8}$$

The elevation changes in a bed cell related to the i th particle (Δz_i) during a time step (Δt) is then:

$$\Delta z_i = (F_{d,i} - F_{e,i}) \frac{\Delta t}{VFS} \tag{9}$$

The volume fraction of sediments (VFS) represents the sediment content in the bed material. The subsequent vertical movement of the grid is then computed by summing Eq. 9 over all the sediment sizes.

According to the sieve analysis of the samples collected from different sections of the Bodendorf reservoir, sediments are categorized into nine size classes for numerical modeling. The density of the sediments was set to 2.55 g/cm³. Table 1 shows the grain size distribution near the weir, middle section, and the head of the reservoir [23]. The particle distribution along the reservoir is linearly interpolated.

Table 1 Sediment characteristics used in the numerical model

	Sediment size class								
	1	2	3	4	5	6	7	8	9
Diameter (mm)	1	2	4	8	16	32	40	64	80
Proportion-inlet (%)	1	1	3	10	15	20	15	10	25
Proportion-center (%)	10	15	20	15	10	10	10	5	5
Proportion-outlet (%)	40	20	15	10	5	7	1	1	1

2.3 Model calibration

During calibration, the model is adapted by modifying input variables to achieve agreement between simulated and observed distributions of dependent variables. Hence, the model results should have a minimum allowable deviation from the values given in the performance criterion. The time-consuming and subjective nature of manual model calibration has prompted the development of optimization-based inverse modeling methods to expedite the procedure and establish an objective framework for model calibration. The three main elements of this approach are: one or more objective functions to quantify the discrepancies between the computed and measured values, an optimization algorithm to sample the parameter space and minimize the disagreements through iterative model runs, and a target convergence threshold to terminate iterations.

The model-independent nonlinear Parameter ESTimation and predictive uncertainty analysis tool PEST [41] is coupled with SSIIM to calibrate the models. This tool has shown satisfactory results regarding sensitivity analysis, parameter estimation, and automatic model calibration in various fields, e.g., hydraulics and sediment transport [42, 43], groundwater [44], stormwater management [45], and hydrological models [46].

PEST uses the gradient-based Gauss–Marquardt–Levenberg (GML) optimization algorithm, which solves nonlinear least-squares problems. The algorithm is a hybrid of gradient descent (first-order gradient-based) and Gauss–Newton (second-order curvature-based) methods. This combination improves efficiency by using the gradient descent method for steep regions of the objective function surface, while the algorithm acts as the Gauss–Newton method for the near-optimum shallow parts.

The relationship between input variables and model outputs is iteratively linearized by formulating a Taylor expansion of the current optimum parameter set (in the case of the first iteration, the initial user-defined values). During each optimization iteration, partial derivatives of outputs are calculated concerning input parameters by using the forward finite differences method and by running the model once for each adjustable parameter to generate an $m \times n$ Jacobian matrix (m = the number of model outputs, n = the number of parameters subject to calibration). Hence, each element of the Jacobian matrix J_{ij} contains the derivative of the i th output with respect to the j th parameter. The new parameter set can then be found by solving the linearized problem. By comparing the objective function value obtained from the latest iteration with those achieved in prior ones, PEST identifies whether another optimization iteration is required; if so, the procedure is repeated until the termination criteria are met. The GML algorithm aims to minimize the sum of the squares of the errors between predictions and observations as the objective function (Φ) through a sequence of parameter update vectors (u_{up}) within the user-specified bounds.

$$\Phi = (y - y')^T W (y - y') = \sum_{i=1}^m (w_i r_i)^2 \quad (10)$$

$$u_{up} = (J^T W J + \lambda I)^{-1} J^T W r \quad (11)$$

where y and y' are vectors of order m that hold observations and calculated values, respectively, W is an m -dimensional diagonal matrix containing squared observation weights w_i (which are taken to be 1 in this study), the superscript T represents matrix transpose, and r_i is the residual of the i th calculated-observed pair (in this study, bed elevations). The parameter upgrade vector u_{up} is calculated in accordance with J = Jacobian matrix containing the

derivatives of simulated values with respect to the calibration parameters, λ = Marquardt lambda as a damping factor, I = an n -dimensional identity matrix, and r = the vector of residuals.

The termination criterion for the optimization algorithm is set in a way that if the relative change of the objective function ($(\Phi_i - \Phi_{min})/\Phi_i$) is less than 0.005 over the four successive iterations, the algorithm stops the inversion process (Φ_i : objective function value at the end of the i th iteration; Φ_{min} : the lowest value of the objective function achieved so far during the whole optimization procedure) [41].

2.4 Calibration parameters

The response of a model to particular input parameter alteration needs to be analyzed in many modeling applications to determine how sensitive it reacts to adjustments. This may serve as the initial stage of the model calibration procedure, whereby key variables are determined. The sensitivity analysis in this study is performed by the SENSitivity ANalyzer tool (SENSAN), as a subset of the PEST program. The sensitivity of simulation results to parameter adjustments is tracked and recorded by successive model runs conducted by SENSAN using specified sets of parameter values. In this study, the following parameters show significant influence on the results and are selected for automatic calibration.

1. Parameters in van Rijn's bedload transport formula ($\alpha_1, \alpha_2, \alpha_3, \alpha_4$):

$$q_b = \alpha_1 \sqrt{\Delta g} \frac{T^{\alpha_2}}{D_*^{\alpha_3}} d_{50}^{\alpha_4} \quad (12)$$

q_b gives the bedload transport rate for particle size range $0.2 \leq d \leq 2$ mm.

- Δ is the submerged relative density of sediments ($= \frac{\rho_s - \rho_w}{\rho_w}$),
 - T is the transport stage parameter ($= \frac{\tau - \tau_c}{\tau_c}$),
 - D_* is known as the particle number ($= d_{50} \left(\frac{\Delta g}{v^2} \right)^{\frac{1}{3}}$),
 - $\alpha_1, \alpha_2, \alpha_3, \alpha_4$ are variables in the van Rijn equation and have the following values in the original formula: 0.053, 2.1, 0.3, 1.5, respectively.
2. Coefficient of Meyer-Peter and Müller's (MPM) sediment transport formula (β):

$$\phi_b = \beta (\tau^* - \tau_c^*)^{1.5} \quad (13)$$

where τ^* and τ_c^* are the bed shear stress and the critical bed shear stress in dimensionless form, respectively. This equation gives the bedload transport intensity verified with experimental data for uniform coarse sand and gravel. The original recommended value for the coefficient is $\beta = 8$. The contribution of other researchers to modify this formula based on different conditions and experimental data can be found in the literature, e.g., $\beta = 5.7$ [47] or $\beta = 12$ [48].

3. Hiding-exposure parameter (ξ):

The hiding-exposure effect of nonuniform sediments is calculated by Wu's correction factor (η_i) for the critical bed shear stress, based on the probabilities of hiding (p_{Hi}) and exposure (p_{Ei}) of the i th size fraction, which is stochastically related to the sediment size and gradation.

Table 2 Parameters for calibration with their initial values and allowable variation range

Parameter variation	Calibration parameters								
	α_1 (-)	α_2 (-)	α_3 (-)	α_4 (-)	β (-)	ξ (-)	k_s (m)	ALT (m)	VFS (%)
Upper boundary	0.106	4.20	0.60	3.00	12	0.9	0.4	1	70
Lower boundary	0.026	1.05	0.15	0.75	6	0.1	0.1	0.1	30
Initial value	0.053	2.10	0.30	1.50	8	0.6	0.2	0.5	50

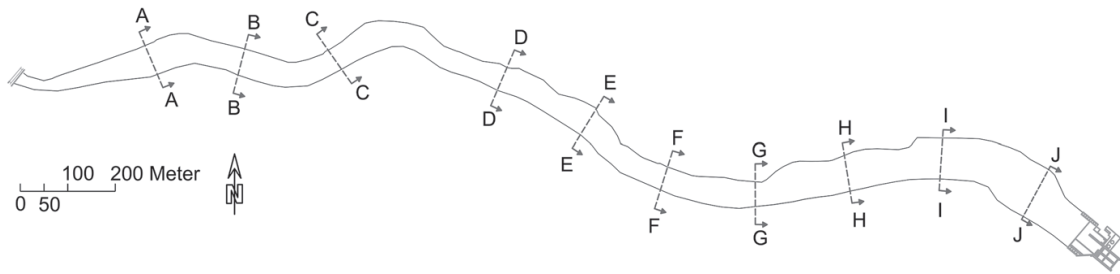


Fig. 4 The location of cross-sections with measured bed elevations used for calibration

$$\eta_i = \left(\frac{p_{Hi}}{p_{Ei}} \right)^\xi \tag{14}$$

the parameter ξ was originally calibrated using laboratory and field data, and a value of $\xi = 0.6$ was suggested.

- Effective bed roughness height (k_s) can be defined as the sum of the grain roughness (skin friction) and the bedform-induced resistance (form friction).

$$k_s = 3d_{90} + 1.1\Delta_d \left(1 - e^{\left(-25 \frac{\Delta_d}{\lambda_d} \right)} \right) \tag{15}$$

where d_{90} is the characteristic sediment size, and Δ_d and λ_d are bedform height and length, respectively.

- Active layer thickness (ALT) is the height of the erodible bed layer, where grain sorting and exchange processes occur, i.e., entrainment and deposition of sediments. The thickness of this layer is usually attributed to the representative grain diameter or the bedform height, depending on the transport regime. The value for this parameter in the numerical model defines the maximum erodible depth within a time step.
- The volume fraction of sediments (VFS) is a parameter to define the proportion of sediments to the water content in the bed deposit. Hence, it can also be expressed as one minus the porosity of the bed material. In the model, a single value is used for the entire modeling domain.

Table 2 summarizes the investigated parameters with their starting values, as well as the maximum and minimum boundary values introduced to the optimization algorithm.

The numerical models are calibrated against the measured bed elevations in 10 cross-sections along the reservoir (about 1300 measured points). Figure 4 depicts the location of the cross-sections.

3 Results and discussion

3.1 Calibrated values

The GML optimization algorithm is applied to three computational models using different sediment transport formulae. It ought to be mentioned that the GML algorithm, as a gradient-based optimization algorithm, initiates the search process from a single point on the objective function surface (i.e., using the initial values presented in Table 2); thus, this approach may lead to the solution getting trapped in local minima points over the search space instead of converging to the global minimum. Therefore, to validate the results, reassessing the calibration procedure with sampling-based optimization algorithms is beneficial. However, it is important to note that such algorithms may require significantly more iterations to sample the entire surface of the objective function and become impractical and inefficient for computationally expensive models, such as models simulating the hydro-morphological processes. The calibration results for the parameters mentioned in Sect. 2.4 are presented in Table 3. The number of model runs varies depending on the number of adjustable parameters since one run per parameter is required to build the Jacobian matrix within each optimization iteration. The lowest number of model runs is for Wu (62 runs), and the highest is for van Rijn (110 runs). The bedload transport formulae of van Rijn and Meyer-Peter and Müller (MPM) can be revised by replacing the values of α_i and β from Table 3 into Eqs. 12 and 13. Regarding van Rijn's formula, all parameters except α_4 , have higher values compared to the original formula. The relative change is in the range of 5 to 25%. The coefficient β in the MPM formula is slightly higher than the recommended value (8.9 compared to 8), resulting in a higher transport rate.

The hiding and exposure parameter is found to be almost half of the recommended ($\xi = 0.6$) value for all three models. The calibrated values for roughness are in the range between 21 and 29 cm, while the active layer thickness has a wide variation range (30–50 cm). The volume fraction of sediments is almost 60% for the models of van Rijn and MPM, whereas a value of 40% yields the best result for the model calculated by Wu's formula.

According to Table 3, it should be noted that the calibrated values are entirely model-dependent, and an identical optimized parameter combination may not be the best set if a model feature is changed. It means calibrating a hydro-morphodynamic model and then applying the optimized values to the same model with a different sediment

Table 3 Results of the three calibrated models using different sediment transport formulae

Model	Calibration parameters									Flushed volume (m ³)	Model runs
	α_1 (–)	α_2 (–)	α_3 (–)	α_4 (–)	β (–)	ξ (–)	k_s (m)	ALT (m)	VFS (%)		
van Rijn	0.067	2.22	0.35	1.05	–	0.24	0.21	0.30	59	52,200	110
MPM	–	–	–	–	8.9	0.29	0.29	0.40	61	37,800	78
Wu	–	–	–	–	–	0.30	0.24	0.50	40	43,900	62

$\alpha_1, \alpha_2, \alpha_3, \alpha_4$ = parameters used in van Rijn's bedload formula; β = coefficient of Meyer-Peter and Müller's bedload formula; ξ = correction factor for critical Shields number considering hiding and exposure effect; k_s = roughness height; ALT = active layer thickness; VFS = volume fraction of sediments in the bed

transport formula, which is a common approach when following the manual model calibration, does not necessarily lead to the best result.

3.2 Statistical performance of the models

To provide a quantitative and comparative evaluation of the model's capability to predict bed level changes, the deviation between calculated and measured bed elevations after flushing is assessed by several statistical indicators (Table 4). As a bias predictor, mean bias error (MBE) shows the model under- or over-estimation. Root mean squared error (RMSE) and mean absolute error (MAE) reflect the average error magnitude. While MAE shows a linear trend of individual errors, RMSE is dominated by large deviations, i.e., it emphasizes big errors by assigning them larger weights and is more sensitive to outliers. Kling–Gupta efficiency (KG) is applied as a composite goodness-of-fit metric, integrating correlation, variability, and bias into a single objective function. It is defined as the geometric mean of the Pearson correlation coefficient, the ratio of the standard deviation of predicted values to observations, and the ratio of the simulation mean to the observation mean. The Brier skill score (BSS), which measures the performance of simulations relative to a reference or baseline prediction (initial bed levels before flushing), is also used. BSS compares the mean squared error (MSE) between the simulation and observation with the MSE between the baseline prediction and observation. The range for BSS is between $-\infty$ and 1.

The negative value of MBE for the van Rijn model shows the overprediction of the bed erosion, while the other two models underpredict the eroded sediments by having positive values. According to their lower MAE and RMSE values, the models using the formulae of van Rijn and Wu have better performance than the model using the formula of MPM. This can further be confirmed by higher values of the Kling–Gupta efficiency and Brier skill score of van Rijn and Wu models. According to van Rijn et al. [49], a value of $0.3 \leq \text{BSS} \leq 0.6$ shows a “reasonable/fair” model prediction. The prediction can be stated as “good” if the value is in the range of 0.6–0.8. Models having BSS values over 0.8 or under 0.3 have “excellent” or “poor” performance, respectively. In the case of a negative value, the model has a “bad” performance. Therefore, both models simulated by the formulae of van Rijn and Wu can be called “good” predictors of the flushing event in this study. The model calculated by the MPM bedload formula also gives a “reasonable/fair” result.

Table 4 Overall statistical performance of the automatically calibrated models regarding bed level changes with different bedload transport formulae

Model	Goodness-of-fit				
	MBE (m)	MAE (m)	RMSE (m)	KG (–)	BSS (–)
van Rijn	–0.11	0.23	0.35	0.98	0.64
MPM	0.13	0.30	0.41	0.95	0.51
Wu	0.08	0.25	0.35	0.97	0.65

MBE mean bias error, *MAE* mean absolute error, *RMSE* root mean squared error, *KG* Kling–Gupta efficiency, *BSS* Brier skill score

3.3 Bed level changes

Figure 5 shows measured bed elevations in 10 cross-sections before and after flushing together with the bed levels from the three automatically calibrated models. The statistical metrics presented in Sect. 3.2 are also used to evaluate the cross-sectional bed level changes (Table 5).

Although the pattern of calculated bed levels after flushing for all three models agrees well with their measured pairs, slight local discrepancies can be seen in some cross-sections. Looking at the most upstream-located cross-section (A–A), the small eroded part at the orographic right river bank cannot be seen in the simulations. In section B–B, a steep drop at the right bank with a sharp rise toward the center can be noticed in the measured bed pattern, which is not the case for the results of the numerical models. This reverse fluctuating pattern compared to the initial bed can be attributed to the occurrence of the lateral sand slide, which is approximated by the program but cannot be resolved [50]. Here, almost the same volume of sliding sediments is deposited in the middle part. Furthermore, cross-section B–B has the highest simulated bed level deviation from the measured data according to MAE and RMSE values in Table 5.

The discrepancies between simulation results and the observed bed pattern after flushing in cross-section C–C can be seen at the left and right edges of the flushing channel, where measurements show an extended channel widening close to the reservoir banks. Particularly for the model using the formula of MPM, the results show an about 1-m bed elevation difference compared to the measurement at distances of 60 and 90 m along the cross-section. A similar issue regarding the depth and width of the eroded part persists for cross-section D–D at the left side and for cross-sections E–E, F–F, G–G, and H–H at the left and right edges of the flushing channel. For the aforementioned sections, the model using the formula of van Rijn gives the closest simulated patterns to the measurements, which can be confirmed by the lowest MAE and RMSE as well as the highest KG and BSS values of the van Rijn model presented in Table 5.

The calculated patterns for two cross-sections adjacent to the weir (I–I and J–J) are almost identical to those observed. Slight differences can be noticed at the left slope of cross-section I–I simulated by the MPM model, as well as the right slope and central part of cross-section J–J calculated by the van Rijn model. Although the predicted bed patterns by all three models are similar in these two cross-sections (almost similar KG efficiency values according to Table 5), other statistical metrics reveal the better performance of the Wu model.

3.4 Flushed volume

The total flushed volume of sediments (presented in Table 3) confirms the trend of over- or underestimation of erosion, which can be seen in the cross-sections in Fig. 5. Compared to the measured flushed volume of 47,300 m³, van Rijn's model overestimates the erosion (52,200 m³), whereas underestimations are found by the models of MPM and Wu (37,800 m³ and 43,900 m³, respectively). The deviation between calculated and measured flushed volumes is about $\pm 10\%$ for van Rijn and Wu models and -20% for MPM.

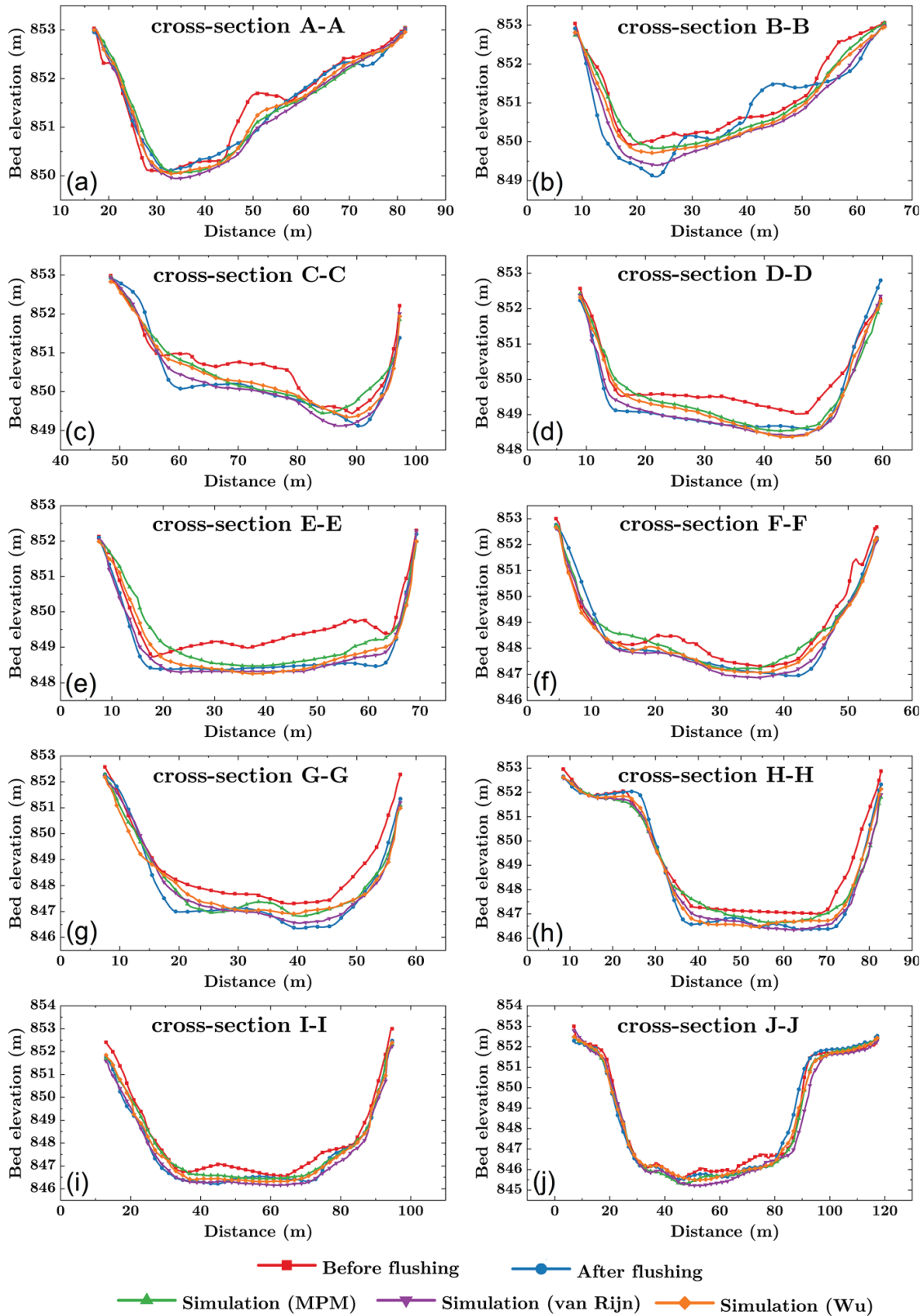


Fig. 5 Simulated bed levels of the Bodendorf reservoir after flushing using the formulae of Meyer-Peter and Müller (MPM), van Rijn, and Wu in 10 cross-sections, including the measured bed levels before and after flushing

Table 5 Cross-sectional goodness-of-fit for models using different bedload transport formulae

Cross-section	Model	Goodness-of-fit				
		MBE (m)	MAE (m)	RMSE (m)	KG (-)	BSS (-)
A-A	van Rijn	-0.10	0.14	0.17	0.91	0.60
	MPM	-0.03	0.13	0.15	0.96	0.66
	Wu	-0.03	0.12	0.14	0.95	0.72
B-B	van Rijn	-0.15	0.35	0.45	0.92	0.45
	MPM	0.12	0.45	0.56	0.85	0.14
	Wu	0.01	0.41	0.50	0.88	0.33
C-C	van Rijn	-0.05	0.16	0.20	0.97	0.83
	MPM	0.18	0.27	0.36	0.87	0.45
	Wu	0.10	0.21	0.28	0.88	0.68
D-D	van Rijn	-0.07	0.16	0.22	0.94	0.85
	MPM	0.14	0.34	0.44	0.87	0.45
	Wu	0.06	0.26	0.33	0.93	0.69
E-E	van Rijn	0.01	0.12	0.15	0.98	0.95
	MPM	0.37	0.39	0.52	0.92	0.52
	Wu	0.13	0.23	0.33	0.94	0.81
F-F	van Rijn	-0.13	0.20	0.26	0.93	0.78
	MPM	0.18	0.34	0.45	0.86	0.33
	Wu	-0.04	0.25	0.38	0.87	0.52
G-G	van Rijn	0.08	0.23	0.31	0.93	0.87
	MPM	0.20	0.35	0.42	0.85	0.75
	Wu	0.16	0.43	0.53	0.79	0.61
H-H	van Rijn	-0.06	0.20	0.24	0.95	0.87
	MPM	0.13	0.39	0.49	0.87	0.46
	Wu	0.02	0.23	0.31	0.94	0.77
I-I	van Rijn	-0.12	0.18	0.23	0.97	0.81
	MPM	0.21	0.24	0.31	0.96	0.68
	Wu	0.08	0.17	0.21	0.98	0.83
J-J	van Rijn	-0.22	0.29	0.49	0.96	0.15
	MPM	-0.15	0.23	0.37	0.98	0.35
	Wu	-0.08	0.19	0.28	0.99	0.41

The best value of different metrics in each cross-section is highlighted in bold form

4 Conclusions

This study employs an automatically calibrated 3D numerical model of the Bodendorf reservoir to simulate the 2004 flushing event. The bed level changes and the volume of flushed sediments are calculated using the formulae of Meyer-Peter and Müller, van Rijn, and Wu. Prior to calibration, a sensitivity analysis is performed to detect the most affecting parameters in the model (i.e., the roughness height, active layer thickness, volume fraction of sediments in bed, hiding-exposure parameter, and empirical factors in the formulae of van Rijn and MPM). The measured bed elevation data from 10 cross-sections (about 1300 points) along the reservoir is used for calibration. The optimization

algorithm runs the models several times based on the number of parameters subject to calibration. The formulae of van Rijn and MPM are modified during the optimization by finding new values for their empirical parameters. The parameter regarding the hiding-exposure behavior of nonuniform sediments introduced by Wu is also modified by a factor of 0.5. The calibration results for the roughness height, active layer thickness, and the volume fraction of sediments are found to be model-dependent, where different sediment transport formulae yield a unique parameter combination leading to an optimized outcome.

The performance of the calibrated models is investigated by different statistical metrics. According to the mean absolute error, root mean squared error, and Kling–Gupta efficiency, the models using the formulae of van Rijn and Wu outperform the model calculated by the MPM formula in terms of error amount and correlation. The two former models show almost equal performance, and no clear statistical evidence of superiority exists among them. This is also confirmed by the Brier skill score, where both van Rijn and Wu models have almost the same score, indicating their “good” performance. According to the evaluation criteria of the Brier skill score, the model simulated by the MPM formula has a “reasonable/fair” performance.

Patterns of simulated bed elevations in 10 cross-sections are compared with the measured data, which are in good agreement with the observations. The discrepancies are limited to the local differences as a result of sand slides in the two most upstream cross-sections, as well as the underestimation of lateral erosion and widening of the flushing channel at middle cross-sections of the reservoir, especially those predicted by the model using the MPM formula. The calculated flushed volume of sediments shows a reasonable agreement (approximately $\pm 10\%$ regarding van Rijn and Wu models and -20% for MPM) compared to the measured flushed volume of $47,300 \text{ m}^3$.

This study provides an overview of applying automatic calibration for hydro-morphodynamic models in a prototype scale and shows how the best fit can be objectively achieved. According to the number of model runs and considering innumerable parameter combinations, it can be concluded that employing optimization algorithms is a suitable and efficient alternative for the widely used subjective trial-and-error calibration approach.

To improve the validity and reliability of the automatic calibration, future work can include a multi-objective optimization approach to consider additional aspects of the model, e.g., measured downstream sediment concentrations during the flushing event to define a second objective function in addition to the bed level changes. Then, instead of achieving a single value for investigated uncertain parameters, a set of equally good and non-dominated solutions (Pareto front) can be found, which would be interesting to be compared with the results of the single-objective method. A challenge in this regard is related to using global optimization algorithms, which require orders of magnitude more model runs for sampling the entire objective function surface. However, the issue can be tackled by applying surrogate modeling techniques [51].

Acknowledgements The first author would like to express his grateful acknowledgment to the Sustainable Water Management-NaWaM program of the German Academic Exchange Service (DAAD). The last author is indebted to the Elite program for Postdocs of the Baden-Württemberg Stiftung.

Author contributions Conceptualization: VS, and SH; Methodology: VS, NRBO, and SH; Formal analysis and investigation: VS, NRBO, and SH; Software: VS and NRBO; Resources: NRBO, and SH; Writing—original draft preparation: VS; Writing—review and editing: VS, SW, NRBO, and SH; Supervision: SW, and SH; Project administration: SH. All authors read and approved the final version of the manuscript.

Funding Open Access funding enabled and organized by Projekt DEAL. This research received no external funding/grant/financial support.

Data availability The data analyzed during the current study are available from the corresponding author upon reasonable request.

Declarations

Conflict of interest The authors declare no conflict of interest.

Open Access This article is licensed under a Creative Commons Attribution 4.0 International License, which permits use, sharing, adaptation, distribution and reproduction in any medium or format, as long as you give appropriate credit to the original author(s) and the source, provide a link to the Creative Commons licence, and indicate if changes were made. The images or other third party material in this article are included in the article's Creative Commons licence, unless indicated otherwise in a credit line to the material. If material is not included in the article's Creative Commons licence and your intended use is not permitted by statutory regulation or exceeds the permitted use, you will need to obtain permission directly from the copyright holder. To view a copy of this licence, visit <http://creativecommons.org/licenses/by/4.0/>.

References


1. Aksoy H, Kavvas ML (2005) A review of hillslope and watershed scale erosion and sediment transport models. *CATENA* 64:247–271. <https://doi.org/10.1016/j.catena.2005.08.008>
2. Minear JT, Kondolf GM (2009) Estimating reservoir sedimentation rates at large spatial and temporal scales: A case study of California. *Water Resour Res*. <https://doi.org/10.1029/2007WR006703>
3. Fan J, Morris GL (1992) Reservoir sedimentation. I: delta and density current deposits. *J Hydraul Eng* 118:354–369. [https://doi.org/10.1061/\(ASCE\)0733-9429\(1992\)118:3\(354\)](https://doi.org/10.1061/(ASCE)0733-9429(1992)118:3(354))
4. Annandale GW (2006) Reservoir sedimentation. In: *Encyclopedia of hydrological sciences*. Wiley, Hoboken. <https://doi.org/10.1002/0470848944.hsa086>
5. Oehy CD, Schleiss AJ (2007) Control of turbidity currents in reservoirs by solid and permeable obstacles. *J Hydraul Eng* 133:637–648. [https://doi.org/10.1061/\(ASCE\)0733-9429\(2007\)133:6\(637\)](https://doi.org/10.1061/(ASCE)0733-9429(2007)133:6(637))
6. Mahmood K (1987) Reservoir sedimentation: impact, extent, and mitigation. Technical paper No. WTP 71, International Bank for Reconstruction and Development, Washington, DC, USA
7. Schleiss AJ, Franca MJ, Juez C, De Cesare G (2016) Reservoir sedimentation. *J Hydraul Res* 54:595–614. <https://doi.org/10.1080/00221686.2016.1225320>
8. Kondolf GM, Gao Y, Annandale GW, Morris GL, Jiang E, Zhang J, Cao Y, Carling P, Fu K, Guo Q, Hotchkiss R, Peteuil C, Sumi T, Wang H-W, Wang Z, Wei Z, Wu B, Wu C, Yang CT (2014) Sustainable sediment management in reservoirs and regulated rivers: experiences from five continents. *Earth's Future* 2:256–280. <https://doi.org/10.1002/2013EF000184>
9. Hauer C, Wagner B, Aigner J, Holzapfel P, Flödl P, Liedermann M, Tritthart M, Sindelar C, Pulg U, Klösch M, Haimann M, Donnum BO, Stickler M, Habersack H (2018) State of the art, shortcomings and future challenges for a sustainable sediment management in hydropower: a review. *Renew Sustain Energy Rev* 98:40–55. <https://doi.org/10.1016/j.rser.2018.08.031>
10. Morris GL, Fan J (1998) Reservoir sedimentation handbook: design and management of dams, reservoirs, and watersheds for sustainable use. McGraw-Hill, New York
11. Atkinson E (1996) The feasibility of flushing sediment from reservoirs. HR Wallingford Report OD 137, London, UK
12. Guertault L, Camenen B, Peteuil C, Paquier A, Faure JB (2016) One-dimensional modeling of suspended sediment dynamics in dam reservoirs. *J Hydraul Eng* 142:04016033. [https://doi.org/10.1061/\(ASCE\)HY.1943-7900.0001157](https://doi.org/10.1061/(ASCE)HY.1943-7900.0001157)
13. Habib-ur-Rehman, Chaudhry MA, Naeem UA, Hashmi HN (2018) Performance evaluation of 1-D numerical model HEC-RAS towards modeling sediment depositions and sediment flushing operations for the reservoirs. *Environ Monit Assess* 190:433. <https://doi.org/10.1007/s10661-018-6755-7>
14. Iqbal M, Ghumman AR, Haider S, Hashmi HN, Khan MA (2019) Application of Godunov type 2D model for simulating sediment flushing in a reservoir. *Arab J Sci Eng* 44:4289–4307. <https://doi.org/10.1007/s13369-018-3381-1>
15. Reisenbüchler M, Bui MD, Skublics D, Rutschmann P (2020) Sediment management at run-of-river reservoirs using numerical modelling. *Water* 12:249. <https://doi.org/10.3390/w12010249>

16. Haun S, Olsen NRB (2012) Three-dimensional numerical modelling of reservoir flushing in a prototype scale. *Int J River Basin Manag* 10:341–349. <https://doi.org/10.1080/15715124.2012.736388>
17. Sawadogo O, Basson GR, Schneiderbauer S (2019) Physical and coupled fully three-dimensional numerical modeling of pressurized bottom outlet flushing processes in reservoirs. *Int J Sediment Res* 34:461–474. <https://doi.org/10.1016/j.ijsrc.2019.02.001>
18. Khanpour M, Zarrati AR, Kolahdoozan M, Shakibaeinia A, Amirshahi SM (2016) Mesh-free SPH modeling of sediment scouring and flushing. *Comput Fluids* 129:67–78. <https://doi.org/10.1016/j.compfluid.2016.02.005>
19. Shoarinezhad V, Wieprecht S, Haun S (2020) Automatic calibration of a 3D morphodynamic numerical model for simulating bed changes in a 180° channel bend. In: Kalinowska MB, Mrokowska MM, Rowiński PM (eds) *Recent trends in environmental hydraulics, geoplanet: earth and planetary sciences*. Springer, Cham, pp 253–262. https://doi.org/10.1007/978-3-030-37105-0_22
20. Shoarinezhad V, Wieprecht S, Haun S (2020) Comparison of local and global optimization methods for calibration of a 3D morphodynamic model of a curved channel. *Water* 12:1333. <https://doi.org/10.3390/w12051333>
21. Mouris K, Acuna Espinoza E, Schwindt S, Mohammadi F, Haun S, Wieprecht S, Oladyskhin S (2023) Stability criteria for Bayesian calibration of reservoir sedimentation models. *Model Earth Syst Environ*. <https://doi.org/10.1007/s40808-023-01712-7>
22. Schwindt S, Callau Medrano S, Mouris K, Beckers F, Haun S, Nowak W, Wieprecht S, Oladyskhin S (2023) Bayesian calibration points to misconceptions in three-dimensional hydrodynamic reservoir modeling. *Water Resour Res* 59:e2022WR033660. <https://doi.org/10.1029/2022WR033660>
23. Badura H (2007) *Feststofftransportprozesse während Spülungen von Flusstauräumen am Beispiel der oberen Mur*. PhD thesis, Schriftenreihe zur Wasserwirtschaft der Technischen Universität Graz 51, Graz, Austria
24. Badura H, Knoblauch H, Schneider J, Harreiter H, Demel S (2007) Wasserwirtschaftliche Optimierung der stauräumspülungen an der oberen mur. *Österr Wasser- Abfallwirtsch* 59:61–68. <https://doi.org/10.1007/s00506-007-0101-6>
25. Olsen NRB (2014) *A three dimensional numerical model for simulation of sediment movement in water intakes with multiblock option*. Department of Hydraulic and Environmental Engineering, The Norwegian University of Science and Technology, Trondheim
26. Haun S, Olsen NRB (2012) Three-dimensional numerical modelling of the flushing process of the Kali Gandaki hydropower reservoir. *Lakes Reserv Sci Policy Manag Sustain Use* 17:25–33. <https://doi.org/10.1111/j.1440-1770.2012.00491.x>
27. Isaac N, Eldho TI (2019) Experimental and numerical simulations of the hydraulic flushing of reservoir sedimentation for planning and design of a hydropower project. *Lakes Reserv Sci Policy Manag Sustain Use* 24:259–274. <https://doi.org/10.1111/lre.12278>
28. Mohammad ME, Al-Ansari N, Knutsson S, Laue J (2020) A computational fluid dynamics simulation model of sediment deposition in a storage reservoir subject to water withdrawal. *Water* 12:959. <https://doi.org/10.3390/w12040959>
29. Esmaeili T, Sumi T, Kantoush SA, Kubota Y, Haun S, Rütther N (2021) Numerical study of discharge adjustment effects on reservoir morphodynamics and flushing efficiency: an outlook for the Unazuki Reservoir, Japan. *Water* 13:1624. <https://doi.org/10.3390/w13121624>
30. Versteeg HK, Malalasekera W (2007) *An introduction to computational fluid dynamics: the finite volume method*, 2nd edn. Pearson Education Ltd, Harlow
31. Launder BE, Spalding DB (1972) *Lectures in mathematical models of turbulence*. Academic Press, London
32. Patankar SV (1980) *Numerical heat transfer and fluid flow*. McGraw-Hill, New York
33. Rhie CM, Chow WL (1983) Numerical study of the turbulent flow past an airfoil with trailing edge separation. *AIAA J* 21:1525–1532. <https://doi.org/10.2514/3.8284>
34. Ferziger JH, Perić M, Street RL (2020) *Computational methods for fluid dynamics*, 4th edn. Springer, Cham. <https://doi.org/10.1007/978-3-319-99693-6>
35. Olsen NRB (2015) Four free surface algorithms for the 3D Navier–Stokes equations. *J Hydroinform* 17:845–856. <https://doi.org/10.2166/hydro.2015.012>
36. Schlichting H, Gersten K (2017) *Boundary-layer theory*, 9th edn. Springer, Berlin. <https://doi.org/10.1007/978-3-662-52919-5>
37. van Rijn LC (1984) Sediment Transport, Part II: Suspended Load Transport. *J Hydraul Eng* 110:1613–1641. [https://doi.org/10.1061/\(ASCE\)0733-9429\(1984\)110:11\(1613\)](https://doi.org/10.1061/(ASCE)0733-9429(1984)110:11(1613))
38. van Rijn LC (1984) Sediment transport, part I: bed load transport. *J Hydraul Eng* 110:1431–1456. [https://doi.org/10.1061/\(ASCE\)0733-9429\(1984\)110:10\(1431\)](https://doi.org/10.1061/(ASCE)0733-9429(1984)110:10(1431))

39. Wu W, Wang SSY, Jia Y (2000) Nonuniform sediment transport in alluvial rivers. *J Hydraul Res* 38:427–434. <https://doi.org/10.1080/00221680009498296>
40. Meyer-Peter E, Müller R (1948) Formulas for bed-load transport. In: Proceedings of the 2nd meeting of the international association for hydraulic structures research, Stockholm, Sweden, pp 39–64
41. Doherty J (2016) PEST model-independent parameter estimation user manual Part I, 6th edn. Watermark Numerical Computing, Brisbane
42. Lavoie B, Mahdi T-F (2020) Manning’s roughness coefficient determination in laboratory experiments using 2D modeling and automatic calibration. *Houille Blanche* 106:22–33. <https://doi.org/10.1051/lhb/2020001>
43. Shoarinezhad V, Wieprecht S, Kantoush SA, Haun S (2023) Applying optimization methods for automatic calibration of 3D morphodynamic numerical models of shallow reservoirs: comparison between lozenge- and hexagon-shaped reservoirs. *J Hydroinform* 25:85–100. <https://doi.org/10.2166/hydro.2022.094>
44. Rajaeian S, Ketabchi H, Ebadi T (2023) Investigation on quantitative and qualitative changes of groundwater resources using MODFLOW and MT3DMS: a case study of Hashtgerd aquifer, Iran. *Environ Dev Sustain*. <https://doi.org/10.1007/s10668-022-02904-4>
45. Perin R, Trigatti M, Nicolini M, Campolo M, Goi D (2020) Automated calibration of the EPA-SWMM model for a small suburban catchment using PEST: a case study. *Environ Monit Assess* 192:374. <https://doi.org/10.1007/s10661-020-08338-7>
46. Alp H, Demirel MC, Aşikoğlu ÖL (2022) Effect of model structure and calibration algorithm on discharge simulation in the Acısu Basin, Turkey. *Climate* 10:196. <https://doi.org/10.3390/cli10120196>
47. Fernandez Luque R, Van Beek R (1976) Erosion and transport of bed-load sediment. *J Hydraul Res* 14:127–144. <https://doi.org/10.1080/00221687609499677>
48. Wilson KC (1966) Bed-load transport at high shear stress. *J Hydraul Div* 92:49–59. <https://doi.org/10.1061/JYCEAJ.0001562>
49. van Rijn LC, Walstra DJR, Grasmeijer B, Sutherland J, Pan S, Sierra JP (2003) The predictability of cross-shore bed evolution of sandy beaches at the time scale of storms and seasons using process-based profile models. *Coast Eng* 47:295–327. [https://doi.org/10.1016/S0378-3839\(02\)00120-5](https://doi.org/10.1016/S0378-3839(02)00120-5)
50. Olsen NRB, Haun S (2020) A numerical geotechnical model for computing soil slides at banks of water reservoirs. *Int J Geo-Eng*. <https://doi.org/10.1186/s40703-020-00129-w>
51. Beckers F, Heredia A, Noack M, Nowak W, Wieprecht S, Oladyshkin S (2020) Bayesian calibration and validation of a large-scale and time-demanding sediment transport model. *Water Resour Res* 56:e2019WR026966. <https://doi.org/10.1029/2019WR026966>

Publisher’s Note Springer Nature remains neutral with regard to jurisdictional claims in published maps and institutional affiliations.

Authors and Affiliations

Vahid Shoarinezhad¹  · Nils Reidar Bøe Olsen²  · Silke Wieprecht¹  · Stefan Haun¹ 

✉ Vahid Shoarinezhad
vahid.shoarinezhad@iws.uni-stuttgart.de

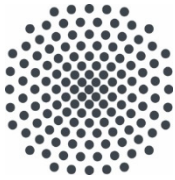
Nils Reidar Bøe Olsen
nils.r.olsen@ntnu.no

Silke Wieprecht
wieprecht@iws.uni-stuttgart.de

Stefan Haun
stefan.haun@iws.uni-stuttgart.de

¹ Institute for Modeling Hydraulic and Environmental Systems, University of Stuttgart, 70569 Stuttgart, Germany

² Department of Civil and Environmental Engineering, Norwegian University of Science and Technology, S.P. Andersens veg 5, 7491 Trondheim, Norway



Institut für Wasser- und Umweltsystemmodellierung Universität Stuttgart

Pfaffenwaldring 61
70569 Stuttgart (Vaihingen)
Telefon (0711) 685 - 60156
Telefax (0711) 685 - 51073
E-Mail: iws@iws.uni-stuttgart.de
<http://www.iws.uni-stuttgart.de>

Direktoren

Prof. Dr.-Ing. Rainer Helmig
Prof. Dr.-Ing. Wolfgang Nowak
Prof. Dr.-Ing. Silke Wieprecht

Emeriti

Prof. Dr.-Ing. habil. Dr.-Ing. E.h. Jürgen Giesecke
Prof. Dr.h.c. Dr.-Ing. E.h. Helmut Kobus, PhD

Lehrstuhl für Wasserbau und Wassermengenwirtschaft

Leiterin: Prof. Dr.-Ing. Silke Wieprecht
Stellv.: Dr.-Ing. Kristina Terheiden
Versuchsanstalt für Wasserbau
Leiter: Stefan Haun, PhD

Lehrstuhl für Hydromechanik und Hydrosystemmodellierung

Leiter: Prof. Dr.-Ing. Rainer Helmig
Stellv.: apl. Prof. Dr.-Ing. Holger Class

Lehrstuhl für Stochastische Simulation und Sicherheitsforschung für Hydrosysteme

Leiter: Prof. Dr.-Ing. Wolfgang Nowak
Stellv.: apl. Prof. Dr.-Ing. Sergey Oladyshkin
Hydrogeophysik der Vadosen Zone
(mit Forschungszentrum Jülich)
Leiter: Prof. Dr. J.A. Sander Huisman

VEGAS, Versuchseinrichtung zur Grundwasser- und Altlastensanierung

Leiter: Dr.-Ing. Simon Kleinknecht
PD Dr.-Ing. Claus Haslauer

Verzeichnis der Mitteilungshefte

- 1 Röhnisch, Arthur: *Die Bemühungen um eine Wasserbauliche Versuchsanstalt an der Technischen Hochschule Stuttgart*, und Fattah Abouleid, Abdel: *Beitrag zur Berechnung einer in lockeren Sand gerammten, zweifach verankerten Spundwand*, 1963
- 2 Marotz, Günter: *Beitrag zur Frage der Standfestigkeit von dichten Asphaltbelägen im Großwasserbau*, 1964
- 3 Gurr, Siegfried: *Beitrag zur Berechnung zusammengesetzter ebener Flächentragwerke unter besonderer Berücksichtigung ebener Stauwände, mit Hilfe von Randwert- und Lastwertmatrizen*, 1965
- 4 Plica, Peter: *Ein Beitrag zur Anwendung von Schalenkonstruktionen im Stahlwasserbau*, und Petrikat, Kurt: *Möglichkeiten und Grenzen des wasserbaulichen Versuchswesens*, 1966
- 5 Plate, Erich: *Beitrag zur Bestimmung der Windgeschwindigkeitsverteilung in der durch eine Wand gestörten bodennahen Luftschicht*, und Röhnisch, Arthur; Marotz, Günter: *Neue Baustoffe und Bauausführungen für den Schutz der Böschungen und der Sohle von Kanälen, Flüssen und Häfen; Gesteigungskosten und jeweilige Vorteile*, sowie Unny, T.E.: *Schwingungsuntersuchungen am Kegelstrahlschieber*, 1967
- 6 Seiler, Erich: *Die Ermittlung des Anlagenwertes der bundeseigenen Binnenschiffahrtsstraßen und Talsperren und des Anteils der Binnenschiffahrt an diesem Wert*, 1967

- 7 *Sonderheft anlässlich des 65. Geburtstages von Prof. Arthur Röhnisch mit Beiträgen von Benk, Dieter; Breitling, J.; Gurr, Siegfried; Haberhauer, Robert; Honekamp, Hermann; Kuz, Klaus Dieter; Marotz, Günter; Mayer-Vorfelder, Hans-Jörg; Miller, Rudolf; Plate, Erich J.; Radomski, Helge; Schwarz, Helmut; Vollmer, Ernst; Wildenhahn, Eberhard; 1967*
- 8 *Jumikis, Alfred: Beitrag zur experimentellen Untersuchung des Wassernachschubs in einem gefrierenden Boden und die Beurteilung der Ergebnisse, 1968*
- 9 *Marotz, Günter: Technische Grundlagen einer Wasserspeicherung im natürlichen Untergrund, 1968*
- 10 *Radomski, Helge: Untersuchungen über den Einfluß der Querschnittsform wellenförmiger Spundwände auf die statischen und rammtechnischen Eigenschaften, 1968*
- 11 *Schwarz, Helmut: Die Grenztragfähigkeit des Baugrundes bei Einwirkung vertikal gezogener Ankerplatten als zweidimensionales Bruchproblem, 1969*
- 12 *Erbel, Klaus: Ein Beitrag zur Untersuchung der Metamorphose von Mittelgebirgsschneedecken unter besonderer Berücksichtigung eines Verfahrens zur Bestimmung der thermischen Schneequalität, 1969*
- 13 *Westhaus, Karl-Heinz: Der Strukturwandel in der Binnenschifffahrt und sein Einfluß auf den Ausbau der Binnenschiffskanäle, 1969*
- 14 *Mayer-Vorfelder, Hans-Jörg: Ein Beitrag zur Berechnung des Erdwiderstandes unter Ansatz der logarithmischen Spirale als Gleitflächenfunktion, 1970*
- 15 *Schulz, Manfred: Berechnung des räumlichen Erddruckes auf die Wandung kreiszylindrischer Körper, 1970*
- 16 *Mobasseri, Manoutschehr: Die Rippenstützmauer. Konstruktion und Grenzen ihrer Standsicherheit, 1970*
- 17 *Benk, Dieter: Ein Beitrag zum Betrieb und zur Bemessung von Hochwasserrückhaltebecken, 1970*
- 18 *Gál, Attila: Bestimmung der mitschwingenden Wassermasse bei überströmten Fischbauchklappen mit kreiszylindrischem Staublech, 1971, vergriffen*
- 19 *Kuz, Klaus Dieter: Ein Beitrag zur Frage des Einsetzens von Kavitationserscheinungen in einer Düsenströmung bei Berücksichtigung der im Wasser gelösten Gase, 1971, vergriffen*
- 20 *Schaak, Hartmut: Verteilleitungen von Wasserkraftanlagen, 1971*
- 21 *Sonderheft zur Eröffnung der neuen Versuchsanstalt des Instituts für Wasserbau der Universität Stuttgart mit Beiträgen von Brombach, Hansjörg; Dirksen, Wolfram; Gál, Attila; Gerlach, Reinhard; Giesecke, Jürgen; Holthoff, Franz-Josef; Kuz, Klaus Dieter; Marotz, Günter; Minor, Hans-Erwin; Petrikat, Kurt; Röhnisch, Arthur; Rueff, Helge; Schwarz, Helmut; Vollmer, Ernst; Wildenhahn, Eberhard; 1972*
- 22 *Wang, Chung-su: Ein Beitrag zur Berechnung der Schwingungen an Kegelstrahlschiebern, 1972*
- 23 *Mayer-Vorfelder, Hans-Jörg: Erdwiderstandsbeiwerte nach dem Ohde-Variationsverfahren, 1972*
- 24 *Minor, Hans-Erwin: Beitrag zur Bestimmung der Schwingungsanfachungsfunktionen überströmter Stauklappen, 1972, vergriffen*
- 25 *Brombach, Hansjörg: Untersuchung strömungsmechanischer Elemente (Fluidik) und die Möglichkeit der Anwendung von Wirbelkammerelementen im Wasserbau, 1972, vergriffen*
- 26 *Wildenhahn, Eberhard: Beitrag zur Berechnung von Horizontalfilterbrunnen, 1972*
- 27 *Steinlein, Helmut: Die Eliminierung der Schwebstoffe aus Flußwasser zum Zweck der unterirdischen Wasserspeicherung, gezeigt am Beispiel der Iller, 1972*
- 28 *Holthoff, Franz Josef: Die Überwindung großer Hubhöhen in der Binnenschifffahrt durch Schwimmerhebewerke, 1973*

- 29 Röder, Karl: *Einwirkungen aus Baugrundbewegungen auf trog- und kastenförmige Konstruktionen des Wasser- und Tunnelbaues*, 1973
- 30 Kretschmer, Heinz: *Die Bemessung von Bogenstau mauern in Abhängigkeit von der Talform*, 1973
- 31 Honekamp, Hermann: *Beitrag zur Berechnung der Montage von Unterwasserpipelines*, 1973
- 32 Giesecke, Jürgen: *Die Wirbelkammertriode als neuartiges Steuerorgan im Wasserbau*, und Brombach, Hansjörg: *Entwicklung, Bauformen, Wirkungsweise und Steuereigenschaften von Wirbelkammerverstärkern*, 1974
- 33 Rueff, Helge: *Untersuchung der schwingungserregenden Kräfte an zwei hintereinander angeordneten Tiefschützen unter besonderer Berücksichtigung von Kavitation*, 1974
- 34 Röhnisch, Arthur: *Einpreßversuche mit Zementmörtel für Spannbeton - Vergleich der Ergebnisse von Modellversuchen mit Ausführungen in Hüllwellrohren*, 1975
- 35 *Sonderheft anlässlich des 65. Geburtstages von Prof. Dr.-Ing. Kurt Petrikat mit Beiträgen von:* Brombach, Hansjörg; Erbel, Klaus; Flinspach, Dieter; Fischer jr., Richard; Gàl, Attila; Gerlach, Reinhard; Giesecke, Jürgen; Haberhauer, Robert; Hafner Edzard; Hausenblas, Bernhard; Horlacher, Hans-Burkhard; Hutarew, Andreas; Knoll, Manfred; Krummet, Ralph; Marotz, Günter; Merkle, Theodor; Miller, Christoph; Minor, Hans-Erwin; Neumayer, Hans; Rao, Syamala; Rath, Paul; Rueff, Helge; Ruppert, Jürgen; Schwarz, Wolfgang; Topal-Gökceli, Mehmet; Vollmer, Ernst; Wang, Chung-su; Weber, Hans-Georg; 1975
- 36 Berger, Jochum: *Beitrag zur Berechnung des Spannungszustandes in rotationssymmetrisch belasteten Kugelschalen veränderlicher Wandstärke unter Gas- und Flüssigkeitsdruck durch Integration schwach singulärer Differentialgleichungen*, 1975
- 37 Dirksen, Wolfram: *Berechnung instationärer Abflußvorgänge in gestauten Gerinnen mittels Differenzenverfahren und die Anwendung auf Hochwasserrückhaltebecken*, 1976
- 38 Horlacher, Hans-Burkhard: *Berechnung instationärer Temperatur- und Wärmespannungsfelder in langen mehrschichtigen Hohlzylindern*, 1976
- 39 Hafner, Edzard: *Untersuchung der hydrodynamischen Kräfte auf Baukörper im Tiefwasserbereich des Meeres*, 1977, ISBN 3-921694-39-6
- 40 Ruppert, Jürgen: *Über den Axialwirbelkammerverstärker für den Einsatz im Wasserbau*, 1977, ISBN 3-921694-40-X
- 41 Hutarew, Andreas: *Beitrag zur Beeinflußbarkeit des Sauerstoffgehalts in Fließgewässern an Abstürzen und Wehren*, 1977, ISBN 3-921694-41-8, vergriffen
- 42 Miller, Christoph: *Ein Beitrag zur Bestimmung der schwingungserregenden Kräfte an unterströmten Wehren*, 1977, ISBN 3-921694-42-6
- 43 Schwarz, Wolfgang: *Druckstoßberechnung unter Berücksichtigung der Radial- und Längsverschiebungen der Rohrwandung*, 1978, ISBN 3-921694-43-4
- 44 Kinzelbach, Wolfgang: *Numerische Untersuchungen über den optimalen Einsatz variabler Kühlsysteme einer Kraftwerkskette am Beispiel Oberrhein*, 1978, ISBN 3-921694-44-2
- 45 Barczewski, Baldur: *Neue Meßmethoden für Wasser-Luftgemische und deren Anwendung auf zweiphasige Auftriebsstrahlen*, 1979, ISBN 3-921694-45-0
- 46 Neumayer, Hans: *Untersuchung der Strömungsvorgänge in radialen Wirbelkammerverstärkern*, 1979, ISBN 3-921694-46-9
- 47 Elalfy, Youssef-Elhassan: *Untersuchung der Strömungsvorgänge in Wirbelkammerdioden und -drosseln*, 1979, ISBN 3-921694-47-7
- 48 Brombach, Hansjörg: *Automatisierung der Bewirtschaftung von Wasserspeichern*, 1981, ISBN 3-921694-48-5
- 49 Geldner, Peter: *Deterministische und stochastische Methoden zur Bestimmung der Selbstdichtung von Gewässern*, 1981, ISBN 3-921694-49-3, vergriffen

- 50 Mehlhorn, Hans: *Temperaturveränderungen im Grundwasser durch Brauchwassereinleitungen*, 1982, ISBN 3-921694-50-7, vergriffen
- 51 Hafner, Edzard: *Rohrleitungen und Behälter im Meer*, 1983, ISBN 3-921694-51-5
- 52 Rinnert, Bernd: *Hydrodynamische Dispersion in porösen Medien: Einfluß von Dichteunterschieden auf die Vertikalvermischung in horizontaler Strömung*, 1983, ISBN 3-921694-52-3, vergriffen
- 53 Lindner, Wulf: *Steuerung von Grundwasserentnahmen unter Einhaltung ökologischer Kriterien*, 1983, ISBN 3-921694-53-1, vergriffen
- 54 Herr, Michael; Herzer, Jörg; Kinzelbach, Wolfgang; Kobus, Helmut; Rinnert, Bernd: *Methoden zur rechnerischen Erfassung und hydraulischen Sanierung von Grundwasserkontaminationen*, 1983, ISBN 3-921694-54-X
- 55 Schmitt, Paul: *Wege zur Automatisierung der Niederschlagsermittlung*, 1984, ISBN 3-921694-55-8, vergriffen
- 56 Müller, Peter: *Transport und selektive Sedimentation von Schwebstoffen bei gestautem Abfluß*, 1985, ISBN 3-921694-56-6
- 57 El-Qawasmeh, Fuad: *Möglichkeiten und Grenzen der Tropfbewässerung unter besonderer Berücksichtigung der Verstopfungsanfälligkeit der Tropfelemente*, 1985, ISBN 3-921694-57-4, vergriffen
- 58 Kirchenbaur, Klaus: *Mikroprozessorgesteuerte Erfassung instationärer Druckfelder am Beispiel seegangsbelasteter Baukörper*, 1985, ISBN 3-921694-58-2
- 59 Kobus, Helmut (Hrsg.): *Modellierung des großräumigen Wärme- und Schadstofftransports im Grundwasser*, Tätigkeitsbericht 1984/85 (DFG-Forschergruppe an den Universitäten Hohenheim, Karlsruhe und Stuttgart), 1985, ISBN 3-921694-59-0, vergriffen
- 60 Spitz, Karlheinz: *Dispersion in porösen Medien: Einfluß von Inhomogenitäten und Dichteunterschieden*, 1985, ISBN 3-921694-60-4, vergriffen
- 61 Kobus, Helmut: *An Introduction to Air-Water Flows in Hydraulics*, 1985, ISBN 3-921694-61-2
- 62 Kaleris, Vassilios: *Erfassung des Austausches von Oberflächen- und Grundwasser in horizontalebene Grundwassermodellen*, 1986, ISBN 3-921694-62-0
- 63 Herr, Michael: *Grundlagen der hydraulischen Sanierung verunreinigter Porengrundwasserleiter*, 1987, ISBN 3-921694-63-9
- 64 Marx, Walter: *Berechnung von Temperatur und Spannung in Massenbeton infolge Hydratation*, 1987, ISBN 3-921694-64-7
- 65 Koschitzky, Hans-Peter: *Dimensionierungskonzept für Sohlbelüfter in Schußrinnen zur Vermeidung von Kavitationsschäden*, 1987, ISBN 3-921694-65-5
- 66 Kobus, Helmut (Hrsg.): *Modellierung des großräumigen Wärme- und Schadstofftransports im Grundwasser*, Tätigkeitsbericht 1986/87 (DFG-Forschergruppe an den Universitäten Hohenheim, Karlsruhe und Stuttgart) 1987, ISBN 3-921694-66-3
- 67 Söll, Thomas: *Berechnungsverfahren zur Abschätzung anthropogener Temperaturanomalien im Grundwasser*, 1988, ISBN 3-921694-67-1
- 68 Dittrich, Andreas; Westrich, Bernd: *Bodenseeufererosion, Bestandsaufnahme und Bewertung*, 1988, ISBN 3-921694-68-X, vergriffen
- 69 Huwe, Bernd; van der Ploeg, Rienk R.: *Modelle zur Simulation des Stickstoffhaushaltes von Standorten mit unterschiedlicher landwirtschaftlicher Nutzung*, 1988, ISBN 3-921694-69-8, vergriffen
- 70 Stephan, Karl: *Integration elliptischer Funktionen*, 1988, ISBN 3-921694-70-1
- 71 Kobus, Helmut; Zilliox, Lothaire (Hrsg.): *Nitratbelastung des Grundwassers, Auswirkungen der Landwirtschaft auf die Grundwasser- und Rohwasserbeschaffenheit und Maßnahmen zum Schutz des Grundwassers*. Vorträge des deutsch-französischen Kolloquiums am 6. Oktober 1988, Universitäten Stuttgart und Louis Pasteur Strasbourg (Vorträge in deutsch oder französisch, Kurzfassungen zweisprachig), 1988, ISBN 3-921694-71-X

- 72 Soyeaux, Renald: *Unterströmung von Stauanlagen auf klüftigem Untergrund unter Berücksichtigung laminarer und turbulenter Fließzustände*, 1991, ISBN 3-921694-72-8
- 73 Kohane, Roberto: *Berechnungsmethoden für Hochwasserabfluß in Fließgewässern mit überströmten Vorländern*, 1991, ISBN 3-921694-73-6
- 74 Hassinger, Reinhard: *Beitrag zur Hydraulik und Bemessung von Blocksteinrampen in flexibler Bauweise*, 1991, ISBN 3-921694-74-4, vergriffen
- 75 Schäfer, Gerhard: *Einfluß von Schichtenstrukturen und lokalen Einlagerungen auf die Längsdispersion in Porengrundwasserleitern*, 1991, ISBN 3-921694-75-2
- 76 Giesecke, Jürgen: *Vorträge, Wasserwirtschaft in stark besiedelten Regionen; Umweltforschung mit Schwerpunkt Wasserwirtschaft*, 1991, ISBN 3-921694-76-0
- 77 Huwe, Bernd: *Deterministische und stochastische Ansätze zur Modellierung des Stickstoffhaushalts landwirtschaftlich genutzter Flächen auf unterschiedlichem Skalenniveau*, 1992, ISBN 3-921694-77-9, vergriffen
- 78 Rommel, Michael: *Verwendung von Kluffdaten zur realitätsnahen Generierung von Kluffnetzen mit anschließender laminar-turbulenter Strömungsberechnung*, 1993, ISBN 3-921694-78-7
- 79 Marschall, Paul: *Die Ermittlung lokaler Stofffrachten im Grundwasser mit Hilfe von Einbohrloch-Meßverfahren*, 1993, ISBN 3-921694-79-5, vergriffen
- 80 Ptak, Thomas: *Stofftransport in heterogenen Porenaquiferen: Felduntersuchungen und stochastische Modellierung*, 1993, ISBN 3-921694-80-9, vergriffen
- 81 Haakh, Frieder: *Transientes Strömungsverhalten in Wirbelkammern*, 1993, ISBN 3-921694-81-7
- 82 Kobus, Helmut; Cirkpa, Olaf; Barczewski, Baldur; Koschitzky, Hans-Peter: *Versuchseinrichtung zur Grundwasser- und Altlastensanierung VEGAS, Konzeption und Programmrahmen*, 1993, ISBN 3-921694-82-5
- 83 Zang, Weidong: *Optimaler Echtzeit-Betrieb eines Speichers mit aktueller Abflußregenerierung*, 1994, ISBN 3-921694-83-3, vergriffen
- 84 Franke, Hans-Jörg: *Stochastische Modellierung eines flächenhaften Stoffeintrages und Transports in Grundwasser am Beispiel der Pflanzenschutzmittelproblematik*, 1995, ISBN 3-921694-84-1
- 85 Lang, Ulrich: *Simulation regionaler Strömungs- und Transportvorgänge in Karstaquiferen mit Hilfe des Doppelkontinuum-Ansatzes: Methodenentwicklung und Parameteridentifikation*, 1995, ISBN 3-921694-85-X, vergriffen
- 86 Helmig, Rainer: *Einführung in die Numerischen Methoden der Hydromechanik*, 1996, ISBN 3-921694-86-8, vergriffen
- 87 Cirkpa, Olaf: *CONTRACT: A Numerical Tool for Contaminant Transport and Chemical Transformations - Theory and Program Documentation -*, 1996, ISBN 3-921694-87-6
- 88 Haberlandt, Uwe: *Stochastische Synthese und Regionalisierung des Niederschlages für Schmutzfrachtberechnungen*, 1996, ISBN 3-921694-88-4
- 89 Croisé, Jean: *Extraktion von flüchtigen Chemikalien aus natürlichen Lockergesteinen mittels erzwungener Luftströmung*, 1996, ISBN 3-921694-89-2, vergriffen
- 90 Jorde, Klaus: *Ökologisch begründete, dynamische Mindestwasserregelungen bei Ausleitungskraftwerken*, 1997, ISBN 3-921694-90-6, vergriffen
- 91 Helmig, Rainer: *Gekoppelte Strömungs- und Transportprozesse im Untergrund - Ein Beitrag zur Hydrosystemmodellierung-*, 1998, ISBN 3-921694-91-4, vergriffen
- 92 Emmert, Martin: *Numerische Modellierung nichtisothermer Gas-Wasser Systeme in porösen Medien*, 1997, ISBN 3-921694-92-2
- 93 Kern, Ulrich: *Transport von Schweb- und Schadstoffen in staugeregelten Fließgewässern am Beispiel des Neckars*, 1997, ISBN 3-921694-93-0, vergriffen
- 94 Förster, Georg: *Druckstoßdämpfung durch große Luftblasen in Hochpunkten von Rohrleitungen* 1997, ISBN 3-921694-94-9

- 95 Cirpka, Olaf: *Numerische Methoden zur Simulation des reaktiven Mehrkomponententransports im Grundwasser*, 1997, ISBN 3-921694-95-7, vergriffen
- 96 Färber, Arne: *Wärmetransport in der ungesättigten Bodenzone: Entwicklung einer thermischen In-situ-Sanierungstechnologie*, 1997, ISBN 3-921694-96-5
- 97 Betz, Christoph: *Wasserdampfdestillation von Schadstoffen im porösen Medium: Entwicklung einer thermischen In-situ-Sanierungstechnologie*, 1998, SBN 3-921694-97-3
- 98 Xu, Yichun: *Numerical Modeling of Suspended Sediment Transport in Rivers*, 1998, ISBN 3-921694-98-1, vergriffen
- 99 Wüst, Wolfgang: *Geochemische Untersuchungen zur Sanierung CKW-kontaminierter Aquifere mit Fe(0)-Reaktionswänden*, 2000, ISBN 3-933761-02-2
- 100 Sheta, Hussam: *Simulation von Mehrphasenvorgängen in porösen Medien unter Einbeziehung von Hysterese-Effekten*, 2000, ISBN 3-933761-03-4
- 101 Ayros, Edwin: *Regionalisierung extremer Abflüsse auf der Grundlage statistischer Verfahren*, 2000, ISBN 3-933761-04-2, vergriffen
- 102 Huber, Ralf: *Compositional Multiphase Flow and Transport in Heterogeneous Porous Media*, 2000, ISBN 3-933761-05-0
- 103 Braun, Christopherus: *Ein Upscaling-Verfahren für Mehrphasenströmungen in porösen Medien*, 2000, ISBN 3-933761-06-9
- 104 Hofmann, Bernd: *Entwicklung eines rechnergestützten Managementsystems zur Beurteilung von Grundwasserschadensfällen*, 2000, ISBN 3-933761-07-7
- 105 Class, Holger: *Theorie und numerische Modellierung nichtisothermer Mehrphasenprozesse in NAPL-kontaminierten porösen Medien*, 2001, ISBN 3-933761-08-5
- 106 Schmidt, Reinhard: *Wasserdampf- und Heißluftinjektion zur thermischen Sanierung kontaminierter Standorte*, 2001, ISBN 3-933761-09-3
- 107 Josef, Reinhold: *Schadstoffextraktion mit hydraulischen Sanierungsverfahren unter Anwendung von grenzflächenaktiven Stoffen*, 2001, ISBN 3-933761-10-7
- 108 Schneider, Matthias: *Habitat- und Abflussmodellierung für Fließgewässer mit unscharfen Berechnungsansätzen*, 2001, ISBN 3-933761-11-5
- 109 Rathgeb, Andreas: *Hydrodynamische Bemessungsgrundlagen für Lockerdeckwerke an überströmbaren Erddämmen*, 2001, ISBN 3-933761-12-3
- 110 Lang, Stefan: *Parallele numerische Simulation instationärer Probleme mit adaptiven Methoden auf unstrukturierten Gittern*, 2001, ISBN 3-933761-13-1
- 111 Appt, Jochen; Stumpp Simone: *Die Bodensee-Messkampagne 2001, IWS/CWR Lake Constance Measurement Program 2001*, 2002, ISBN 3-933761-14-X
- 112 Heimerl, Stephan: *Systematische Beurteilung von Wasserkraftprojekten*, 2002, ISBN 3-933761-15-8, vergriffen
- 113 Iqbal, Amin: *On the Management and Salinity Control of Drip Irrigation*, 2002, ISBN 3-933761-16-6
- 114 Silberhorn-Hemminger, Annette: *Modellierung von Kluftaquifersystemen: Geostatistische Analyse und deterministisch-stochastische Kluftgenerierung*, 2002, ISBN 3-933761-17-4
- 115 Winkler, Angela: *Prozesse des Wärme- und Stofftransports bei der In-situ-Sanierung mit festen Wärmequellen*, 2003, ISBN 3-933761-18-2
- 116 Marx, Walter: *Wasserkraft, Bewässerung, Umwelt - Planungs- und Bewertungsschwerpunkte der Wasserbewirtschaftung*, 2003, ISBN 3-933761-19-0
- 117 Hinkelmann, Reinhard: *Efficient Numerical Methods and Information-Processing Techniques in Environment Water*, 2003, ISBN 3-933761-20-4
- 118 Samaniego-Eguiguren, Luis Eduardo: *Hydrological Consequences of Land Use / Land Cover and Climatic Changes in Mesoscale Catchments*, 2003, ISBN 3-933761-21-2
- 119 Neunhäuserer, Lina: *Diskretisierungsansätze zur Modellierung von Strömungs- und Transportprozessen in geklüftet-porösen Medien*, 2003, ISBN 3-933761-22-0

- 120 Paul, Maren: *Simulation of Two-Phase Flow in Heterogeneous Poros Media with Adaptive Methods*, 2003, ISBN 3-933761-23-9
- 121 Ehret, Uwe: *Rainfall and Flood Nowcasting in Small Catchments using Weather Radar*, 2003, ISBN 3-933761-24-7
- 122 Haag, Ingo: *Der Sauerstoffhaushalt staugeregelter Flüsse am Beispiel des Neckars - Analysen, Experimente, Simulationen -*, 2003, ISBN 3-933761-25-5
- 123 Appt, Jochen: *Analysis of Basin-Scale Internal Waves in Upper Lake Constance*, 2003, ISBN 3-933761-26-3
- 124 Hrsg.: Schrenk, Volker; Batereau, Katrin; Barczewski, Baldur; Weber, Karolin und Koschitzky, Hans-Peter: *Symposium Ressource Fläche und VEGAS - Statuskolloquium 2003, 30. September und 1. Oktober 2003*, 2003, ISBN 3-933761-27-1
- 125 Omar Khalil Ouda: *Optimisation of Agricultural Water Use: A Decision Support System for the Gaza Strip*, 2003, ISBN 3-933761-28-0
- 126 Batereau, Katrin: *Sensorbasierte Bodenluftmessung zur Vor-Ort-Erkundung von Schadensherden im Untergrund*, 2004, ISBN 3-933761-29-8
- 127 Witt, Oliver: *Erosionsstabilität von Gewässersedimenten mit Auswirkung auf den Stofftransport bei Hochwasser am Beispiel ausgewählter Stauhaltungen des Oberrheins*, 2004, ISBN 3-933761-30-1
- 128 Jakobs, Hartmut: *Simulation nicht-isothermer Gas-Wasser-Prozesse in komplexen Kluft-Matrix-Systemen*, 2004, ISBN 3-933761-31-X
- 129 Li, Chen-Chien: *Deterministisch-stochastisches Berechnungskonzept zur Beurteilung der Auswirkungen erosiver Hochwasserereignisse in Flussstauhaltungen*, 2004, ISBN 3-933761-32-8
- 130 Reichenberger, Volker; Helmig, Rainer; Jakobs, Hartmut; Bastian, Peter; Niessner, Jennifer: *Complex Gas-Water Processes in Discrete Fracture-Matrix Systems: Up-scaling, Mass-Conservative Discretization and Efficient Multilevel Solution*, 2004, ISBN 3-933761-33-6
- 131 Hrsg.: Barczewski, Baldur; Koschitzky, Hans-Peter; Weber, Karolin; Wege, Ralf: *VEGAS - Statuskolloquium 2004*, Tagungsband zur Veranstaltung am 05. Oktober 2004 an der Universität Stuttgart, Campus Stuttgart-Vaihingen, 2004, ISBN 3-933761-34-4
- 132 Asie, Kemal Jabir: *Finite Volume Models for Multiphase Multicomponent Flow through Porous Media*. 2005, ISBN 3-933761-35-2
- 133 Jacoub, George: *Development of a 2-D Numerical Module for Particulate Contaminant Transport in Flood Retention Reservoirs and Impounded Rivers*, 2004, ISBN 3-933761-36-0
- 134 Nowak, Wolfgang: *Geostatistical Methods for the Identification of Flow and Transport Parameters in the Subsurface*, 2005, ISBN 3-933761-37-9
- 135 Süß, Mia: *Analysis of the influence of structures and boundaries on flow and transport processes in fractured porous media*, 2005, ISBN 3-933761-38-7
- 136 Jose, Surabhin Chackiath: *Experimental Investigations on Longitudinal Dispersive Mixing in Heterogeneous Aquifers*, 2005, ISBN: 3-933761-39-5
- 137 Filiz, Fulya: *Linking Large-Scale Meteorological Conditions to Floods in Mesoscale Catchments*, 2005, ISBN 3-933761-40-9
- 138 Qin, Minghao: *Wirklichkeitsnahe und recheneffiziente Ermittlung von Temperatur und Spannungen bei großen RCC-Staumauern*, 2005, ISBN 3-933761-41-7
- 139 Kobayashi, Kenichiro: *Optimization Methods for Multiphase Systems in the Subsurface - Application to Methane Migration in Coal Mining Areas*, 2005, ISBN 3-933761-42-5
- 140 Rahman, Md. Arifur: *Experimental Investigations on Transverse Dispersive Mixing in Heterogeneous Porous Media*, 2005, ISBN 3-933761-43-3
- 141 Schrenk, Volker: *Ökobilanzen zur Bewertung von Altlastensanierungsmaßnahmen*, 2005, ISBN 3-933761-44-1

- 142 Hundecha, Hirpa Yeshewatesfa: *Regionalization of Parameters of a Conceptual Rainfall-Runoff Model*, 2005, ISBN: 3-933761-45-X
- 143 Wege, Ralf: *Untersuchungs- und Überwachungsmethoden für die Beurteilung natürlicher Selbstreinigungsprozesse im Grundwasser*, 2005, ISBN 3-933761-46-8
- 144 Breiting, Thomas: *Techniken und Methoden der Hydroinformatik - Modellierung von komplexen Hydrosystemen im Untergrund*, 2006, ISBN 3-933761-47-6
- 145 Hrsg.: Braun, Jürgen; Koschitzky, Hans-Peter; Müller, Martin: *Ressource Untergrund: 10 Jahre VEGAS: Forschung und Technologieentwicklung zum Schutz von Grundwasser und Boden*, Tagungsband zur Veranstaltung am 28. und 29. September 2005 an der Universität Stuttgart, Campus Stuttgart-Vaihingen, 2005, ISBN 3-933761-48-4
- 146 Rojanschi, Vlad: *Abflusskonzentration in mesoskaligen Einzugsgebieten unter Berücksichtigung des Sickerraumes*, 2006, ISBN 3-933761-49-2
- 147 Winkler, Nina Simone: *Optimierung der Steuerung von Hochwasserrückhaltebeckensystemen*, 2006, ISBN 3-933761-50-6
- 148 Wolf, Jens: *Räumlich differenzierte Modellierung der Grundwasserströmung alluvialer Aquifere für mesoskalige Einzugsgebiete*, 2006, ISBN: 3-933761-51-4
- 149 Kohler, Beate: *Externe Effekte der Laufwasserkraftnutzung*, 2006, ISBN 3-933761-52-2
- 150 Hrsg.: Braun, Jürgen; Koschitzky, Hans-Peter; Stuhmann, Matthias: *VEGAS-Statuskolloquium 2006*, Tagungsband zur Veranstaltung am 28. September 2006 an der Universität Stuttgart, Campus Stuttgart-Vaihingen, 2006, ISBN 3-933761-53-0
- 151 Niessner, Jennifer: *Multi-Scale Modeling of Multi-Phase - Multi-Component Processes in Heterogeneous Porous Media*, 2006, ISBN 3-933761-54-9
- 152 Fischer, Markus: *Beanspruchung eingeerdeter Rohrleitungen infolge Austrocknung bindiger Böden*, 2006, ISBN 3-933761-55-7
- 153 Schneck, Alexander: *Optimierung der Grundwasserbewirtschaftung unter Berücksichtigung der Belange der Wasserversorgung, der Landwirtschaft und des Naturschutzes*, 2006, ISBN 3-933761-56-5
- 154 Das, Tapash: *The Impact of Spatial Variability of Precipitation on the Predictive Uncertainty of Hydrological Models*, 2006, ISBN 3-33761-57-3
- 155 Bielinski, Andreas: *Numerical Simulation of CO₂ sequestration in geological formations*, 2007, ISBN 3-933761-58-1
- 156 Mödinger, Jens: *Entwicklung eines Bewertungs- und Entscheidungsunterstützungssystems für eine nachhaltige regionale Grundwasserbewirtschaftung*, 2006, ISBN 3-933761-60-3
- 157 Manthey, Sabine: *Two-phase flow processes with dynamic effects in porous media - parameter estimation and simulation*, 2007, ISBN 3-933761-61-1
- 158 Pozos Estrada, Oscar: *Investigation on the Effects of Entrained Air in Pipelines*, 2007, ISBN 3-933761-62-X
- 159 Ochs, Steffen Oliver: *Steam injection into saturated porous media – process analysis including experimental and numerical investigations*, 2007, ISBN 3-933761-63-8
- 160 Marx, Andreas: *Einsatz gekoppelter Modelle und Wetterradar zur Abschätzung von Niederschlagsintensitäten und zur Abflussvorhersage*, 2007, ISBN 3-933761-64-6
- 161 Hartmann, Gabriele Maria: *Investigation of Evapotranspiration Concepts in Hydrological Modelling for Climate Change Impact Assessment*, 2007, ISBN 3-933761-65-4
- 162 Kebede Gurmessa, Tesfaye: *Numerical Investigation on Flow and Transport Characteristics to Improve Long-Term Simulation of Reservoir Sedimentation*, 2007, ISBN 3-933761-66-2
- 163 Trifković, Aleksandar: *Multi-objective and Risk-based Modelling Methodology for Planning, Design and Operation of Water Supply Systems*, 2007, ISBN 3-933761-67-0
- 164 Göttinger, Jens: *Distributed Conceptual Hydrological Modelling - Simulation of Climate, Land Use Change Impact and Uncertainty Analysis*, 2007, ISBN 3-933761-68-9

- 165 Hrsg.: Braun, Jürgen; Koschitzky, Hans-Peter; Stuhmann, Matthias: *VEGAS – Kolloquium 2007*, Tagungsband zur Veranstaltung am 26. September 2007 an der Universität Stuttgart, Campus Stuttgart-Vaihingen, 2007, ISBN 3-933761-69-7
- 166 Freeman, Beau: *Modernization Criteria Assessment for Water Resources Planning; Klamath Irrigation Project, U.S.*, 2008, ISBN 3-933761-70-0
- 167 Dreher, Thomas: *Selektive Sedimentation von Feinstschwebstoffen in Wechselwirkung mit wandnahen turbulenten Strömungsbedingungen*, 2008, ISBN 3-933761-71-9
- 168 Yang, Wei: *Discrete-Continuous Downscaling Model for Generating Daily Precipitation Time Series*, 2008, ISBN 3-933761-72-7
- 169 Kopecki, Ianina: *Calculational Approach to FST-Hemispheres for Multiparametrical Benthos Habitat Modelling*, 2008, ISBN 3-933761-73-5
- 170 Brommundt, Jürgen: *Stochastische Generierung räumlich zusammenhängender Niederschlagszeitreihen*, 2008, ISBN 3-933761-74-3
- 171 Papafotiou, Alexandros: *Numerical Investigations of the Role of Hysteresis in Heterogeneous Two-Phase Flow Systems*, 2008, ISBN 3-933761-75-1
- 172 He, Yi: *Application of a Non-Parametric Classification Scheme to Catchment Hydrology*, 2008, ISBN 978-3-933761-76-7
- 173 Wagner, Sven: *Water Balance in a Poorly Gauged Basin in West Africa Using Atmospheric Modelling and Remote Sensing Information*, 2008, ISBN 978-3-933761-77-4
- 174 Hrsg.: Braun, Jürgen; Koschitzky, Hans-Peter; Stuhmann, Matthias; Schrenk, Volker: *VEGAS-Kolloquium 2008 Ressource Fläche III*, Tagungsband zur Veranstaltung am 01. Oktober 2008 an der Universität Stuttgart, Campus Stuttgart-Vaihingen, 2008, ISBN 978-3-933761-78-1
- 175 Patil, Sachin: *Regionalization of an Event Based Nash Cascade Model for Flood Predictions in Ungauged Basins*, 2008, ISBN 978-3-933761-79-8
- 176 Assteerawatt, Anongnart: *Flow and Transport Modelling of Fractured Aquifers based on a Geostatistical Approach*, 2008, ISBN 978-3-933761-80-4
- 177 Karnahl, Joachim Alexander: *2D numerische Modellierung von multifraktionalem Schwebstoff- und Schadstofftransport in Flüssen*, 2008, ISBN 978-3-933761-81-1
- 178 Hiester, Uwe: *Technologieentwicklung zur In-situ-Sanierung der ungesättigten Bodenzone mit festen Wärmequellen*, 2009, ISBN 978-3-933761-82-8
- 179 Laux, Patrick: *Statistical Modeling of Precipitation for Agricultural Planning in the Volta Basin of West Africa*, 2009, ISBN 978-3-933761-83-5
- 180 Ehsan, Saqib: *Evaluation of Life Safety Risks Related to Severe Flooding*, 2009, ISBN 978-3-933761-84-2
- 181 Prohaska, Sandra: *Development and Application of a 1D Multi-Strip Fine Sediment Transport Model for Regulated Rivers*, 2009, ISBN 978-3-933761-85-9
- 182 Kopp, Andreas: *Evaluation of CO₂ Injection Processes in Geological Formations for Site Screening*, 2009, ISBN 978-3-933761-86-6
- 183 Ebigbo, Anozie: *Modelling of biofilm growth and its influence on CO₂ and water (two-phase) flow in porous media*, 2009, ISBN 978-3-933761-87-3
- 184 Freiboth, Sandra: *A phenomenological model for the numerical simulation of multiphase multicomponent processes considering structural alterations of porous media*, 2009, ISBN 978-3-933761-88-0
- 185 Zöllner, Frank: *Implementierung und Anwendung netzfreier Methoden im Konstruktiven Wasserbau und in der Hydromechanik*, 2009, ISBN 978-3-933761-89-7
- 186 Vasin, Milos: *Influence of the soil structure and property contrast on flow and transport in the unsaturated zone*, 2010, ISBN 978-3-933761-90-3
- 187 Li, Jing: *Application of Copulas as a New Geostatistical Tool*, 2010, ISBN 978-3-933761-91-0
- 188 AghaKouchak, Amir: *Simulation of Remotely Sensed Rainfall Fields Using Copulas*, 2010, ISBN 978-3-933761-92-7

- 189 Thapa, Pawan Kumar: *Physically-based spatially distributed rainfall runoff modelling for soil erosion estimation*, 2010, ISBN 978-3-933761-93-4
- 190 Wurms, Sven: *Numerische Modellierung der Sedimentationsprozesse in Retentionsanlagen zur Steuerung von Stoffströmen bei extremen Hochwasserabflussereignissen*, 2011, ISBN 978-3-933761-94-1
- 191 Merkel, Uwe: *Unsicherheitsanalyse hydraulischer Einwirkungen auf Hochwasserschutzdeiche und Steigerung der Leistungsfähigkeit durch adaptive Strömungsmodellierung*, 2011, ISBN 978-3-933761-95-8
- 192 Fritz, Jochen: *A Decoupled Model for Compositional Non-Isothermal Multiphase Flow in Porous Media and Multiphysics Approaches for Two-Phase Flow*, 2010, ISBN 978-3-933761-96-5
- 193 Weber, Karolin (Hrsg.): *12. Treffen junger WissenschaftlerInnen an Wasserbauinstituten*, 2010, ISBN 978-3-933761-97-2
- 194 Blifernicht, Jan-Geert: *Probability Forecasts of Daily Areal Precipitation for Small River Basins*, 2011, ISBN 978-3-933761-98-9
- 195 Hrsg.: Koschitzky, Hans-Peter; Braun, Jürgen: *VEGAS-Kolloquium 2010 In-situ-Sanierung - Stand und Entwicklung Nano und ISCO -*, Tagungsband zur Veranstaltung am 07. Oktober 2010 an der Universität Stuttgart, Campus Stuttgart-Vaihingen, 2010, ISBN 978-3-933761-99-6
- 196 Gafurov, Abror: *Water Balance Modeling Using Remote Sensing Information - Focus on Central Asia*, 2010, ISBN 978-3-942036-00-9
- 197 Mackenberg, Sylvia: *Die Quellstärke in der Sickerwasserprognose: Möglichkeiten und Grenzen von Labor- und Freilanduntersuchungen*, 2010, ISBN 978-3-942036-01-6
- 198 Singh, Shailesh Kumar: *Robust Parameter Estimation in Gauged and Ungauged Basins*, 2010, ISBN 978-3-942036-02-3
- 199 Doğan, Mehmet Onur: *Coupling of porous media flow with pipe flow*, 2011, ISBN 978-3-942036-03-0
- 200 Liu, Min: *Study of Topographic Effects on Hydrological Patterns and the Implication on Hydrological Modeling and Data Interpolation*, 2011, ISBN 978-3-942036-04-7
- 201 Geleta, Habtamu Itefa: *Watershed Sediment Yield Modeling for Data Scarce Areas*, 2011, ISBN 978-3-942036-05-4
- 202 Franke, Jörg: *Einfluss der Überwachung auf die Versagenswahrscheinlichkeit von Stau-stufen*, 2011, ISBN 978-3-942036-06-1
- 203 Bakimchandra, Oinam: *Integrated Fuzzy-GIS approach for assessing regional soil erosion risks*, 2011, ISBN 978-3-942036-07-8
- 204 Alam, Muhammad Mahboob: *Statistical Downscaling of Extremes of Precipitation in Mesoscale Catchments from Different RCMs and Their Effects on Local Hydrology*, 2011, ISBN 978-3-942036-08-5
- 205 Hrsg.: Koschitzky, Hans-Peter; Braun, Jürgen: *VEGAS-Kolloquium 2011 Flache Geothermie - Perspektiven und Risiken*, Tagungsband zur Veranstaltung am 06. Oktober 2011 an der Universität Stuttgart, Campus Stuttgart-Vaihingen, 2011, ISBN 978-3-933761-09-2
- 206 Haslauer, Claus: *Analysis of Real-World Spatial Dependence of Subsurface Hydraulic Properties Using Copulas with a Focus on Solute Transport Behaviour*, 2011, ISBN 978-3-942036-10-8
- 207 Dung, Nguyen Viet: *Multi-objective automatic calibration of hydrodynamic models – development of the concept and an application in the Mekong Delta*, 2011, ISBN 978-3-942036-11-5
- 208 Hung, Nguyen Nghia: *Sediment dynamics in the floodplain of the Mekong Delta, Vietnam*, 2011, ISBN 978-3-942036-12-2
- 209 Kuhlmann, Anna: *Influence of soil structure and root water uptake on flow in the unsaturated zone*, 2012, ISBN 978-3-942036-13-9

- 210 Tuhtan, Jeffrey Andrew: *Including the Second Law Inequality in Aquatic Ecodynamics: A Modeling Approach for Alpine Rivers Impacted by Hydropeaking*, 2012, ISBN 978-3-942036-14-6
- 211 Tolossa, Habtamu: *Sediment Transport Computation Using a Data-Driven Adaptive Neuro-Fuzzy Modelling Approach*, 2012, ISBN 978-3-942036-15-3
- 212 Tatomir, Alexandru-Bodgan: *From Discrete to Continuum Concepts of Flow in Fractured Porous Media*, 2012, ISBN 978-3-942036-16-0
- 213 Erbertseder, Karin: *A Multi-Scale Model for Describing Cancer-Therapeutic Transport in the Human Lung*, 2012, ISBN 978-3-942036-17-7
- 214 Noack, Markus: *Modelling Approach for Interstitial Sediment Dynamics and Reproduction of Gravel Spawning Fish*, 2012, ISBN 978-3-942036-18-4
- 215 De Boer, Cjstmir Volkert: *Transport of Nano Sized Zero Valent Iron Colloids during Injection into the Subsurface*, 2012, ISBN 978-3-942036-19-1
- 216 Pfaff, Thomas: *Processing and Analysis of Weather Radar Data for Use in Hydrology*, 2013, ISBN 978-3-942036-20-7
- 217 Lebreuz, Hans-Henning: *Addressing the Input Uncertainty for Hydrological Modeling by a New Geostatistical Method*, 2013, ISBN 978-3-942036-21-4
- 218 Darcis, Melanie Yvonne: *Coupling Models of Different Complexity for the Simulation of CO₂ Storage in Deep Saline Aquifers*, 2013, ISBN 978-3-942036-22-1
- 219 Beck, Ferdinand: *Generation of Spatially Correlated Synthetic Rainfall Time Series in High Temporal Resolution - A Data Driven Approach*, 2013, ISBN 978-3-942036-23-8
- 220 Guthke, Philipp: *Non-multi-Gaussian spatial structures: Process-driven natural genesis, manifestation, modeling approaches, and influences on dependent processes*, 2013, ISBN 978-3-942036-24-5
- 221 Walter, Lena: *Uncertainty studies and risk assessment for CO₂ storage in geological formations*, 2013, ISBN 978-3-942036-25-2
- 222 Wolff, Markus: *Multi-scale modeling of two-phase flow in porous media including capillary pressure effects*, 2013, ISBN 978-3-942036-26-9
- 223 Mosthaf, Klaus Roland: *Modeling and analysis of coupled porous-medium and free flow with application to evaporation processes*, 2014, ISBN 978-3-942036-27-6
- 224 Leube, Philipp Christoph: *Methods for Physically-Based Model Reduction in Time: Analysis, Comparison of Methods and Application*, 2013, ISBN 978-3-942036-28-3
- 225 Rodríguez Fernández, Jhan Ignacio: *High Order Interactions among environmental variables: Diagnostics and initial steps towards modeling*, 2013, ISBN 978-3-942036-29-0
- 226 Eder, Maria Magdalena: *Climate Sensitivity of a Large Lake*, 2013, ISBN 978-3-942036-30-6
- 227 Greiner, Philipp: *Alkoholinjektion zur In-situ-Sanierung von CKW Schadensherden in Grundwasserleitern: Charakterisierung der relevanten Prozesse auf unterschiedlichen Skalen*, 2014, ISBN 978-3-942036-31-3
- 228 Lauser, Andreas: *Theory and Numerical Applications of Compositional Multi-Phase Flow in Porous Media*, 2014, ISBN 978-3-942036-32-0
- 229 Enzenhöfer, Rainer: *Risk Quantification and Management in Water Production and Supply Systems*, 2014, ISBN 978-3-942036-33-7
- 230 Faigle, Benjamin: *Adaptive modelling of compositional multi-phase flow with capillary pressure*, 2014, ISBN 978-3-942036-34-4
- 231 Oladyskhin, Sergey: *Efficient modeling of environmental systems in the face of complexity and uncertainty*, 2014, ISBN 978-3-942036-35-1
- 232 Sugimoto, Takayuki: *Copula based Stochastic Analysis of Discharge Time Series*, 2014, ISBN 978-3-942036-36-8
- 233 Koch, Jonas: *Simulation, Identification and Characterization of Contaminant Source Architectures in the Subsurface*, 2014, ISBN 978-3-942036-37-5

- 234 Zhang, Jin: *Investigations on Urban River Regulation and Ecological Rehabilitation Measures, Case of Shenzhen in China*, 2014, ISBN 978-3-942036-38-2
- 235 Siebel, Rüdiger: *Experimentelle Untersuchungen zur hydrodynamischen Belastung und Standsicherheit von Deckwerken an überströmbaren Erddämmen*, 2014, ISBN 978-3-942036-39-9
- 236 Baber, Katherina: *Coupling free flow and flow in porous media in biological and technical applications: From a simple to a complex interface description*, 2014, ISBN 978-3-942036-40-5
- 237 Nuske, Klaus Philipp: *Beyond Local Equilibrium — Relaxing local equilibrium assumptions in multiphase flow in porous media*, 2014, ISBN 978-3-942036-41-2
- 238 Geiges, Andreas: *Efficient concepts for optimal experimental design in nonlinear environmental systems*, 2014, ISBN 978-3-942036-42-9
- 239 Schwenck, Nicolas: *An XFEM-Based Model for Fluid Flow in Fractured Porous Media*, 2014, ISBN 978-3-942036-43-6
- 240 Chamorro Chávez, Alejandro: *Stochastic and hydrological modelling for climate change prediction in the Lima region, Peru*, 2015, ISBN 978-3-942036-44-3
- 241 Yulizar: *Investigation of Changes in Hydro-Meteorological Time Series Using a Depth-Based Approach*, 2015, ISBN 978-3-942036-45-0
- 242 Kretschmer, Nicole: *Impacts of the existing water allocation scheme on the Limarí watershed – Chile, an integrative approach*, 2015, ISBN 978-3-942036-46-7
- 243 Kramer, Matthias: *Luftbedarf von Freistrahlturbinen im Gegendruckbetrieb*, 2015, ISBN 978-3-942036-47-4
- 244 Hommel, Johannes: *Modeling biogeochemical and mass transport processes in the sub-surface: Investigation of microbially induced calcite precipitation*, 2016, ISBN 978-3-942036-48-1
- 245 Germer, Kai: *Wasserinfiltration in die ungesättigte Zone eines makroporösen Hanges und deren Einfluss auf die Hangstabilität*, 2016, ISBN 978-3-942036-49-8
- 246 Hörning, Sebastian: *Process-oriented modeling of spatial random fields using copulas*, 2016, ISBN 978-3-942036-50-4
- 247 Jambhekar, Vishal: *Numerical modeling and analysis of evaporative salinization in a coupled free-flow porous-media system*, 2016, ISBN 978-3-942036-51-1
- 248 Huang, Yingchun: *Study on the spatial and temporal transferability of conceptual hydrological models*, 2016, ISBN 978-3-942036-52-8
- 249 Kleinknecht, Simon Matthias: *Migration and retention of a heavy NAPL vapor and remediation of the unsaturated zone*, 2016, ISBN 978-3-942036-53-5
- 250 Kwakye, Stephen Oppong: *Study on the effects of climate change on the hydrology of the West African sub-region*, 2016, ISBN 978-3-942036-54-2
- 251 Kissinger, Alexander: *Basin-Scale Site Screening and Investigation of Possible Impacts of CO₂ Storage on Subsurface Hydrosystems*, 2016, ISBN 978-3-942036-55-9
- 252 Müller, Thomas: *Generation of a Realistic Temporal Structure of Synthetic Precipitation Time Series for Sewer Applications*, 2017, ISBN 978-3-942036-56-6
- 253 Grüninger, Christoph: *Numerical Coupling of Navier-Stokes and Darcy Flow for Soil-Water Evaporation*, 2017, ISBN 978-3-942036-57-3
- 254 Suroso: *Asymmetric Dependence Based Spatial Copula Models: Empirical Investigations and Consequences on Precipitation Fields*, 2017, ISBN 978-3-942036-58-0
- 255 Müller, Thomas; Mosthaf, Tobias; Gunzenhauser, Sarah; Seidel, Jochen; Bárdossy, András: *Grundlagenbericht Niederschlags-Simulator (NiedSim3)*, 2017, ISBN 978-3-942036-59-7
- 256 Mosthaf, Tobias: *New Concepts for Regionalizing Temporal Distributions of Precipitation and for its Application in Spatial Rainfall Simulation*, 2017, ISBN 978-3-942036-60-3

- 257 Fenrich, Eva Katrin: *Entwicklung eines ökologisch-ökonomischen Vernetzungsmodells für Wasserkraftanlagen und Mehrzweckspeicher*, 2018, ISBN 978-3-942036-61-0
- 258 Schmidt, Holger: *Microbial stabilization of lotic fine sediments*, 2018, ISBN 978-3-942036-62-7
- 259 Fetzer, Thomas: *Coupled Free and Porous-Medium Flow Processes Affected by Turbulence and Roughness—Models, Concepts and Analysis*, 2018, ISBN 978-3-942036-63-4
- 260 Schröder, Hans Christoph: *Large-scale High Head Pico Hydropower Potential Assessment*, 2018, ISBN 978-3-942036-64-1
- 261 Bode, Felix: *Early-Warning Monitoring Systems for Improved Drinking Water Resource Protection*, 2018, ISBN 978-3-942036-65-8
- 262 Gebler, Tobias: *Statistische Auswertung von simulierten Talsperrenüberwachungsdaten zur Identifikation von Schadensprozessen an Gewichtsstaumauern*, 2018, ISBN 978-3-942036-66-5
- 263 Harten, Matthias von: *Analyse des Zuppinger-Wasserrades – Hydraulische Optimierungen unter Berücksichtigung ökologischer Aspekte*, 2018, ISBN 978-3-942036-67-2
- 264 Yan, Jieru: *Nonlinear estimation of short time precipitation using weather radar and surface observations*, 2018, ISBN 978-3-942036-68-9
- 265 Beck, Martin: *Conceptual approaches for the analysis of coupled hydraulic and geomechanical processes*, 2019, ISBN 978-3-942036-69-6
- 266 Haas, Jannik: *Optimal planning of hydropower and energy storage technologies for fully renewable power systems*, 2019, ISBN 978-3-942036-70-2
- 267 Schneider, Martin: *Nonlinear Finite Volume Schemes for Complex Flow Processes and Challenging Grids*, 2019, ISBN 978-3-942036-71-9
- 268 Most, Sebastian Christopher: *Analysis and Simulation of Anomalous Transport in Porous Media*, 2019, ISBN 978-3-942036-72-6
- 269 Buchta, Rocco: *Entwicklung eines Ziel- und Bewertungssystems zur Schaffung nachhaltiger naturnaher Strukturen in großen sandgeprägten Flüssen des norddeutschen Tieflandes*, 2019, ISBN 978-3-942036-73-3
- 270 Thom, Moritz: *Towards a Better Understanding of the Biostabilization Mechanisms of Sediment Beds*, 2019, ISBN 978-3-942036-74-0
- 271 Stolz, Daniel: *Die Nullspannungstemperatur in Gewichtsstaumauern unter Berücksichtigung der Festigkeitsentwicklung des Betons*, 2019, ISBN 978-3-942036-75-7
- 272 Rodriguez Pretelin, Abelardo: *Integrating transient flow conditions into groundwater well protection*, 2020, ISBN: 978-3-942036-76-4
- 273 Weishaupt, Kilian: *Model Concepts for Coupling Free Flow with Porous Medium Flow at the Pore-Network Scale: From Single-Phase Flow to Compositional Non-Isothermal Two-Phase Flow*, 2020, ISBN: 978-3-942036-77-1
- 274 Koch, Timo: *Mixed-dimension models for flow and transport processes in porous media with embedded tubular network systems*, 2020, ISBN: 978-3-942036-78-8
- 275 Gläser, Dennis: *Discrete fracture modeling of multi-phase flow and deformation in fractured poroelastic media*, 2020, ISBN: 978-3-942036-79-5
- 276 Seitz, Lydia: *Development of new methods to apply a multi-parameter approach – A first step towards the determination of colmation*, 2020, ISBN: 978-3-942036-80-1
- 277 Ebrahim Bakhshipour, Amin: *Optimizing hybrid decentralized systems for sustainable urban drainage infrastructures planning*, 2021, ISBN: 978-3-942036-81-8
- 278 Seitz, Gabriele: *Modeling Fixed-Bed Reactors for Thermochemical Heat Storage with the Reaction System $\text{CaO}/\text{Ca}(\text{OH})_2$* , 2021, ISBN: 978-3-942036-82-5
- 279 Emmert, Simon: *Developing and Calibrating a Numerical Model for Microbially Enhanced Coal-Bed Methane Production*, 2021, ISBN: 978-3-942036-83-2
- 280 Heck, Katharina Klara: *Modelling and analysis of multicomponent transport at the interface between free- and porous-medium flow - influenced by radiation and roughness*, 2021, ISBN: 978-3-942036-84-9

- 281 Ackermann, Sina: *A multi-scale approach for drop/porous-medium interaction*, 2021, ISBN: 978-3-942036-85-6
- 282 Beckers, Felix: *Investigations on Functional Relationships between Cohesive Sediment Erosion and Sediment Characteristics*, 2021, ISBN: 978-3-942036-86-3
- 283 Schlabing, Dirk: *Generating Weather for Climate Impact Assessment on Lakes*, 2021, ISBN: 978-3-942036-87-0
- 284 Becker, Beatrix: *Efficient multiscale multiphysics models accounting for reversible flow at various subsurface energy storage sites*, 2021, ISBN: 978-3-942036-88-7
- 285 Reuschen, Sebastian: *Bayesian Inversion and Model Selection of Heterogeneities in Geo-statistical Subsurface Modeling*, 2021, ISBN: 978-3-942036-89-4
- 286 Michalkowski, Cynthia: *Modeling water transport at the interface between porous GDL and gas distributor of a PEM fuel cell cathode*, 2022, ISBN: 978-3-942036-90-0
- 287 Koca, Kaan: *Advanced experimental methods for investigating flow-biofilm-sediment interactions*, 2022, ISBN: 978-3-942036-91-7
- 288 Modiri, Ehsan: *Clustering simultaneous occurrences of extreme floods in the Neckar catchment*, 2022, ISBN: 978-3-942036-92-4
- 289 Mayar, Mohammad Assem: *High-resolution spatio-temporal measurements of the col-mation phenomenon under laboratory conditions*, 2022, ISBN: 978-3-942036-93-1
- 290 Schäfer Rodrigues Silva, Aline: *Quantifying and Visualizing Model Similarities for Multi-Model Methods*, 2022, ISBN: 978-3-942036-94-8
- 291 Moreno Leiva, Simón: *Optimal planning of water and renewable energy systems for copper production processes with sector coupling and demand flexibility*, 2022, ISBN 978-3-942036-95-5
- 292 Schönau, Steffen: *Modellierung von Bodenerosion und Sedimentaustrag bei Hochwasserereignissen am Beispiel des Einzugsgebiets der Rems*, 2022, ISBN 978-3-942036-96-2
- 293 Glatz, Kumiko: *Upscaling of Nanoparticle Transport in Porous Media*, 2022, ISBN 978-3-942036-97-9
- 294 Pavia Santolamazza, Daniela: *Event-based flood estimation using a random forest algorithm for the regionalization in small catchments*, 2022, ISBN 978-3-942036-98-6
- 295 Haun, Stefan: *Advanced Methods for a Sustainable Sediment Management of Reservoirs*, 2022, ISBN 978-3-942036-99-3
- 296 Herma, Felix: *Data Processing and Model Choice for Flood Prediction*, 2022, ISBN 978-3-910293-00-7
- 297 Weinhardt, Felix: *Porosity and permeability alterations in processes of biomineralization in porous media - microfluidic investigations and their interpretation*, 2022, ISBN 978-3-910293-01-4
- 298 Sadid, Najibullah: *Bedload Transport Estimation in Mountainous Intermittent Rivers and Streams*, 2023, ISBN 978-3-910293-02-1
- 299 Mohammadi, Farid: *A Surrogate-Assisted Bayesian Framework for Uncertainty-Aware Validation Benchmarks*, 2023, ISBN 978-3-910293-03-8
- 300 Praditia, Timothy: *Physics-informed Neural Networks for Learning Dynamic, Distributed and Uncertain Systems*, 2023, ISBN 978-3-910293-04-5
- 301 Gyawali, Dhiraj Raj: *Development and parameter estimation of conceptual snow-melt models using MODIS snow-cover distribution*, 2023, ISBN 978-3-910293-05-2
- 302 Görtz, Jan: *Coupled modeling approach for physico-chemical processes during the deterioration of cement-based structures*, 2023, ISBN 978-3-910293-06-9
- 303 Veyskarami, Maziar: *Coupled free-flow-porous media flow processes including drop formation*, 2023, ISBN 978-3-910293-07-6
- 304 El Hachem, Abbas: *Spatial Extent of Precipitation Extremes in Hydrology*, 2023, ISBN 978-3-910293-08-3

- 305 Banerjee, Ishani: *Stochastic Model Comparison and Refinement Strategies for Gas Migration in the Subsurface*, 2023, ISBN 978-3-910293-09-0
- 306 Anwar, Faizan: *Spatial aspects of hydrological extremes: Description and simulation*, 2024, ISBN 978-3-910293-10-6
- 307 Mouris, Kilian: *A holistic approach to assess the impact of global change on reservoir sedimentation*, 2024, ISBN 978-3-910293-11-3
- 308 Ejaz, Fahad: *Long-term lumped projections of groundwater balances in the face of limited data*, 2024, ISBN 978-3-910293-12-0
- 309 Shoarinezhad, Vahid: *Applying automatic calibration for three-dimensional numerical modeling of hydro-morphological changes in channels and reservoirs*, 2024, ISBN 978-3-910293-13-7

Die Mitteilungshefte ab der Nr. 134 (Jg. 2005) stehen als pdf-Datei über die Homepage des Instituts: www.iws.uni-stuttgart.de zur Verfügung.